ULTRASONIC AND VISCOELASTIC STUDIES ON LIQUIDS AT DIFFERENT PRESSURES

A THESIS

SUBMITTED TO THE

DEPARTMENT OF PURE AND APPLIED CHEMISTRY

OF THE

UNIVERSITY OF SALFORD

BY

JESSIE ELLIS

FOR THE DEGREE OF

DOCTOR OF PHILOSOPHY

DECLARATION

The work contained in this thesis was carried out by myself at the University of Salford and the Physical Laboratories of Shell Research Limited, Chester, during the period 1973 - 1976 and has not to my knowledge been currently submitted in part or in total as fulfilment for any other degree of this or any other University.

SIGNED ..... Jessie Ellis .....

DATE ..... May 4th 1976 .....

CONTENTS

LIST OF SYMBOLS

Symbol	Definition	Units
a_r	Ratio of $\eta_s(0)_{T1} : \eta_s(0)_{T2}$	
a + ib	Propagation constant of fused quartz	
A	Parameter in the single relaxation equation	Nepers $m^{-1}s^2$
A	Amplitude of longitudinal wave	dB
A_o	Amplitude of unattenuated longitudinal wave	dB
b.p.	Boiling point	K
b_r	Ratio $G(\infty)_{T1} : G(\infty)_{T2}$	
B	Parameter in the single relaxation equation	Nepers $m^{-1}s^2$
C	(1 + R) dB/(1 - R)	decibels
C_p	Specific heat at constant pressure	J mol^{-1}
C_v	Specific heat at constant volume	J mol^{-1}
d	Length of cable (velocimeter)	cm
dB	Decibel = 10 $\log_{10}$ (I_1/I_2)	
D	Internal diameter of the densitometer	m
f	Frequency = velocity/wavelength	s^{-1}
f_c	Characteristic frequency = $1/2\pi\tau$	s^{-1}
ΔE	The energy difference between two states	J mol^{-1}
G	Shear modulus - the ratio of a shearing stress to its corresponding shearing strain	N m^{-2}
$G^*(\omega)$	Complex shear modulus (complex sum of the moduli)	N m^{-2}
$G'(\omega)$	Real part of G^* or storage modulus, the ratio of the stress which is in phase with the sinusoidal strain of angular frequency, ω, to the strain	N m^{-2}

Symbol	Definition	Units
$G''(\omega)$	Imaginary part of G^* or loss modulus, the ratio of stress which has a phase lag of 90° with the sinusoidal strain of angular frequency, ω, to the strain	$N\ m^{-2}$
$G(\infty)$	Limiting shear modulus at infinite frequency	$N\ m^{-2}$
ΔG	Gibbs free energy difference	J
H	Enthalpy	$J\ mol^{-1}$
ΔH	Enthalpy of activation	$J\ mol^{-1}$
i	$\sqrt{-1}$	
J	Shear compliance - the ratio of a strain to its corresponding stress	$(N\ m^{-2})^{-1}$
$J^*(\omega)$	Complex shear compliance	"
$J'(\omega)$	Real part of J^*, the ratio of the strain which in phase with the sinusoidal stress of angular frequency, ω, to the stress	"
$J''(\omega)$	Imaginary part of J^*, the ratio of the strain which has a phase lag of 90° with a sinusoidal stress of angular frequency, ω, to the stress	"
$J(\infty)$	Limiting shear compliance	"
J_r	Retardation compliance - represents the delayed storage of energy under stress	"
J_r^*	Complex retardation compliance	"
J_1	Real part of J_r^*	"
J_2	Imaginary part of J_r^*	"
k	Parameter in the modified B.E.L. equation	
k	Constant for the couette viscometer	$N\ rad\ m^{-2}$
k_a	Association rate constant	$dm^3\ mol^{-1}s^{-1}$
k_d	Dissocation rate constant	s^{-1}
k_B	Boltzman's constant	$J\ deg^{-1}$

Symbol	Definition	Units
k_b	Reaction rate from state I to II	s^{-1}
k_c	Reaction rate from state II to I	s^{-1}
K	Bulk modulus, the ratio of isotropic stress to the relative change of volume	$N\ m^{-2}$
$K^*(\omega)$	Complex bulk modulus	"
$K'(\omega)$	Real part of K^*	"
$K''(\omega)$	Imaginary part of K^*	"
$K(0)$	Bulk modulus at low frequency	"
$K(\infty)$	Bulk modulus at infinite frequency	"
K_2	$K(\infty) - K(0)$	"
K'	Equilibrium constant	
L	Path length change	m
L	Length of cable (X_s measurements)	cm
L	Spacer length (velocimeter)	m
M	Mass	Kg
m.p.	Melting point	K
$M^*(\omega)$	Complex longitudinal modulus	$N\ m^{-2}$
$M'(\omega)$	Real part of M^*	"
$M''(\omega)$	Imaginary part of M^*	"
$M(0)$	Longitudinal modulus at low frequency	"
$M(\infty)$	Longitudinal modulus at infinite frequency	"
$\overline{Mn}$	Number average molecular weight	
$\overline{Mw}$	Weight average molecular weight	
P	Pressure	$N\ m^{-2}$

Symbol	Definition	Units
Q	$= 2R/(1 + R)^2$	
R	Gas constant	J deg^{-1}
R	Radius of crystal (transducer)	mm
R	Reflection coefficient	
R^*	Complex reflection coefficient	
R_L	Real part of the longitudinal impedance	N s m^{-3}
R_{QL}	Real part of the longitudinal impedance of quartz	"
R_{FL}	Real part of the longitudinal impedance of test liquid	"
R_{TL}	Real part of the longitudinal impedance of reference liquid	"
R_S	Real part of the complex shear impedance	"
R_{QS}	Real part of the complex shear impedance of quartz	"
R_{FS}	Real part of the complex shear impedance of test liquid	"
R_{TS}	Real part of the complex shear impedance of reference liquid	"
$R_{Newt.}$	Newtonian value of the real part of the impedance	"
S	Stress (force per unit area)	N m^{-2}
S	Entropy	J $mol^{-1}K^{-1}$
ΔS	Entropy of activation	J $mol^{-1}K^{-1}$
t	Thickness of crystal	m
t	Time for fractional part of a wavelength (velocimeter)	s
T	Temperature	K

Symbol	Definition	Units
T_g	Glass transition temperature	K
T^*	Transmission factor	
u	Particle displacement	m
V	Velocity = frequency . wavelength	m s^{-1}
V_L	Longitudinal velocity	"
V_S	Shear velocity	"
V^*	Complex velocity	"
V(0)	Limiting low frequency velocity	"
$V(\infty)$	Limiting high frequency velocity	"
V	Molar volume	dm^{-3}
ΔV	Volume change	"
$\overline{V}$	Partial molar volume	"
W	Velocity of particles in a wave	m s^{-1}
X_L	Imaginary part of the complex longitudinal impedance	N s m^{-3}
X_S	Imaginary part of the complex shear impedance	N s m^{-3}
x, y, z	Distances or directions (Cartesian co-ordinates)	
x	Coefficient in equations	
Y	Admittance - reciprocal impedance	$(N\ s\ m^{-3})^{-1}$
Z	Impedance = R + iX. Complex ratio of a force like quantity to a related velocity like quantity	N s m^{-3}
Z_L	Longitudinal impedance	"
Z_{QL}	Longitudinal impedance of quartz	"

Symbol	Definition	Units
Z_{FL}	Longitudinal impedance of test liquid	N s m^{-3}
Z_S	Shear impedance	"
Z_{QS}	Shear impedance of quartz	"
Z_{FS}	Shear impedance of test liquid	"
Z_{TS}	Shear impedance of reference liquid	"
$\alpha + i\beta$	Propagation constant of a liquid	
α	Absorption coefficient	Nepers m^{-1}
α_{Cl}	Classical absorption coefficient	"
α_{th}	Absorption coefficient arising from thermal conductivity	"
β	Coefficient of compressibility (reciprocal bulk modulus)	$(N\ m^{-2})^{-1}$
β	Parameter	
γ	Shear strain	
γ	Ratio of specific heats C_p/C_v	
δ	Phase angle	rad.
ε	Strain measured by strain guage bridge	
η_s	Coefficient of viscosity, the ratio of the shearing stress to the rate of shear	N s m^{-2}
η^*	Complex viscosity, ratio of complex modulus to frequency = $\eta' - i\eta''$	"
η'	Real part of η^* - dynamic viscosity	"
η''	Imaginary part of η^*	"
$\eta_s(0)$	Viscosity at low or zero shear rate	"
η_v	Volume or bulk viscosity - viscosity of volume flow .	"

Symbol	Definition	Units
η_v^*	Complex bulk viscosity	N s m^{-2}
$\eta_{Newt.}$	Viscosity of a Newtonian liquid	"
θ	Phase angle	deg.
θ	Thermal expansion coefficient	K^{-1}
κ	Thermal conductivity	
λ	Wavelength	m
μ	Absorption per wavelength = $\alpha\lambda$	Nepers
ν	Kinematic viscosity - the ratio of viscosity to density	m^2 s^{-1}
ρ	Density	Kg m^{-3}
σ	Shear stress	N m^{-2}
τ	Relaxation time, the time taken for the internal stress to drop to $^1/e$ of its initial value under constant strain	s
τ_m	Maxwell relaxation time = $\eta_s(0)/G(\infty)$	s
τ_v	Volume retardation time	s
τ_r	Characteristic retardation time, the time taken by the strain to fall to $^1/e$ of its original value in an elastic after effect	s
ϕ	Angle of incidence	rad.
ϕ	Angle of refraction	"
ω	Angular frequency $2\pi f$	s^{-1}
Ω	Angular velocity	rad s^{-1}
Γ	Propagation constant = $i\omega\rho/z$	

Definitions

Hookean solid - an ideal elastic solid for which the shearing stress is proportional to the shear, straining and recovery taking place near sonic speeds.

Liquid crystal - a liquid whose molecules show a degree of order but maintain some mobility relative to each other.

Nematic phase - a form of liquid crystal whose molecules lie with their long axis parallel to one another but are not arranged in layers.

Newtonian liquid - an ideal liquid, devoid of shear elasticity, for which the shearing stress is proportional to the rate of shear.

Smectic phase - a form of liquid crystal whose molecules lie with their long axes parallel to one another and are arranged in layers that are free to slide over one another.

Cholesteric phase - This is intermediate between Nematic and Smectic. The molecules are arranged in layers like Smectic but within each layer there is a parallel arrangement of molecules like the Nematic phase.

Comparison of Units.

1 dyne s cm^{-3} ≡ 10 N s m^{-3} (impedance)

1 dyne cm^{-2} ≡ 0.1 N m^{-2} (pressure or modulus)

1 poise ≡ 0.1 N s m^{-2} (viscosity)

Symbols used on figures.

Symbol	Frequency/MHz	
	Longitudinal	Shear
□	5	6
△	15	18
+	25	
0	35	30
X	55	
▽	75	78

ACKNOWLEDGEMENTS

The author wishes to thank Mr. J.C. Hawkes and Professor W.J. Orville Thomas for providing the opportunity to undertake this research.

The encouragement and guidance of Mr. J.F. Hutton and Dr. E. Wyn-Jones are most gratefully acknowledged.

Dr. M.C. Phillips is thanked for his interesting discussions.

Members of the Tribology and Applied Physics Sections at Shell Research Limited, Chester, are thanked for their help and friendship. In particular, Mr. M. Davies and Mr. B. Jones are thanked for their assistance with the Shear Relaxation Spectrometer and high pressure equipment respectively.

Sincere thanks are given to Mrs. R.M. Verrall for typing and suggestions for the presentation of this thesis.

Finally, the author gratefully acknowledges the financial support provided by the Science Research Council and Shell Research Limited. The research was conducted partly at the University of Salford and partly at Thornton Research Centre.

SUMMARY

This thesis describes experimental researches in ultrasonic and viscoelastic relaxation in pure liquids, mixtures and a polymer solution. The measurements were made over a range of temperatures and pressures in the frequency range 5 to 78 MHz.

Density, steady flow viscosity, real part and imaginary part of the shear impedance were measured on five liquids. Four of the liquids obeyed the Time-Temperature Superposition principle and could be described by the Barlow, Erginsav and Lamb (B.E.L,) model. The fifth liquid did not obey the Time-Temperature Superposition principle and deviated from the model. This was attributed to the distribution of relaxation times widening as the temperature is decreased.

The shear compliance ($J(\infty)$) for all five liquids varied linearly with temperature at atmospheric pressure. At higher pressures it was the shear modulus ($G(\infty)$) that varied linearly with pressure.

Both low and high frequency longitudinal velocities were found to vary linearly with temperature at atmospheric pressure, while at higher pressures only the low frequency velocity varied linearly with pressure, the high frequency velocity results were too scattered.

Values of the bulk moduli obtained from the longitudinal moduli and shear moduli were normalised and the variation with reduced frequency was found to be of the same shape as for the shear moduli but displaced along the reduced frequency axis. Therefore the shear and bulk relaxation properties have a common origin. From this displacement and the values of $G(\infty)$ and the relaxing part of the bulk modulus $(K(\infty) - K(0))$ the ratio of volume to shear viscosity was calculated for three liquids at atmospheric pressure and two liquids at higher pressures. The ratio η_v/η_s varied from 2.7 to 4.2 at atmospheric pressure with slightly lower values at higher pressures but the difference was not statistically significant.

Measurements of density and velocity were made on solutions of a surfactant at elevated pressures. The density measurements were fitted to the linear secant modulus equation. Investigation of the shear properties of a gel-soap solution showed that it was thixotropic.

Finally, a conformational analysis at pressures above atmospheric pressure showed that the relaxation frequency was not significantly changed by increasing the pressure.

CHAPTER I

INTRODUCTION

The main objective of this research is to simulate in the laboratory, the conditions which exist in heavily loaded gears and ball bearings lubricated under elastohydrodynamic conditions. In heavily loaded gears and ball bearings the lubricant is entrained between two surfaces by rolling and is subjected to very high pressures (1 GN m^{-2}) and shear rates (10^5 s^{-1}). The liquid transit time is short (10^{-5} s) and during this time the liquid's volume is decreased and its viscosity increased. However, at these high pressures volume retardation occurs with a time constant τ_v ($\tau_v \approx 10^{-4}$ s) and therefore since the transit time is less than this, volume retardation effects can be important. The shear relaxation time τ_s ($= \eta_s/G(\infty)$) is also of the order of the transit time so that the shear viscosity (η_s) will again be time dependent[1]. For a Newtonian liquid the product of shear viscosity and shear rate ($\dot{\gamma}$) is the shear stress (σ) and is much less than the shear modulus ($G(\infty) \approx 1$ GN m^{-2}). Under conditions of elastohydrodynamic lubrication (E.H.L.) the shear stress is of the same order of magnitude as the shear modulus, so that large elastic strains will occur. Therefore the shear stress will be non linearly dependent on shear rate and the viscosity will be shear rate dependent, i.e. non-Newtonian viscosity (η_{Newt} = shear stress/shear rate).

To have a better understanding of E.H.L., measurements of volume (or bulk) and shear viscosities at high shear rates, shear modulus and bulk modulus are required. To reproduce the above conditions in a controlled experiment in the laboratory would be extremely difficult, probably the only way is in the actual E.H.L. contact, this does not allow any time for measurements. Attempts[2] to measure viscosity in such situations using disc machines have given results smaller than the values expected from reasonable extrapolations of measurements made in low shear rate viscometers operating at high static pressures. Fein[3] suggested that the liquid fails to respond to the rapid increase in pressure which occurs in a very short period

of time and therefore it does not reach the equilibrium state corresponding to this pressure, which leads to a lower value of viscosity. Paul and Cameron[4] have shown that there is a definite time delay of the viscosity rise after the pressure step, the viscosity at 800 MN m^{-2} varies from 3×10^4 N s m^{-2} after 0.015 s to 3×10^8 N s m^{-2} after 105 s.

To overcome these difficulties of measurement other techniques have been used, namely ultrasonics, high rates of shear can be obtained for short durations, use is then made of the analogy between the behaviour of viscoelastic fluids in oscillatory and continuous shear.

There are two types of elastic waves, longitudinal and shear. In longitudinal waves the particles in the medium move in the direction of propagation of the wave while in shear or transverse waves the displacement of the particles is at right angles to the direction of propagation. In this work elastic waves in the range 5 MHz to 78 MHz (ultrasonic frequency) have been used.

Sinusoidally alternating shear and longitudinal waves of ultrasonic frequency are propagated into fluids and from the response of the fluid to these waves, information regarding shear and bulk properties can be obtained. It is possible to produce pure shear waves but not pure compressional waves.

The techniques used today have been developed over many years starting with the 'classical' absorption of sound in gases by Stokes[5], Biquard[6] made the first quantitative measurements in liquids and later Pellam and Galt[7] developed the Pulse Technique. They used piezoelectric transducers excited by pulsed electrical oscillations to produce a pulse of ultrasound which was propagated in the liquid and detected by a second identical transducer and reconverted to electrical energy for measurement. This technique is suitable for longitudinal waves (often referred to as ultrasonic waves)

but owing to the high absorption of shear waves in a liquid, the technique has to be modified. This has been carried out initially by Mason[8] and further developed by Barlow and Lamb[9]. Since longitudinal waves propagate more easily through a liquid than do shear waves, their absorption coefficient and velocity can be determined whereas shear wave techniques rely on the reflection of a wave at the interface.

The behaviour of a liquid to an elastic wave depends upon the frequency of that wave, i.e. for longitudinal waves it depends upon the period of compression. If the period of alternating compression is short the wave will propagate adiabatically and the local temperature will alter in phase with its changing volume, hence any equilibria which are sensitive to temperature or pressure changes will be disturbed by the wave. This disturbance is detected by an increase in the attenuation of the longitudinal wave, the maximum attenuation will occur at a frequency f_c ($= {}^1/2\pi\tau$) where τ is the relaxation time of the equilibrium. Equilibria studied include chemical reactions, molecular energy transfer between translational, vibrational and rotational degrees of freedom, rotational isomerisation in liquids and the flow of molecules between regions of high and low density. It is possible that more than one type of equilibrium may be taking place at any one time giving rise to more than one relaxation time[10].

When a liquid is subjected to a shear wave there is no volume change and a negligibly small temperature change and hence chemical equilibria which are present are not disturbed. The medium responds to the shear wave by viscous flow (liquid), by elastic deformation (solid) or by some combination of the two (viscoelastic). Whether viscous, viscoelastic or elastic properties are observed depends on the period of the shear wave. If the period is long compared to the time required for the liquid to return to equilibrium

after the application of the strain, then the liquid will respond to the oscillating strain and the behaviour of the liquid is referred to as Newtonian, i.e. shear viscosity is independent of rate of deformation. If the period is small compared to the time for the liquid to return to equilibrium then there will be no molecular diffusion and no flow, any energy is now stored, not dissipated as before, and the liquid behaves as an amorphous solid with Hookean elasticity. The change from viscous to elastic behaviour (viscoelastic relaxation) occurs when the period of the shear wave becomes comparable to the time for molecular diffusion. This time may range from seconds in polymers to 10^{-13} secs in liquid argon. There are many examples of materials which exhibit both elastic and viscous properties depending on the time scale, e.g. glass will flow over many years and pitch can be shattered by a sharp blow.

In practice the change in amplitude and phase of the shear wave are measured to give the reactive and resistive parts of the shear impedance and the absorption and velocity of longitudinal waves are measured. From these measurements a shear and volume viscosity and the various moduli can be calculated. Results to date have shown that if the components of the shear modulus (or reactive and resistive parts of the impedance) and bulk modulus are plotted in normalised form, they do not fit models of viscoelasticity based upon a single relaxation time, however the results can be described by assuming a distribution of relaxation times[9]. An empirical model based upon the impedance of the viscoelastic fluid being a parallel combination of the impedance of a Newtonian liquid and an elastic solid has been shown to account for the results for pure liquids[11] but the model has to be slightly modified to account for the behaviour of liquid mixtures[12]. A theoretical treatment by Phillips[13] gave the same equation for the relaxation function as developed by Barlow[11], this treatment was based on a defect diffusion model which was an extension

of Glarum's defect diffusion model[14]. Barlow[15,16,17] has shown that the compressional or bulk modulus can be treated in the same way as the shear modulus, with the assumption that both the volume viscosity and relaxing part of the compressional modulus are constant multiples of the shear viscosity and shear modulus.

To date only a few liquids have been studied in detail, the results of these studies are given in Tables 1,2 in Appendix I. There has been no correlation between the ratio of volume viscosity to shear viscosity and molecular structure, but there is a difference in the temperature dependence of this ratio between associated and unassociated structures[18,19]. The unassociated liquids exhibit a positive slope for temperature against coefficient of absorption and a temperature dependent ratio of experimental absorption (α exp) to the classical absorption (α_{Cl}). This behaviour is attributed to thermal relaxation processes due to temperature changes produced by the ultrasonic wave and these are the predominant mechanisms for volume viscosity in these liquids. A temperature independant ratio of α_{exp}/α_{Cl} lying between 1 and 3 is found in associated liquids. The absorption coefficient decreases with increase in temperature as in the 'classical' absorption. The mechanism responsible for the volume viscosity in associated liquids is closely related to the mechanism for the shear viscosity. Structural relaxation processes connected with volume changes among different molecular rearrangements and produced by pressure changes of the sound waves are assumed to occur.

Likewise with the shear modulus no theory or experiment has shown any relationship between chemical structure and viscoelastic properties for non-polymeric liquids. Initially, Barlow and Lamb[9] gave an interpretation in terms of hydrocarbon type and later Hutton[20] showed that this was an incorrect interpretation. This has been confirmed by work on unrelated molecular structures which showed no significant difference in shear properties[11,21] although impurities

in samples can lead to small differences[11].

The liquids so far investigated have either been 'supercooled' or have a viscosity about 1 N s m^{-2} at ambient temperature. Supercooling is usually limited to asymmetric molecules (symmetric molecules crystallise readily, e.g. benzene crystallises at a much higher temperature than toluene). For symmetrical molecules, only translation to a suitable site is required whereas for asymmetric molecules, translation and rotation of the molecule is usually necessary, the latter requiring more energy.

In Chapter II the theory of ultrasonic and viscoelastic relaxation is discussed and the terminology used is introduced. The relationships between experimentally measured quantities and the various moduli are derived. The experimental measurements made and apparatus used are described in Chapter III. The viscoelastic properties of two bitumen samples have been investigated, the experimental results are given in Chapter IV, together with a discussion of the results. In Chapter V the results of shear and ultrasonic relaxation measurements are given for three 'supercooled' liquids at atmospheric and high pressure. The analysis of these results to give the ratio of shear to volume viscosity and a discussion of them is given in Chapter VI. The above forms the bulk of the work presented, however, to take advantage of the high pressure equipment two minor pieces of work have been carried out. The first being the effect of pressure on a micelle system, the theory and experimental results for the work are presented and discussed in Chapter VII; also included in this chapter are some shear measurements on a 'liquid crystal system'. The second is the effect of pressure on a rotational isomerisation equilibrium - conformational analysis, the theory and results are presented and discussed in Chapter VIII. Chapter IX is devoted to an assessment of the work and general conclusions. The experimental data are given in the appendices, appendix numbers

correspond with the chapters, i.e. results for Chapter IV are given in Appendix IV.

CHAPTER II

THEORY

2.1 Introduction - longitudinal waves.

From classical theory Stokes[5] showed that the longitudinal sound absorption (α) depends on the shear viscosity (η_s) by the following relationship

$$\alpha = \frac{8}{3} \frac{\pi^2 \eta_s f^2}{\rho v^3} \quad ..(2.1)$$

where ρ is the density of the medium,

v is the velocity of sound in the medium,

f is the frequency of the sound.

Usually this equation is re-written as follows:

$$\alpha/f^2 = \frac{8}{3} \frac{\pi^2 \eta_s}{\rho v^3} \quad ..(2.2)$$

α/f^2 is a constant at a particular temperature for some liquids, e.g. water, carbon tetrachloride. The shear viscosity is well known and was defined by Newton as the ratio of tangential force per unit area (σ) to the shear rate ($\frac{\partial \gamma}{\partial t}$) or rate of strain. This ratio is often constant over a limited range of shear rates and when independant of shear rate the fluid is said to behave in a Newtonian manner. The fluids described in this work are mainly studied in the non-Newtonian range. In practice the measured absorption (α_{exp}) is not equal to the classical absorption given by equation (2.1). The difference is caused by volume and pressure changes in the fluid, the molecules in the fluid have to flow from a more compact to a less compact structure in the direction of the motion imposed by the sound wave. A fluid can therefore have a volume or bulk viscosity (η_v) defined as the viscosity of volume flow (Stokes assumed $\eta_v = 0$). This volume viscosity can arise from structural changes and various equilibria. The 'classical' absorption given by equation (2.1) is modified to give

$$\alpha = \frac{2\pi^2}{\rho v^3} (4/3 \eta_s + \eta_v) f^2 \quad ..(2.3)$$

Kirchoff showed that α is also a function of the thermal conductivity (κ)

of the fluid, α_{th}, absorption due to thermal conductivity is given by

$$\alpha_{th} = \frac{2\pi^2}{\rho V^3} \frac{(y-1)\ \kappa\ f^2}{Cp} \qquad ..(2.4)$$

where $y = {}^{Cp}/_{Cv}$ and Cp is specific heat at constant pressure,

Cv is specific heat at constant volume.

The contribution to α from α_{th} is negligible for all liquids except liquid metals.

2.2 Propagation of longitudinal waves.

The amplitude of the waves is small so that heating of the liquid is insignificant but, locally there is a significant temperature rise in a sound wave to cause chemical reactions to occur. The temperature variations are in the region of 0.002 deg.[22]. The wave motion is described by the following two dimensional wave equation

$$V_L^2 \frac{\partial^2 u}{\partial x^2} = \frac{\partial^2 u}{\partial t^2} \qquad ..(2.5)$$

where u is the particle displacement in the direction (x) of the wave motion,

V_L is the phase velocity.

The solution of equation (2.5) is obtained by the method of separation of variables and after substitution of the boundary conditions the following is obtained,

$$u(x,t) = u_o \exp i\omega(t - {}^{x}/_{V_L}) + u_o' \exp i\omega(t + {}^{x}/_{V_L}) \qquad ..(2.6)$$

u_o and u_o' are constants,

$\omega = (2\pi f)$ is the angular frequency,

t = time.

The first term represents a wave travelling in the positive x direction and the second term a wave travelling in the negative direction, both with velocity V_L. u_o' is zero when there is no reflection (which is true in the work in this thesis) and therefore there is a single progressive wave with maximum amplitude u_o. This equation (2.6)

assumes no attenuation in the medium and has to be modified to account for the attenuation. Equations (2.7) and (2.8) give the modified wave equation and solution.

$$\frac{\partial^2 u}{\partial t^2} = V_L^2 \frac{\partial^2 u}{\partial x^2} + 4/3 \frac{\eta_s}{\rho} \frac{\partial^3 u}{\partial x^2 \partial t} \qquad ..(2.7)$$

$$u(x,t) = u_o \exp\left[i\omega\left(t - x\left(\frac{1}{V_L} - \frac{i\alpha_L}{\omega}\right)\right)\right] \qquad ..(2.8)$$

α_L is the longitudinal sound absorption (the subscript L refers to longitudinal sound waves - in the remaining chapters this subscript is omitted).

$\left(\frac{1}{V_L} - \frac{i\alpha_L}{\omega}\right)^{-1}$ is the complex velocity V^* of the sound wave.

$$\frac{1}{V^*} = \frac{1}{V_L} - \frac{i\alpha}{\omega} \qquad ..(2.9)$$

The wave equation can also be written in the following form

$$M^* \frac{\partial^2 u}{\partial x^2} = \rho \frac{\partial u^2}{\partial t^2} \qquad ..(2.10)$$

The longitudinal modulus M^*, a complex quantity, is related to the complex velocity

$$M^* = \rho(V^*)^2 \qquad ..(2.11)$$

$$\text{and} \quad M^* = M' + iM'' \qquad ..(2.12)$$

where M' and M'' are the real and imaginary parts of the longitudinal modulus respectively.

By a simple mathematical procedure from equations (2.9) and (2.11) it can be shown that

$$M^* = \rho(V^*)^2 = \frac{\rho(\omega^4 V_L^2 - \alpha_L^2 \omega^2 V_L^4) + i\, 2\rho\, \alpha_L \omega^3 V_L^3}{(\omega^2 + \alpha_L^2 V_L^2)^2} \qquad ..(2.13)$$

$$\text{and hence} \qquad M' = \frac{\rho V_L^2 \left[1 - \left(\frac{\alpha_L V_L}{\omega}\right)^2\right]}{\left[1 + \left(\frac{\alpha_L V_L}{\omega}\right)^2\right]^2} \qquad ..(2.14)$$

$$M'' = \frac{2\rho V_L^2 \ \frac{\alpha_L V_L}{\omega}}{\left[1 + \left(\frac{\alpha_L V_L}{\omega}\right)^2\right]^2} \qquad ..(2.15)$$

We now have the real and imaginary parts of the longitudinal modulus in terms of the measured quantities namely α_L, V_L and ω. Singh and Mishra[23] have identified a relationship between frequency and α/f^2, $\left[\log_{10} \alpha_{max}/f^2 = -1.075 \log_{10} f - 3.512\right]$; their findings have been confirmed in this work. It is therefore possible to give an estimate of the maximum and minimum values of $\alpha_L V_L/\omega$ in the range of frequencies used in the present study. $\alpha_L V_L/\omega$ ranges from 0.004 to 0.060.

When $\alpha_L V_L/\omega$ is small then from equation (2.14)

$$M' = \rho V_L^2 = M(0) \qquad ..(2.16)$$

$$(V_L = V_L(0))$$

M(0) is the low frequency longitudinal modulus.

If the frequency is greatly increased above the relaxation frequency then $\alpha_L V_L/\omega$ will again be small and

$$M' = \rho V_L^2 = M(\infty) \qquad ..(2.17)$$

$$(V_L = V_L(\infty))$$

$M(\infty)$ is the longitudinal modulus at infinite frequency.

M'' in both the above conditions becomes very small and M'' goes through a maximum as the frequency is increased from a low to a high value.

In viscous liquids ($\eta_s(0) > 100$ N s m^{-2}) it is experimentally difficult to measure the absorption coefficient and velocity directly. Reflection techniques are then used to measure the impedance of the liquid. The longitudinal impedance (Z_L) is the ratio of force to particle velocity and is related to the complex velocity by the following

$$Z_L = R_L + iX_L = \rho V_L^* \qquad ..(2.18)$$

where R_L is the real or resistive part of the impedance,

and X_L is the imaginary or reactive part of the impedance.

From equation (2.9) then

$$Z_L = \rho \left(\frac{1}{V_L} - \frac{i\alpha}{\omega} \right)^{-1} \qquad ..(2.19)$$

and at high frequency the equation reduces to

$$Z_L(\infty) = R_L(\infty) = \rho V_L(\infty) \qquad X_L = 0 \qquad ..(2.20)$$

the velocity is obtained from the impedance and the density.

To complete the relationships, from equations (2.11) and (2.18)

$$M^* = \frac{Z_L^2}{\rho} = \frac{(R_L + iX_L)^2}{\rho} \qquad ..(2.21)$$

and $$M' = \frac{R_L^2 - X_L^2}{\rho} \quad , \quad M'' = \frac{2R_L X_L}{\rho} \qquad ..(2.22)$$

2.3 Viscoelastic Response.

When a solid is subjected to a shear stress (σ) it experiences a shear strain (γ) and the ratio of these two quantities is the shear modulus (G).

$$\sigma = G\gamma \qquad ..(2.23)$$

A liquid responds to a shear stress by flowing and the relative motion of the different layers of the flowing liquid leads to a resistance to the flow and energy is dissipated, the liquid is said to exhibit viscosity and obey Newton's law

$$\sigma = \eta_s \frac{\partial \gamma}{\partial t} \qquad ..(2.24)$$

Deviations from these ideal Hookean and Newtonian behaviour occur and the material is then said to be viscoelastic. A shear stress is produced in a liquid by shear waves and unlike longitudinal waves no volume or temperature change takes place, the temperature rise resulting from viscous flow appears as a random increase in the translational

energy of the molecules, therefore any temperature sensitive equilibria will not be affected by the shear wave. Shear waves can be used to study molecular diffusional motion in the medium and will not be complicated by other relaxation processes.

2.4 Propagation of shear waves.

The amplitude of the shear wave is small so that heating of the liquid is insignificant and only the linear viscoelastic response is determined, higher orders can be neglected. When shear waves are propagated into a medium the displacement of the particles in the medium is perpendicular to the direction of motion. Using normal Cartesian co-ordinates the x axis gives the direction of propagation and the displacement is in the z direction. The shear stress (σ_{xz}) is given by equation (2.23) and the strain $\gamma = {}^{\partial u}/_{\partial z}$, where u is the particle displacement in the z direction. For a unit volume the driving force is the product of mass and acceleration giving

$$\rho \frac{\partial^2 u}{\partial t^2} = \frac{\partial \sigma_{xz}}{\partial z} \qquad ..(2.25)$$

Differentiation of equation (2.23) with respect to the z direction and after substitution of γ we have

$$\rho \frac{\partial^2 u}{\partial t^2} = G^* \frac{\partial^2 u}{\partial z^2} \qquad ..(2.26)$$

(This equation is analogous to (2.10) for longitudinal waves). The solution of (2.26) is given by the method of separation of variables

$$u(z,t) = u_o \exp\left[i\omega \left(t - z \left(\frac{1}{V_s} - \frac{i\alpha_s}{\omega}\right)\right)\right] \qquad ..(2.27)$$

where u_o is the initial value of u,

V_s and α_s are the velocity and absorption coefficient of the shear wave respectively,

ω ($= 2\pi f$) is the angular frequency.

The complex shear velocity (V_s^*) is given by

$$V_s^{*} = \left[\frac{1}{V_s} - \frac{i\alpha_s}{\omega}\right]^{-1} \qquad ..(2.28)$$

$$\text{and } (V_s^{*})^2 = G^{*}/\rho \qquad ..(2.29)$$

G^{*} is the frequency dependant complex shear modulus.

$$G^{*} = G' + iG'' \qquad ...(2.30)$$

where G' is the real part and is described as storage modulus and G" is the imaginary or loss modulus. Experimentally the complex shear impedance (Z_s) is measured which is defined as the negative ratio of shear stress to particle velocity.

$$Z_s = R_s + iX_s = -\sigma_{xz}/(\partial u/\partial t) \qquad ..(2.31)$$

where R_s is the real or resistive part of Z_s

and X_s is the imaginary or reactive part of Z_s.

Substitution for σ_{xz} from (2.23) gives

$$Z_s = -G^{*}\,(\partial u/\partial z)/(\partial u/\partial t) \qquad ..(2.32)$$

$$= -G^{*}\,\partial z/\partial t = -G^{*}/V_s^{*} \qquad ..(2.33)$$

and substitution for V_s^{*} from (2.29) gives

$$Z_s^2 = \rho G^{*} \qquad ..(2.34)$$

Equating real and imaginary parts of (2.34) we have

$$G' = \frac{R_s^2 - X_s^2}{\rho} \qquad ..(2.35)$$

$$G'' = \frac{2R_sX_s}{\rho} \qquad ..(2.36)$$

$$\text{or} \quad R_s^2 = \frac{\rho G'}{2}\left[\left(1 + \left(\frac{G''}{G'}\right)^2\right)^{\frac{1}{2}} + 1\right] \qquad ..(2.37)$$

$$X_s^2 = \frac{\rho G'}{2}\left[\left(1 + \left(\frac{G''}{G'}\right)^2\right)^{\frac{1}{2}} - 1\right] \qquad ..(2.38)$$

Two other complex quantities can be defined namely, complex viscosity

$$\eta_s^* = \eta_s' - i\eta_s'' = G^*/i\omega \qquad ..(2.39)$$

where $\eta_s' = G''/\omega$ and $\eta_s'' = G'/\omega$ ..(2.40)

and complex compliance $J^* = {}^1/G^*$

$$J^* = J' - iJ'' \qquad ..(2.41)$$

giving

$$J' = \frac{G'}{G'^2 + G''^2} \quad , \quad J'' = \frac{G''}{G'^2 + G''^2} \qquad ..(2.42)$$

In the Newtonian limit $G' = 0$ by definition $\therefore \eta'' = 0$ and $J' = 0$

$$\text{but} \quad G'' = \omega\eta_s' = \frac{2R_sX_s}{\rho}$$

and since $G' = 0$, $R_s(0)^2 = X_s(0)^2$.

$$\text{Then} \quad R_s(0) = X_s(0) = \left(\frac{\omega\eta_s(0)\rho}{2}\right)^{\frac{1}{2}} \qquad ..(2.43)$$

$R_s(0)$, $X_s(0)$ in equation (2.43) are the Newtonian values and

$$Z_{\text{Newtonian}} = (1 + i)\left(\frac{\omega\eta_s\rho}{2}\right)^{\frac{1}{2}} \qquad ..(2.44)$$

The absorption coefficient (α_s) and velocity (V_s) for a Newtonian liquid can be obtained in terms of density, viscosity and angular frequency from (2.28), (2.29) and (2.33).

$$V_s = \left(\frac{2\omega\eta_s}{\rho}\right)^{\frac{1}{2}} \quad \text{and} \quad \alpha_s = \left(\frac{\omega\rho}{2\eta_s}\right)^{\frac{1}{2}} \qquad ..(2\ 45)$$

It can be seen that the absorption coefficient is extremely large, for water at 298.2 K and $\omega = 2\pi\ 10^6\ s^{-1}$.

$$\alpha_s = 1.8 \times 10^6 \text{ nepers } m^{-1}.$$

giving a skin depth ${}^1/\alpha_s = 5.6 \times 10^{-7}$ m.

For a perfect Hookean solid where $\eta' = 0$ by definition $G'' = 0$ and $J'' = 0$. G' is equal to the shear modulus and

$$R_s = (\rho G^{\ast})^{\frac{1}{2}} \qquad X_s = 0 \qquad ..(2.46)$$

$G^{\ast} = G(\infty)$ the shear modulus at infinite frequency

$$\text{and} \quad V_s(\infty) = (G(\infty)/\rho)^{\frac{1}{2}} \qquad \alpha_s = 0 \qquad ..(2.47)$$

2.5 The relationship of longitudinal modulus to shear modulus.

Both the complex longitudinal modulus and complex shear modulus are frequency dependant and can therefore be written $M^{\ast}(\omega)$ and $G^{\ast}(\omega)$ respectively. The longitudinal modulus is a linear combination of the shear modulus and the bulk modulus $K^{\ast}(\omega)$, which is also complex,

$$M^{\ast}(\omega) = K^{\ast}(\omega) + {}^{4}/_{3}\, G^{\ast}(\omega) \qquad ..(2.48)$$

$$\text{and} \quad K^{\ast}(\omega) = K'(\omega) + K''(\omega)$$

where $K'(\omega)$ is the real part of the bulk modulus and $K''(\omega)$ is the imaginary part. $K^{\ast}(\omega)$ cannot be obtained by experiment and therefore is obtained by the above relationship.

$$M^{\ast}(\omega) = K'(\omega) + {}^{4}/_{3}\, G'(\omega) + i(K''(\omega) + {}^{4}/_{3}\, G''(\omega)) \qquad ..(2.49)$$

separating into real and imaginary parts gives

$$M'(\omega) = K'(\omega) + {}^{4}/_{3}\, G'(\omega) \qquad ..(2.50)$$

$$\text{and} \quad M''(\omega) = K''(\omega) + {}^{4}/_{3}\, G''(\omega) \qquad ..(2.51)$$

At low frequencies (Newtonian liquids) $G'(0) = 0$

$$M'(\omega) = M(0)$$

$$M(0) = K'(0) = K(0) \qquad ..(2.52)$$

where $K(0)$ is the low frequency bulk modulus.

At high frequency $M'(\omega)$ becomes $M(\infty)$ and $M'(\infty) = 0$.

$$\text{Then} \quad M(\infty) = K(0) + K'(\infty) + {}^{4}/_{3}\, G(\infty) \qquad ..(2.53)$$

$K'(\infty) = (K_{\infty} - K_0)$ is the relaxing part of the bulk modulus and is usually denoted by K_2.

Relationship of viscosities.

From equation (2.39)

$$G^{\ast} = i\omega\eta_s^{\ast}$$

and by using a similar approach to that used for shear waves it can be shown that

$$M^{*} = i\omega\eta_L^{*} \qquad ..(2.54)$$

where η_L^{*} is the complex longitudinal viscosity.

Substitution of (2.39) and (2.54) into (2.48) gives

$$i\omega\eta_L^{*} = K^{*}(\omega) + {}^{4}/_{3}\, i\omega\eta_s^{*} \qquad ..(2.55)$$

Rearranging equation (2.55) gives

$$K^{*}(\omega) = i\omega(\eta_L^{*} - {}^{4}/_{3}\, \eta_s^{*}) \qquad ..(2.56)$$

and $$\eta_V^{*} = \eta_L^{*} - {}^{4}/_{3}\, \eta_s^{*} \qquad ..(2.57)$$

where η_V^{*} is the complex bulk viscosity.

From (2.56) and (2.57)

$$K^{*}(\omega) = i\omega\eta_V^{*} \qquad ..(2.58)$$

2.6 Models of viscoelastic liquids.

2.6.1 Maxwell model.

The simplest model was formulated by Maxwell and is given by the addition of the compliances of the two elements (elastic and viscous) of the fluid. The total strain rate $(\frac{\partial\gamma}{\partial t})$ is given by

$$\frac{\partial\gamma}{\partial t} = \frac{\partial\sigma}{\partial t}\frac{1}{G(\infty)} + \frac{\sigma}{\eta_s(0)} \qquad ..(2.59)$$

or alternatively,

$$\frac{\partial\gamma}{\partial t} = \frac{1}{G(\infty)}\frac{\partial\sigma}{\partial t} + \frac{1}{G(\infty)}\frac{\sigma}{\tau_m} \qquad ..(2.60)$$

where τ_m is the Maxwell relaxation time, a single relaxation time. By a suitable choice of boundary conditions this equation reduces to either Hookes Law or Newtons Law.

If the strain and stress are sinusoidal then

$$\gamma = \gamma_o \exp(i\omega t) \qquad ..(2.61)$$

$$\sigma = \sigma_o \exp(i\omega t) \qquad ..(2.62)$$

Differentiation with respect to t of (2.61) and (2.62) and substitution into (2.60) gives

$$\sigma + i\omega\tau_m\sigma = i\omega\tau_m G(\infty)\gamma \qquad ..(2.63)$$

and $$\frac{\sigma}{\gamma} = \frac{i\omega\tau_m G(\infty)}{1 + i\omega\tau_m} \qquad ..(2.64)$$

The complex shear modulus ($G^* = \sigma/\gamma$) can be separated into the real and imaginary parts giving, from equation (2.64),

$$G' = \frac{G(\infty)\ \omega^2\ \tau_m^2}{(1 + \omega^2\ \tau_m^2)} \quad , \quad G'' = \frac{G(\infty)\ \omega\ \tau_m}{(1 + \omega^2\ \tau_m^2)} \qquad ..(2.65)$$

or the viscosities from equation (2.40) can be given by

$$\eta_s' = \frac{G(\infty)\ \tau_m}{(1 + \omega^2\ \tau_m^2)} \quad , \quad \eta_s'' = \frac{G(\infty)\ \omega\ \tau_m^2}{(1 + \omega^2\ \tau_m^2)} \qquad ..(2.66)$$

R_s and X_s are then given from equations (2.37), (2.38) and (2.65).

$$R_s = (\rho G(\infty))^{\frac{1}{2}} \left[\frac{(\omega\tau_m)^2 + \omega\tau_m(1 + (\omega\tau_m)^2)^{\frac{1}{2}}}{2\left[1 + (\omega\tau_m)^2\right]}\right]^{\frac{1}{2}} \qquad ..(2.67)$$

and $$X_s = (\rho G(\infty))^{\frac{1}{2}} \left[\frac{-(\omega\tau_m)^2 + \omega\tau_m(1 + (\omega\tau_m)^2)^{\frac{1}{2}}}{2\left[1 + (\omega\tau_m)^2\right]}\right]^{\frac{1}{2}} \qquad ..(2.68)$$

The usual quantities plotted are $R_s/(\rho G(\infty))^{\frac{1}{2}}$ and $X_s/(\rho G(\infty))^{\frac{1}{2}}$ against a reduced frequency ($\omega\tau_m$) (where $\tau_m = \eta_s(0)/G(\infty)$). ($G'/G(\infty)$, $G''/G(\infty)$ and $\eta_s'/\eta_s(0)$ are occasionally plotted against $\omega\tau_m$).

The Maxwell model predicts that the viscoelastic region (defined as the region in which $G'/G\infty$ varies from 0.05 to 0.95) extends over two decades of reduced frequency ($\omega\tau_m$). However, for most liquids studied the region extends over four or more decades, but Mikhailov[24] suggests that soyabean and cotton-seed oils have a single relaxation.

The behaviour of the viscoelastic fluids cannot be characterised by a single relaxation time but by a distribution of relaxation

times[9] and equation (2.64) is then written as follows

$$G^{*}(\omega) = \sum_{j=1}^{N} \frac{G_j \, i\omega(\tau_m)_j}{1 + i\omega(\tau_m)_j} \qquad ..(2.69)$$

where G_j is the contribution of the j^{th} process to $G(\infty)$ and $(\tau_m)_j$ is its relaxation time. In the limiting condition of a continuous distribution of relaxation times the summation may be replaced by an integral

$$G^{*}(\omega) = G(\infty) \int_{0}^{\infty} \frac{g(\tau_m) \, i\omega\tau_m}{1 + i\omega\tau_m} \, d\tau_m \qquad ..(2.70)$$

where $g(\tau_m)$ represents the distribution of relaxation times and $G(\infty)$ $g\tau_m \, d\tau_m$ is the contribution to $G(\infty)$ from those processes which have relaxation times in the interval τ_m to $\tau_m + d\tau_m$.

2.6.2 The Barlow, Erginsav and Lamb (B.E.L.) model.

Barlow, Erginsav and Lamb[11] found that their data for pure liquids could be fitted within experimental error to a model based on a parallel combination of the shear impedances of a Newtonian liquid (Z_N) and a Hookean solid (Z_H) as follows

$$\frac{1}{Z} = \frac{1}{Z_N} + \frac{1}{Z_H} \qquad ..(2.71)$$

where Z is the impedance of the viscoelastic fluid.

Substituting for Z_N and Z_H from (2.44) and (2.46)

$$\frac{1}{Z} = \frac{1}{(1 + i)(\pi f \eta_s \rho)^{\frac{1}{2}}} + \frac{1}{(\rho G\infty)^{\frac{1}{2}}} \qquad ..(2.72)$$

rearranging then gives

$$Z = \frac{(i\omega\rho\eta_s)^{\frac{1}{2}}}{1 + (i\omega\tau)^{\frac{1}{2}}} \qquad ..(2.73)$$

The usual form of the model is written in terms of the compliance $J^{*}(\omega)$

$$J^{*}(\omega) = \frac{\rho}{Z^2} = \frac{1}{G(\infty)} \left[1 + \frac{1}{i\omega\tau} + \frac{2}{(i\omega\tau)^{\frac{1}{2}}} \right] \qquad ..(2.74)$$

Comparing equation (2.74) with (2.64) for the Maxwell model we see there is an additional term, $2/G(\infty)(i\omega\tau)^{\frac{1}{2}}$.

Separating equation (2.74) into real and imaginary parts and equating to $J^{*} = J' - iJ''$ gives

$$J' = \frac{1}{G(\infty)} \left[1 + \frac{1}{(1/2\ \omega\tau)^{\frac{1}{2}}} \right] \qquad ..(2.75)$$

$$\text{and} \quad J'' = \frac{1}{G(\infty)} \left[\frac{1}{\omega\tau} + \frac{1}{(1/2\ \omega\tau)^{\frac{1}{2}}} \right] \qquad ..(2.76)$$

Although the experimental results for fairly pure compounds fitted this model, it was not consistent with binary mixtures[12], the deviations were found to be greatest when the components of the mixture differed significantly in molecular weight. In order to describe these results an empirical modification was made by multiplying the additional term by a parameter (k) in equation (2.74), which becomes

$$J^{*} = \frac{1}{G(\infty)} \left[1 + \frac{1}{i\omega\tau} + \frac{2k}{(1/2\ i\omega\tau)^{\frac{1}{2}}} \right] \qquad ..(2.77)$$

k is a measure of the width of the distribution times, the larger k values corresponding to a wider distribution. k = 1 corresponds to the original B.E.L. model and k = 0 to the Maxwell model. The same results are plotted as for the Maxwell model, namely $R_s/(\rho G\infty)^{\frac{1}{2}}$ and $X_s/(\rho G\infty)^{\frac{1}{2}}$ against $\omega\tau$. The following relationships are obtained from (2.42), (2.75) and (2.76)

$$\frac{G'}{G(\infty)} = \frac{1 + \dfrac{k}{(1/2\ \omega\tau)^{\frac{1}{2}}}}{\left[1 + \dfrac{k}{(1/2\ \omega\tau)^{\frac{1}{2}}}\right]^2 + \left[\dfrac{1}{\omega\tau} + \dfrac{k}{(1/2\ \omega\tau)^{\frac{1}{2}}}\right]^2} \qquad ..(2.78)$$

$$\frac{G''}{G(\infty)} = \frac{\dfrac{1}{\omega\tau} + \dfrac{k}{(1/2\ \omega\tau)^{\frac{1}{2}}}}{\left[1 + \dfrac{k}{(1/2\ \omega\tau)^{\frac{1}{2}}}\right]^2 + \left[\dfrac{1}{\omega\tau} + \dfrac{k}{(1/2\ \omega\tau)^{\frac{1}{2}}}\right]^2} \qquad ..(2.79)$$

$$\frac{R_s^2}{\rho G(\infty)} = \frac{J'G(\infty)}{2\left[(J'G\infty)^2 + (J''G\infty)^2\right]}\left\{\left[1 + \left(\frac{J''}{J'}\right)^2\right]^{\frac{1}{2}} + 1\right\} \quad ..(2.80)$$

$$\frac{X_s^2}{\rho G(\infty)} = \frac{J'G\infty}{2\,(J'G\infty)^2 + (J''G\infty)^2}\left\{\left[1 + \left(\frac{J''}{J'}\right)^2\right]^{\frac{1}{2}} - 1\right\} \quad ..(2.81)$$

or alternatively

$$\frac{R_s}{(\rho G(\infty))^{\frac{1}{2}}} = \frac{\left(\frac{\omega\tau}{2}\right)^{\frac{1}{2}}\left[1 + (2\omega\tau)^{\frac{1}{2}}\right]}{\left(1 + \left(\frac{\omega\tau}{2}\right)^{\frac{1}{2}}\right)^2 + \left(\frac{\omega\tau}{2}\right)} \quad ..(2.82)$$

$$\frac{X_s}{(\rho G(\infty))^{\frac{1}{2}}} = \frac{\left(\frac{\omega\tau}{2}\right)^{\frac{1}{2}}}{\left[1 + \left(\frac{\omega\tau}{2}\right)^{\frac{1}{2}}\right]^2 + \left(\frac{\omega\tau}{2}\right)} \quad ..(2.83)$$

In all the above equations τ may be replaced by $\eta_s(0)/G(\infty)$.

The model, which predicts a behaviour in cyclic shear in agreement with experimental results over the frequencies and temperatures employed, does not explain satisfactorily the creep behaviour[12], it leads to the prediction of unlimited creep strain which is physically unrealistic, i.e. the delayed elastic strain increases indefinitely as $t^{\frac{1}{2}}$. This defect with the model led the authors to look deeper into the ill-defined region between Newtonian behaviour and the onset of the viscoelastic relaxation region[25,26]. From these measurements a new model was proposed giving the following equation which is analogous to an equation used by Davidson and Cole[27] in dielectric studies.

$$J^*(\omega) = J(\infty) + \frac{1}{i\omega\eta_s} + \frac{J_r}{(1 + i\omega\tau_r)\beta} \quad ..(2.84)$$

where J_r is the retardation compliance which represents the delayed storage of energy under stress through reorientational changes; τ_r is the retardation time and β is an adjustable parameter similar to that used by Davidson and Cole for dielectric relaxation in supercooled liquids. The complex retardational compliance $J_r^*(\omega)$ is given by the

following expression

$$J_r^*(\omega) = \frac{J_r}{(1 + i\omega\tau_r)\beta} = J_1(\omega) - iJ_2(\omega) \qquad ..(2.85)$$

where $J_1(\omega)$ and $J_2(\omega)$ are the real and imaginary parts of the complex retardational compliance. $J_1(\omega)$ and $J_2(\omega)$ can be calculated from the measured quantities by the following equations

$$J_1(\omega) = \frac{\rho(R_s^2 - X_s^2)}{(R_s^2 + X_s^2)^2} - J(\infty) \qquad ..(2.86)$$

$$\text{and} \quad J_2(\omega) = \frac{2\rho R_s X_s}{(R_s^2 + X_s^2)^2} - \frac{1}{\omega\eta_s} \qquad ..(2.87)$$

The B.E.L. model has been used to describe volume relaxations[15,16,28], the equations are similar to those for shear relaxation and are given by the following:

$$\frac{K'}{K_2} = \frac{1 + \frac{1}{\left(\frac{\omega\tau_v}{2}\right)^{\frac{1}{2}}}}{\left[1 + \frac{1}{\left(\frac{\omega\tau_v}{2}\right)^{\frac{1}{2}}}\right]^2 + \left[\frac{1}{\omega\tau_v} + \frac{1}{\left(\frac{\omega\tau_v}{2}\right)^{\frac{1}{2}}}\right]^2} \qquad ..(2.88)$$

$$\frac{K''}{K_2} = \frac{\frac{1}{\omega\tau_v} + \frac{1}{\left(\frac{\omega\tau_v}{2}\right)^{\frac{1}{2}}}}{\left[1 + \frac{1}{\left(\frac{\omega\tau_v}{2}\right)^{\frac{1}{2}}}\right]^2 + \left[\frac{1}{\omega\tau_v} + \frac{1}{\left(\frac{\omega\tau_v}{2}\right)^{\frac{1}{2}}}\right]^2} \qquad ..(2.89)$$

where τ_v is the volume relaxation time ($= \eta_v/K_2$). η_v is not obtainable directly by experiment and therefore K'/K_2 and/or K''/K_2 are plotted against the reduced frequency $\omega\eta_s(0)/K_2$ [or $\omega\eta_s(0)/G(\infty)$ if K_2 is not available]. The shape of these curves is identical to those obtained from plotting $G'/G(\infty)$ and $G''/G(\infty)$ against reduced frequency, but they are usually shifted along the reduced frequency axis. If the assumption is made that η_s is a constant multiple of η_v and $G(\infty)$ is a constant multiple of K_2, the amount of shift will give $\eta_v G(\infty)/\eta_s K_2$ or

if $K_2 = G(\infty)$ it will give η_v/η_s.

2.7 The method of reduced variables.

It was stated in the previous sections that the liquids to be investigated have a distribution of relaxation times extending over three to four decades of frequency. Therefore, with the experimental techniques available (less than two decades of frequency can be obtained) it would not be possible to study the complete relaxation. This disadvantage is overcome by varying the temperature (or pressure) and using Time Temperature (pressure) Superposition - effectively altering $G(\infty)$ and $\eta_s(0)$ of the liquid. The viscosity, which changes far more rapidly with temperature and pressure than $G(\infty)$, must be changed by at least four decades. Lamb[29] gives the characteristic frequency corresponding to $\omega\tau_m = 1$ as $0.8/\eta_s(0)$ (GHz) and therefore liquids with a viscosity of about 10 N s m^{-2} are used. The method of reduced variables does not apply across a first order phase change and therefore the 'liquid' should remain in the liquid state until a viscosity of 10^5 N s m^{-2} is reached and preferably reach the glass transition temperature or pressure before crystallisation takes place.

It is assumed that changes in temperature (or pressure) affect all relaxation frequencies by the same factor (a_r). Now if two experiments are carried out at the same frequency but at different temperatures, T_1 and T_2, then the relaxation times (assumed single relaxation), τ_{T_1} and τ_{T_2}, can be related as follows:

$$\tau_{T_2} = a_r \tau_{T_1} \qquad ..(2.90)$$

and

$$G(\infty)T_2 = b_r G(\infty)T_1 \qquad ..(2.91)$$

where a_r and b_r depend on τ_{T_2}, τ_{T_1} and $G(\infty)T_2$, $G(\infty)T_1$ respectively. The ratio of viscosities $(\eta_s)_{T_1} : (\eta_s)_{T_2}$ at these two temperatures can be obtained as follows:

$$(\eta_s)_{T_2} = \tau_{T_2} G(\infty)_{T_2}$$

$$= a_r b_r \, G(\infty)_{T_1} \, \tau_{T_1}$$

$$= a_r b_r \, (\eta_s)_{T_1} \qquad ..(2.92)$$

From (2.92) the ratio of the steady flow viscosity at two temperatures will give the product $a_r b_r$, b_r is usually close to unity[9]. Hence, if $(\eta_s)_{T_2}/(\eta_s)_{T_1} \approx 10^4$, the effective frequency $a_r\omega \approx 10^4\,\omega$. This method has been used widely to extend the frequency range of various techniques.

2.8 Summary of important equations.

$$M^*(\omega) = K^*(\omega) + {}^4/3\, G^*(\omega) \qquad ..(2.48)$$

$$R_s(0) = X_s(0) = (0.5\,\omega\eta_s(0)\rho)^{\frac{1}{2}} \qquad ..(2.43)$$

$$R_s(\infty) = (\rho G(\infty))^{\frac{1}{2}} \qquad ..(2.46)$$

$$G'(\omega) = (R_s^2 - X_s^2)/\rho \qquad ..(2.35)$$

$$G''(\omega) = 2R_s X_s/\rho \qquad ..(2.36)$$

$$\eta_s'(\omega) = G''/\omega \qquad ..(2.40)$$

$$\eta_s''(\omega) = G'/\omega \qquad ..(2.40)$$

$$G' = \frac{J'}{J'^2 + J''^2} \qquad ..(2.42)$$

$$G'' = \frac{J''}{J'^2 + J''^2} \qquad ..(2.42)$$

For B.E.L. model

$$J' = \frac{1}{G(\infty)}\left[1 + \left(\frac{1}{1/2\ \omega\tau}\right)^{\frac{1}{2}}\right] \qquad ..(2.75)$$

and $$J'' = \frac{1}{G(\infty)}\left[\frac{1}{\omega\tau} + \left(\frac{1}{1/2\ \omega\tau}\right)^{\frac{1}{2}}\right] \qquad ..(2.76)$$

$$\tau_m = \eta_s(0)/G(\infty)$$

$$M(0) = K(0) = \rho(V_L(0))^2 \qquad ..(2.16)\quad(2.52)$$

$$M(\infty) = \rho(V_L(\infty))^2 \qquad ..(2.17)$$

$$M' = \frac{\rho V_L^2 \left[1 - (\frac{aV}{\omega})^2\right]}{\left[1 + (\frac{aV}{\omega})^2\right]^2} \quad ..(2.14)$$

$$M'' = \frac{2\rho V_L^2 \frac{aV}{\omega}}{\left[1 + (\frac{aV}{\omega})^2\right]^2} \quad ..(2.15)$$

$$Z_L = \rho V_L(\infty) \quad ..(2.20)$$

$$K'(\omega) = -K(0) + M'(\omega) - {}^4/3\ G'(\omega) \quad ..(2.50)$$

$$K''(\omega) = M''(\omega) - {}^4/3\ G''(\omega) \quad ..(2.51)$$

CHAPTER III

EXPERIMENTAL TECHNIQUES

3.1 Generation of longitudinal and shear waves of ultrasonic frequency.

The required frequencies can be generated by using piezo-electric crystals, these are unsymmetric crystals. Quartz, which is the most well known and belongs to the trigonal crystallographic system, is particularly suited for this type of work; it is inert and has a very high melting point (~ 1500 K). Whether longitudinal or shear waves are produced depends on the way the crystal is cut. X-cut crystals with faces parallel to each other and normal to the X-axis are used to generate longitudinal waves and AT-cut crystals which are Y-cut rotated about the X-axis to make an angle of 49^{o} with the Z-axis are used to generate shear waves. When these crystals (or transducers) are metal plated (gold or silver with resistance < 10Ω) on opposite parallel faces and an alternating voltage of frequency (f) applied across, the crystal will vibrate at this frequency. The oscillations will be of small amplitude unless f coincides with the natural frequency of the quartz transducer, the amplitude will then increase giving the most efficient conversion of electrical to mechanical energy. This is known as the fundamental frequency of the transducer, the thickness of the transducer required is calculated from the formula given by Mason[30]

$$t = \frac{1}{2f}\sqrt{\frac{C'_{66}}{\rho}} \qquad ..(3.1)$$

where t = thickness (m) $\qquad C'_{66}$ = elastic constant (N m^{-2})

f = frequency (Hz)

ρ = density (Kg m^{-3})

For longitudinal waves of 5 MHz fundamental frequency t ≈ 0.5 mm, and for shear waves of 6 MHz fundamental frequency t ≈ 0.3 mm. If the electrical frequency is equal to (2n + 1)f (i.e. odd harmonic of the fundamental frequency) the amplitude is high but as n increases the amplitude decreases, n is usually less than ten giving a frequency range of less than two decades. The transducers, which are usually circular or rectangular plates, must have parallel faces (parallel to

6 seconds of arc) and be flat to $\lambda/8$ (of sodium light). It is necessary to mount these transducers on to quartz bars (delay lines) their main use being to delay the signal thereby allowing the transmitted and detected signal to be separated in time. The transducer is attached to the delay line by some bonding agent, this agent should transmit the mechanical vibrations with no attenuation, it should be thin, homogeneous and must be capable of producing a parallel film so that the transducer and face of the delay line will be parallel to each other. Many materials have been used in the past but the best to date is indium, the whole process is carried out under vacuum (Gooch and Housego - Ilminster). This bond has reproducible properties and is suitable for use at high pressures (700 MN m^{-2}).

3.2 Real and imaginary parts of the shear mechanical impedance.

In principle the components of the complex shear modulus can be obtained from measurements of the velocity and attenuation of plane shear waves propagated through a liquid, but experimentally this is not feasible because of the very high attenuation of shear waves at these frequencies. The technique used is to measure the complex reflection coefficient R^*.

$$R^* = \frac{Z_{FS} - Z_{QS}}{Z_{FS} + Z_{QS}} = Re^{-i(\pi+\theta)} \qquad ..(3.2)$$

3.2.1 Theory.

The theory has been developed by O'Neil[31]. For a wave propagating through the solid at angle of incidence ϕ some of the wave is reflected at an angle ϕ and some is refracted into the liquid at an angle ϕ. If the interface lies in the plane $y = 0$ then the particles in both media move parallel to the Z direction with velocities given by the following equations:

$$W_1 = W_o e^{-\Gamma_Q (x \sin\phi + y \cos\phi)} \qquad ..(3.3)$$

$$W_2 = W_o e\, T^* e^{-\Gamma_F (x \sin\phi + y \cos\phi)} \qquad ..(3.4)$$

$$W_3 = W_o \, e \, R^{*} \, e^{-\Gamma Q \, (x \, \mathrm{Sin} \, \phi \; - \; y \, \mathrm{Cos} \, \phi)} \qquad ..(3.5)$$

where W_1 is the velocity of particles for the incident wave,

W_2 " " " " " " " " refracted wave,

W_3 " " " " " " " " reflected wave,

W_o " " " " " when x = 0,

Γ is a propagation constant = $i\omega\rho/z$

suffixes F and Q refer to liquid and fused quartz respectively,

T^{*} is a transmission factor,

R^{*} is a reflection constant.

Equation (3.4) is only valid if the attenuation in the liquid is much greater than that in the solid. This is true for shear waves refracted at a quartz/liquid interface.

Using the assumption that at the interface there is no slip and the shear stress ($\sigma = ZW$) suffers no change across the interface we have

$$W_1 = W_2 + W_3 \qquad ..(3.6)$$

and $$\sigma_1 + \sigma_3 = \sigma_2 \qquad ..(3.7)$$

Rewritting equation (3.7) in terms of the impedance and particle velocities from equations (3.3), (3.4) and (3.5) gives the following equation

$$Z_{QS} \, (1 + R^{*}) \, \mathrm{Cos} \, \phi = Z_{FS} \, T^{*} \, \mathrm{Cos} \, \phi \qquad ..(3.8)$$

where suffix S refers to shear waves.

Since $T^{*} = 1 - R^{*}$, then

$$Z_{FS} = \frac{Z_{QS} \, (1 + R^{*}) \, \mathrm{Cos} \, \phi}{(1 - R^{*}) \, \mathrm{Cos} \, \phi} \qquad ..(3.9)$$

If the liquid is replaced by a vacuum or rarefied gas the refracted wave will not exist and the reflection factor is equal to -1. Now R^{*} is a complex quantity and can be written as follows:

$$R^{*} = R \, e^{-i(\pi+\theta)} \qquad ..(3.10)$$

where R is the relative reduction in amplitude and $(\pi+\theta)$ is the total phase change, π due to the phase change at the interface and θ due to applying the liquid. By substituting equation (3.10) into equation (3.9) and rearranging we have

$$Z_{FS} = Z_{QS} \frac{\text{Cos } \phi}{\text{Cos } \phi} \left\{\frac{1 - R^2 + 2\, i\, R \text{ Sin } \theta}{1 + R^2 + 2 R \text{ Cos } \theta}\right\} \qquad ..(3.11)$$

$$(Z_{FS} \sim 0.1\ Z_{QS})$$

Cos ϕ can be put equal to unity and since θ is less than 5° Cos θ can also be put equal to unity. Then equating real and imaginary parts of equation (3.11) gives:

$$R_{FS} = Z_{QS} \text{ Cos } \phi \ \frac{1 - R}{1 + R} \qquad ..(3.12)$$

where R_{FS} is the real part of Z_{FS}

$$\text{and} \quad X_{FS} = Z_{QS} \frac{\text{Cos } \phi \ 2R \text{ Sin } \theta}{(1 + R)^2} \qquad ..(3.13)$$

To simplify the calculations in terms of the measured quantities dB and θ we define two quantities C and Q where

$$\frac{dB}{C} = \frac{1-R}{1+R} \quad \text{and} \quad Q = \frac{2R}{(1 + R)^2} \qquad ..(3.14)$$

$$\text{and} \quad dB = 20 \log_{10} R.$$

C and Q have been calculated for various values of dB[32, 33]. θ is small and cannot be measured accurately when $\phi = 0$ (normal incidence technique), however the sensitivity can be increased if the angle of incidence (ϕ) is increased. ($\phi = 77^{\circ}\ 38'$ for inclined incidence).

At pressures greater than atmospheric pressure a reference fluid other than air has to be chosen. For normal incidence Cos ϕ can be put equal to unity and then from equation (3.9)

$$R^{*} = \frac{Z_{FS} - Z_{QS}}{Z_{FS} + Z_{QS}} \qquad ..(3.15)$$

for amplitude ratio from air to liquid and

$$R_R^{*} = \frac{Z_{TS} - Z_{QS}}{Z_{TS} + Z_{QS}} \qquad ..(3.16)$$

for amplitude ratio from air to reference liquid, where the suffix T refers to the reference liquid.

$$\text{Then} \quad \frac{R^{*}}{R_R^{*}} = \frac{Z_{FS} - Z_{QS}}{Z_{FS} + Z_{QS}} \cdot \frac{Z_{TS} - Z_{QS}}{Z_{TS} + Z_{QS}} \qquad ..(3.17)$$

Rearranging and putting $\frac{R^{*}}{R_R^{*}} = R_R$

$$\text{then} \quad Z_{RS} = Z_{QS}\left[\frac{Z_{QS}(1 - R_R) + Z_{TS}(1 + R_R)}{Z_{QS}(1 + R_R) + Z_{TS}(1 - R_R)}\right] \qquad ..(3.18)$$

where $dB = 20 \log_{10} R_R$, and

$$Z_{TS} = (0.5\ \rho\ \omega\ \eta_s(0))^{\frac{1}{2}} \qquad ..(3.19)$$

The reference liquid is chosen to behave as a Newtonian liquid throughout the experimental range.

The experiments yield values of dB and θ, Z_{QS}, Z_{RS} and ϕ are known, hence R_{FS} and X_{FS} can be calculated at atmospheric pressure and R_{FS} at pressures greater than atmospheric.

3.2.2 Measurement of amplitude change for R_{FS}.

The shear waves produced by the transducer (diameter 12.5 mm) travel down the delay line (length 50 mm, diameter 15 mm). They are reflected normally from the end face and travel back to the transducer where they are detected. The shear waves are produced in pulses at intervals of 20 ms and the pulse duration which can be varied from 2 to 10 μs is shorter than the time taken to travel twice through the delay line; the transducer is then quiescent and acts as a receiver for the returning pulse, part of the returning pulse is reflected and will travel up and down the delay line many times with ever-decreasing amplitude. There will be a train of reflected pulses (echoes) of decreasing amplitude displayed on the oscilloscope. The amplitude of these echoes is measured by using a comparison pulse. This comparison

pulse is produced by a comparison oscillator of the same frequency but is pulsed a short time after the main transmitter pulse. The comparison pulse, which can be made equal in duration to the sample pulses, is passed through a calibrated piston attenuator which is used to adjust the comparison pulse amplitude; the position of the comparison pulse on the oscilloscope screen can be altered so that it can be placed side by side with each echo in turn. A set of readings is obtained of pulse amplitudes up to the n^{th} reflection. After applying a liquid to the end of the delay line the reduced pulse amplitudes are measured. The difference in amplitude, which is obtained from the difference of the two measurements, is plotted against reflection number, the gradient of the graph then gives the amplitude per reflection (A). The amplitude, which is measured in terms of a change of distance between the coils in the attenuator, must be converted to dB. This is achieved by multiplying A by the piston attenuator constant which is obtained from the geometry of the attenuator (1.675 dB mm^{-1}).

For measurements at atmospheric pressure air is used for the first measurements. However, at higher pressures air cannot be used, therefore some suitable fluid has to be chosen; the fluid should have a low viscosity ($< 10^{-2}$ N s m^{-2}) and be liquid over the pressure range up to 700 MN m^{-2} and temperature range down to 243 K. The fluid used is isopentane (99% ex. B.D.H.), the viscosity and density have been determined over the pressure and temperature ranges by Bridgeman[34]. The data have been fitted to the Roelands equation for viscosity and linear secant modulus equation for density by Phillips[35]. Bridgeman's data has recently been confirmed by Houck[36]. The shear impedance of isopentane is obtained from equation (3.19).

3.2.3 Measurement of phase change for X_{FS}.

Phase change measurements are possible only at atmospheric pressure because no suitable apparatus has yet been designed for use at high pressure. Two identical transducers (19 mm x 12.5 mm) and quartz

bars (see diagram 3.2 for details) are required. The two quartz bars are initially free of liquid. The signal from the reference bar is passed through a variable delay line and variable piston attenuator and adjusted to be equal in amplitude and opposite in phase with the signal from the test bar. The two signals are derived from the same source, therefore they are coherent and able to interfere destructively when brought together in the receiver. After cancellation of the first echo, the reading of the variable delay line is noted and the procedure repeated for each echo. The liquid from the trough is applied to the test bar and again the cancellation procedure carried out. The difference between the two readings is then plotted against reflection number (only even reflections are obtained) and the gradient gives the length of delay line per reflection. The variable delay line consists of fixed lengths of coaxial cable and a telescopic line for fine adjustment. The conversion of length of delay line (L) into phase change (θ) is given by:

$$\theta = 0{\cdot}01818 \cdot L \cdot f \qquad \text{where } f \text{ in MHz} \qquad ..(3.20)$$

L in cm

θ in degrees

X_{FS} is calculated from equation (3.13).

The frequency is measured by adding a signal from a standard signal generator (Marconi Inst. Ltd. No. TF 1444/4) which can be varied until the condition of zero beating with the reference pulse is obtained, this standard signal is measured on a frequency meter (A.M.F. Venner, model 7736).

3.2.4 Apparatus.

The shear relaxation spectrometer is based on apparatus developed by Mason and McSkimin[8] and refined by Barlow and Lamb[9], a block diagram is shown in Figure 3.1. The dotted parts are not required for amplitude measurements and the sample trapezium bar used for inclined incidence measurements is replaced by a cylindrical bar

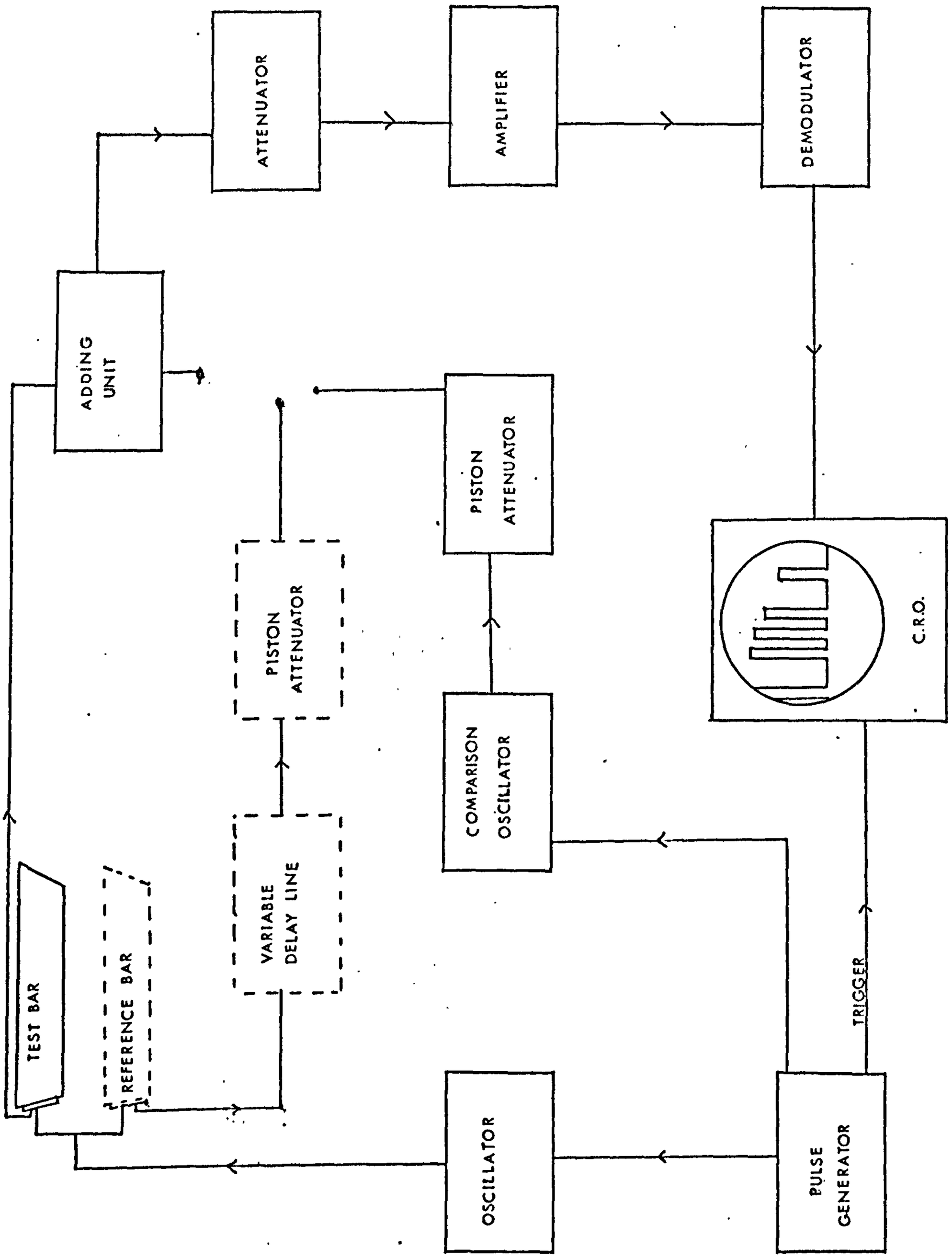

FIG. 3·1 SCHEMATIC DIAGRAM OF THE SHEAR RELAXATION SPECTROMETER

for normal incidence. The spectrometer operates at four frequencies, the fundamental 6 MHz and three odd harmonics (18, 30 and 78 MHz). The apparatus has been described in general by Powell[28] and in detail by Barlow and Subramanian[33]. Both the atmospheric and high pressure normal incidence cells have been described in detail by Powell[28]. The inclined incidence cell is shown in Figure 3.2, the two identical quartz bars are side by side but separated by a metal partition, the quartz transducers are bonded to the end of each bar and electrically connected to the spectrometer via coaxial cable taken through a metal tube. Above the test bar is a trough which can be rotated from outside the vessel, the trough is filled with liquid and after the initial measurements is rotated to allow the liquid to flow over the surface of the bar. The whole apparatus is fitted into a glass-fronted sealed container which can be immersed in a bath and brought to the required temperature.

3.2.5 Sampling technique.

Normal incidence, at temperatures at which the test liquid flowed readily (viscosity < 10 N s m^{-2}) the liquid was placed in the bottom of the tube and after the initial measurements the tube was tilted and the delay line pushed into the liquid. The tube was returned to its initial position and the second measurements taken. With increasing viscosity ($> 10^2$ N s m^{-2}) this technique became unusable because it was not possible to push the delay line or bar into the liquid so that the surface of the bar was completely covered by the liquid. Other techniques were tried, unsuccessfully, but finally a technique was used which seemed to overcome the difficulty of keeping out moisture and ensuring the end of the bar was covered with liquid. The holder for the quartz bar and transducer was bent to form a $\cup$, and sellotape was placed around the free end of the bar extending about 0.01 m above the bar. A piece of sellotape was placed over the top of the first piece of sellotape, thus sealing the face of the bar from the

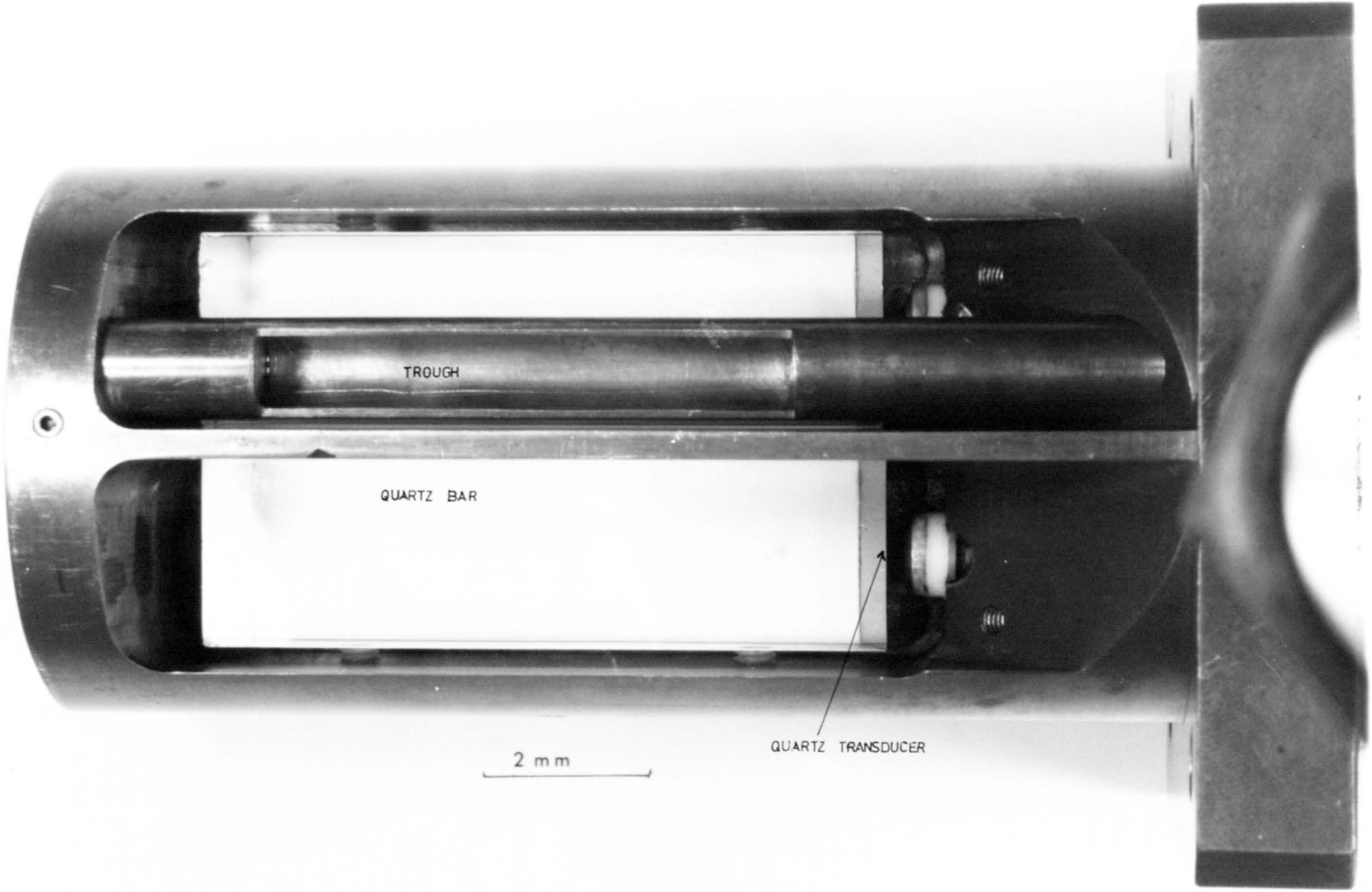

FIG. 3·2 INCLINED INCIDENCE CELL

atmosphere. The holder containing the quartz bar was placed in a sealed glass tube containing molecular sieve to absorb any moisture present. After the initial measurements the warmed liquid was injected by a syringe or pasteur pipette through the sellotape on to the face of the bar. The final measurements were taken after allowing time for the liquid to reach the temperature of the bath.

Inclined incidence:- The apparatus was designed for liquids which flowed easily and therefore could be poured from the trough onto the bar. If this technique was not possible then the apparatus had to be removed from the bath, opened and the warmed liquid poured onto the bar, and then placed back in the bath and re-establish the initial conditions. An initial experiment showed that the initial conditions could be re-established, i.e. the first and second measurements concurred. This technique was used once for a bitumen sample.

3.2.6 Accuracy.

The accuracy of the technique depends to a great extent on the stability of temperature, pressure and electronics of the instrument. At atmospheric pressure they can be made stable over the period of measurement, but at higher pressures where longer times are required stability can be a problem. The measurements are checked by re-establishing some reference condition after making a deliberate change; if these measurements do not agree the experiment is repeated. The amplitude changes can be measured to $\pm$ 0.05 dB in the range 1 to 3 dBs for low attenuation, i.e. at 6 to 30 MHz. At 78 MHz the attenuation is high and leads to larger errors in measurement, frequently less than three echoes can be measured. Results at the low frequencies are better than $\pm$ 5% but at 78 MHz they are less accurate. Phase change measurements can be made to 0.5 cm of delay line cable leading to an error in θ of 0.055° in 3° to 5° at 6 MHz and 0.71° at 78 MHz.

3.3 The measurement of the sound absorption coefficient (α).

3.3.1 Theory.

The absorption coefficient is the absorption of sound per unit distance, the usual units are nepers per meter. The amplitude (A) of the attenuated wave is related to α by the following equation

$$A = A_o \exp\left[- \alpha x + i\omega (t - xV^{-1}) \right] \qquad ..(3.21)$$

where A_o is the amplitude of the unattenuated sound wave,

x is the acoustic path length,

ω is the angular frequency of the sound wave $= 2\pi f$,

V is the phase velocity of the sound wave in the liquid.

Experimentally changes of path length can be measured with greater accuracy than absolute values of path length, therefore by measuring the amplitude at two path lengths the difference between the two being known, A_o can be eliminated.

Taking the real part of equation (3.21) we have

$$\ln \frac{A_1}{A_o} = - \alpha x_1 \qquad ..(3.22)$$

where x_1 is the first path length, and

$$\ln \frac{A_2}{A_o} = - \alpha x_2 \qquad ..(3.23)$$

where x_2 is the second path length.

Eliminating A_o between (3.22) and (3.23) gives

$$\ln \frac{A_1}{A_2} = \alpha(x_2 - x_1) \qquad ..(3.24)$$

A plot of amplitude versus path length will then give α (slope of the graph). α is usually measured in decibels but is converted to nepers by the following relationship, Neper = dB/8.686.

3.3.2 Apparatus.

The apparatus is a modified design of Andreae et al[37] and is based on the pulse technique developed by Pellam and Galt[7]. A

block diagram of the apparatus is shown in Figure (3.3). Two cells are used with the apparatus (a) atmospheric cell and (b) high pressure acoustic absorptiometer. Both cells have been fully described[28]. Some small modifications were made to the high pressure cell for ease of handling. The jack plug was changed to one identical in design to that of the viscometer so avoiding the necessity of breaking electrical connections when interchanging the viscometer and absorptiometer. Also to avoid breaking electrical connections the floating piston was held in place by two special screws inserted through the jack plug.

The apparatus operates at a fundamental frequency of 5 MHz and the following odd haromincs; 15, 25, 35, 55 and 75 MHz. There is also a comparison channel for each frequency. The launching transducer (atmospheric cell 15.5 mm diameter, high pressure cell 12.5 mm diameter) in both cells is bonded to the fixed delay line. It is pulsed at intervals of 4 ms with a pulse duration of 2-10 μs, this is less than the time (~ 50 μs) required to travel through the fixed delay line, liquid and movable delay line onto which is bonded the receiving transducer (15.5 mm diameter). The signal is detected by this transducer, amplified, demodulated and finally displayed on the oscilloscope screen, together with the delayed comparison pulse. It is extremely important for the production of a good signal that the faces of the two delay lines should be parallel to each other, the atmospheric cell is designed so that this can be achieved easily, the high pressure cell has been designed so that the faces are parallel.

3.3.3 Measurement.

The amplitude of the first echo, which must be free from any beating with other echoes, is measured by adjusting the amplitude of the comparison pulse until equal in amplitude to the first echo. (In the atmospheric pressure cell the comparison pulse is placed adjacent to the first echo, whereas in the high pressure cell it is placed to the right of the train of echoes because there is insufficient space

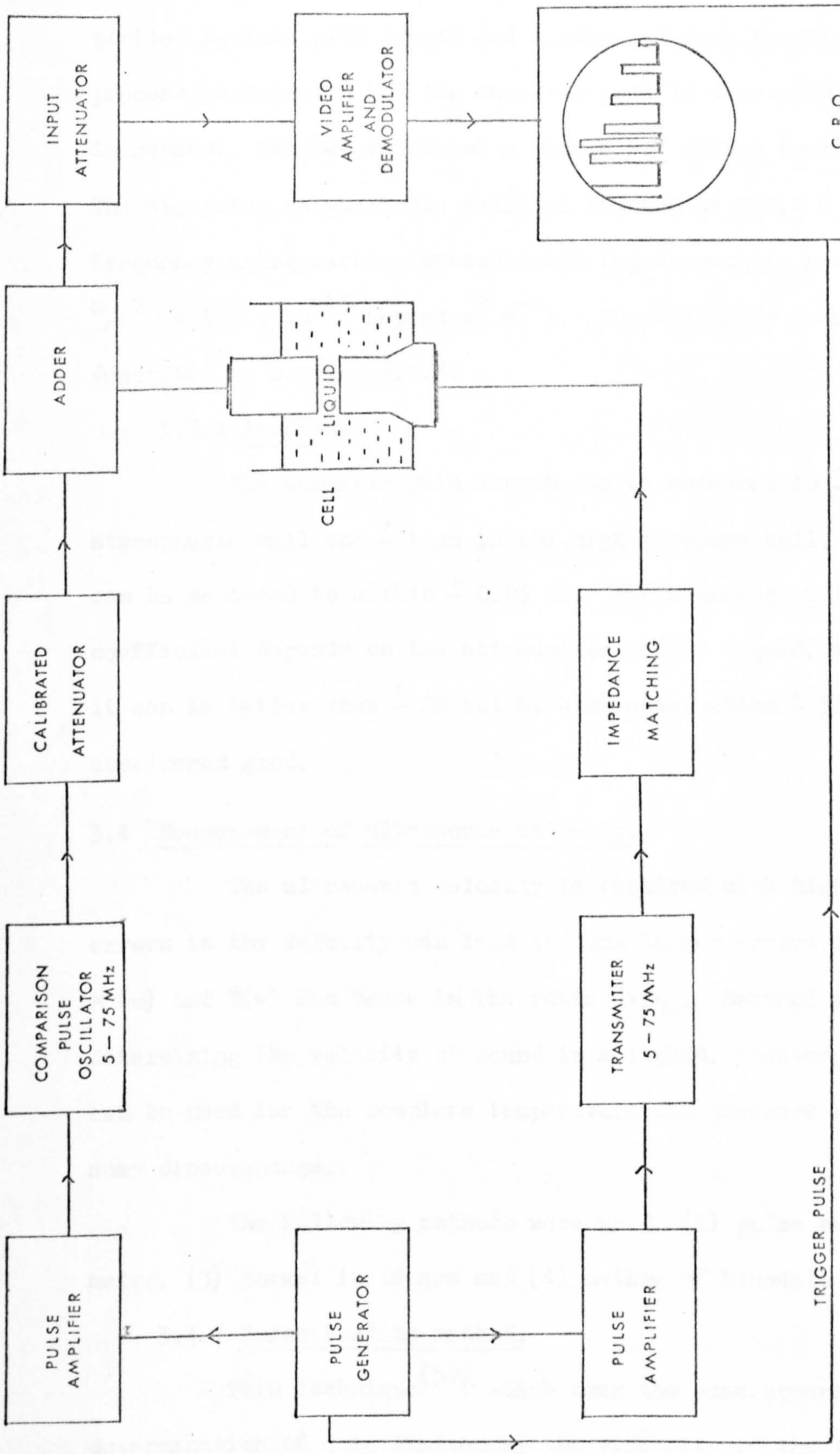

FIG. 3·3 SCHEMATIC DIAGRAM OF THE ULTRASONIC APPARATUS

between the echoes). The distance between the delay line is increased a known amount and again the amplitude is measured. This process is repeated until there is a decrease of about 30 dB. The amplitude is plotted against path length and α obtained from the slope. The whole process is repeated but the acoustic path is decreased instead of increased. The two values of α should not differ by more than $\pm$ 2%. The apparatus (atmospheric cell) is checked at 298.2 K for each frequency using carbon tetrachloride (spectroscopic grade, B.D.H., $\alpha/f^2 = 550 \cdot 10^{-15}$ Nepers s^2 m^{-1}). The frequency is measured as described in Section 3.2.3.

3.3.4 Accuracy.

The acoustic path length can be measured to $\pm$ 0.01 mm in the atmospheric cell and $\pm$ 1 μm in the high pressure cell. The amplitude can be measured to within $\pm$ 0.05 dB. The accuracy of the absorption coefficient depends on the attenuation of the liquid, at low attenuation it can be better than $\pm$ 2% but at high attenuation $\pm$ 5% would be considered good.

3.4 Measurement of ultrasonic velocity.

The ultrasonic velocity is required with high accuracy, small errors in the velocity can lead to much larger errors in $M(0)$, $M'(\omega)$, $M''(\omega)$ and $M(\infty)$ and hence in the ratio η_v/η_s. Several methods exist for determining the velocity of sound in a liquid, however no single method can be used for the complete temperature and pressure range, each has some disadvantage.

The following methods were used, (1) pulse beating, (2) velocimeter, (3) normal incidence and (4) method of Blundell and Wyn-Jones.

3.4.1 Pulse beating method.

This technique[37] which uses the same apparatus used for the determination of α is limited by the viscosity of the liquid, since at viscosities greater than 10^5 N s m^{-2} the delay lines cannot be moved.

For low attenuated liquids beating can be observed on the first echo at small acoustic path lengths when the path length is changed. This is due to interference between the first echo and echoes reflected from the quartz faces. Moving the delay line through $\lambda/2$ causes a complete beat, hence knowing the frequency, the velocity can be determined. To increase the accuracy many beats and the corresponding path lengths are measured. When the above method is used with high attenuated liquids only a small number of beats are obtained, leading to loss of accuracy. To overcome this the upper delay line is replaced by a shorter delay line, thus allowing the transmitter pulse to interfere with the first received echo. Changing the path length now causes beating of these two, but now a complete beat occurs when the delay line is moved through λ. In the high pressure cell the movable delay line is sufficiently short to allow overlap of the first echo with the transmitter pulse.

3.4.1A Theory.

If n complete beats are obtained for an acoustic path change L, the wavelength of the sound wave is given by

$$\lambda = L\frac{2}{n} \qquad ..(3.25)$$

or $\lambda = \frac{L}{n}$ for shorter delay line.

and $V = f\lambda$ ..(3.26)

3.4.1B Accuracy.

The accuracy of the technique depends on (a) visually observing the point at which a complete beat occurs, by measuring a large number of beats the accuracy can be increased; (b) measuring the distance moved by the delay line and (c) the accuracy of the frequency measurement. The frequency can be measured to $\pm$ 0.02 MHz, the distance to $\pm$ 0.005 mm and better than quarter of a beat can be seen easily. Under the most favourable conditions, i.e. low attenuation and low frequency, velocity can be determined to within $\pm$ 1%, but as the frequency increases and attenuation is high it can only be determined

to within $\pm$ 5%.

3.4.2 Velocimeter method.

This method designed by Barlow and Yazgan[38,39] is based on a fixed path acoustic system developed by McSkimin[40]. The method is only suitable for liquids with a low absorption coefficient (α < 200 Neper m^{-1}), and is used here to measure V(0)..

The transducer (11 mm diameter) has a fundamental frequency of 10 MHz and will also operate at the third harmonic (30 MHz). The principle of the method is to measure the time taken for a longitudinal wave of known frequency to travel a fixed path length of liquid. The cell consists of two quartz rods (41 mm x 15 mm diameter; 13 mm x 15 mm diameter) separated by a fused quartz spacer ring (7.747 mm). A transducer (11 mm diameter) is bonded to the longer rod. A pulse of sound waves (duration variable 1 to 35 μ secs) travels from the transducer down the longer delay line and is partially reflected at the first quartz/liquid interface, the remainder travels through the liquid, is reflected at the second interface and back through the liquid to the transducer. These two reflected pulses are out of phase, the phase difference between the two can be determined by cancelling each separately against a continuous reference signal. The phase difference gives the wavelength difference between the two pulses but does not give the number of complete wavelengths forming the major part of the total phase difference; this number may be evaluated if measurements are made at a slightly different frequency obtained from a second oscillator, the two frequencies differing by only a few parts in a thousand. The system used for cancelling the pulses is identical to that described for X_{FS} measurements, i.e. the continuous reference signal is passed through varying lengths of co-axial cable until cancellation is achieved.

3.4.2A Calculation.

Let f_1 be the first frequency, and let d_1 and d_2 be the

lengths of cable (in cm) required to cancel the first and second pulses respectively. The wavelength, λ_1, ($\approx$ 660 cm at 30 MHz) is obtained by cancelling the first pulse a second time, the difference between these two cancellations gives the length of cable equivalent to one wavelength.

Let t_1 be the time for the fractional part of the wavelength with frequency f_1.

Then $t_1 = \frac{d_2 - d_1}{f_1\lambda_1}$ or $\frac{d_2 + \lambda_1 - d_1}{f_1\lambda_1}$ if $d_1 > d_2$.

Let f_2 be the second frequency, $f_2 > f_1$.

Let d_1' and d_2' be the lengths of cables (in cm) required to cancel the first and second pulses at frequency f_2.

λ_2 is obtained as for λ_1 using frequency f_2.

Let t_2 be the time for the fractional part of the wavelength with frequency f_2.

Then $t_2 = \frac{d_2' - d_1'}{f_2\lambda_2}$ or $\frac{d_2' + \lambda_2 - d_1'}{f_2\lambda_2}$ if $d_1' > d_2'$

Let n_1 be the number of complete wavelengths.

Then $n_1 + \frac{1}{2} = \frac{f_1 f_2}{f_2 - f_1}(t_2 - t_1) + \frac{x}{f_2}$ $\quad x = 0$ if $t_2 - t_1$ +ve; $x = 1$ if $t_2 - t_1$ -ve

and $V_1 = \frac{2L}{(n_1 + \frac{1}{2})f_1 + t_1}$ or $V_2 = \frac{2L}{(n_2 + \frac{1}{2})f_2 + t_2}$

$n_2 = n_1 + 1$, or $n_2 = n_1$.

V_1 should not differ from V_2 by more than 0.02 m per sec.

3.4.2 B Theory.

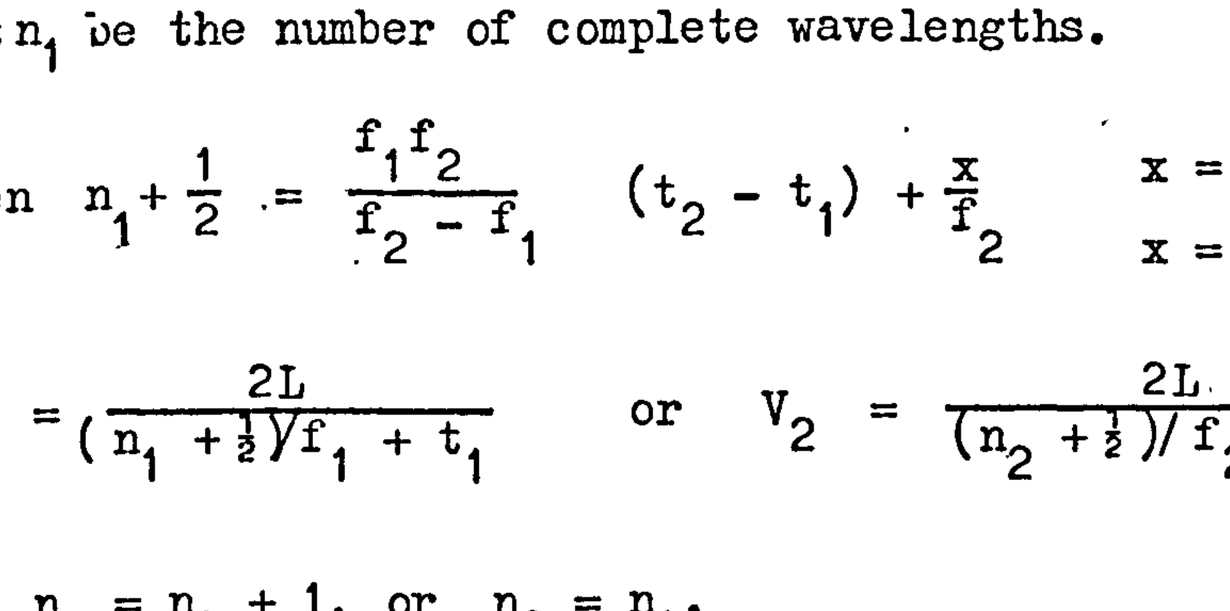

FIG. 3·4 ACOUSTIC SYSTEM

Let E_Q, E_L be the waves reflected from the first and second interface respectively. The relationship between the amplitudes of these two waves is given by

$$\frac{E_Q}{E_L} = \frac{-4 Z_L Z_Q}{(Z_L + Z_Q)^2} \exp\{-2l(\alpha + i\beta)\} \qquad ..(3.27)$$

l is the thickness of the spacer and $(\alpha + i\beta)$ is the propagation constant.

For the liquids investigated $\beta >> \alpha$, giving

$$Z_L \approx |Z_L| \exp(i\, \alpha/\beta) \qquad ..(3.28)$$

and $$Z_Q \approx |Z_Q| \exp(i\, a/b) \qquad ..(3.29)$$

where $a + ib$ $(b >> a)$ is the propagation constant of fused quartz.

$$(Z_L + Z_Q)^2 = |Z_L + Z_Q|^2 \exp(i\, 2\gamma) \qquad ..(3.30)$$

where $\gamma = \dfrac{\alpha b^2 \rho_L + a\beta^2 \rho_Q}{b\beta(\rho_L b + \rho_Q \beta)}$

ρ_Q density of quartz

ρ_L density of liquid.

Substituting (3.28), (3.29), (3.30) into (3.27) gives

$$E_L = E_Q \frac{4\,|Z_L|\,|Z_Q|}{|Z_L + Z_Q|^2} \exp(-2l\alpha) \exp\left[-i\left(2l\beta - \frac{\alpha}{\beta} - \frac{a}{b} + 2\gamma - \pi\right)\right] \qquad ..(3.31)$$

If the phase delay of the reference for the two cancellations is θ radians

$$\text{then} \quad 2l\beta - \frac{\alpha}{\beta} - \frac{a}{b} + 2\gamma - \pi = 2n\pi + \theta \qquad ..(3.32)$$

$-\frac{\alpha}{\beta} - \frac{a}{b} - 2\gamma$ is negligible under the conditions of the experiment.

Let $\beta = \omega/V$.

$$\text{Then} \quad 2l\omega_1/V - \pi = 2\pi n_1 + \theta_1 \qquad ..(3.33)$$

$$\text{and} \quad 2l\omega_2/V - \pi = 2\pi n_2 + \theta_2 \qquad ..(3.34)$$

By putting $n_2 = n_1 + x$, $\theta_1 = t_1 2\pi f_1$ and $\theta_2 = t_2 2\pi f_2$.

$$n_1 + \frac{1}{2} = \frac{f_1 f_2}{f_2 - f_1}\left[(t_2 - t_1) + \frac{x}{f_2}\right] \qquad ..(3.35)$$

$x = 0$ if $t_2 - t_1$ is +ve and $x = 1$ if $t_2 - t_1$ is -ve.

In general, n_1 will not be an integer since experimental errors are finite. However, the nearest integer to the value obtained is taken as n_1; the following equations are then obtained from equations (3.33) and (3.34):

$$V_1 = \frac{2L}{(n_1 + \frac{1}{2})/f_1 + t_1} \qquad ..(3.36)$$

$$V_2 = \frac{2L}{(n_2 + \frac{1}{2})/f_2 + t_2} \qquad ..(3.37)$$

3.4.2C Apparatus and Accuracy.

The apparatus which has been described by Powell[28] is shown schematically in Figure 3.5. The accuracy depends on the stability of temperature and pressure, and measurement of the spacer length, delay line length and frequency. Temperature and pressure must be extremely stable, the temperature to better than 0.01 degree and pressure 0.01 MN m^{-2}. Any change in either temperature or pressure was easily detected since phase cancellations were impossible to achieve or, if achieved, it was very quickly lost. The instrument is a very sensitive detector of changes of temperature and pressure. At 30 MHz, 7 degrees or 2 to 4 MN m^{-2} are sufficient for the phase to go through a complete cycle (≡ 660 cm of delay line). A similar technique has been used by Angel and Bean[41] to measure temperature and pressure.

The frequency measured directly (digital counter A.M.F. Venner model 7736) was accurate to $\pm$ 0.1 kHz, and the delay line measurements were accurate to $\pm$ 0.1 cm, both these measurements did not affect the accuracy of the velocity greater than 0.01%. The spacer length was measured with slip guages to $\pm$ 0.001" (≡ $\pm$ 0.02 mm), giving an accuracy of $\pm$ 3 m s^{-1} in the velocity. The calculation of n is important, a difference of 1 in the value of n gives a difference of $\pm$ 5 m s^{-1} in the velocity.

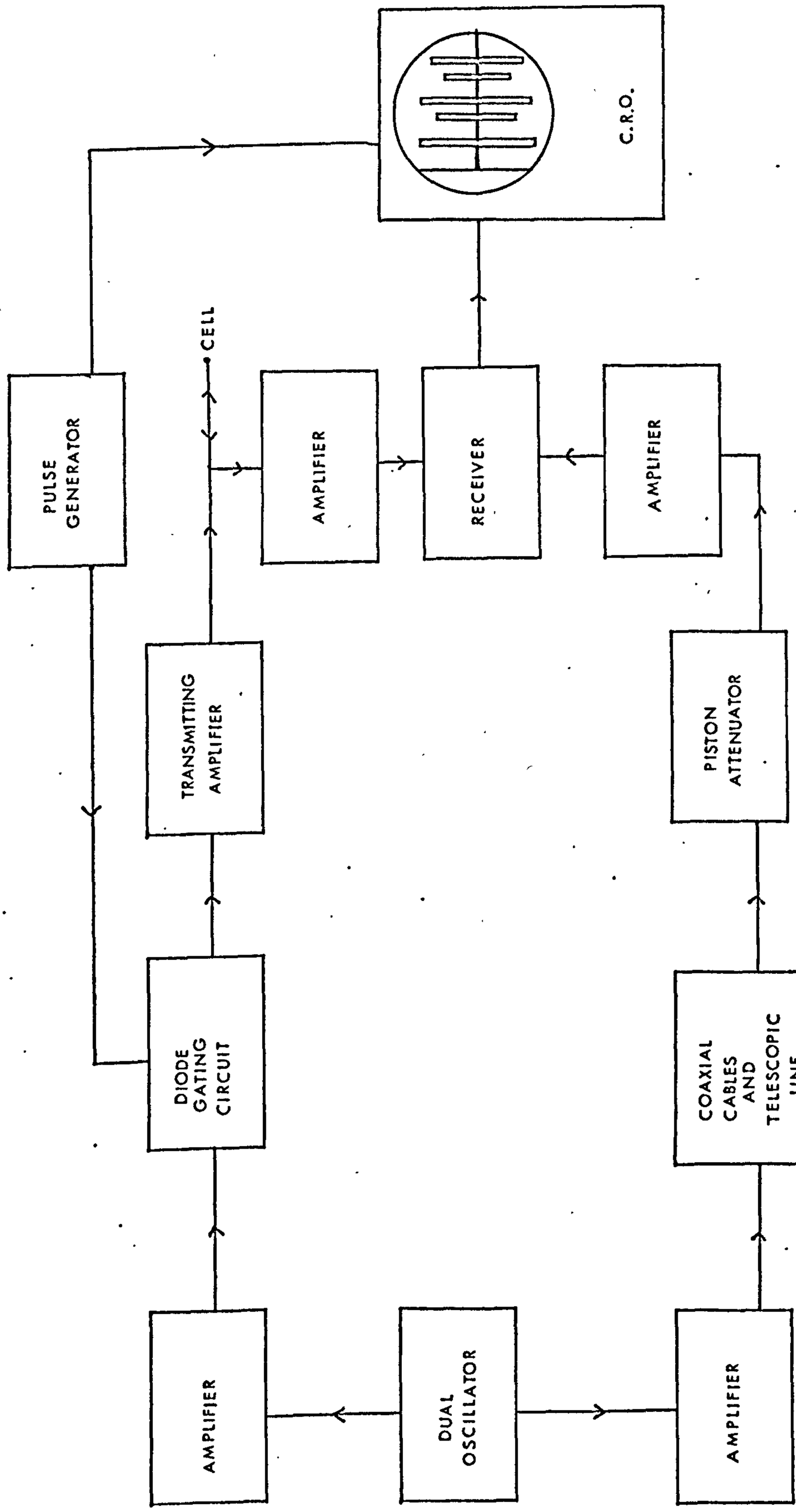

FIG. 3.5 SCHEMATIC DIAGRAM OF THE VELOCIMETER

Providing the temperature and pressure are stable and the spacer length is known accurately the velocity can be obtained to better than $\pm$ 0.01%.

3.4.3 Normal incidence technique.

This technique is used when the pulse beating technique becomes inoperable due to the high viscosity of the sample (i.e. at low temperatures and high pressures). It is based on the same principle as that used for determining the real part of the shear impedance of liquids[9]. The only change to the apparatus is the replacement of the A.T. quartz crystal with an X-cut crystal to generate the longitudinal waves.

3.4.3A Theory

An analogous equation to (3.18) can be written for longitudinal waves

$$Z_{FL} = Z_{QL}\left[\frac{Z_{QL}(1 - R) + Z_{TL}(1 + R)}{Z_{QL}(1 + R) + Z_{TL}(1 - R)}\right] \qquad ..(3.38)$$

where the subscript L refers to longitudinal waves and F, Q and T are sample liquid, quartz and reference liquid respectively, R is the amplitude ratio, where $20 \log_{10} R$ = dB.

When the reference fluid is air the equation reduces to

$$Z_{FL} = Z_{QL}\frac{(1 - R)}{(1 + R)} \qquad ..(3.39)$$

The impedance Z_{FL} is related to the phase velocity (V_L) by the following equation,

$$Z_{FL} = V_L \rho \qquad ..(3.40)$$

providing $(\alpha/\omega)^2 << 1$

where ρ is the density of the sample liquid

and therefore the velocity can be determined from the impedance and the density. At high pressures isopentane is used as the reference fluid and the longitudinal impedance Z_{TL} is obtained from the velocity and

density of isopentane using equation (3.40).

3.4.3B Accuracy.

The error in the phase velocity depends on the error in the impedance measurements and density measurements, density can be measured to better than $\pm$ 1% and impedance to about $\pm$ 3 to 5%.

3.4.4 Wyn-Jones and Blundell method.

The method used by Wyn-Jones and Blundell[42] for solid discs was adapted for liquids as follows. Using the apparatus and atmospheric cell for longitudinal absorption, the pulsed sound wave was passed through the liquid and after detection the undemodulated signal was displayed on the oscilloscope screen. Into the second channel of the oscilloscope a signal of frequency 1 MHz (accuracy 0.005% at 298.2 K) was added. This signal was used to measure the time change since the time between two adjacent waves was one micro-second. The undemodulated signal was superimposed on one of the 1 MHz signal waves and the position noted. After a change of temperature or pressure the position of the signal was again noted and the time change measured. Initial measurements showed this time to be very small. However, when calculations were carried out for the change of time with temperature for quartz and the liquid, they were found to be -16.5×10^{-10} s per degree, and $+15.0 \times 10^{-10}$ s per degree respectively. Therefore, after correcting for the quartz the errors could be considerably larger than existing methods. The method used by Blundell and Jones did not involve any change in temperature or pressure, the solid sample was moved in and out of the sound path.

3.5 Measurement of Density.

3.5.1 Atmospheric pressure.

Densities were determined using a density bottle calibrated with double distilled water. The density bottle was used in accordance with A.S.T.M. Standard D.1481. The accuracy of the method is better than 0.5%. In samples measured the density was found to vary linearly

with temperature.

3.5.2 Pressures greater than atmospheric.

The method depends on measuring the decrease in volume of a known weight of liquid with increase in pressure. The densitometer has been described previously[28]. The volume at atmospheric pressure is obtained from the weight of the sample and its density. The decrease in volume is measured by determining the distance a floating piston moves as the pressure is increased and the internal cross-sectional area of the densitometer. The results of the density determinations are fitted to the linear secant modulus equation[43].

3.5.3 Theory.

The change in volume (ΔV) is given by the following equation:

$$\Delta V = \Delta x \frac{\pi D^2}{4} \qquad ..(3.41)$$

where Δx is the distance moved by the floating piston,

D is the internal diameter of the densitometer.

Now, if V_F is the final volume and V_I the initial volume

$$\text{then} \quad V_F = V_I - \Delta V \qquad ..(3.42)$$

$$\text{and} \quad \frac{V_F}{M} = \frac{V_I}{M} - \frac{\Delta x \pi D^2}{4M} \qquad ..(3.43)$$

where M is the mass of the liquid.

The density $\rho(P)$ is then given by

$$\rho(P)^{-1} = \rho(0)^{-1} - \Delta x \frac{\pi D^2}{4M} \qquad ..(3.44)$$

where $\rho(0)$ is the density at atmospheric pressure.

The distance can be measured to $\pm$ 5 μm and the volume at atmospheric pressure is known to 0.5%, giving an overall accuracy of 0.5%.

3.6 Measurement of the Steady Flow Viscosity.

3.6.1 Atmospheric pressure.

Kinematic viscosities were measured with calibrated suspended

level viscometers BS/IP/SL (S) , which were used in accordance with A.S.T.M. Standard D445. The kinematic viscosity (ν) ranged from 10^{-5} to 10^{-2} m^2 s^{-1}. The zero shear viscosity ($\eta_s(0)$) is obtained from the kinematic viscosity by the following relationship

$$\eta_s(0) = \rho \nu \qquad ..(3.45)$$

The viscosity can be measured to an accuracy of $\pm$ 1%. To obtain viscosities greater than 20 N s m^{-2}, the high pressure viscometer described below was used. The results of the viscosity measurements were fitted to Roelands' equation(44).

3.6.2 Pressures greater than atmospheric pressure.

For measurements at pressures above atmospheric, a Couette viscometer designed by Hutton and Phillips(45) was used. The zero shear viscosity is given by(46)

$$\eta_s(0) = \frac{k \varepsilon}{\Omega} \qquad ..(3.46)$$

where k is a constant for the viscometer,

ε is the strain in the strain gauge bridge,

Ω is the relative angular velocity of the cylinders.

The viscometer constant was obtained from the geometry of the apparatus and by measurement with liquids of known viscosity. The two values agreed to better than 1% ($k = 0.580$ N.rad.m.$^{-2}$). The relative angular velocity can be varied from 150 to 0.005 rads per second, but in practice was used in the range 5.0 to 0.05. The strain was measured by a 'Budd' strain gauge bridge calibrated in microstrain; measurements with weights hanging on the torsion springs showed that the bridge was only linear to $\pm$ 200 $\mu\varepsilon$. The measured viscosity is accurate to $\pm$ 5%. The results are fitted to the high pressure form of Roelands' equation(44).

3.7 Temperature Control and Measurement.

At atmospheric pressure two baths were used, a Townson and Mercer X27 for operation at and above room temperature, and a laboratory-

built bath below ambient. Water was used from 298 K to 340 K and oil above 340 K in the Townson and Mercer bath. The laboratory-built bath consisted of a stainless steel dewar into which was placed a smaller glass dewar. The space between the two dewars was partly filled with liquid nitrogen. The level of liquid nitrogen was maintained by pressure sensors placed in the nitrogen; these sensors activated a low pressure nitrogen gas supply to the vapour space in the nitrogen container and nitrogen was blown over until the required level was reached. The inner dewar, which was filled with Industrial Methylated Spirits (I.M.S.) (10 d m^3) for temperatures from 298 K to 220 K and isopentane for temperatures below 220 K, was fitted with a heater, stirrer and platinum resistance thermometer from which the temperature was controlled by an A.E.I. (RT3/R, MK2) controller.

The bath used for the high pressure studies was larger than the atmospheric pressure bath to accommodate the stainless steel high pressure vessel. The bath consists of an inner and outer vessel. The outer vessel which is thermally insulated on the outside, contains the cooling coil and a bimetallic strip controller. It is filled with I.M.S. (50 d m^{-3}). The aluminium inner vessel is surrounded by three layers of glass matting which are bonded to the vessel with a special low temperature epoxy resin. The inner vessel is fitted with a stirrer, two heaters and a platinum resistance thermometer connected to an A.E.I. RT3/RMK2 controller and contains I.M.S. (40 d m^{-3}) and sodium nitrite (0.5% $^{w}/_{v}$). The temperature in the outer vessel is controlled by the bimetallic strip which activates an electrical relay. The relay operates a heater (5 W) inside a closed dewar containing liquid nitrogen. The nitrogen boils and the increased pressure forces liquid nitrogen through the cooling coil and out into the I.M.S. On sufficient cooling the bimetallic strip breaks the electrical circuit, the heater is switched off and the dewar is vented to atmosphere. The temperature cycle is $\pm$ 3 K. The temperature in the inner vessel is controlled by the platinum

resistance thermometer to ± 0.05 K. The bath and operation has been described by Hutton and Phillips[47]. All temperatures were measured with mercury or alcohol thermometers which had been calibrated against standard National Physical Laboratory (N.P.L.) thermometers; temperatures recorded are correct to 0.1 degree.

3.8 High Pressure Apparatus.

The high pressure vessel is a stainless steel (3.5% NCMV) tube with internal diameter 25.5 mm, external diameter 152.4 mm and length 638.2 mm. The vessel is sealed at each end with special plugs containing three rubber 'O' rings and each end plug is kept in place by a backing nut. The lower end plug contains an inlet for the pressurising fluid and electrical connections for the Couette viscometer and absorptiometer. These electrical leads are sealed into the end plug with an epoxy resin (AY 103 + HY 951 ex. Ciba-Geigy). Two upper end plugs are used, one containing only electrical connections used for the normal incidence and velocimeter cells, and a second containing both electrical connections and a rotary seal. In the second one the electrical connections are used for the absorptiometer and densitometer. The rotary seal, which comprises a steel rod and a close-fitting hole, allows a linear motion for these two pieces of equipment and a rotary motion for the viscometer. The end of the rod which goes into the pressure vessel has a thread 0.5 mm pitch, the other end is attached to a device for measuring the rotary motion. One revolution of the thread is equivalent to 500 divisions on the meter (hence 1 division ≡ 1 μm linear motion). For the operation of the viscometer the part of the rod outside the vessel is coupled to a gearbox and synchronous motor, thus enabling a range of constant rotational velocities to be selected. All three end plugs have been described in detail by Powell[28] and Hutton[47].

High pressure is generated in a pressure transmitting fluid (AeroShell Fluid 4) by a hydraulic intensifier (Powermatic Century

100,000 p.s.i. pump, Olin Matheson). The pump is driven by the laboratory high pressure air supply (0.65 MN m^{-2}) and each reciprocation of the pump delivers a small volume (100 mm^3) of fluid through a check valve and at a pressure controlled by the air inlet pressure. Pressures up to 700 MN m^{-2} can be attained. The pressure can be increased or decreased (by a let down valve) at a slow rate (1 MN $m^{-2}s^{-1}$). The test fluid is isolated from the pressurizing fluid by seals within the particular pieces of equipment, the pressure is transmitted by the use of floating pistons, bellows or diaphragms. These seals were often found to distort owing to elastoplastic flow of the rubber (Viton) but the original shape was soon recovered by warming. If any leakage of the pressurizing fluid into the test liquid occurred it could easily be detected by its pink colour.

Inside the intensifier were three small 'O' rings; the nearest to the high pressure side was teflon, this was required to be replaced every two to three months when the pump was in constant use. The pressure is measured in the hydraulic circuit outside the pressure vessel by a Manganin resistance piezometer (HP 200E Coleraine Instrument Company), the output is displayed on a digital voltmeter in units of 1 MN m^{-2}. The piezometer was calibrated against a 100,000 p.s.i. dead weight tester and was found to be accurate to $\pm$ 1 MN m^{-2}.

3.9 6 MHz Results.

3.9.1 Introduction.

With all the liquids studied the results at 6 MHz measured with the normal incidence apparatus have always been poor compared to the results at other frequencies. In some measurements the attenuation versus reflection number graphs have shown a 'S' shape instead of the linear relationship shown with the other frequencies. The first three points lie more or less on a straight line and then after a decrease in the rate of rise of attenuation the curve shows a marked increase. This effect has also been seen in the measurements of M.C. Phillips.

3.9.2 Observations.

There are many variables in the system, some of which would affect all frequencies and can be eliminated. The nature of the sample at different temperatures required the use of different sampling techniques and with some techniques an improvement was noticed. Different crystals for normal incidence were used but with no improvement. The results improved when the temperature was decreased. However, the inclined incidence apparatus gave good results even at the higher temperatures. Crystal bonding agents were not suspected because indium was used with all crystals. Degassing a sample showed no improvement. The results suggest that the size of the crystal and rod may be causing this effect since most other variables could be eliminated.

Pinkerton[1] showed that the graph of attenuation versus reflection number is linear for distances less than R^2/λ (where R is the radius of the crystal) but as the distance increases we move from the Fresnel region to the Fraunhoffer region where the graph is not linear. At 6 MHz in quartz $\lambda = 0.63$ mm and $R^2/\lambda = 62.5$ mm. Since the normal incidence rods are longer than $R^2/2\lambda$ this may be the cause of these poor results, although it would not explain the good results at lower temperatures and high pressures. A shorter rod (40 mm) and larger crystal (30 mm diameter) was used at the higher temperature giving good results at 6 MHz and the other frequencies.

Whenever the technique discussed in Section 3.2.5 was used good results were obtained at all temperatures with the 50 mm quartz rods and 12.5 mm crystals. The only significant difference between this technique and the previously used push-in technique was that only the face of the rod was wetted by the liquid, the sides were unchanged. In the high pressure cell only the face of the rod is wetted by the liquid and may account for the good results obtained at 6 MHz using the high pressure cell.

Finally, two more experiments were carried out using the 'push-in' technique, the difference between the two was in the second experiment the sides of the rod were protected with several layers of sellotape. The first gave the poor results at 6 MHz whereas the second gave good results at all frequencies. This result provides an explanation for the good results at low temperatures.

It can be concluded that the curvature in the graphs of attenuation against reflection number with the normal incidence equipment operated at 6 MHz occurs when a substantial part of the sides of the quartz rod are wetted by the liquid. An increase in diameter/length ratio of the rod diminishes the curvature when the sides are wetted.

CHAPTER IV

VISCOELASTICITY OF BITUMENS

4.1 Introduction.

Bitumens are viscoelastic fluids prepared from crude oil distillation residues, their composition varies depending on their origin. They usually contain asphaltenes, tars and different oils. Asphalt is a thermoplastic high molecular component of the colloid structure formed by micelles in the oil liquid environment. Bitumens are used as bonding agents on roads and therefore their flow properties are important. The viscous and viscoelastic properties are quite well known, but their elastic properties are not so well known and have, in the past, been obtained from low frequency measurements[48,49]. The elastic properties can be obtained by either using low temperatures or high frequencies (equivalent to short time scales). By using shear waves in the frequency range 6 - 78 MHz the elastic properties can be investigated. Although bitumen becomes brittle at low temperatures, brittleness should not become a problem because the strain levels are low ($\sim 10^{-5}$). In practical applications both linear and non-linear behaviour is encountered, but in the present experimental arrangement only the linear behaviour can be determined.

Two samples of bitumen have been studied; sample (a) Kuwait SB 80/100 (glass transition temperature (T_g) = 263.2 $\pm$ 2 K) is a typical bitumen used for road construction and sample (b) Miri 150/250 thought to be a Maxwell liquid. It was decided to look at sample (b) because of the anomalous results with sample (a).

4.2 Experimental Results.

4.2.1 Kuwait SB 80/100.

The density and viscosity had been determined previously and the data fitted to the equations which are given in Appendix IV, Tables AIV.1 and 2. R_s and X_s were measured as described in Chapter III, R_s over the temperature range 250 to 390 K and X_s above 300 K. The shear modulus ($G(\infty)$) was obtained from low temperature measurements of R_s

where there was no dispersion with frequency. At slightly higher temperatures $R_s(\infty)$ was obtained by the extrapolation procedure of Hutton and Phillips[50]. $G(\infty)$ was found not to vary linearly with temperature but the compliance $J(\infty)$ does vary linearly with temperature and is given by the following equation,

$$J(\infty)/(GN\ m^{-2})^{-1} = -2.305 + 0.0133 \cdot T/K \qquad ..(4.1)$$

The variation of $G(\infty)$ and $J(\infty)$ with temperature is illustrated in Figure 4.1. $R_s(\infty)$ is obtained from equation (4.1) $(R(\infty)^2 = \rho/J(\infty))$ for all temperatures and the ratio $R_s(\omega)/R_s(\infty)$ known as the reduced impedance is plotted against a reduced frequency $\omega\eta_s(0)/G(\infty)$ to give a reduced variables plot, illustrated in Figure 4.2. The numerical values of reduced impedance and frequency are given in Table AIV.3.

4.2.2 Miri 150/250.

This sample is very similar to one reported by Jongepier and Kuilman, sample A in (51) and sample 1 in (49). The viscosity data were fitted by Jongepier and Kuilman to the equation given in (51), the parameters for the viscosity and density equations are given in Tables AIV.1 and 2; R_s, X_s and values of $R_s(\infty)$ were obtained as for Kuwait SB 80/100. Table AIV.4 contains values of $R_s(\infty)$ and $G(\infty)$ calculated from $R_s(\infty)$ at various temperatures. The variation of $R_s(\omega)$, $G(\infty)$ and $J(\infty)$ with temperature is shown in Figures 4.3, 4.4b and 4.4a respectively. $J(\infty)$ was found to vary linearly with temperature (from 270 K upwards) according to equation (4.2).

$$J(\infty)/(GN\ m^{-2})^{-1} = -3.714 + 0.0173\ T/K \qquad ..(4.2)$$

The reduced impedance and reduced frequency calculated from the above are given as a function of temperature and frequency in Table AIV.5 and the resulting reduced variables plot is shown in Figure 4.5.

4.3 Discussion of results.

Viscosity curves of the logarithm of viscosity against temperature were of similar shape for the two samples, but sample (b)

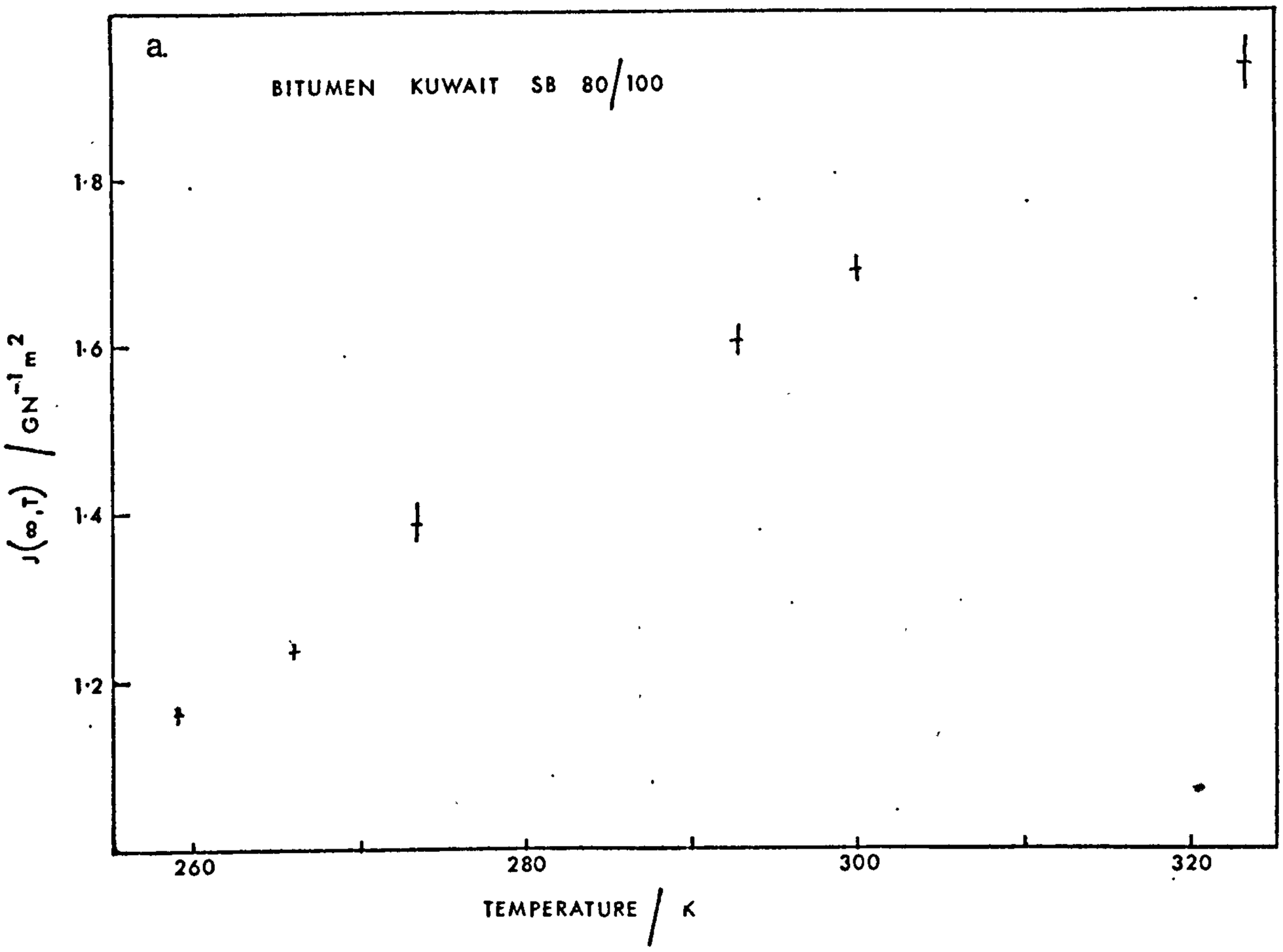

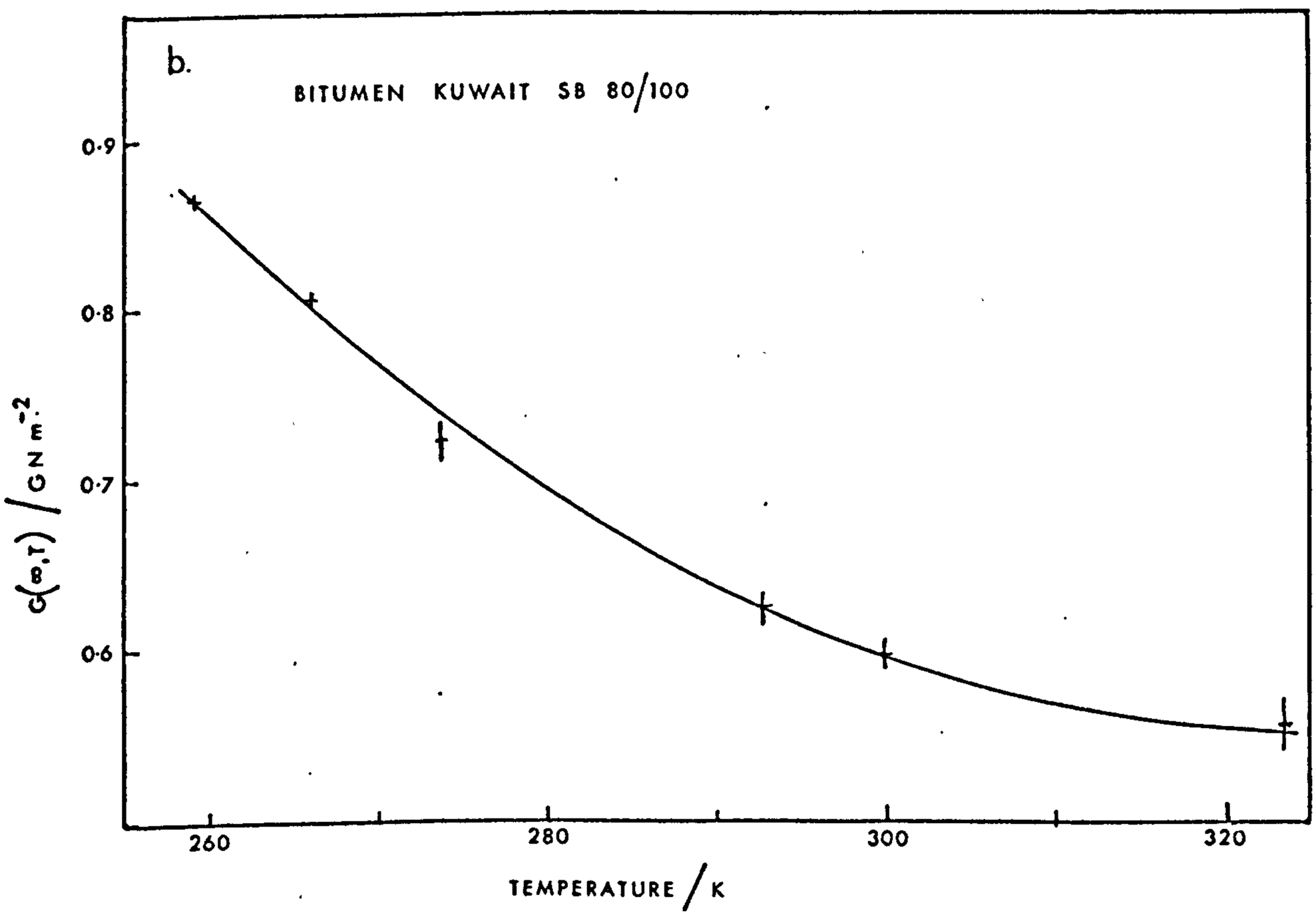

FIG. 4·1 THE VARIATION OF a. J(∞) AND b. G(∞) WITH TEMPERATURE.

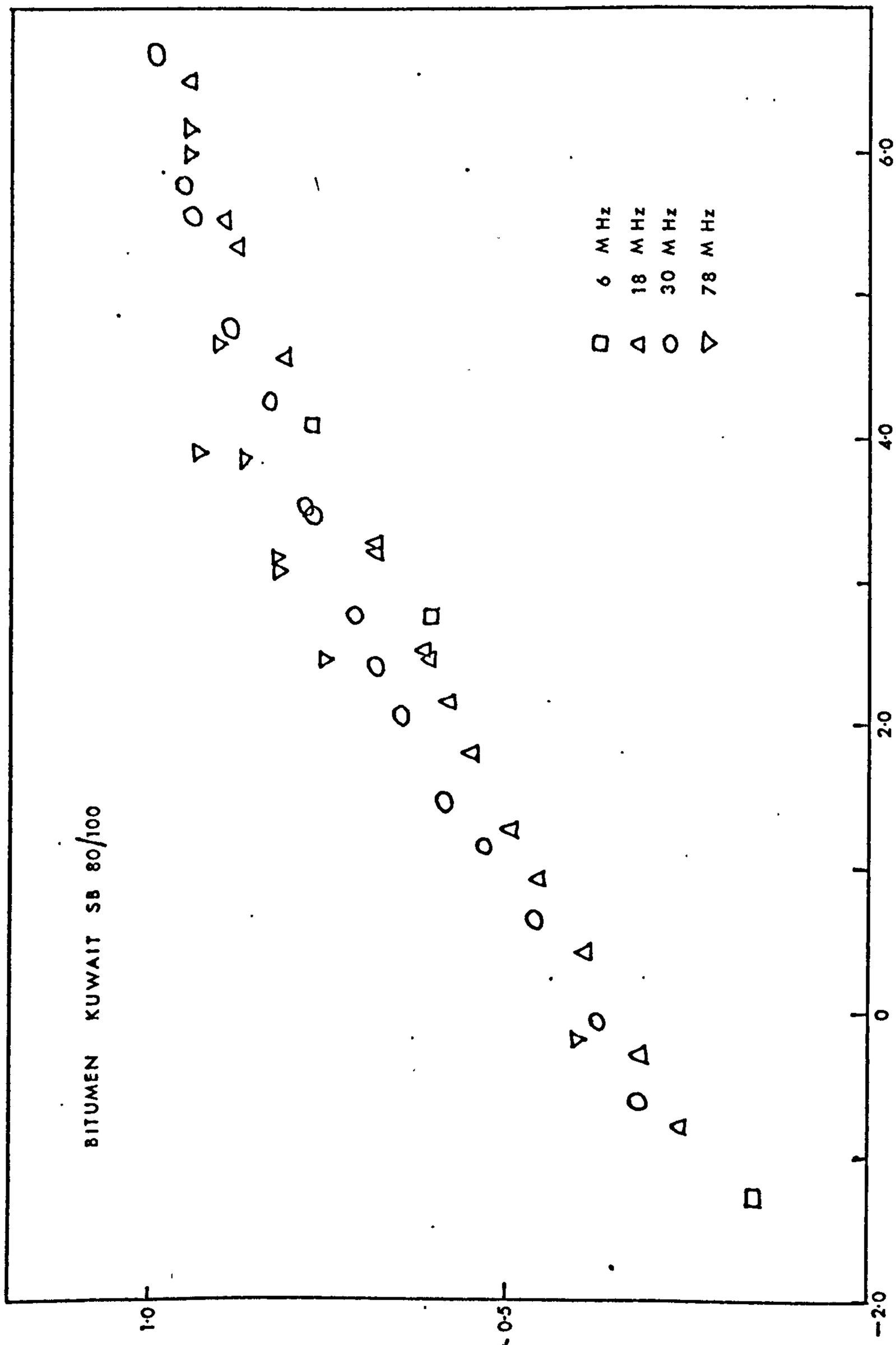

FIG. 4·2 REDUCED VARIABLES PLOT.

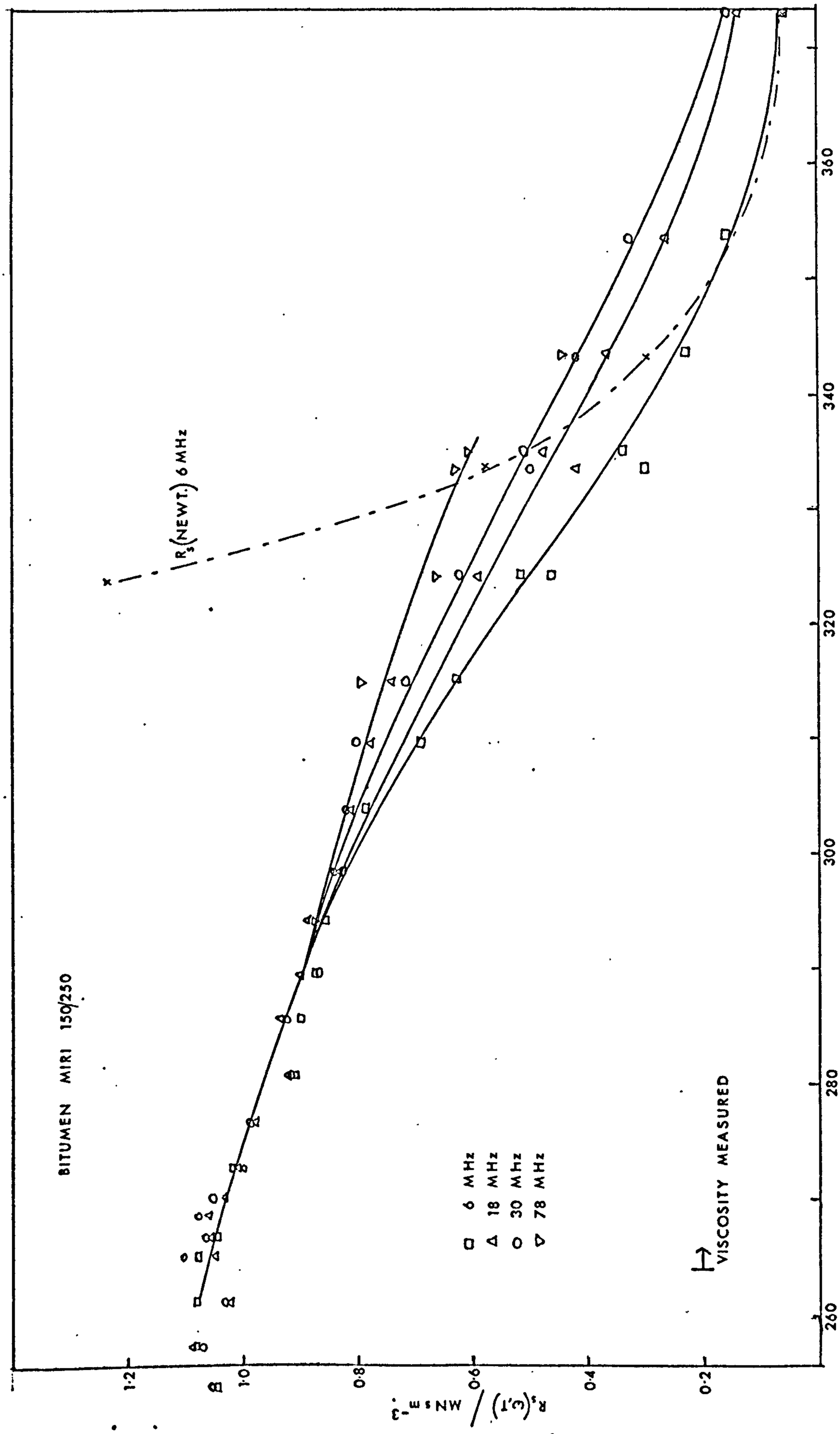

FIG. 4·3 THE VARIATION OF IMPEDANCE, R_s, WITH TEMPERATURE.

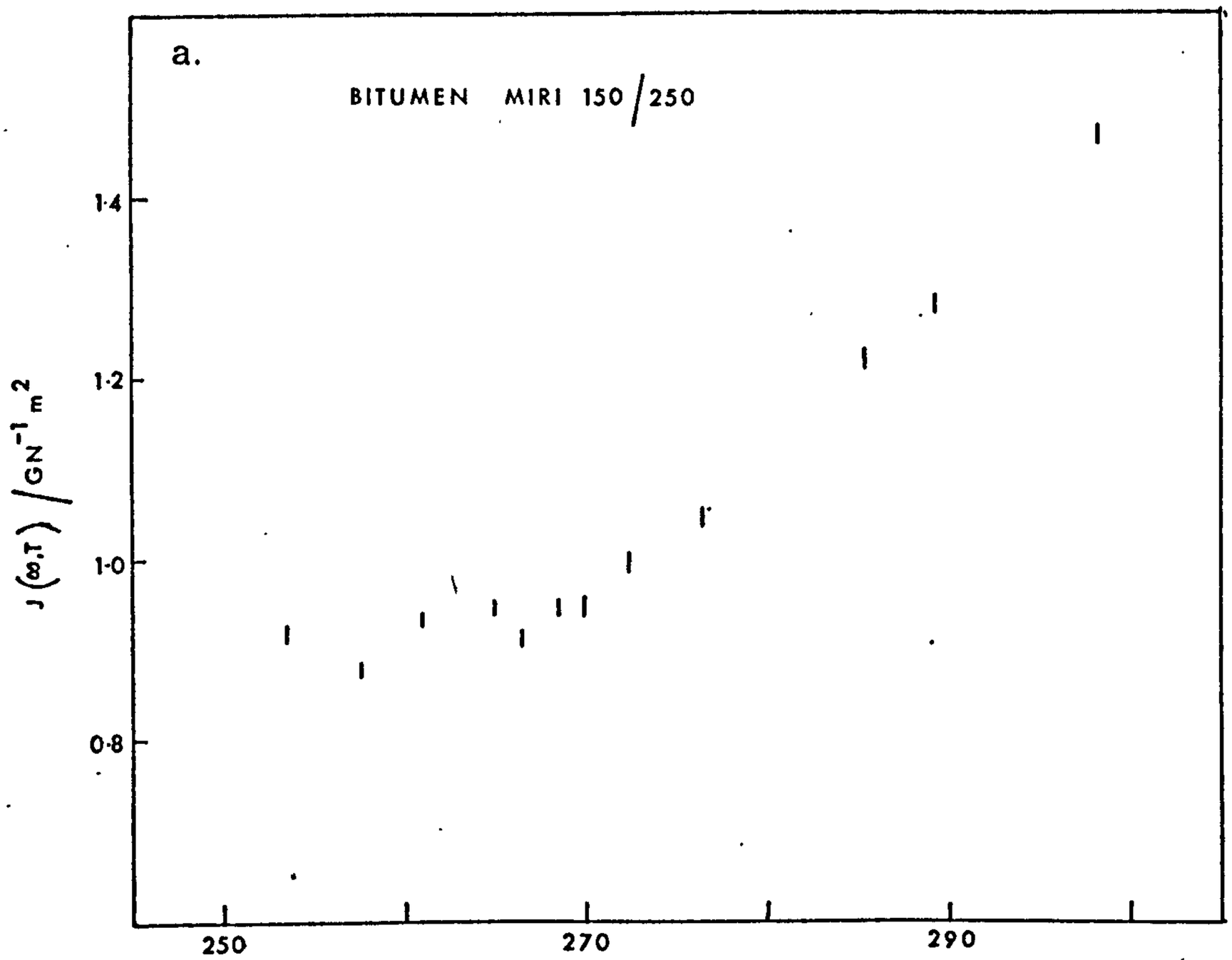

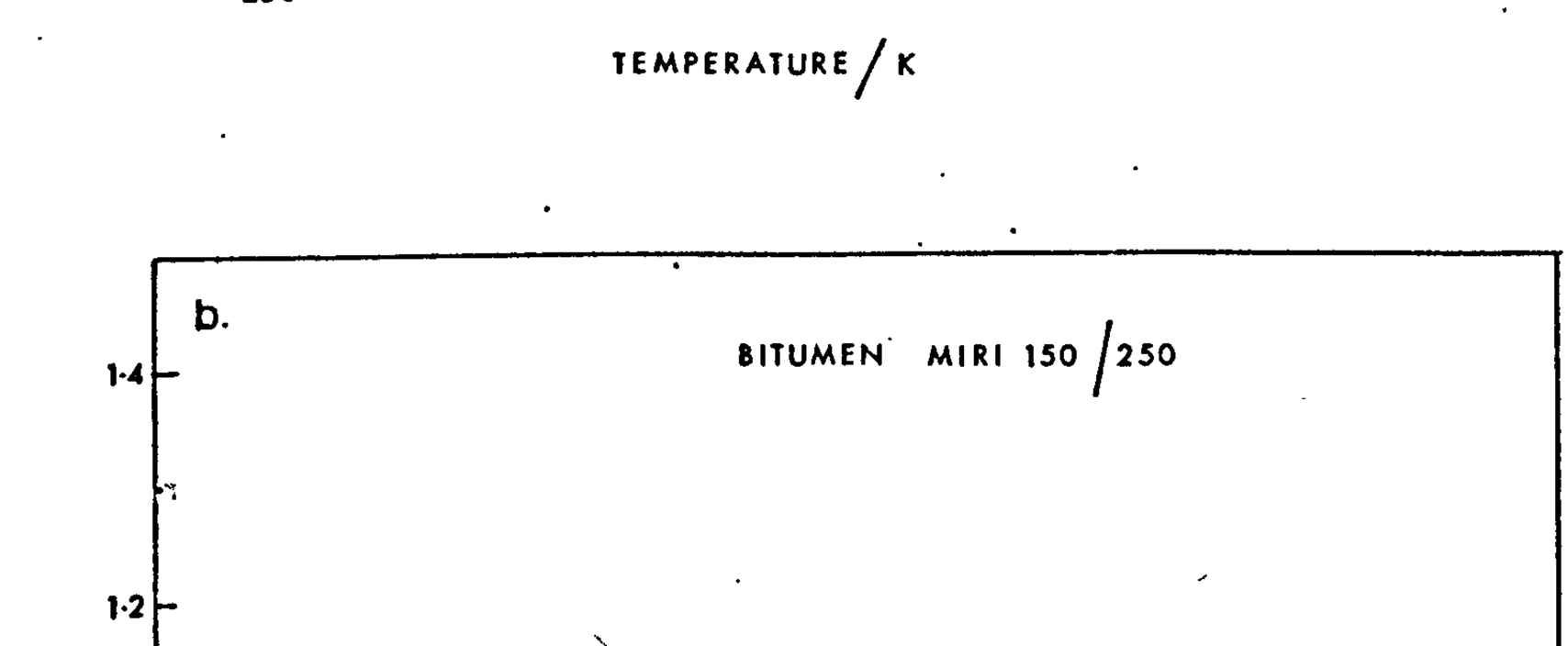

FIG. 4·4 THE VARIATION OF a. J(∞) AND b. G(∞) WITH TEMPERATURE.

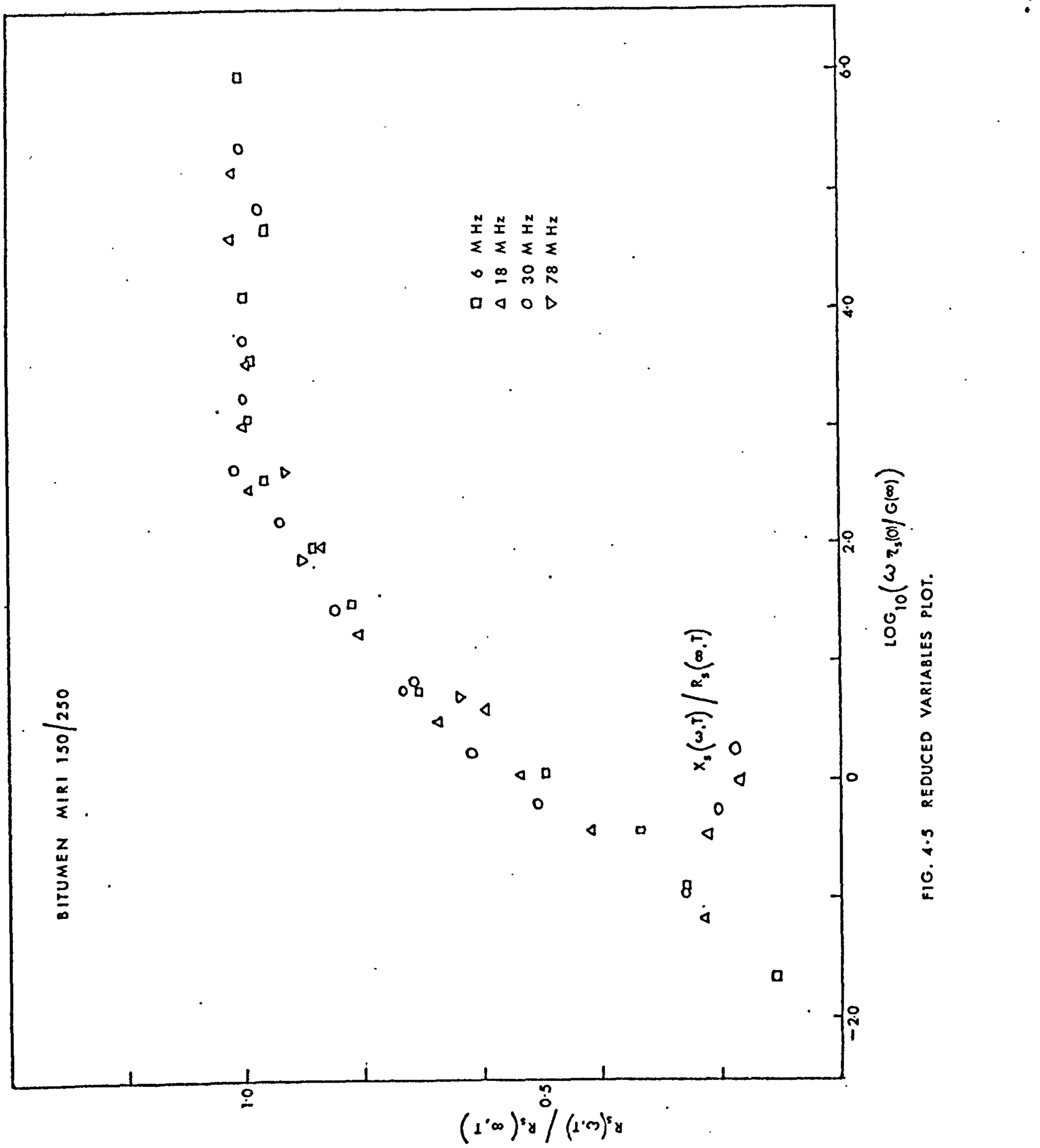

FIG. 4·5 REDUCED VARIABLES PLOT.

was shifted by -1 on the logarithm scale. The two samples gave very different reduced variables plots. Similar behaviour was found by Jongepier and Kuilman for various bitumens[49]. Sample (b) showed the behaviour of a typical organic liquid described as 'thermo-rheologically simple'[52]. If the reduced variables plot of sample (b) is compared with graph 1 in the back cover then it can be seen that it is identical to the B.E.L. model with a k value of 1.0. Sample (a) could not be reduced successfully and will be discussed in section 4.4. Comparing with graph 1 gave a k value between 4 and 5.

Values of the shear modulus lay between 0.5 and 1.0 GN m^{-2} over the temperature range measured. These values agree with the work of Jongepier and Kuilman[49] but not with the work of Isayev et al[48]. Isayev attributes the difference to the group composition and the quality of asphaltenes. Their properties are influenced by temperature and sample history[53]. The cooling of bitumen is accompanied by the formation of asphaltene associates[48]. For ease of handling it was necessary to heat the samples prior to applying to the quartz rod and then to cool to the required temperature. The samples had therefore undergone an ageing process prior to measurement. The value of the shear modulus was lower for sample (a) than sample (b).

4.4 Attempts to reduce variables for Kuwait SB 80/100.

From Figure 4.2 it can be seen that the results at different frequencies do not superimpose. The scatter is greater than for other liquids and the 6 MHz results are smaller than 18 MHz, the 18 MHz smaller than 30 MHz and so on. Barlow et al[12] showed that for a number of different liquids, the results for each liquid could be reduced onto a single curve, although the k values differed slightly from 1.0 for some liquids, except for castor oil which had a k value of 2.9. Although no previous work has been reported to show this breakdown of time-temperature superposition, many earlier results were obtained at only one frequency where the effect would not be seen.

A more critical assessment of the measurements was made and revealed some slight deviation from linearity of the amplitude versus reflection number graphs. [This was also noticed with other fluids measured]. Nevertheless, for this first liquid only the results which showed no deviation from linearity were retained. The effect of this was to reduce the number of 6 and 78 MHz results but with little effect on the reduced variables plot. After other liquids had been studied, and about four to twelve months after the first measurements, more measurements were obtained on sample (a) but no improvement in results was noticed. It is therefore concluded that this anomalous reduced variables plot is real and not caused by some instrument or operator fault. Plotting $R(\omega)$ against $\log(\omega\eta_s(0))$ instead of the more usual reduced variables showed the same effect. However, in the range $\log(\omega\eta_s(0))$ 9 to 14 the results at a fixed temperature had the same slope, giving

$$R(\omega) = M \log(\omega\eta_s(0)) + C \qquad ..(4.3)$$

where M is the slope independent of temperature and C is a constant dependent on temperature. If the temperature is altered then the viscosity changes and therefore C depends on the viscosity. To change C would require a new viscosity function but at present there is no reason to suspect that the viscosity function should be altered.

The value of k is frequency dependent, the higher the frequency the smaller the k value. Replacing ω by $f(\omega)$, where $f(\omega)$ is given by equation (4.4),

$$f(\omega) = \frac{\omega_x \cdot \omega_x}{\omega_{30}} \qquad ..(4.4)$$

where x refers to the frequency,

and plotting $R_s(\omega)/R_s(\infty)$ against $\log(f(\omega)\ \eta_s(0)/G(\infty))$ showed a trend in the right direction, but although the results could be reduced onto a single curve within experimental error, they were not random; the 18 MHz results were always below the 30 MHz results. The experimental

results could be synthesised by replacing k in the B.E.L. equation by $k(\omega)$, given by

$$k(\omega) = k + \left[\frac{\omega_{30}}{\omega_x} - 1\right] \qquad ..(4.5)$$

There is no physical or theoretical explanation for the above but it does suggest that the viscosity should depend on frequency. Barlow et al[54] found that for poly-1-butenes as the molecular weight increased the deviation from the B.E.L. model increased and they suggested that the relaxation mechanism involved only part of the steady flow viscosity. The steady flow viscosity can be calculated from the measured quantities using the B.E.L. model by the following equation

$$\eta_{cal.} = \frac{(R_s^2 + X_s^2)^2}{2\rho\omega X_s^2} \qquad ..(4.6)$$

The viscosity calculated from equation (4.6), see Appendix Table AIV.6, is less than the measured steady flow viscosity and decreases with increase in frequency. Replacement of $\eta_s(0)$ by $\eta_{cal.}$ or the dynamic viscosity (η') would increase the difference between the results at different frequencies. When $\eta_s(0)$ was replaced by the ratio $\eta_s(0)/\eta_{cal.}$, the few results obtained gave a better reduced plot with a slightly lower k value. Two things must be borne in mind before too much emphasis is put on the last result, namely the inaccuracy in the measured values of R_s and, particularly, X_s leading to inaccuracy in $\eta_{cal.}$ and equation (4.6) which assumes k is equal to 1.0.

4.5 Physical Characteristics.

The two samples were different in appearance, sample (b) resembled treacle whereas sample (a) was a darker, heavier material with less lustre. During sample preparation, sample (a) gave a deposit with hydrocarbon solvent but this was not seen with sample (b). A fine precipitate was obtained from sample (b) when pentane was used as solvent. The precipitate from sample (a) was filtered off to give a black

crystalline material (m.p. > 473.2 K, 17.3%). The infrared spectrum (3.46% $^{w}/_{v}$ in CCl_4, 0.1 mm) was that of an aliphatic hydrocarbon. This solid material may have been present in the original sample or precipitated by the solvent. It was impossible to obtain without pre-treatment a suitable film for the optical microscope. The sample was frozen in liquid nitrogen and fractured to give a good surface for electron microscopy. The pretreatment for the scanning electron microscope involves the deposition of an electrical conducting surface layer which is accomplished under vacuum. During this process the samples were distorted and also under the electron beam the samples tended to melt. It was possible to see fragments on the surface of sample (a) but not on sample (b). Electron probe microanalysis of these fragments showed them to contain traces of calcium, silicon, magnesium, aluminium and chlorine, together with a reduction in the sulphur content compared to a part of the surface free of the fragments. Analysis of the crystalline material showed only a trace of sulphur, much less than obtained in the bulk sample. From the electron microprobe analysis there does appear to be additional material in sample (a) but the evidence is not conclusive.

The wavelength of the shear waves used is about 0.5 mm at 6 MHz falling to 0.04 mm at 78 MHz. If the particles in the bitumen were of similar size to the wavelength some scattering may occur, particularly if the particles migrated to the surface on cooling. The effect of this would be for R_s to be increased the higher the frequency. This may account for the results. At low frequencies (100 Hz) as used by Jongepier[49] the wavelength would be about 10 meters, very much larger than the size of any particles which may be present.

4.6 Discussion.

The shear wave is attenuated by exp (-2π) per wavelength[55] and therefore penetrates to a depth less than the wavelength. Only the surface layer is being investigated with the shear waves whereas the

the shear viscosity is that of the bulk material. It is conceivable that the viscosity of this surface layer is not equal to that of the bulk material. The viscosity at the surface could be less than that of the bulk, bitumens are known to 'sweat', i.e. a layer of oil is seen on the surface, particularly after air blowing (a technique used to produce rubbery bitumens). However, it is not so easily understood that the surface viscosity could be higher than that of the bulk sample which would imply that particles were suspended in the surface layer or some change in the nature of the surface.

Following up these two possibilities, if the viscosity was lower at the surface the points on the reduced variables plot (Figure 4.2) would be shifted to the left and may be reduced on to the B.E.L. curve with k = 1, i.e. equivalent to sample (b). At high temperatures the points do lie on this curve, but as the temperature is lowered the situation gets worse requiring a greater difference between the viscosity of the surface and that of the bulk. The other possibility where the surface viscosity is higher than the bulk sample would move the points on the reduced variables plot to the right, i.e. on the curve with k = 8. Also, as the temperature is lowered the situation gets better, this would be expected since the movement of particles would be restricted. Assuming this latter situation, the viscosity was calculated which would reduce the values onto a curve with k = 8. The logarithm of viscosity was found to decrease linearly with depth of penetration. At lower temperatures the values are lying on the curve with k = 8.

Discussions with experts in Bitumen Chemistry[56] indicated that the surface viscosity would probably be lower than the bulk value. It was suggested that high frequency shear measurements should be made on a sample of the bitumen (a) from which the asphalt was removed. (Asphalt content, sample (a) ~10%, sample (b) 0.02%). The asphalt was removed by precipitation with petroleum spirit 60-80 and the petrol removed from the filtered solution by a vacuum rotary evaporator.

Because of the limited sample size measurements were made at 293.2, 298.2 and 313.5 K and the viscosity was measured with a Hallikainen micro viscometer[56]. At 298.2 and 313.5 K the R_s values were lower than for the untreated bitumen but at 293.2 K they were closer to the original values at the same temperature, the viscosities were also lower than the original viscosities at the same temperatures. The limited number of results prevented the calculation of $R(\infty)$ and $G(\infty)$, therefore the values were plotted on the graph of $R(\omega)$ against $\log_{10}(\omega\eta_s(0))$ obtained previously. The values superimposed on the previous results, although shifted down the curve, but not on the graph of the Miri results. It is therefore doubtful whether the asphalt can be the cause of the anomalous results; the petrol treatment would also remove any inorganic material which may have been present.

The only explanation for the results of the Kuwait SB 80/100 bitumen sample is probably that the surface of the sample changes with temperature. At the higher temperatures the results fall onto a curve predicted by the B.E.L. model with $k = 1$, thus showing the presence of a commonly-observed distribution of relaxation times. However, at lower temperatures the distribution of relaxation times widens. On the other hand, in sample (b) (Miri 150/250) the distribution does not change as the temperature is lowered. Miles and Hamamoto[61] found for hexachloro-biphenyl that the width of the distribution was temperature dependent with a broader distribution at lower temperatures.

4.7 Conclusions.

The present work has shown some unexpected features for certain bitumens compared with other organic fluids. Nevertheless, the findings in no way contradict previous work[49]. The value of the shear modulus (~ 1 GN m^{-2}) is in agreement with other fluids and varies slowly with temperature. It is seen that the value of k in the B.E.L. model (k is a parameter which depends on the width of the distribution of relaxation times) increases with decrease in frequency. (For much lower frequencies[49]

k was 8). In this work there appears to be a breakdown of the Time Temperature Superposition.

However, further work would be required before any firm conclusions could be reached, i.e. the frequency range should be extended to cover the region 100 Hz to 1 MHz and also various particle sizes should be dispersed in a bitumen type medium. This would require a knowledge of all components present in bitumen and the effect of temperature on the migration of these components.

CHAPTER V

SHEAR AND LONGITUDINAL MEASUREMENTS

5.1 Introduction

The samples chosen for investigation must satisfy certain criteria, namely they should be fairly viscous at ambient temperature and should remain liquid or in a glassy state until a viscosity of 10^5 Nsm^{-2} is reached. There should be no phase change throughout a series of measurements at varying temperatures and pressures. They should be inert to normal atmospheric conditions and the surface should be representative of the bulk sample. The following three liquids were chosen.

A. 4-phenyl dibenzofuran

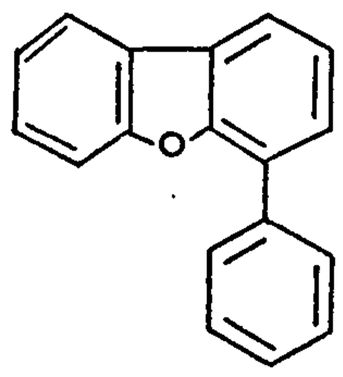

I

4-phenyl dibenzofuran(I) (m.p. 307-308 K, b.p. 676 K) was known from previous industrial experience to supercool. Details of the preparation are given in Appendix III. It is a pale yellow viscous liquid at ambient temperature and at all temperatures at which measurements were made there was no evidence of crystallisation in the sample. The 1, 2 and 3-phenyl dibenzofurans have much higher melting points with the lowest as expected for the 1-phenyl dibenzofuran. The ultraviolet absorption spectrum showed that there is hindrance to conjugation in the 1 and 4 phenyl substituted derivatives of dibenzofuran. The lowering of the melting point in the 4 phenyl derivative is thought to be due to the ortho hydrogen atoms of the phenyl group interfering with the bulky heterocyclic atom and therefore twisting the phenyl ring out of the plane of the dibenzofuran nucleus.

Thermogravimetric analysis (T.G.A.) showed it to be stable in air to 473 K and Differential Thermal Analysis (D.T.A.) gave a glass transition temperature of about 257 K.

B. Epoxy Resin MY 750 (ex Ciba Geigy)

The major component determined by Nuclear Magnetic Resonance (N.M.R.) was diglycidyl ether of bisphenol A (II).

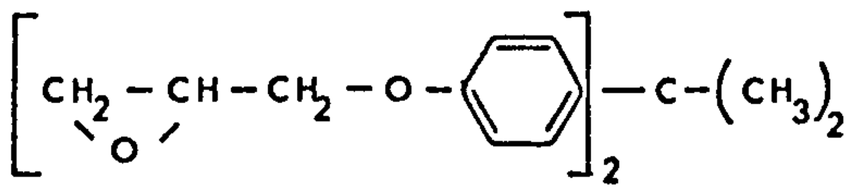

II

Mass Spectrometric analysis showed smaller amounts of material of higher molecular weight but of similar structure and a chlorohydrin - probably partially reacted starting material. It is a pale yellow viscous liquid at ambient temperature and there was no evidence for crystallisation at any temperature or pressure at which it was used. T.G.A. showed it to be stable to 513 K and the glass transition temperature determined by D.T.A. was about 264 K.

C. Styrene ethylene-propylene copolymer (S.E.P.) in Di-2-ethylhexyl phthalate

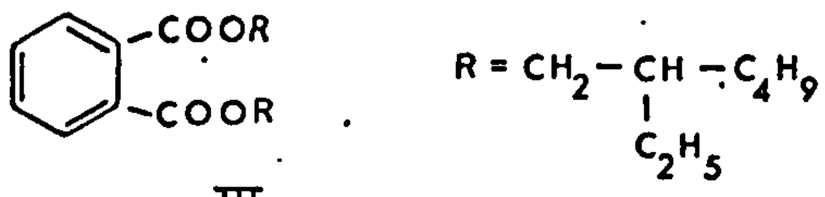

III

The preparation of this solution is given in Appendix III. Di-2-ethylhexyl phthalate(III)(ex Lankro Chemicals Ltd.) which is used as a synthetic lubricant has been investigated by others[16,28,57]. S.E.P. is a block copolymer of styrene ($\bar{M}n$ = 30,000) and ethylene propylene ($\bar{M}n$ = 50,000) $\bar{M}w/\bar{M}n \sim 1.2$. Polymers are frequently added to lubricating oils to improve the viscosity characteristics and S.E.P. is such a polymer. The glass transition temperature determined by D.T.A. was 190 ± 3 K.

In the remaining part of this chapter the experimental results are given in the following order, 4-phenyl dibenzofuran, Epoxy Resin MY 750 atmospheric and high pressures and finally S.E.P. in Di-2-ethylhexyl phthalate at atmospheric and high pressures.

5.2 4-phenyl dibenzofuran

The density was measured at five temperatures between 298.2 K and 353.2 K and found to vary linearly with temperature according to equation (5.1).

$$\rho = A + BT \qquad ..(5.1)$$

Numerical values of A and B are given in Table AV.1. The viscosity was measured between 290 K and 340 K and the values fitted to Roelands'[44] equation, the parameters of which are given in Table AV.2. Plotting the logarithm of viscosity against reciprocal temperature gave two straight lines intersecting at 0.5 Nsm^{-2} and 307 K with an activation energy for viscous flow at the higher temperatures of 32 kJ. The density and viscosity equations are used to interpolate and extrapolate to temperatures at which measurements were not obtained.

The absorption coefficient and velocity of the longitudinal waves were determined as a function of temperature and the results are listed in Table AV.6. Figures 5.1 and 5.2 show the absorption coefficient and velocity as a function of temperature respectively. The low frequency velocity was found to vary linearly with temperature, parameters of the linear equation are given in Table AV.5. The high frequency velocity was also assumed to vary linearly with temperature according to equation (5.2).

$$V(\infty)/ms^{-1} = 3931.1 - 6.10\ T/K \qquad ..(5.2)$$

Both linear equations (V(0) and $V(\infty)$) are used to extrapolate to the relaxation region. The absorption shows the expected increase followed by a decrease and the velocity shows a dispersion with decrease in temperature, typical of a structural relaxation. The logarithm of maximum α/f^2 was found to vary linearly with the logarithm of frequency as given by Mishra and Singh[23] and also to have very similar values.

Results of the normal incidence measurements to give the resistive or real part of the shear impedance are given in Table AV.7

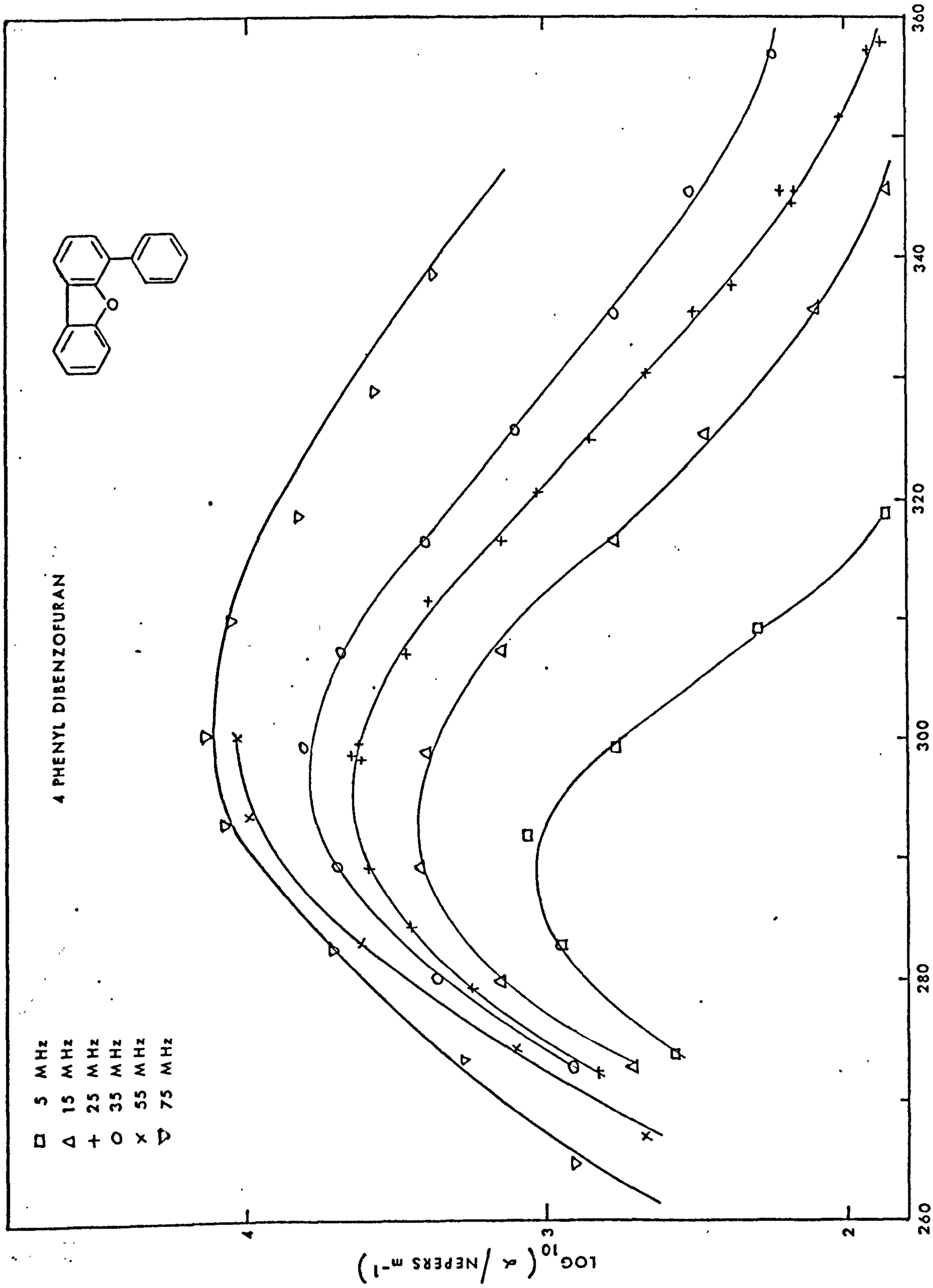

FIG. 5·1 THE VARIATION OF ABSORPTION COEFFICIENT, α, WITH TEMPERATURE

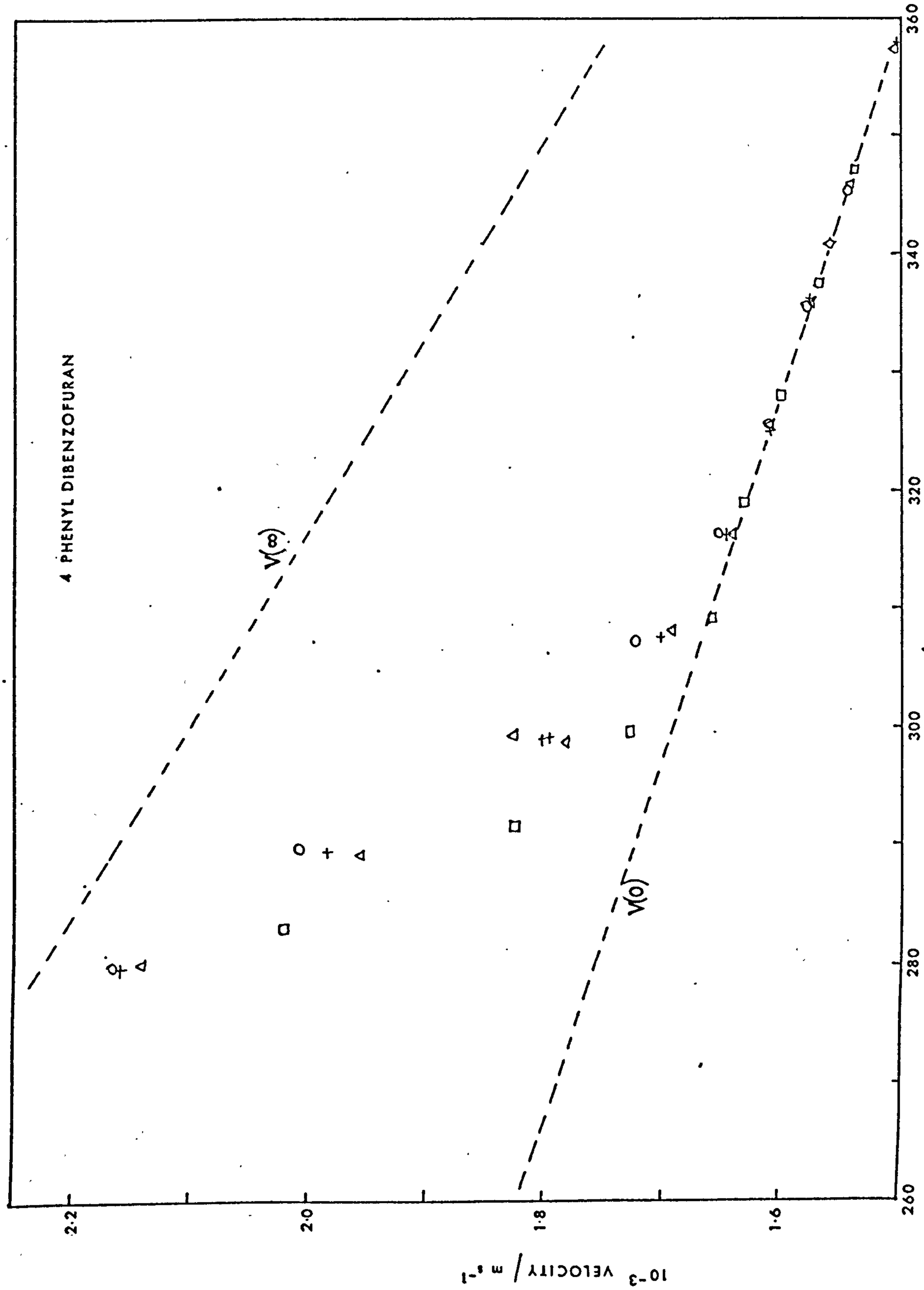

FIG. 5·2 THE VARIATION OF LONGITUDINAL SOUND VELOCITY WITH TEMPERATURE

and illustrated in Figure 5.3. The figure shows the typical visco-elastic response. The dashed line gives the values of R_s (calculated from equation 2.43) as a function of temperature assuming a Newtonian liquid at a frequency of 78 MHz. A few values were obtained of the reactive part of the shear impedance, these were used to calculate the dynamic viscosity ($\eta'(\omega)$) and storage modulus ($G'(\omega)$) which are given in Table AV.8. $G(\infty)$ was calculated from the low temperature values of R_s and the density. The variation of $G(\infty)$ and $J(\infty)$ with temperature are illustrated in Figure 5.4 which shows the compliance to vary linearly with temperature, the parameters for the linear equation are given in Table AV.9. The reduced variables plot, shown in Figure 5.5, was obtained from the values given in Table AV.11. Superimposing graph I (contained in the back cover) shows that the results can be described by the B.E.L. model with a k value just less than 1.0.

5.3 Epoxy Resin MY 750.

5.3.1 Atmospheric pressure.

The density was measured at eleven temperatures between 293.2 K and 358.2 K and found to vary linearly with temperature. The values of the viscosity determined at twelve temperatures between 288 K and 356 K were fitted to Roelands' equation. Parameters for the density and viscosity equations are given in Tables AV.1 and 2 respectively. The graph of logarithm of viscosity against reciprocal temperature gave two straight lines intersecting at ~ 0.5 N s m^{-2} and 319 K and the activation energy of viscous flow at the higher temperatures was 25.7 kJ.

The absorption coefficient and velocity were measured at temperatures between 270 K and 360 K. The values are given in Table AV.12. The low frequency velocity was found to vary linearly with temperature, the parameters of the equation are given in Table AV.5. At low temperatures, < 280 K, the velocity was measured using the normal incidence technique, values obtained were more scattered than the low

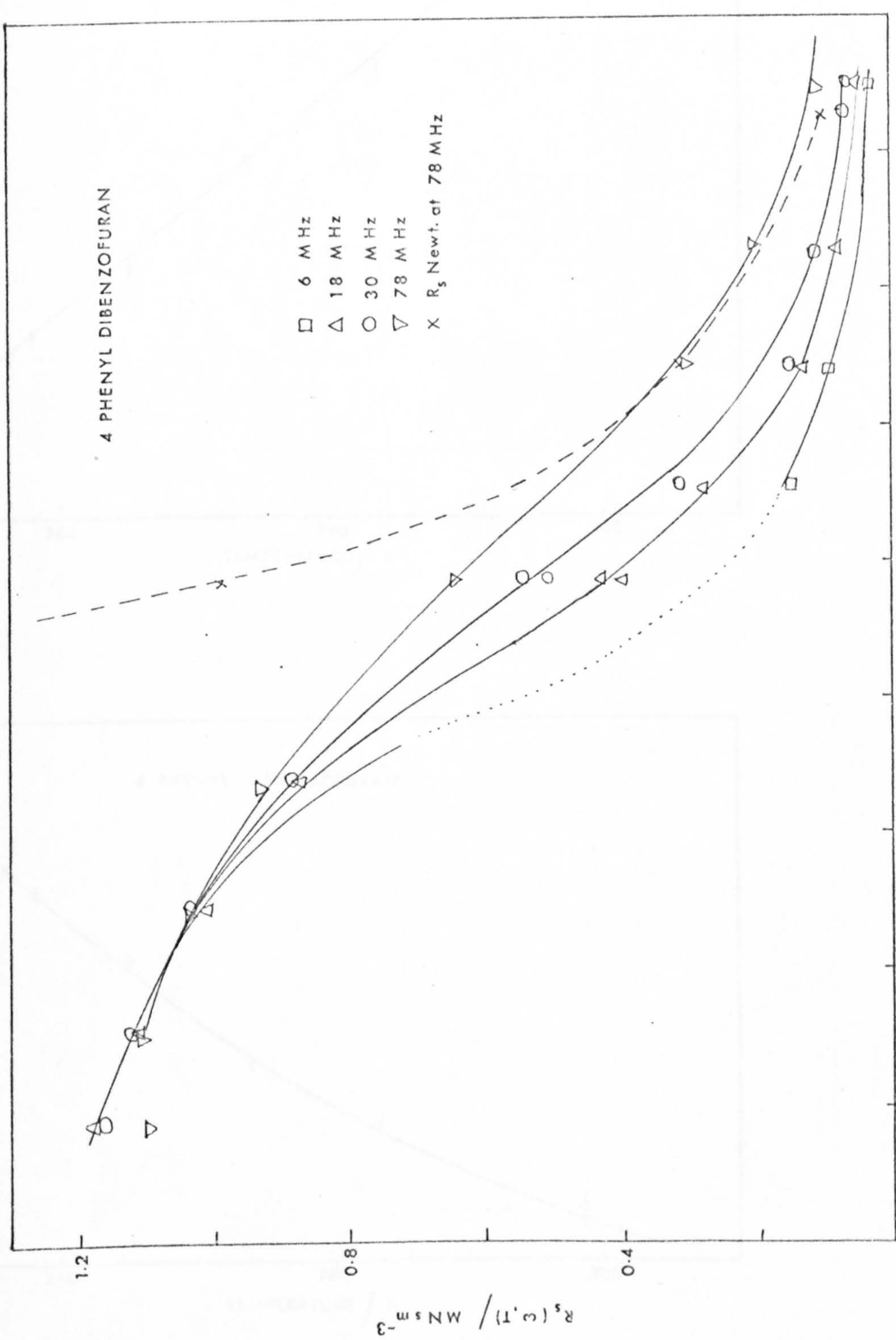

FIG. 5·3 THE VARIATION OF THE SHEAR IMPEDANCE, R_s, WITH TEMPERATURE.

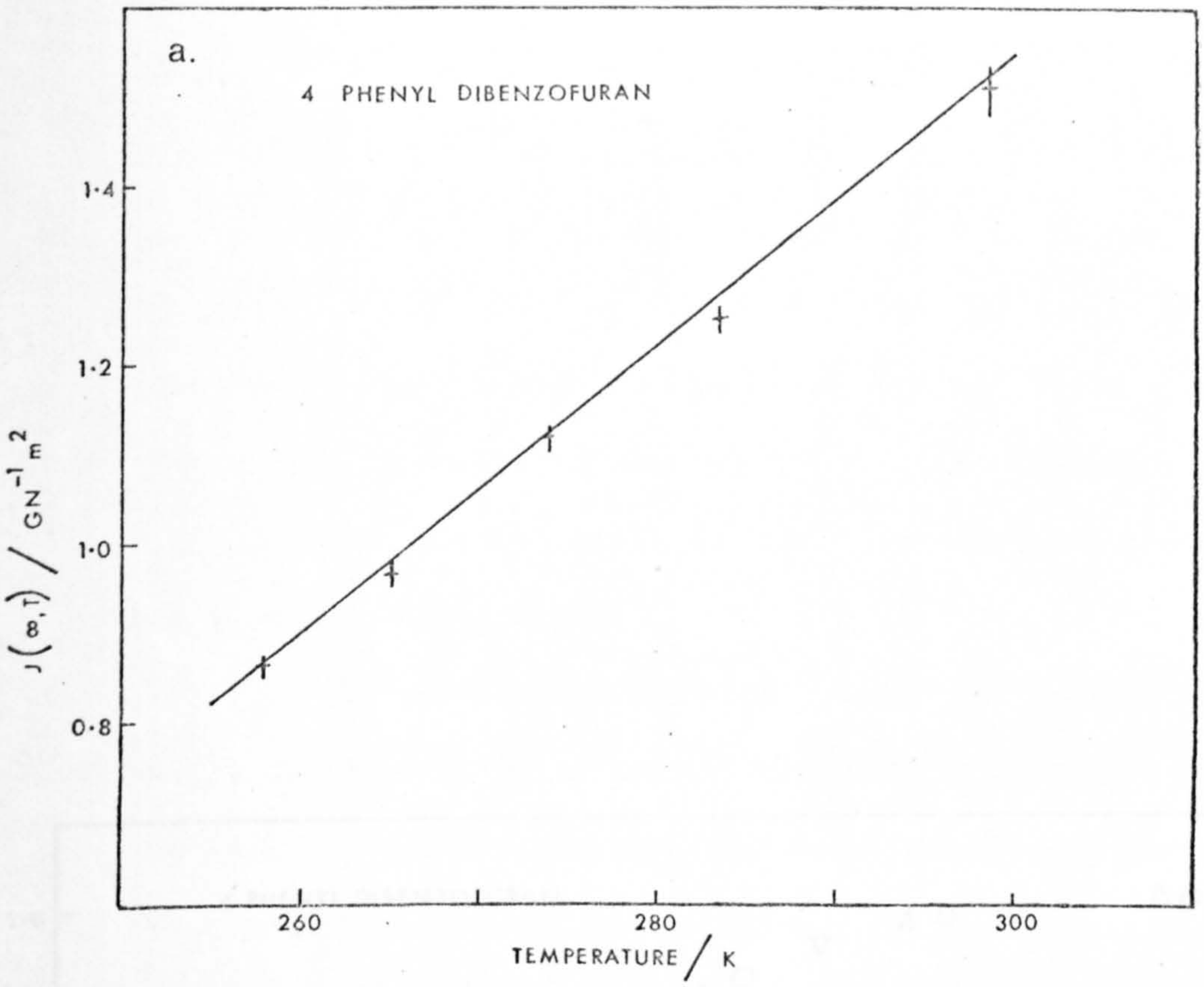

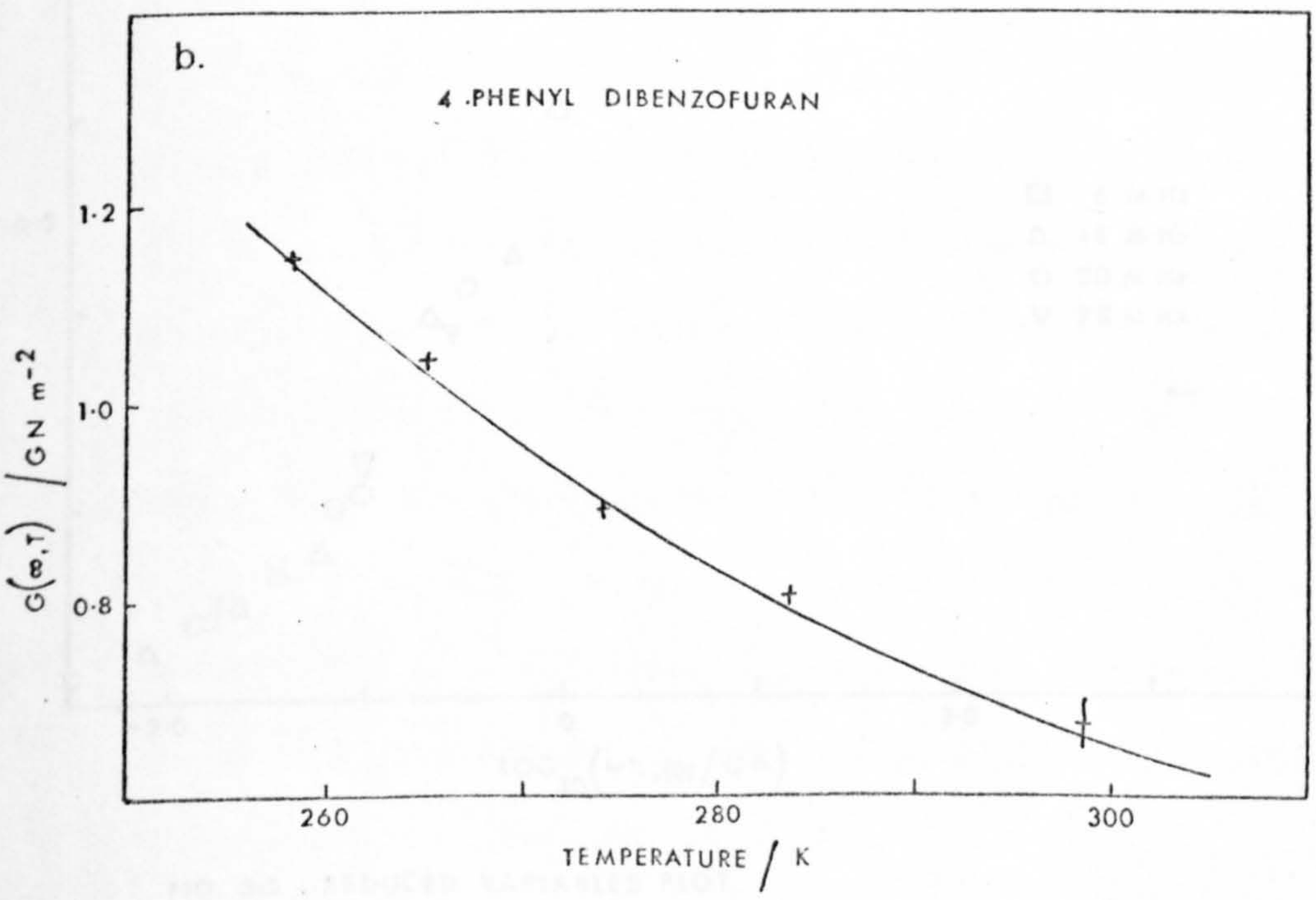

FIG. 5·4 THE VARIATION OF a. SHEAR COMPLIANCE, $J(\infty,T)$, AND b. SHEAR MODULUS, $G(\infty,T)$, WITH TEMPERATURE.

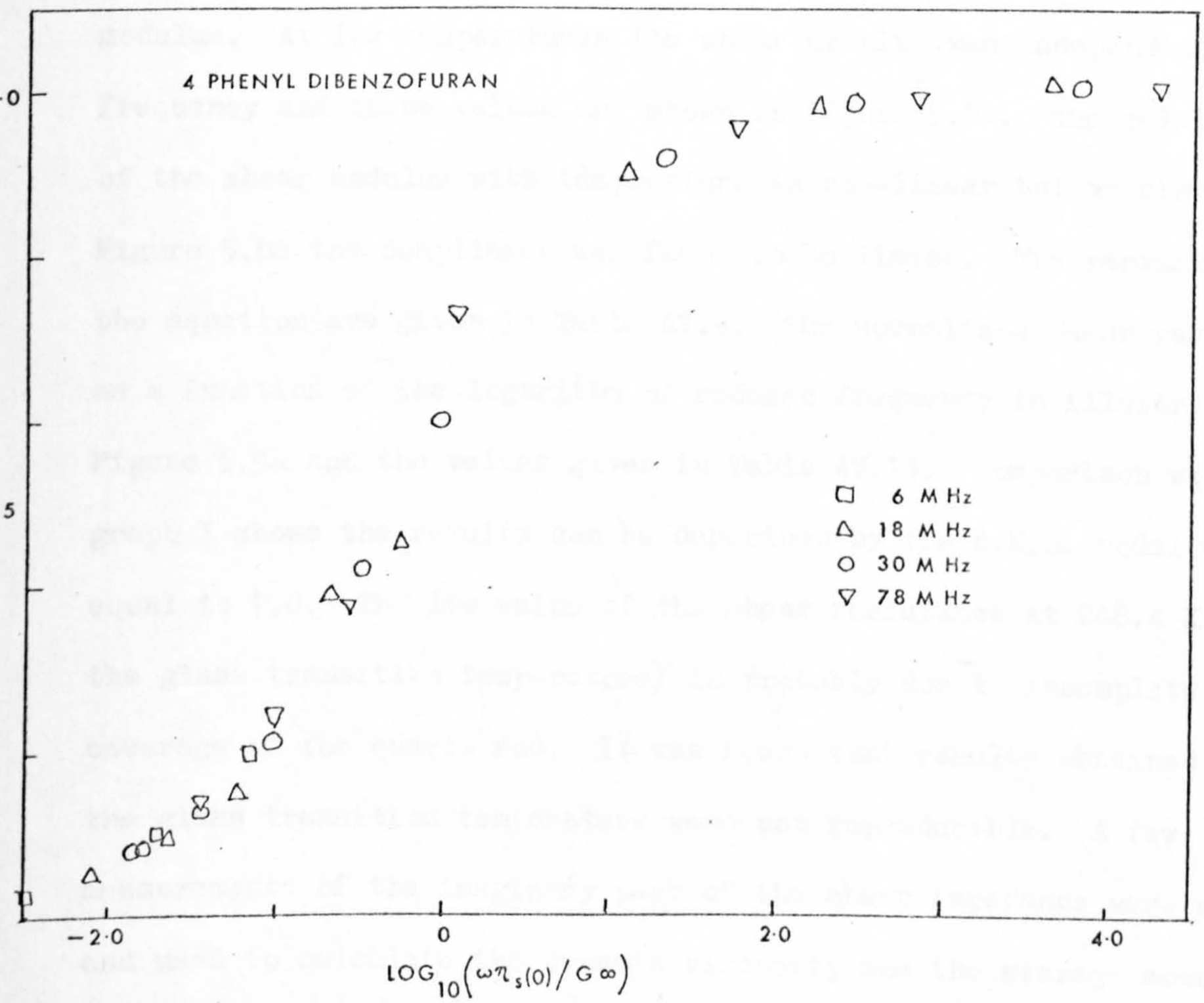

FIG. 5·5 REDUCED VARIABLES PLOT.

frequency velocity values obtained at higher temperatures. The values of the velocity at low temperatures were fitted to a linear equation to give

$$V(\infty)/ms^{-1} = 4322.2 - 7.52\ T/K \qquad ..(5.3)$$

Figures 5.6 and 5.7 illustrate the absorption coefficient and velocity as a function of temperature respectively. The dashed lines give the variation of V(0) and V(∞) obtained by extrapolating the linear equations. The figures show that a structural relaxation is taking place. The logarithm of maximum α/f^2 plotted against logarithm of frequency was found to be linear and to concur with the values obtained for 4-phenyl dibenzofuran.

The real part of the shear impedance (values given in Table AV.13) together with the density was used to calculate the shear modulus. At low temperatures the shear modulus was independent of frequency and these values are shown in Figure 5.8b. The relationship of the shear modulus with temperature is non-linear but as shown in Figure 5.8a the compliance was found to be linear. The parameters for the equation are given in Table AV.9. The normalized shear resistance as a function of the logarithm of reduced frequency is illustrated in Figure 5.9a and the values given in Table AV.14. Comparison with graph I shows the results can be described by the B.E.L. model with k equal to 1.0. The low value of the shear resistance at 248.4 K (below the glass transition temperature) is probably due to incomplete coverage of the quartz rod. It was found that results obtained below the glass transition temperature were not reproducible. A few measurements of the imaginary part of the shear impedance were made and used to calculate the dynamic viscosity and the storage modulus, the results are given in Table AV.8.

5.3.2 Pressures above atmospheric.

Figure 5.10 shows the variation of density with pressure at

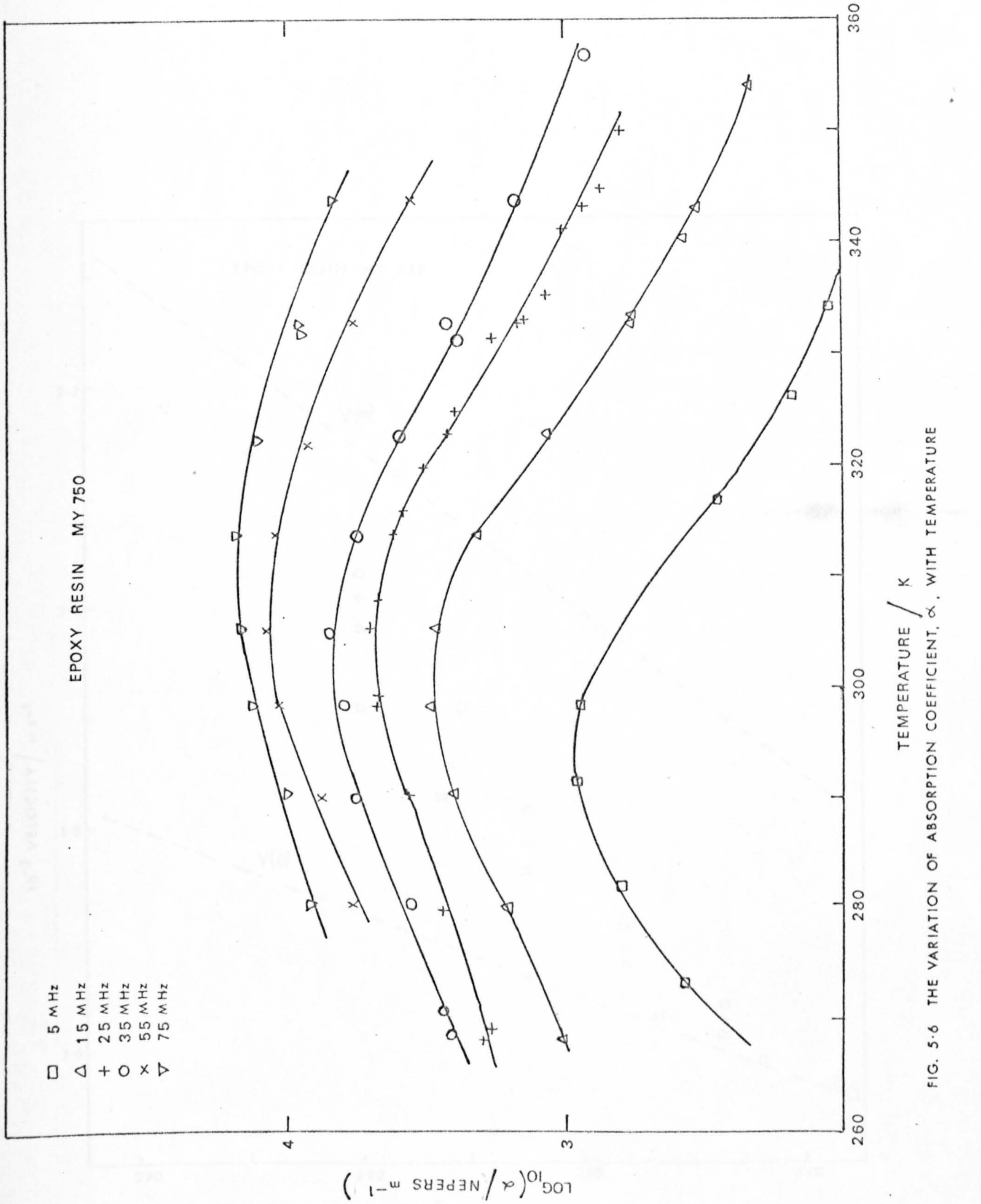

FIG. 5·6 THE VARIATION OF ABSORPTION COEFFICIENT, α, WITH TEMPERATURE

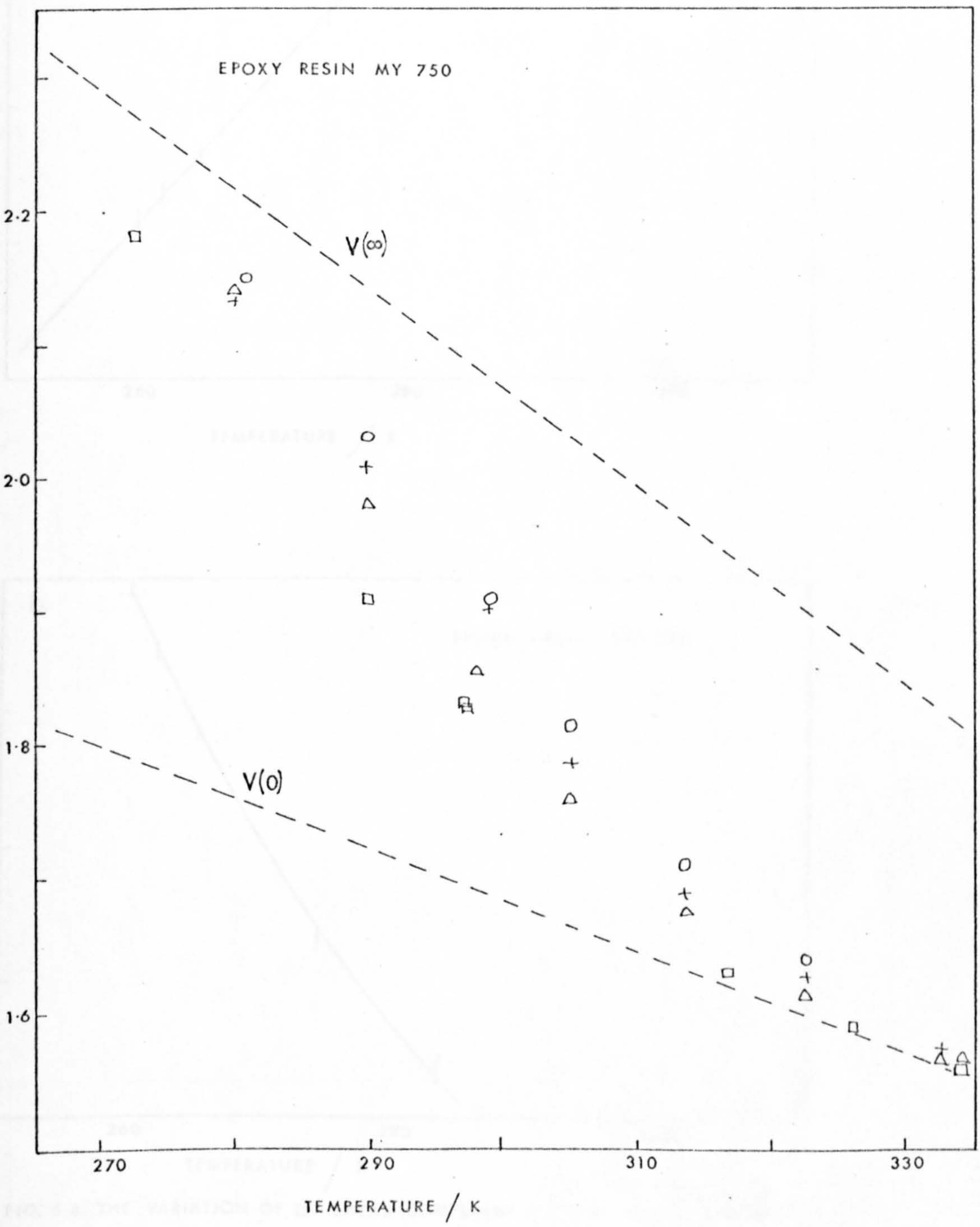

FIG. 5·7 THE VARIATION OF LONGITUDINAL SOUND VELOCITY WITH TEMPERATURE

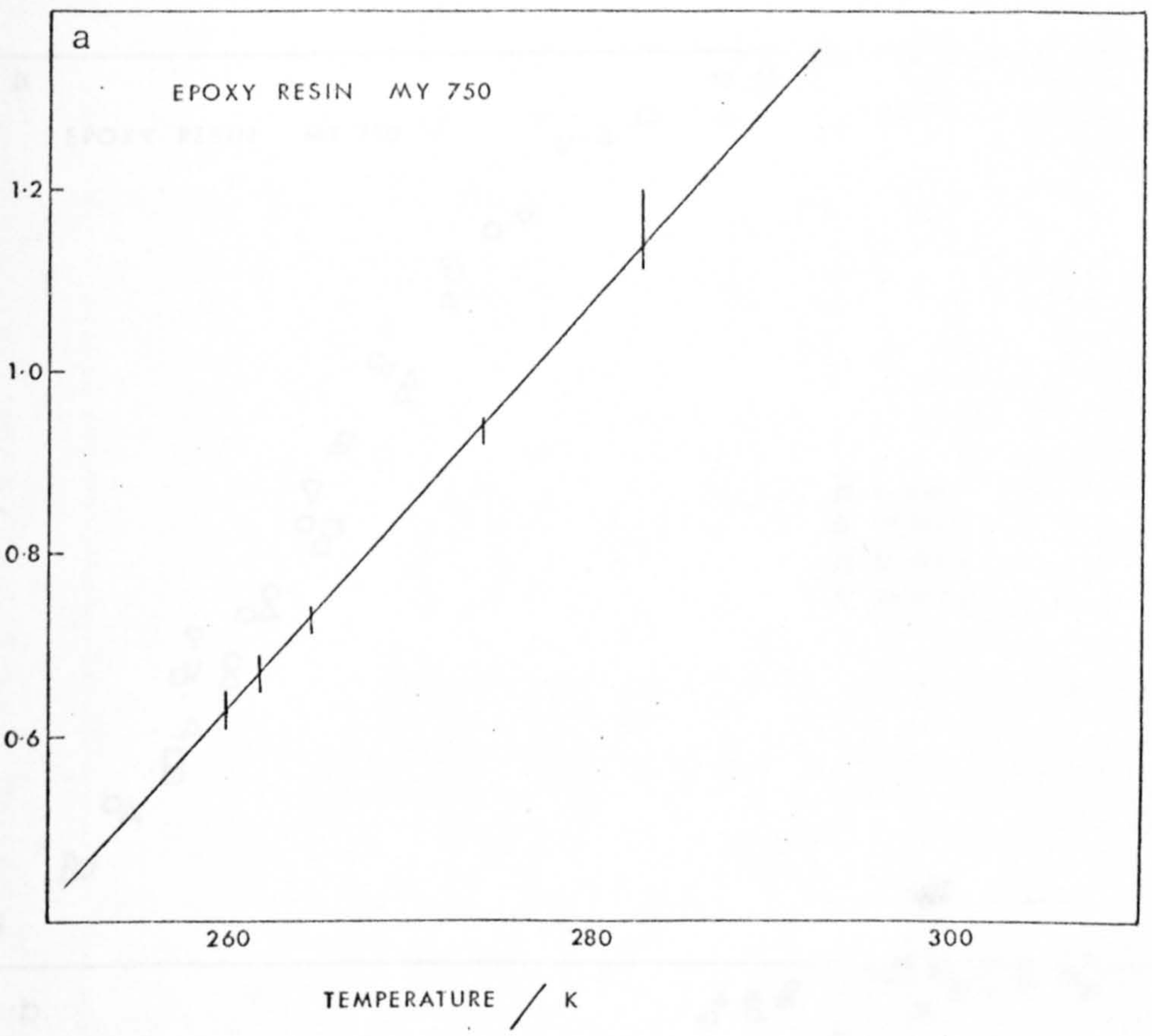

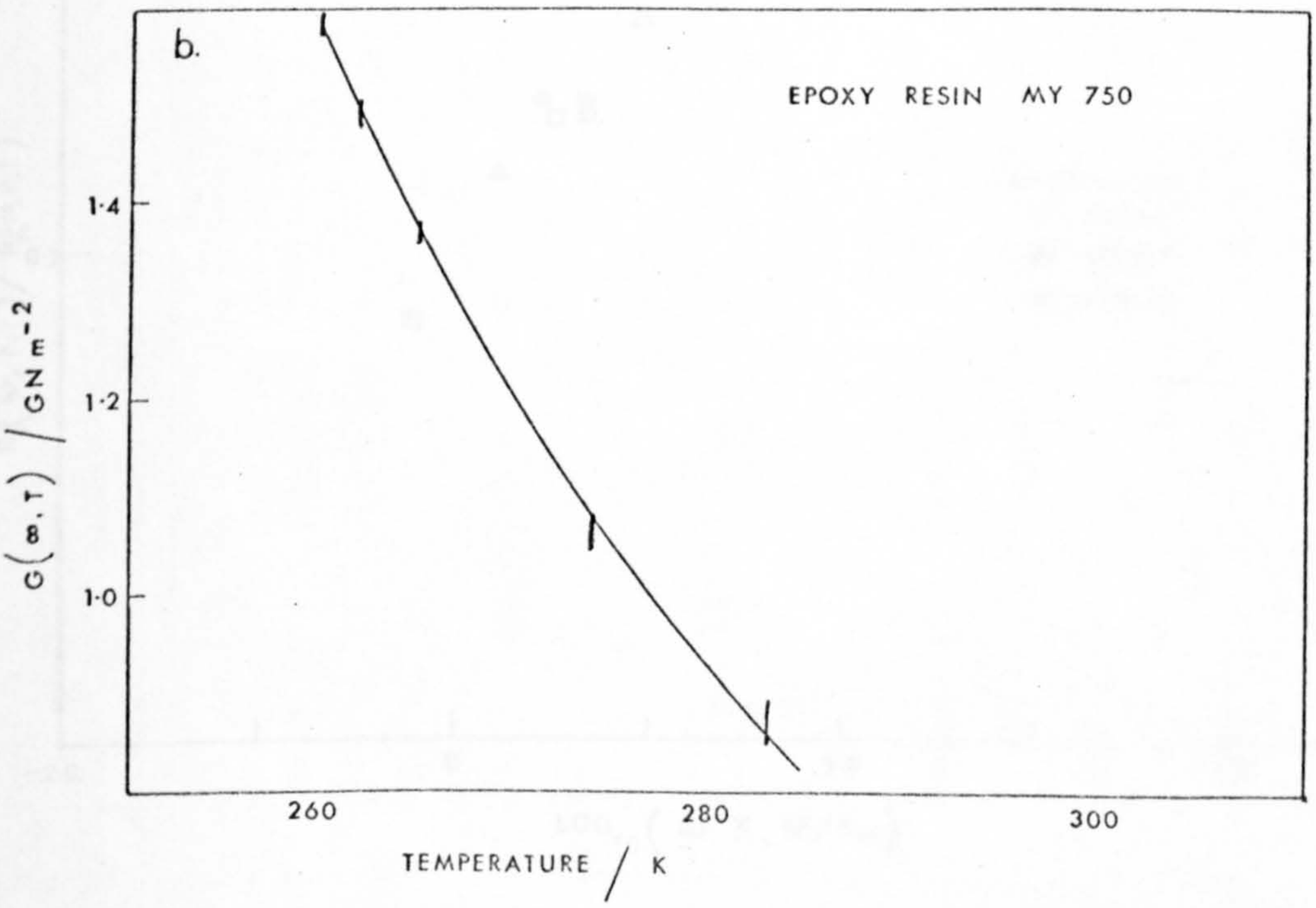

FIG. 5·8 THE VARIATION OF a. SHEAR COMPLIANCE, $J(\infty,T)$, AND b. SHEAR MODULUS, $G(\infty,T)$, WITH TEMPERATURE

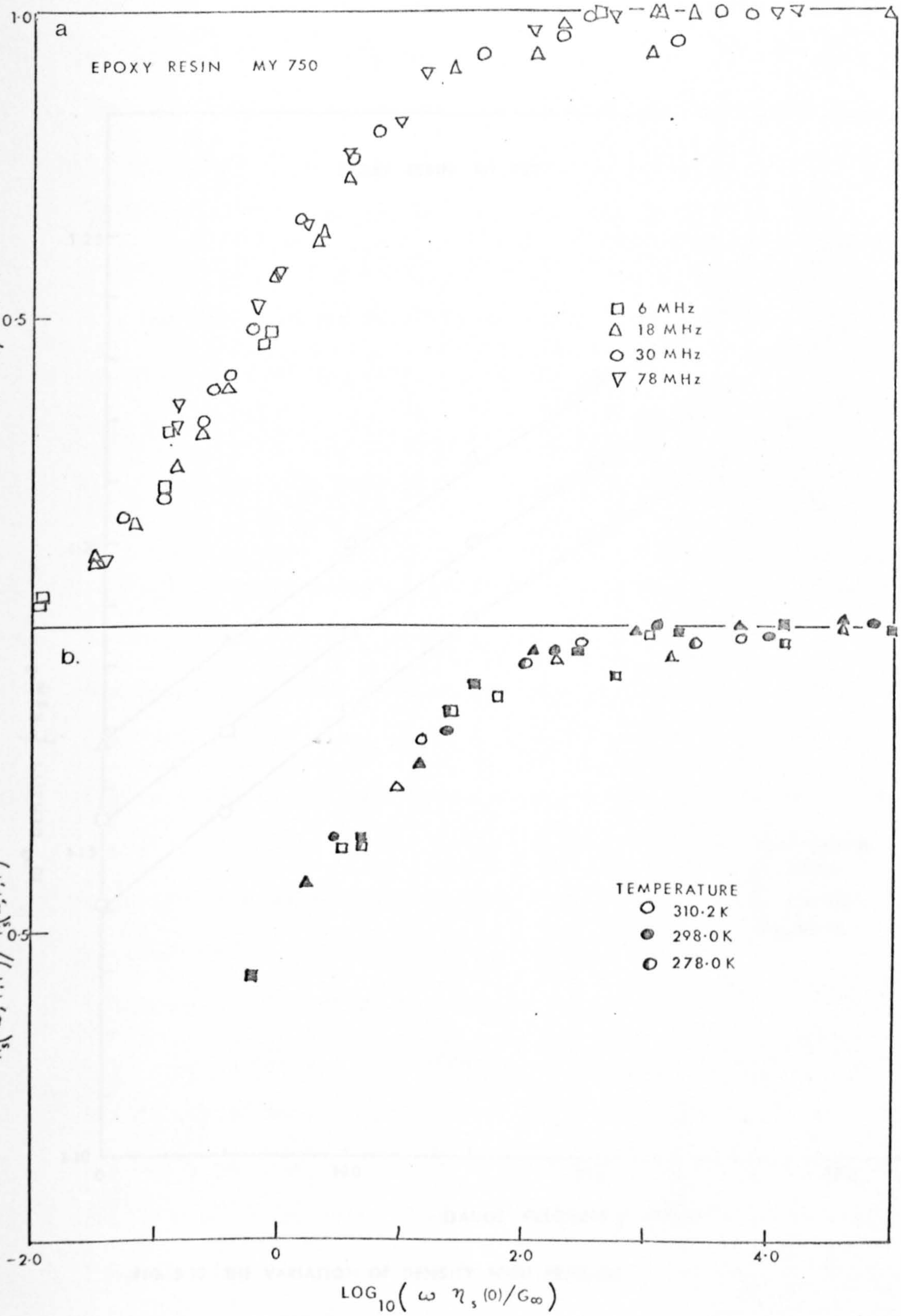

FIG. 5·9 REDUCED VARIABLES PLOT a . TEMPERATURE, b. TEMPERATURE AND PRESSURE

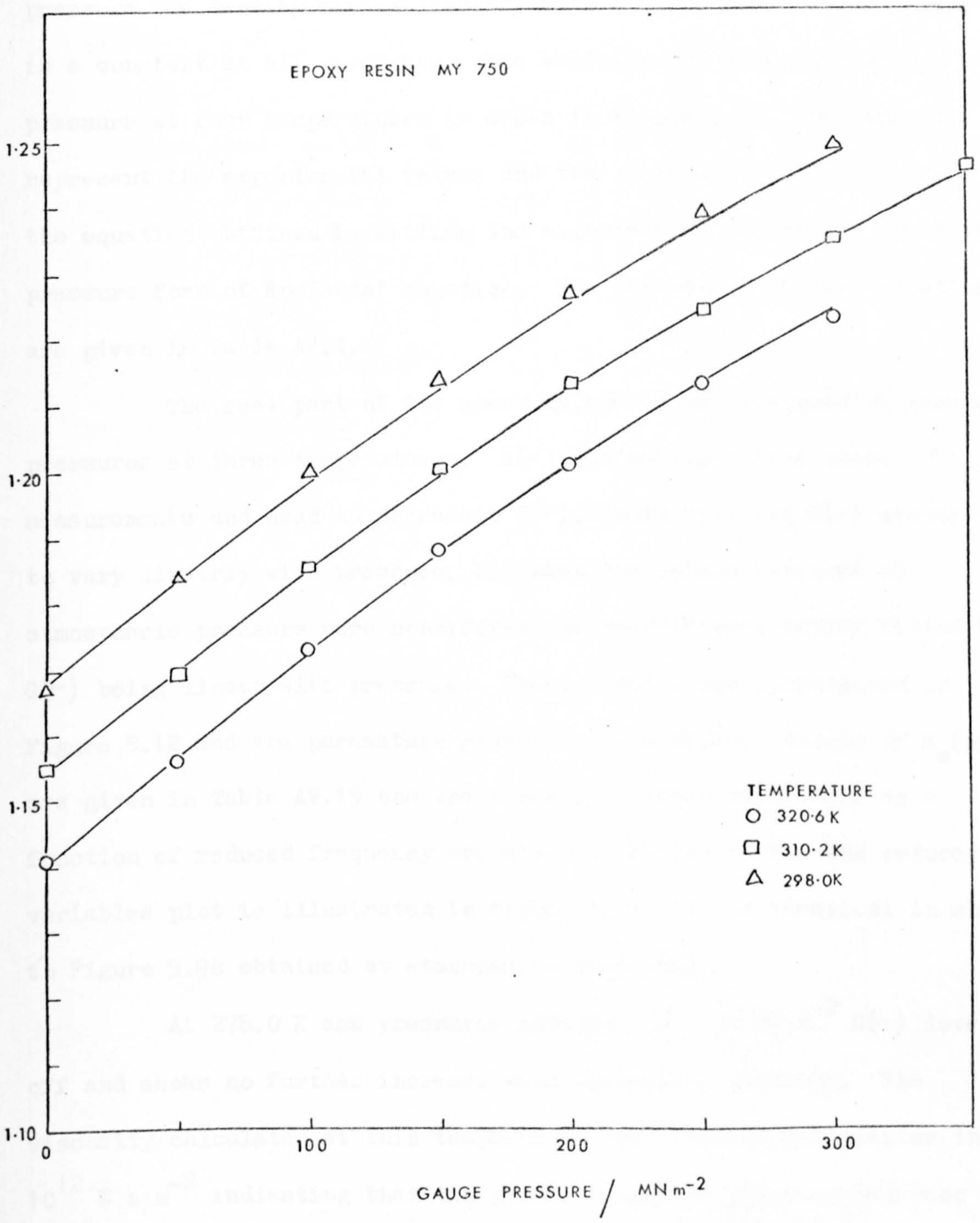

FIG. 5·10 THE VARIATION OF DENSITY WITH PRESSURE

three temperatures, the symbols represent the experimental measurements and the lines are calculated from the equation obtained by fitting the results to the linear secant modulus equation, the parameters of which are given in Table AV.3. The lines are parallel to each other indicating that, within the temperature range used, at any fixed pressure the density varies linearly with temperature, i.e. $(\partial\rho/\partial T)p$ is a constant at all pressures. The variation of viscosity with pressure at four temperatures is shown in Figure 5.11, the symbols represent the experimental values and the lines are calculated from the equation obtained by fitting the experimental results to the high pressure form of Roelands' equation. The parameters of this equation are given in Table AV.4.

The real part of the shear impedance was measured at various pressures at three temperatures. $R(\infty)$ was obtained from these measurements and used to calculate $G(\infty)$. Both $R(\infty)$ and $G(\infty)$ appeared to vary linearly with pressure, but when the values obtained at atmospheric pressure were considered the results were better fitted by $G(\infty)$ being linear with pressure. These results are illustrated in Figure 5.12 and the parameters given in Table AV.10. Values of $R_s(\omega)$ are given in Table AV.15 and the normalised shear resistance as a function of reduced frequency are given in Table AV.16. The reduced variables plot is illustrated in Figure 5.9b. It is identical in shape to Figure 5.9a obtained at atmospheric pressure.

At 278.0 K and pressures greater than 250 MN m^{-2} $G(\infty)$ levels off and shows no further increase with increasing pressure. The viscosity calculated at this temperature and pressure was greater than 10^{12} N s m^{-2} indicating that the glass transition pressure had been reached. It is also seen at higher temperatures that $G(\infty)$ increases beyond the maximum value at 278.0 K. Although this has not been noticed in the literature, calculations on the results for Aroclor[28] and di-2-ethylhexyl phthalate[57] indicate that this would be true for

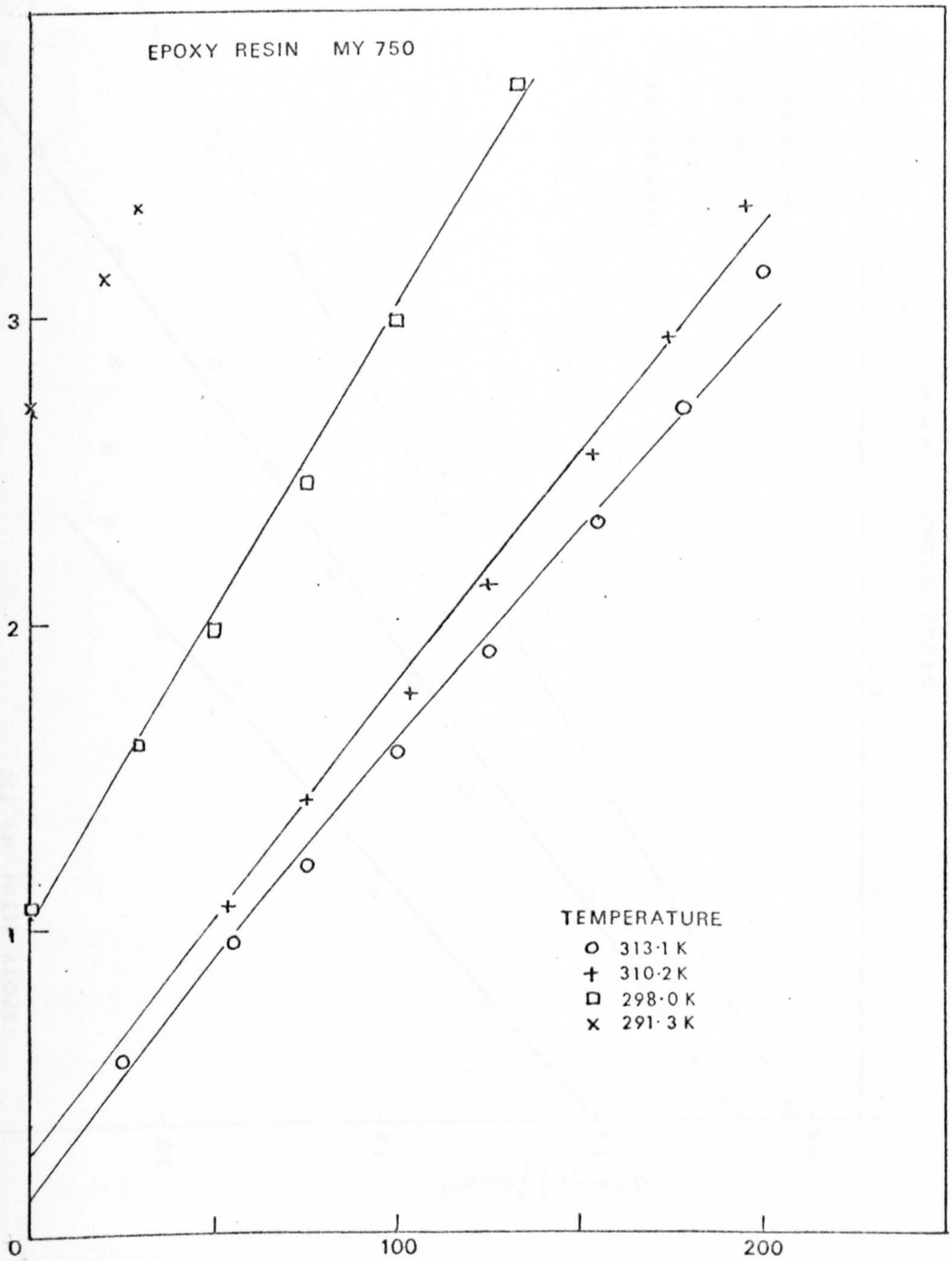

FIG. 5·11 THE VARIATION OF VISCOSITY, $\eta_s(0)$, WITH PRESSURE

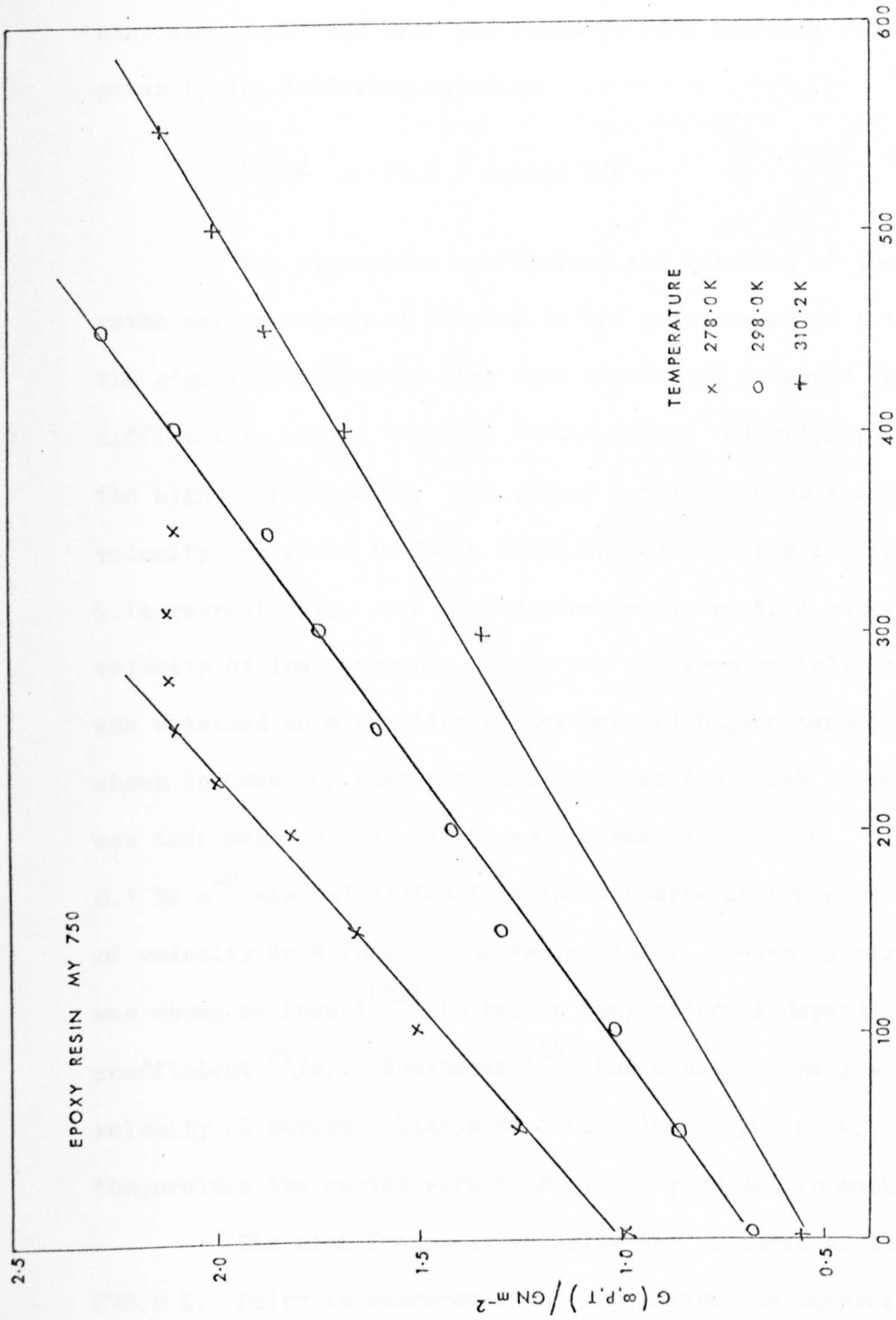

FIG. 5·12 THE VARIATION OF SHEAR MODULUS WITH PRESSURE

these liquids also. There was insufficient data given for castor oil[58] to calculate, but the formula given suggests that as the temperature is raised, the pressure of the glass transition is raised and since $G(\infty)$ varies more with pressure than temperature $G(\infty)$ will also increase. $\partial G(\infty)/\partial P$ was found to vary linearly with temperature given by the following equation

$$\frac{\partial G(\infty)}{\partial P} = 15.6 - 0.0408\ T/K \qquad ..(5.4)$$

The absorption coefficient and velocity of the longitudinal waves were measured at 310.2 K in the pressure range 0.1 to 200 MN m^{-2}. The signal decreased in size with increasing pressure thus making it difficult to obtain accurate values of the velocity, particularly at the higher frequencies. The values for the absorption coefficient and velocity are given in Table AV.17 and illustrated in Figures 5.13 and 5.14 respectively. The dashed line in Figure 5.14 represents the velocity at low frequency. This was obtained as follows. The velocity was obtained as a function of pressure at higher temperatures and shown to have the same pressure dependence at each temperature. It was then assumed that $\partial V/\partial P$ was the same at 310.2 K. The value at 0.1 MN m^{-2} was calculated from the atmospheric pressure relationship of velocity as a function of temperature. Di-2-ethylhexyl phthalate was shown by Powell[28] to have a temperature independent pressure coefficient $^{\partial V}/_{\partial P}$. Boelhouwer[59] has measured the low frequency velocity of several alkanes as a function of pressure, and at each temperature the curves were found to be parallel to each other.

The high frequency velocity was measured at low temperature, 278.0 K. Prior to measurement an experiment was carried out outside the pressure vessel to establish whether the path length of liquid in the pressure cell would be sufficient. If it was too short the sound waves would be reflected or absorbed by the rubber diaphragm and a decrease in the signal, or unwanted signal, would be present. It was

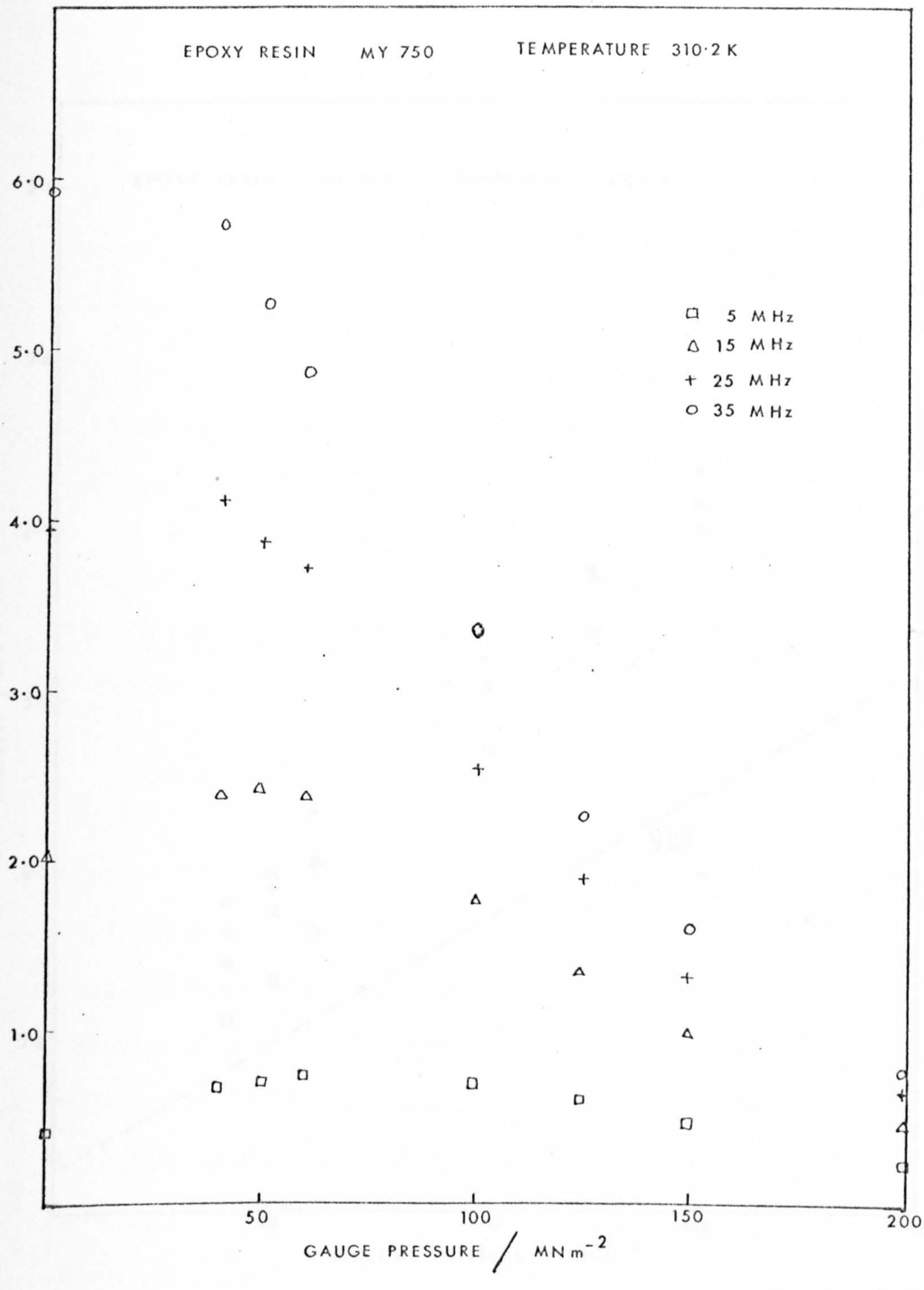

FIG. 5·13 THE VARIATION OF THE ABSORPTION COEFFICIENT, α, WITH PRESSURE AT 310·2 K

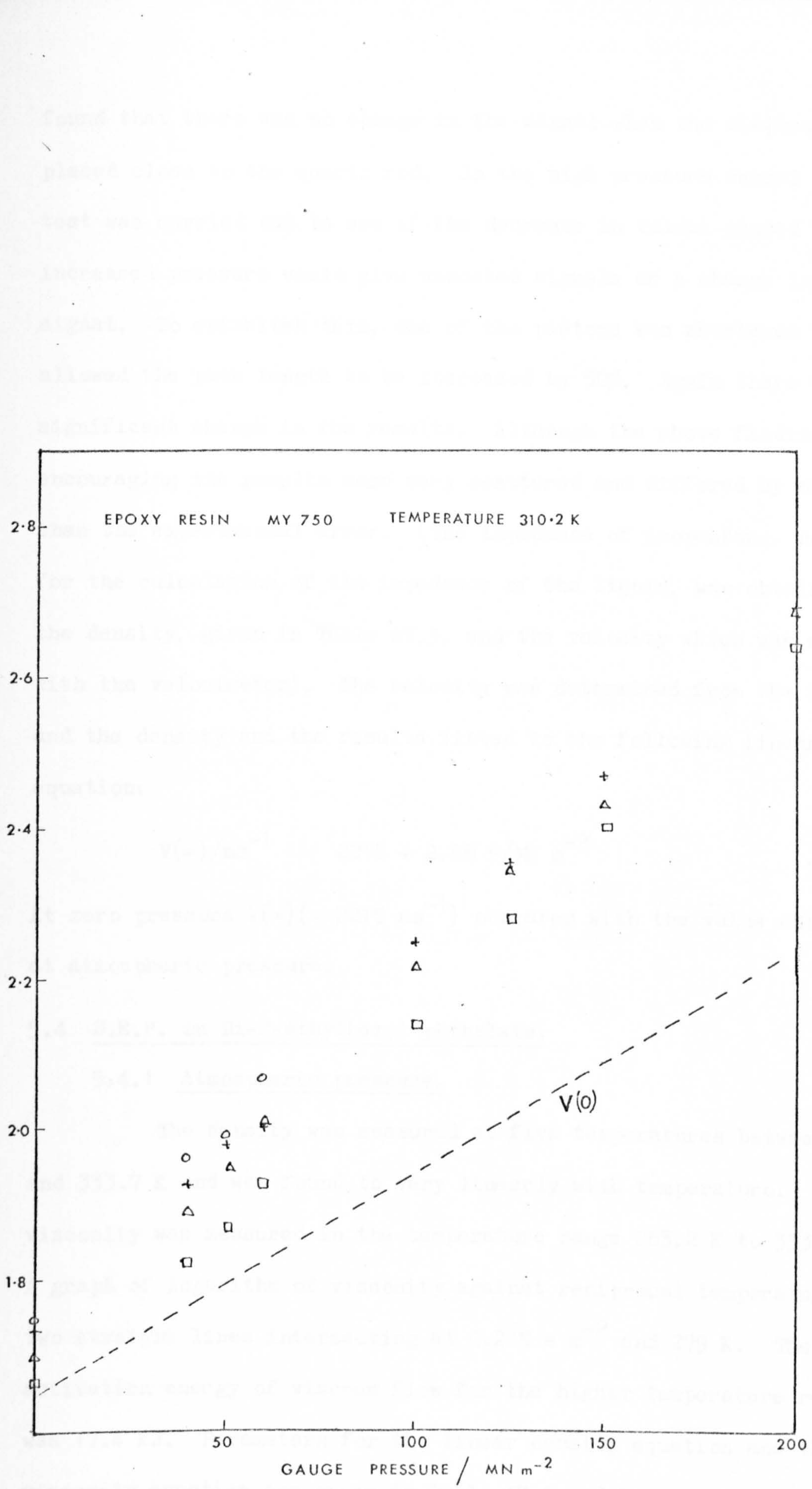

FIG. 5·14 THE VARIATION OF THE LONGITUDINAL SOUND VELOCITY WITH PRESSURE AT 310·2 K

found that there was no change in the signal when the diaphragm was placed close to the quartz rod. In the high pressure vessel a further test was carried out to see if the decrease in volume caused by the increased pressure would give unwanted signals or a change in the signal. To establish this, one of the pistons was shortened which allowed the path length to be increased by 50%. Again there was no significant change in the results. Although the above findings were encouraging the results were very scattered and differed by much more than the experimental error. (The impedance of isopentane, required for the calculation of the impedance of the liquid, was obtained from the density, given in Table AV.3, and the velocity which was measured with the velocimeter). The velocity was determined from the impedance and the density and the results fitted to the following linear equation:

$$V(\infty)/ms^{-1} = 2215 + 2.88\ P/MN\ m^{-2} \qquad ..(5.5)$$

At zero pressure $V(\infty)(= 2215\ ms^{-1})$ compares with the value obtained at atmospheric pressure.

5.4 S.E.P. in Di-2-ethylhexyl phthalate.

5.4.1 Atmospheric pressure.

The density was measured at five temperatures between 294.9 K and 333.7 K and was found to vary linearly with temperature. The viscosity was measured in the temperature range 263.2 K to 333.7 K. A graph of logarithm of viscosity against reciprocal temperature gave two straight lines intersecting at 0.2 N s m^{-2} and 279 K. The activation energy of viscous flow for the higher temperature region was 17.4 kJ. Parameters for the linear density equation and the viscosity equation are given in Table AV.1 and 2 respectively.

The absorption coefficient and velocity were measured as a function of temperature and the values given in Table AV.18. Figures 5.15 and 5.16 illustrate the absorption coefficient and velocity as

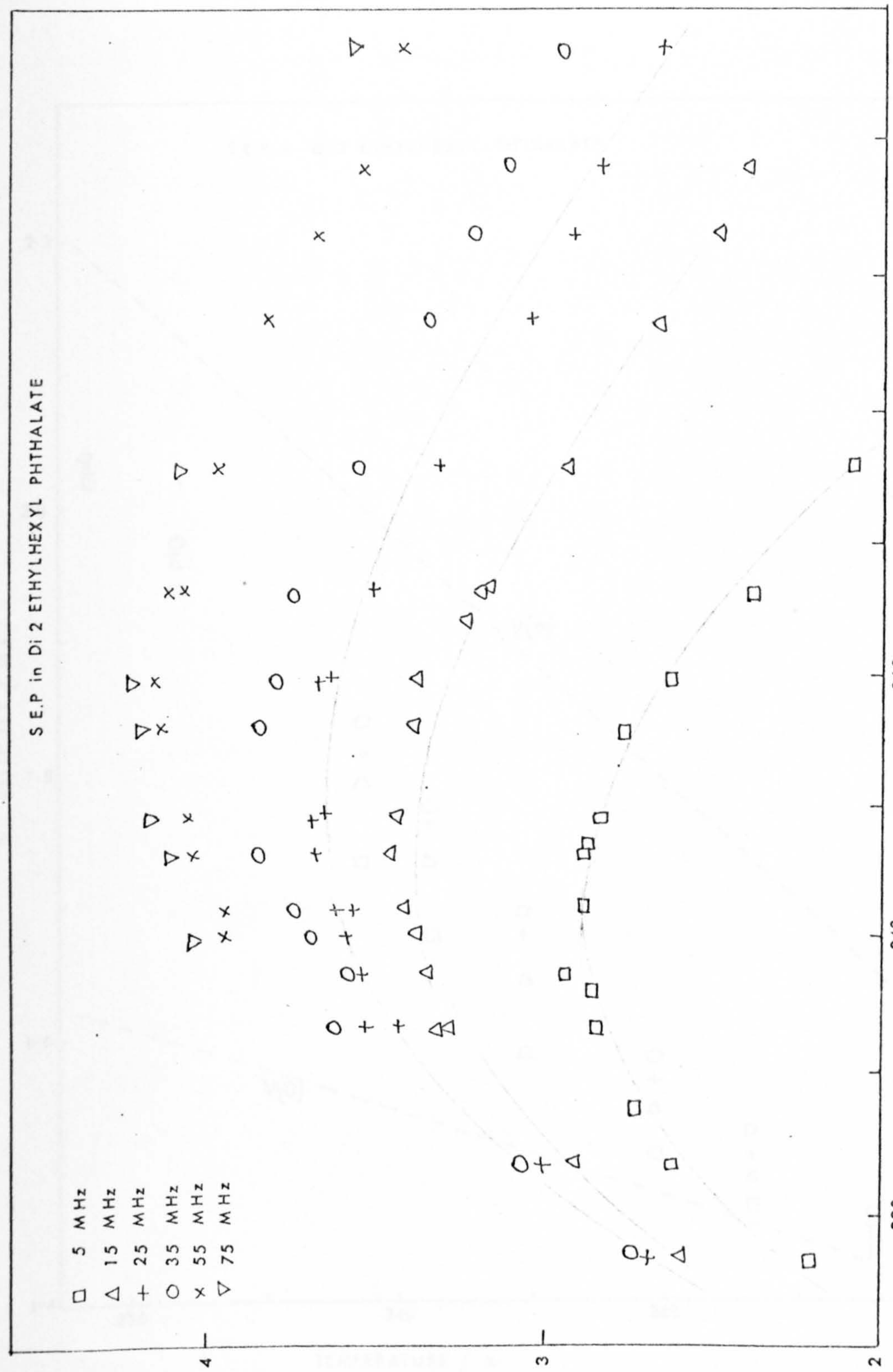

FIG. 5·15 THE VARIATION OF ABSORPTION COEFFICIENT, α, WITH TEMPERATURE

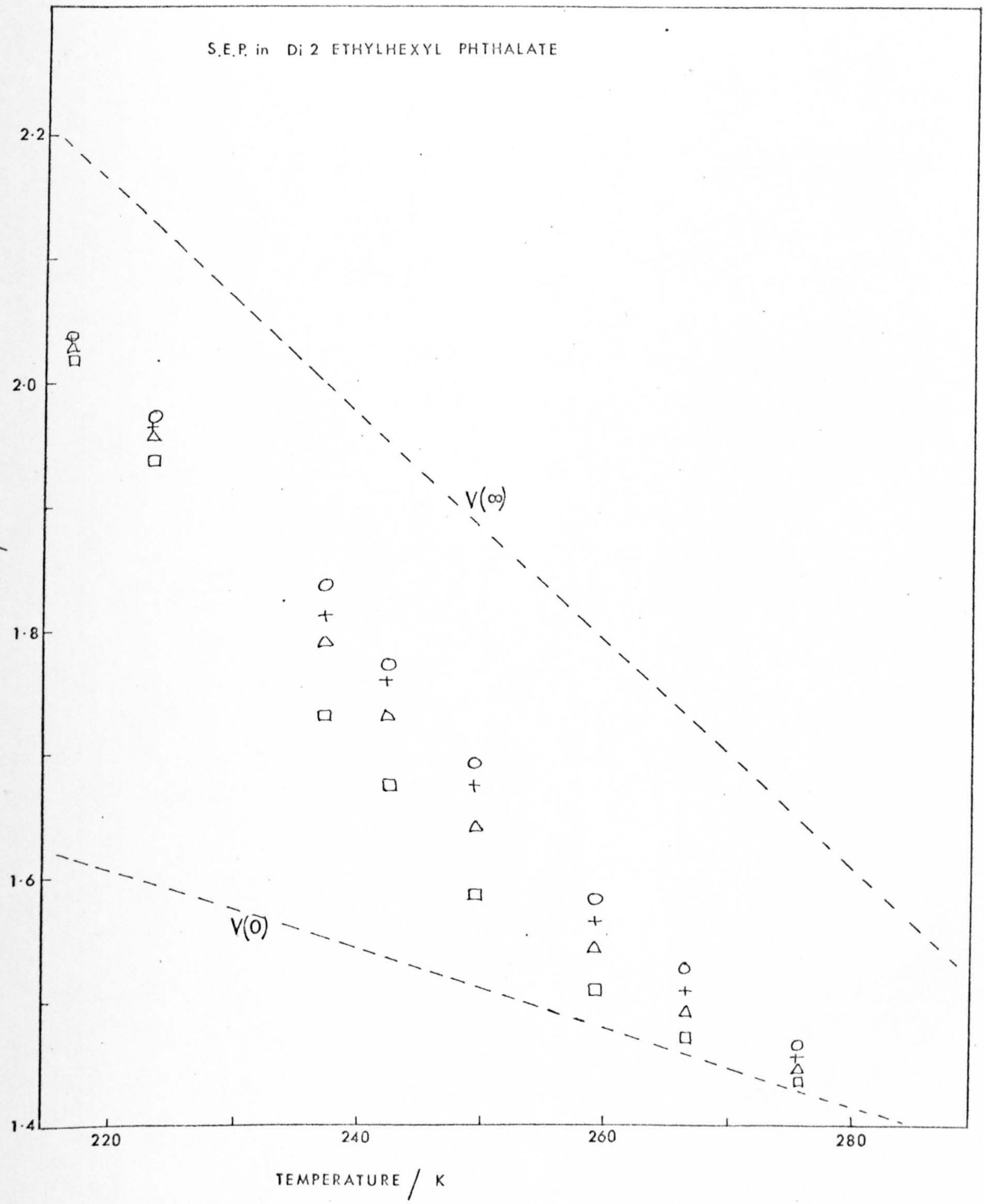

FIG. 5·16 THE VARIATION OF LONGITUDINAL SOUND VELOCITY WITH TEMPERATURE

a function of temperature respectively. The dashed lines in Figure 5.16 represent the variation of the low frequency velocity and high frequency velocity. The low frequency velocity varied linearly with temperature, the parameters for this linear relationship are given in Table AV.5. The high frequency velocity is given by the following equation:

$$V(\infty)/ms^{-1} = 4218.5 - 9.35\ T/K \qquad ..(5.6)$$

The absorption coefficient and velocity show the characteristics typical of a structural relaxation and the logarithm of maximum α/f^2 showed the same linear dependence on logarithm of f as the two previous liquids. There was no significant difference between the graphs of absorption against temperature (Figure 5.15) of S.E.P. in Di-2-ethyl-hexyl phthalate and Di-2-ethylhexyl phthalate[28]. To check this observation a concentrated solution of S.E.P. in cyclohexane was prepared (maximum concentration obtained = 6.7% w/v) and the absorption coefficient was determined at a few temperatures. The results agreed within experimental error with those of cyclohexane indicating that S.E.P. is not contributing significantly to the absorption of the Di-2-ethylhexyl phthalate solution, at least at temperatures between 280-300 K.

The real part of the shear impedance was measured between 194.7 K and 298.2 K and showed a viscoelastic response. The values are given in Table AV.19. A few values of the imaginary part of the impedance were obtained and used together with the real part to give the dynamic viscosity and storage modulus given in Table AV.8. $G(\infty)$ and $J(\infty)$ were calculated as before and $J(\infty)$ was found to be linear with temperature, the parameters for the linear equation are given in Table AV.9. The variation of $G(\infty)$ and $J(\infty)$ with temperature is illustrated in Figures 5.17a and b respectively. The normalised impedance values as a function of reduced frequency are given in

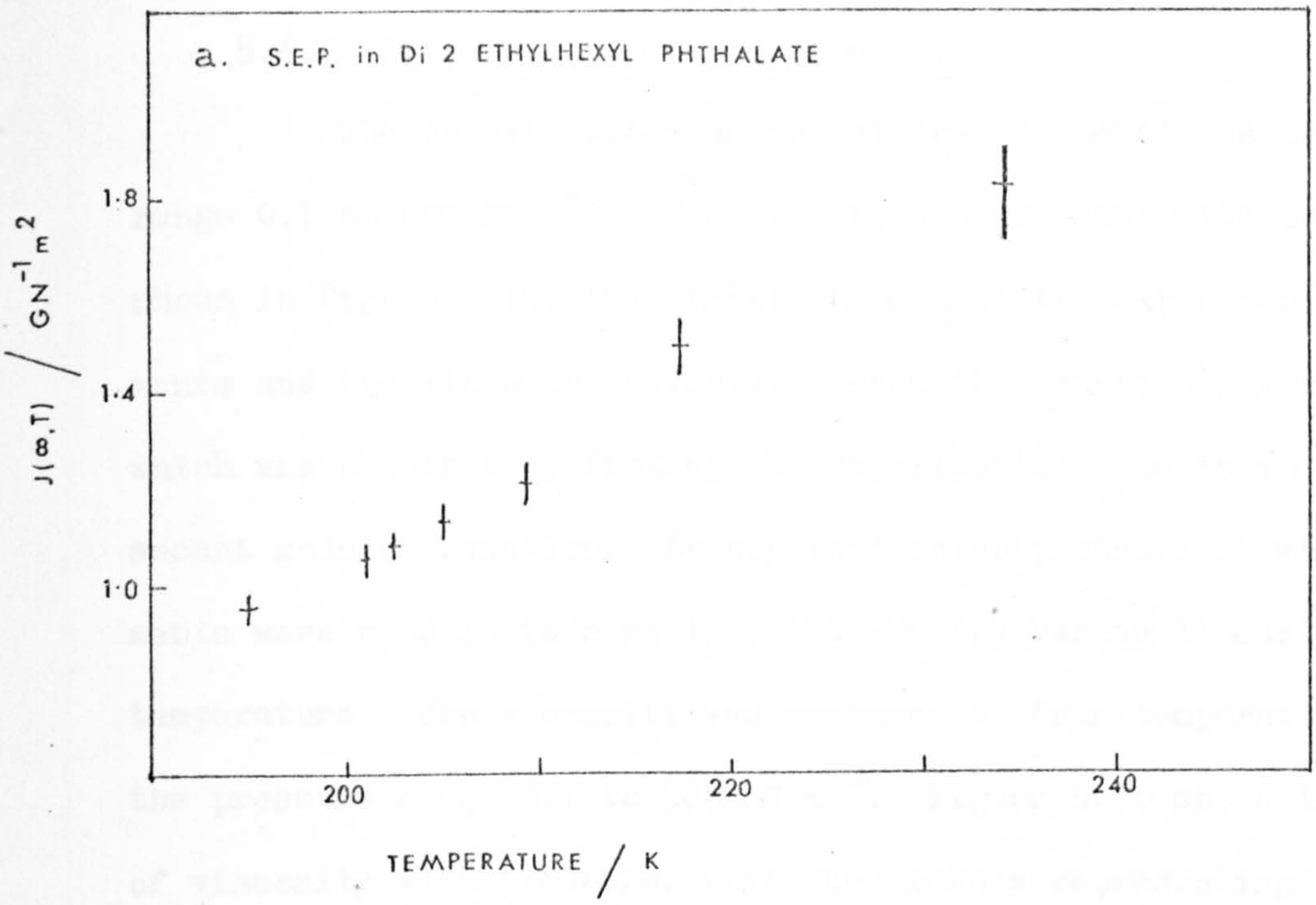

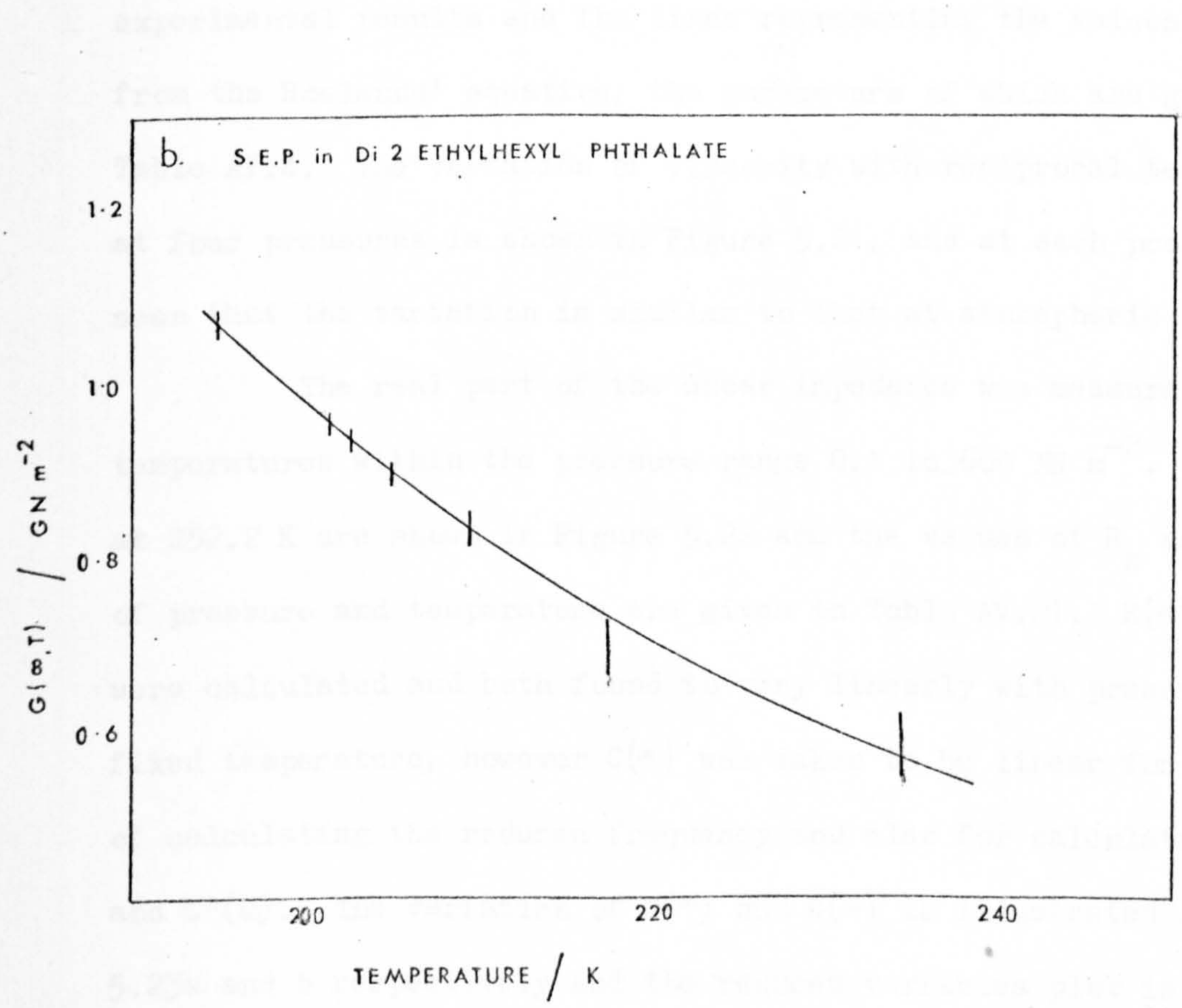

FIG. 5·17 THE VARIATION OF a. J(∞) AND b. G(∞) WITH TEMPERATURE

Table AV.20 and the resulting reduced variables plot is shown in Figure 5.18a. The results can be described by the B.E.L. model with $k = 1.0$.

5.4.2 Pressures above atmospheric.

The density was measured at four temperatures in the pressure range 0.1 to 400 MN m^{-2}. The variation of density with pressure is shown in Figure 5.19, the symbols represent the experimental measurements and the lines are calculated from the equation given in Table AV.3 which was obtained by fitting the experimental results to the linear secant modulus equation. At any particular pressure at which measurements were made it is seen that the density varies linearly with temperature. The viscosity was measured at four temperatures within the pressure range 0.1 to 500 MN m^{-2}. Figure 5.20 shows the variation of viscosity with pressure, with the symbols representing the experimental results and the lines representing the values calculated from the Roelands' equation, the parameters of which are given in Table AV.4. The variation of viscosity with reciprocal temperature at four pressures is shown in Figure 5.21, and at each pressure it is seen that the variation is similar to that at atmospheric pressure.

The real part of the shear impedance was measured at three temperatures within the pressure range 0.1 to 600 MN m^{-2}. The results at 252.2 K are shown in Figure 5.22 and the values of R_s as a function of pressure and temperature are given in Table AV.21. $R(\infty)$ and $G(\infty)$ were calculated and both found to vary linearly with pressure at a fixed temperature, however $G(\infty)$ was taken to be linear for the purpose of calculating the reduced frequency and also for calculation of $G'(\omega)$ and $G''(\omega)$. The variation of $R(\infty)$ and $G(\infty)$ is illustrated in Figure 5.23a and b respectively and the reduced variables plot is shown in Figure 5.18b. The values of the normalised shear resistance as a function of reduced frequency at three temperatures are given in Table AV.22. The variation of $\partial G(\infty)/\partial P$ with temperature could not be

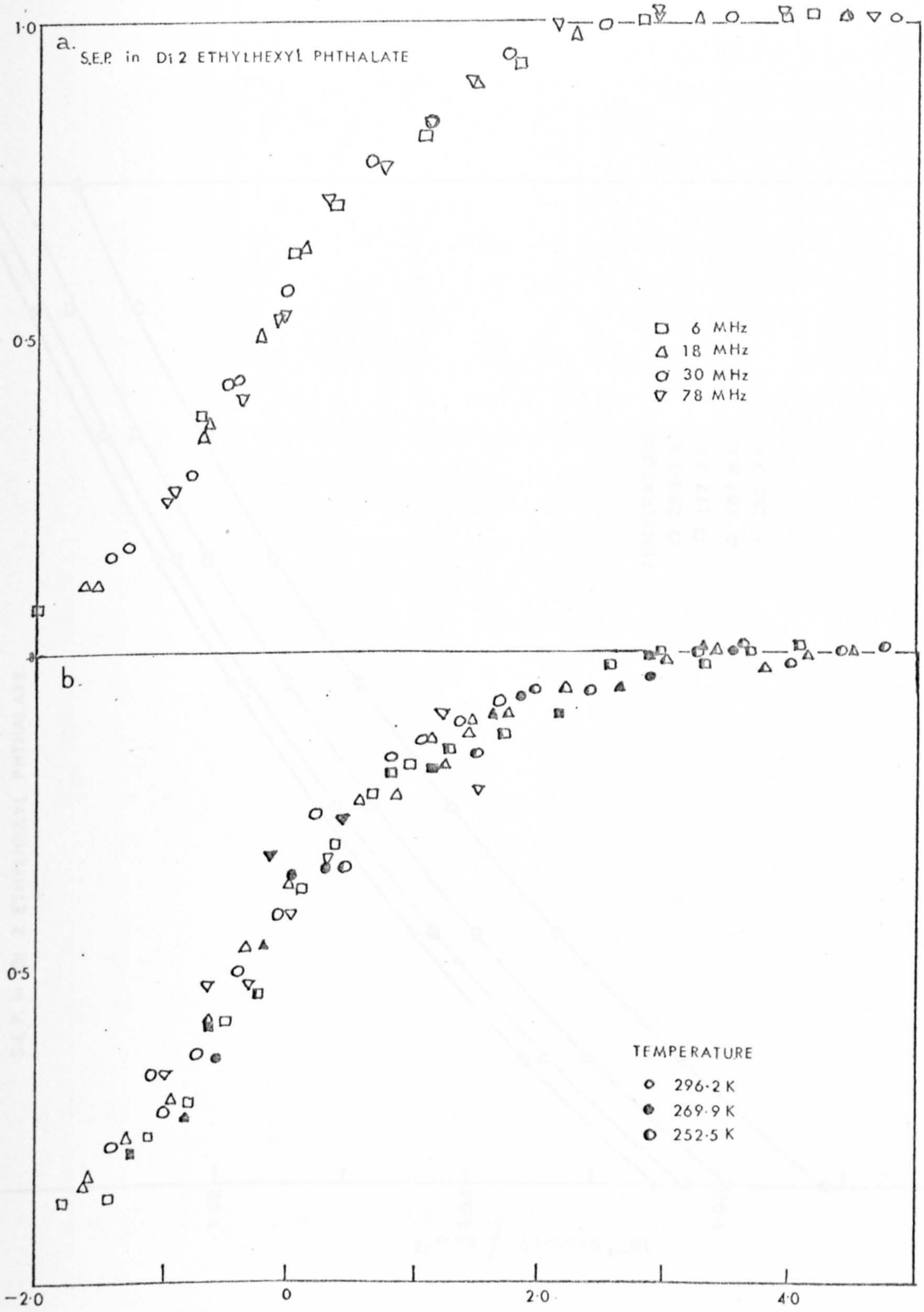

FIG. 5·18 REDUCED VARIABLES PLOT a. AT TEMPERATURE b. AT TEMPERATURE AND PRESSURE

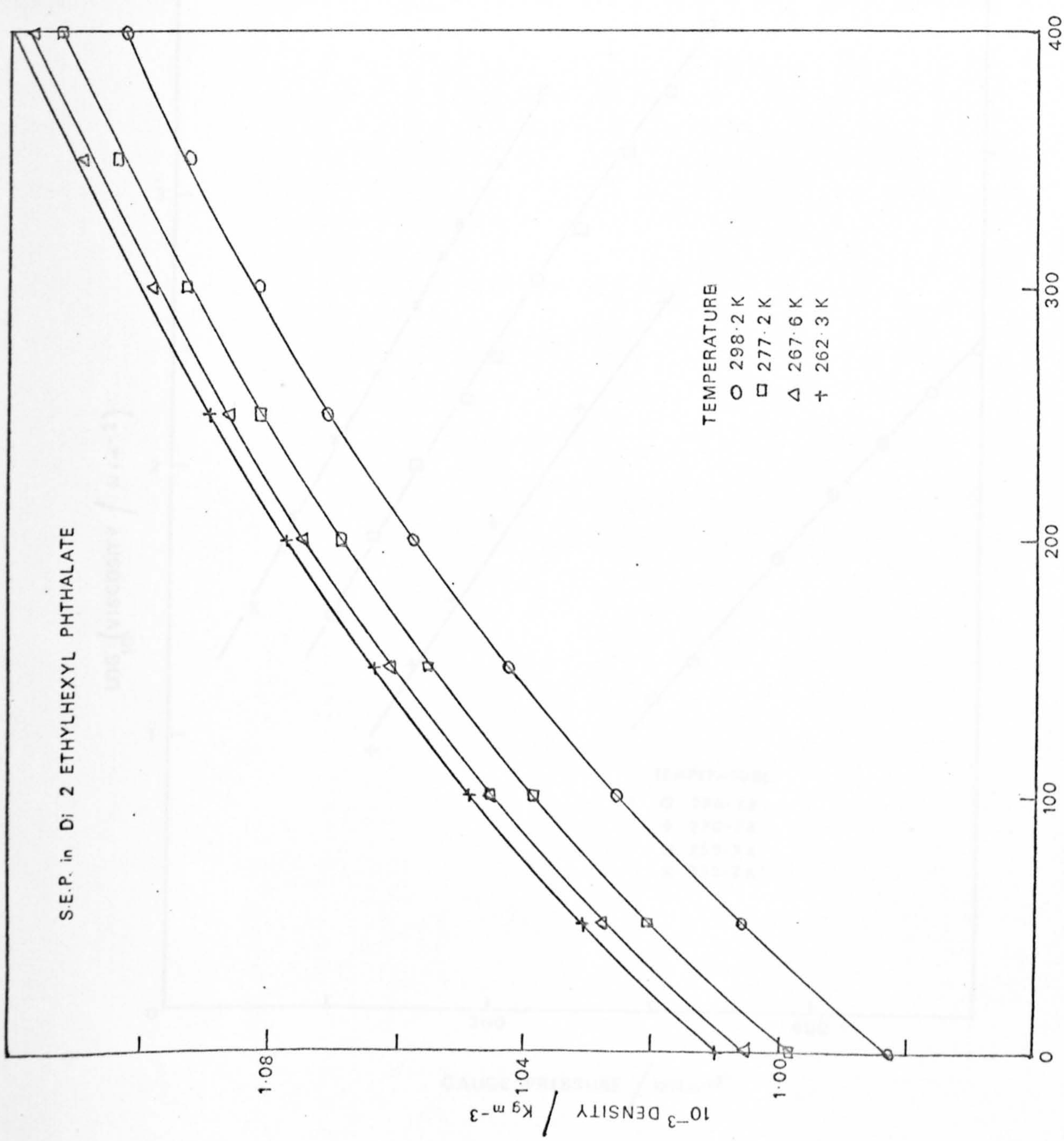

FIG. 5·19 THE VARIATION OF DENSITY WITH PRESSURE

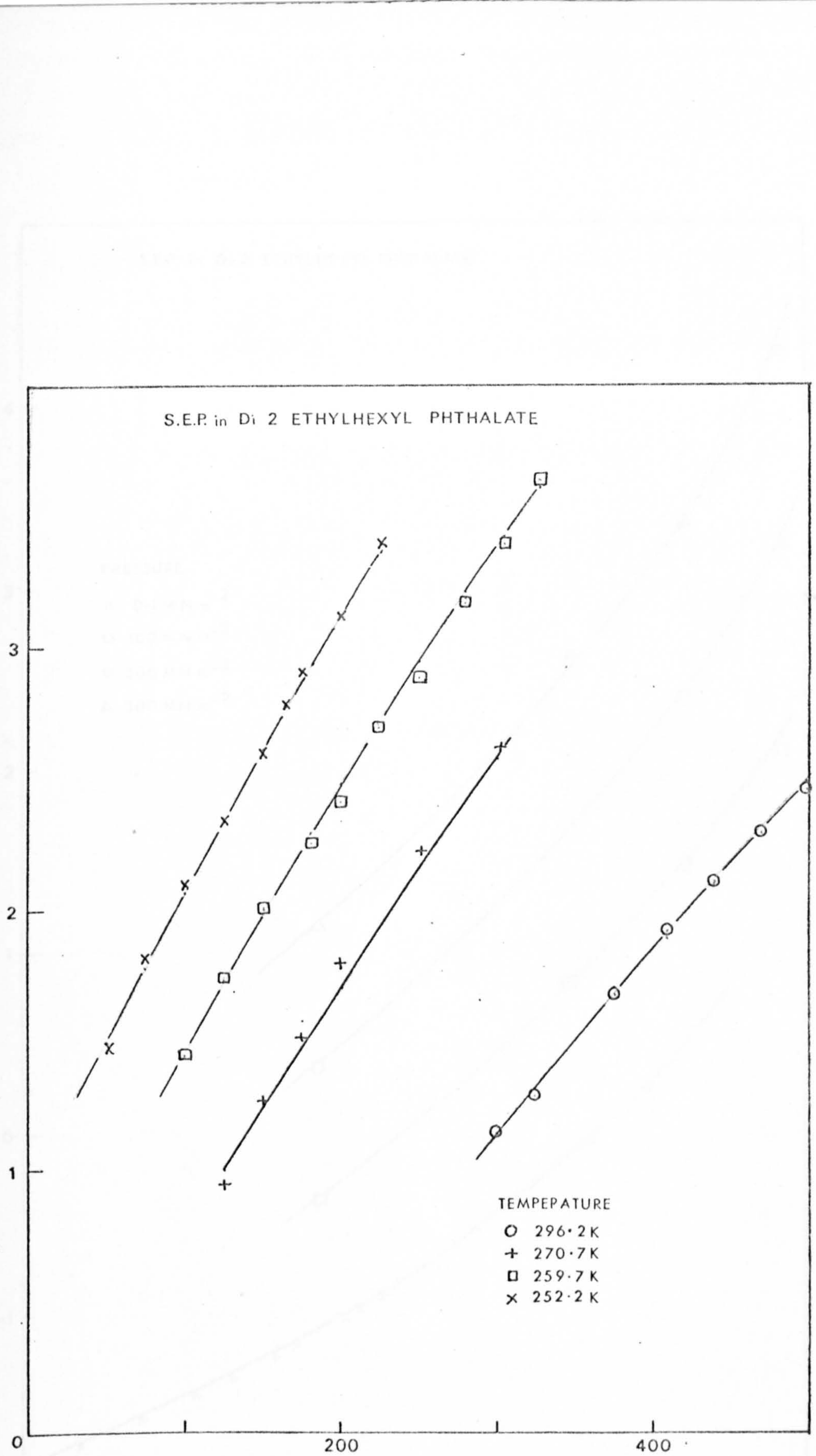

FIG. 5·20 THE VARIATION OF VISCOSITY WITH PRESSURE

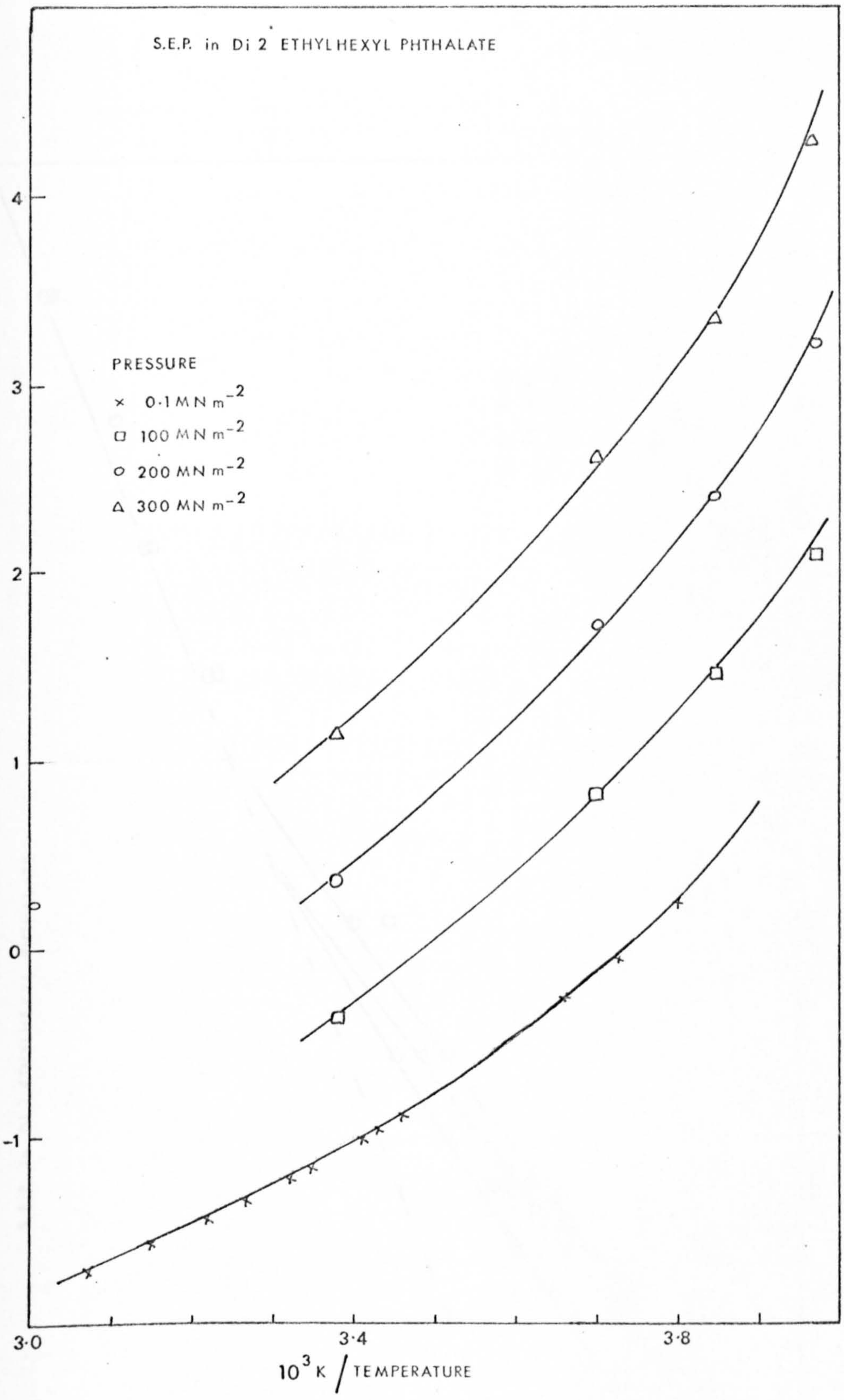

FIG. 5·21 THE VARIATION OF VISCOSITY WITH RECIPROCAL TEMRERATURE

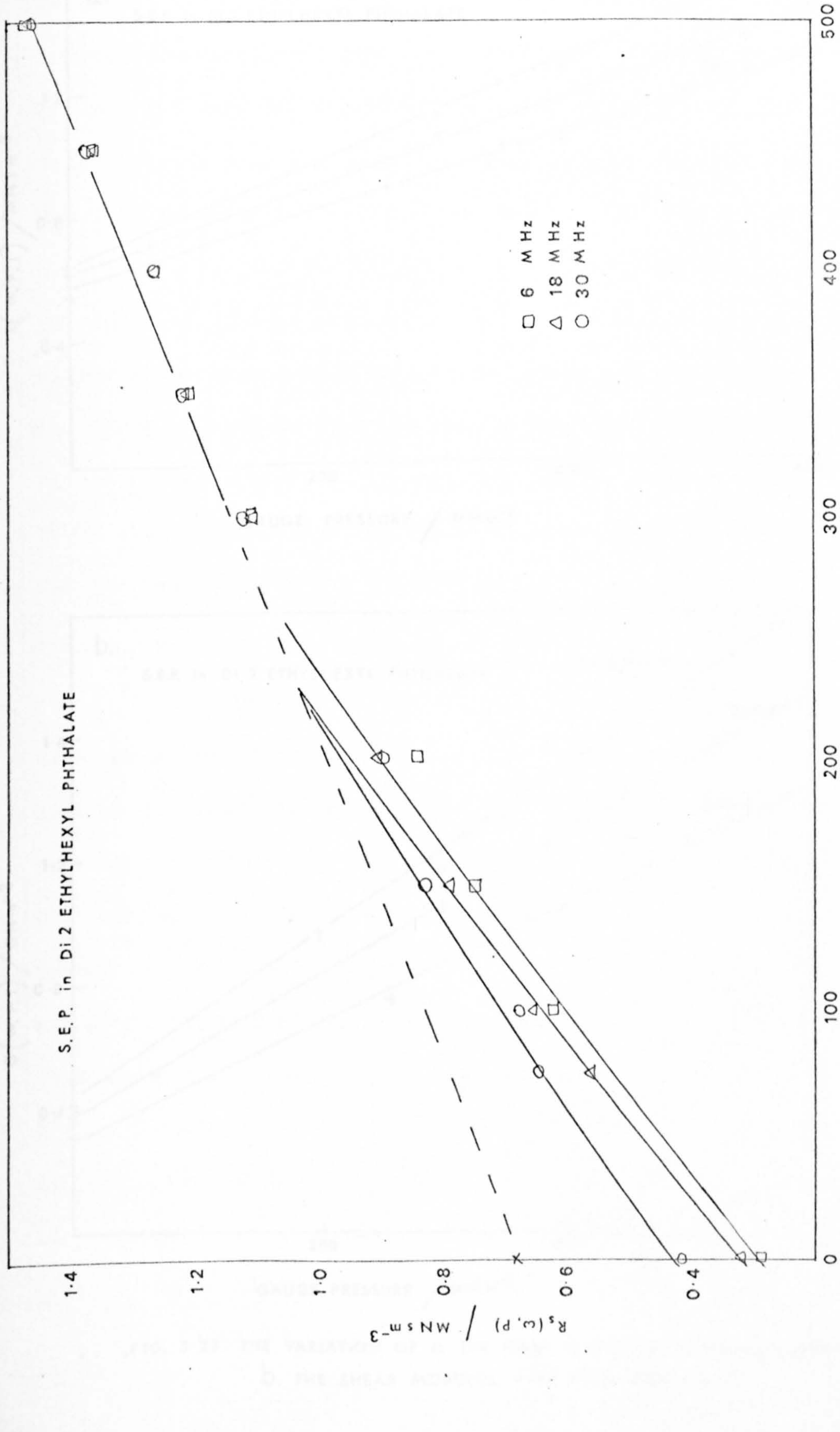

FIG. 5·22 THE VARIATION OF IMPEDANCE, R_s, WITH PRESSURE AT

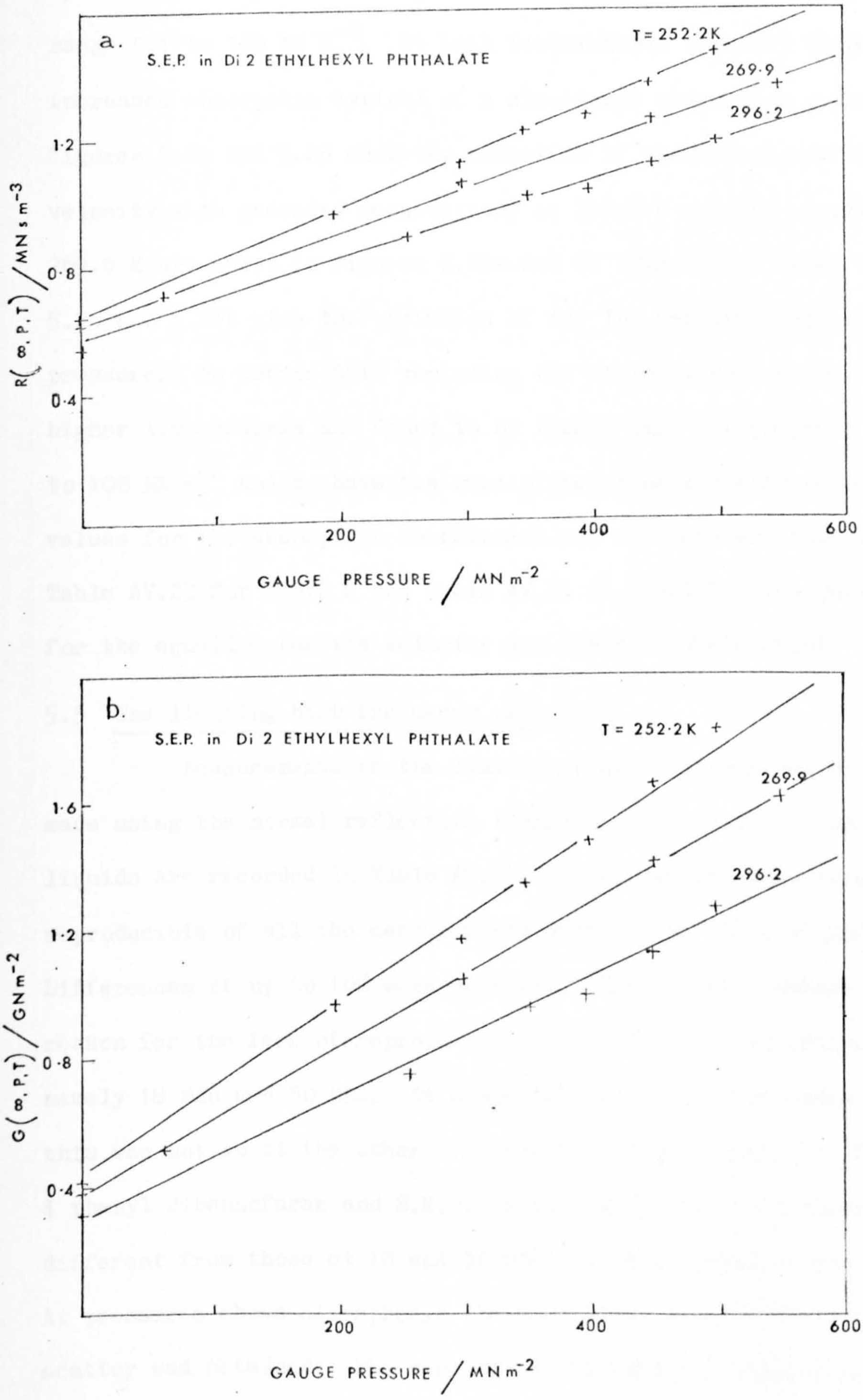

FIG. 5·23 THE VARIATION OF a. THE HIGH FREQUENCY IMPEDANCE, R(∞), b. THE SHEAR MODULUS G(∞) WITH RRESSURE

fitted by a linear equation, but the variation with temperature was smaller than for Epoxy Resin MY 750.

The absorption coefficient and velocity were measured at 296.2 K in the pressure range 0.1 to 400 MN m^{-2} and at 269.9 K in the range 0.1 to 100 MN m^{-2}. At both temperatures velocity dispersion and increased absorption typical of a structural relaxation were observed. Figures 5.24 and 5.25 show the variation of absorption coefficient and velocity with pressure respectively at 296.2 K and the results at 269.9 K are shown in Figures 5.26a and b. The dashed lines on Figures 5.25 and 5.26b give the variation of the low frequency velocity with pressure. To obtain this variation the velocity was measured at two higher temperatures and found to be linear over the pressure range 0.1 to 100 MN m^{-2} and to have the same slope at each temperature. The values for the absorption coefficient and velocity are tabulated in Table AV.23 for 296.2 K and Table AV.24 at 269.9 K. The parameters for the equation for the velocity are given in Table AV.5b.

5.5 The limiting high frequency velocity.

Measurements of the limiting high frequency velocity were made using the normal reflection technique. The results for the three liquids are recorded in Table AV.25. These measurements were the least reproducible of all the measurements made on the three liquids. Differences of up to 10% were obtained. There didn't appear to be any reason for the lack of reproducibility between the two frequencies, namely 18 MHz and 30 MHz. At 6 MHz the pulse shape was very poor but this was not so at the other frequencies. Measurements at 78 MHz in 4 phenyl dibenzofuran and S.E.P. in Di-2-ethylhexyl phthalate were different from those at 18 and 30 MHz and were therefore neglected. At pressures above atmospheric the same lack of reproducibility and scatter was obtained. The results at atmospheric pressure and above would only allow a linear relationship. A linear relationship has

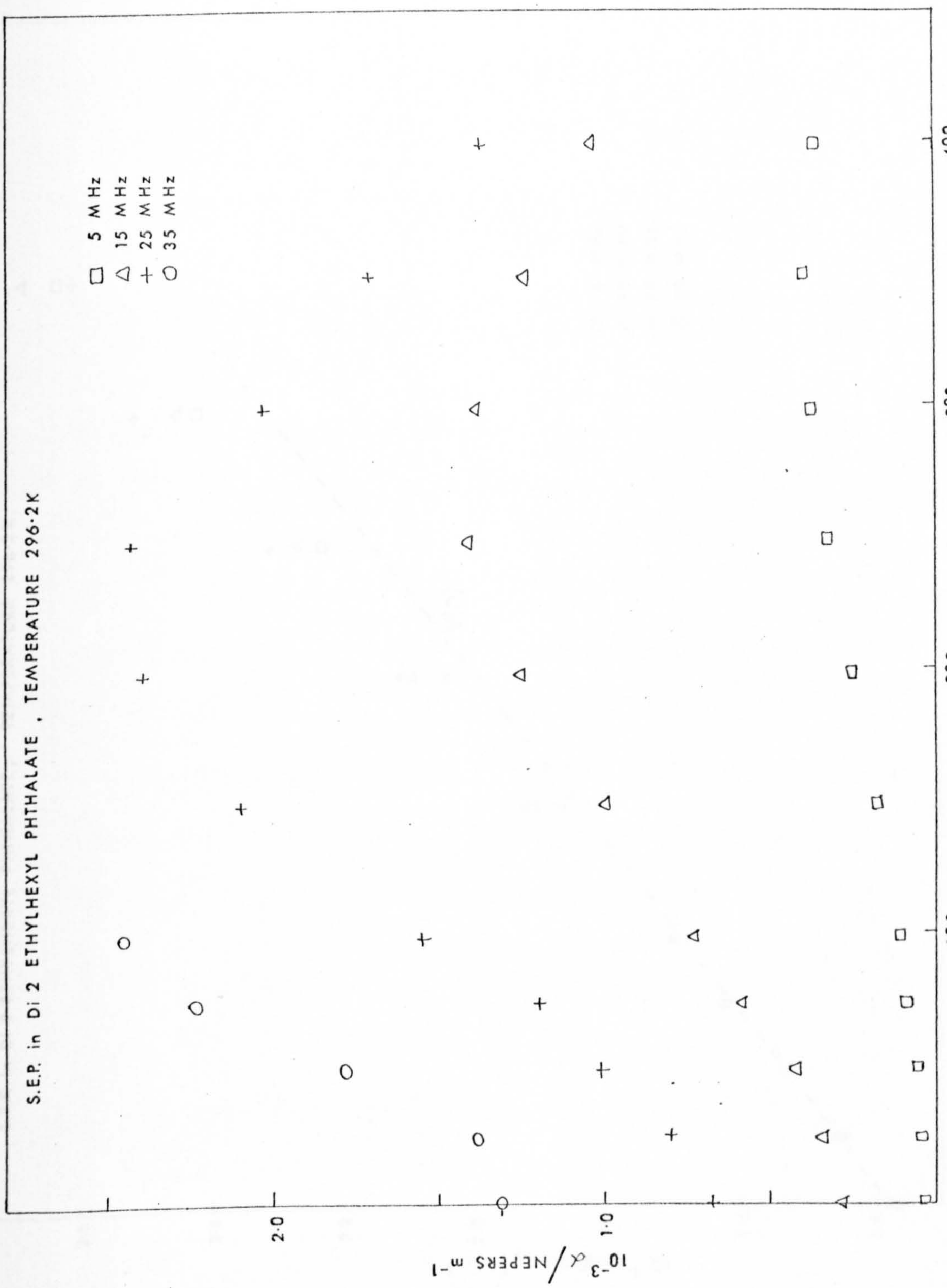

FIG. 5·24 THE VARIATION OF ABSORPTION COEFFICIENT, α, WITH PRESSURE

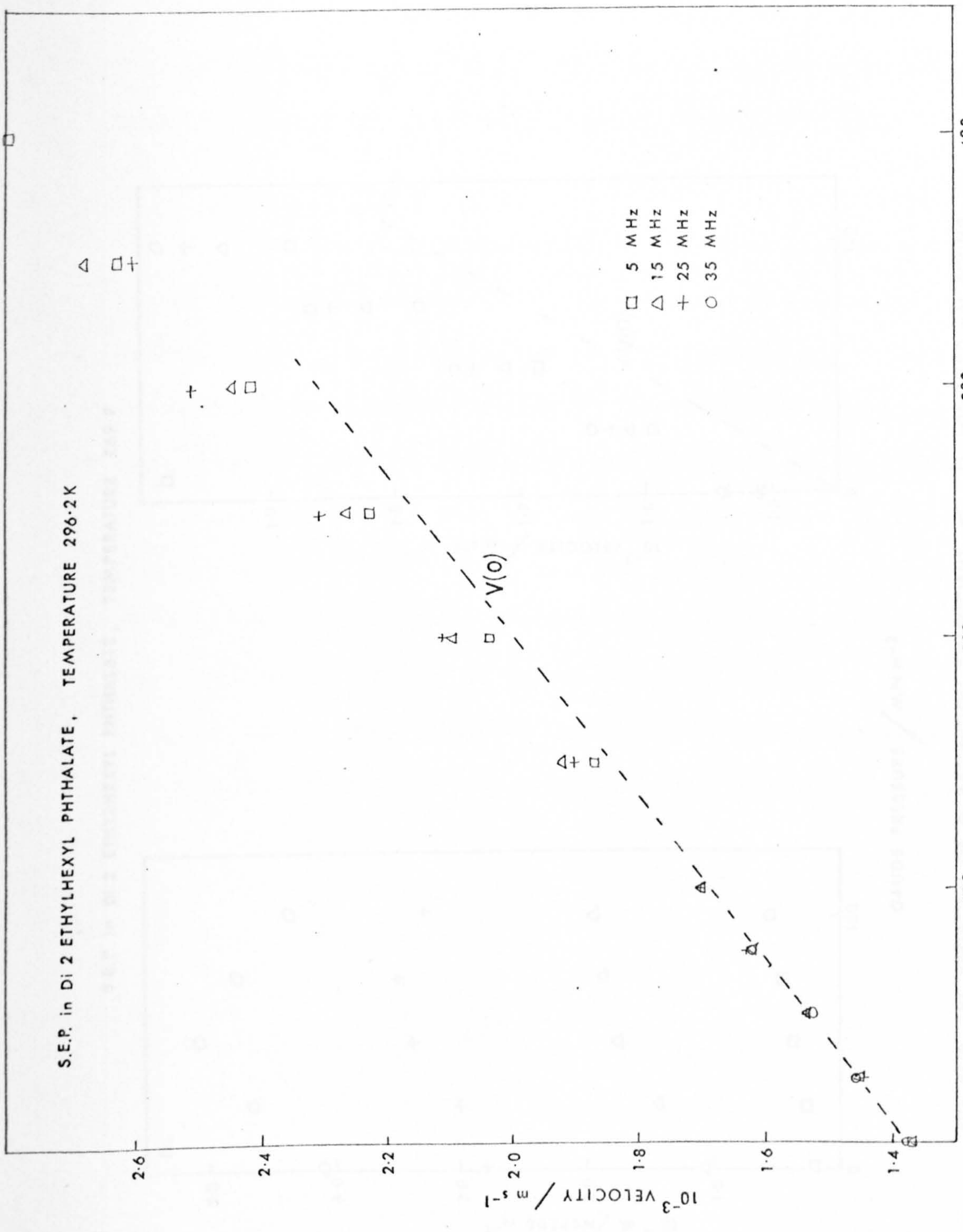

FIG. 5·25 THE VARIATION OF LONGITUDINAL SOUND VELOCITY WITH PRESSURE

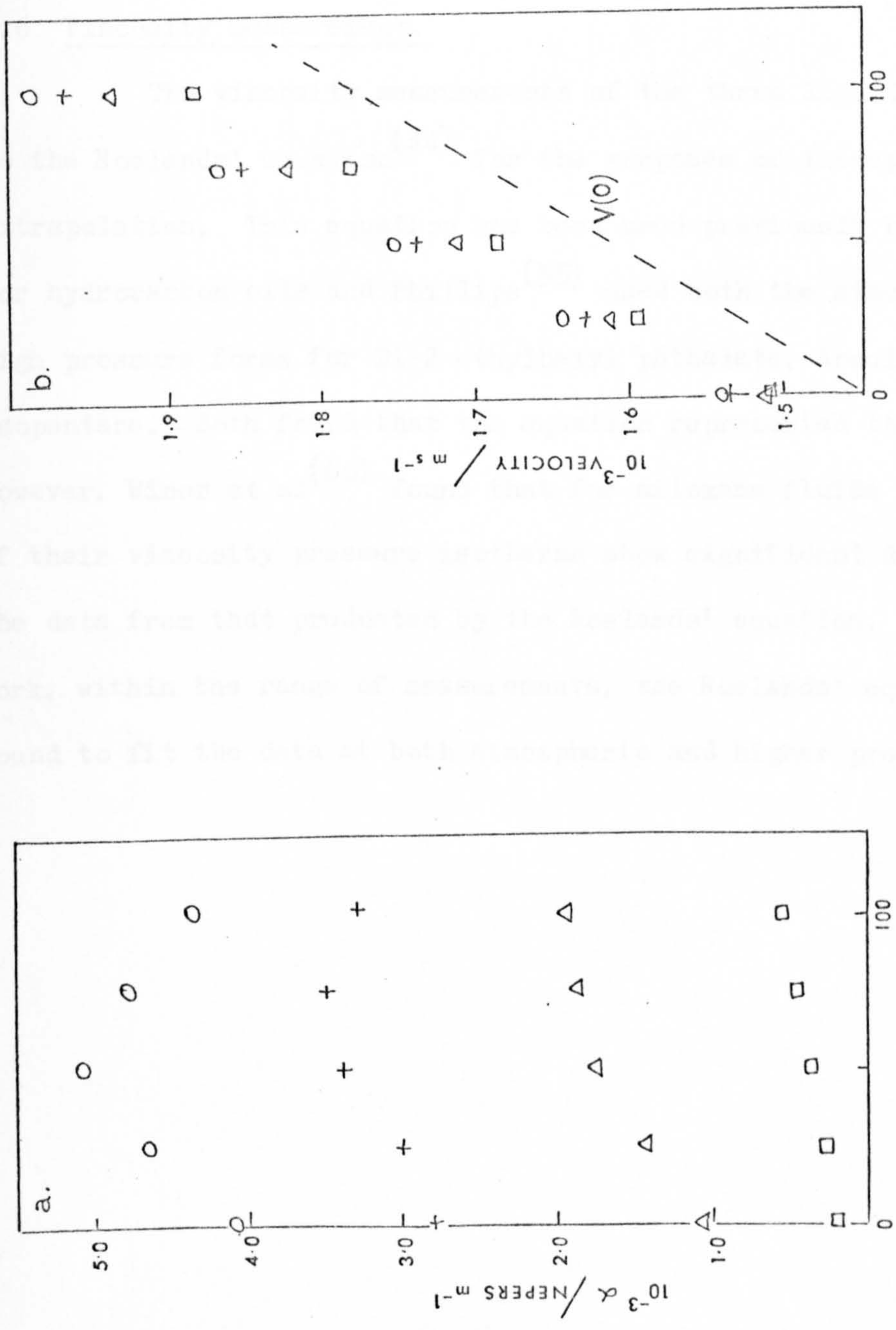

FIG. 5·26 THE VARIATION OF a. ABSORPTION COEFFICIENT, α. b. LONGITUDINAL SOUND VELOCITY WITH PRESSURE

been reported by Litovitz[55] for Aroclor, $V(\infty)$ is linear with temperature, it was also found for liquids that the ratio $\partial V(\infty)/\partial T$: $\partial V(0)/\partial T$ ranged from 2.0 for Aroclor to 3.58 for 2-methyl 2,4-di-hydroxy pentane. In the present work for 4-phenyl dibenzofuran, Epoxy Resin MY 750 and S.E.P. in Di-2-ethylhexyl phthalate the values were 1.9, 2.0 and 3.0 respectively, again the more viscous the material at the same temperature the lower the value.

5.6 Viscosity measurement.

The viscosity measurements of the three liquids were fitted to the Roelands' equation[44] for the purposes of interpolation and extrapolation. This equation has been used previously by Hutton[20] for hydrocarbon oils and Phillips[35] used both the atmospheric and high pressure forms for Di-2-ethylhexyl phthalate, Aroclor 1254 and isopentane. Both found that the equation represented their data. However, Winer et al[60] found that for siloxane fluids less than half of their viscosity pressure isotherms show significant deviations of the data from that predicted by the Roelands' equation. In the present work, within the range of measurements, the Roelands' equation has been found to fit the data at both atmospheric and higher pressures.

CHAPTER VI

BULK MODULUS AND VOLUME VISCOSITY

6.1 Introduction.

The results given in Chapter V will now be used to determine the various bulk moduli and viscosities. To completely determine all the moduli the following are required: $G(\infty)$, $G'(\omega)$, $G''(\omega)$, $M(0)\left[=K(0)\right]$, $M(\infty)$, $M'(\omega)$ and $M''(\omega)$. There is no equivalent of $M(0)$ in shear because a liquid cannot support a continuous shear stress. The relationship of $G(\infty)$ with temperature and/or pressure has been given in Chapter V and at a few selected temperatures $G'(\omega)$ and $G''(\omega)$ were obtained from measurements of the real and imaginary parts of the impedance. To calculate $G'(\omega)$ and $G''(\omega)$ for the whole range of temperature and/or pressure it is assumed that the liquids can be described by the B.E.L. model. This has been shown to be a valid assumption for the three liquids; the values of $R_s(\omega,P,T)/R_s(\infty,P,T)$ plotted against reduced frequency do fall on to the B.E.L. curve. Any errors obtained by this method will be small and will not seriously affect the values of $K'(\omega)$ and $K''(\omega)$.

From the absorption coefficient and velocity of the longitudinal waves, $M'(\omega)$ and $M''(\omega)$ are calculated and hence $K'(\omega)$ and $K''(\omega)$ according to equations (2.50), (2.51) (page 27). An error in the absorption coefficient can affect $M''(\omega)$ far more than $M'(\omega)$, errors of $\pm$ 10% cause $K''(\omega)$ to be meaningless when compared with $K'(\omega)$. On the other hand, an error in the velocity affects the value of $M'(\omega)$ more than $M''(\omega)$, errors of $\pm$ 1% can make $K'(\omega)$ have a negative value or have a very large value.

$K(0)$ and $M(\infty)$ are important values, $K(0)$ for both $K'(\omega)$ and $\left[K(\infty) - K(0)\right] = K_2$ and $M(\infty)$ for the latter. The magnitude of $K(0)$ compared to $G'(\omega)$ and $K'(\omega)$ makes it extremely important that this quantity is accurately known. At temperatures above which relaxation occurs it is possible to measure the velocity accurately ($\sim$ 0.1%) but within the relaxation region extrapolation is required. This procedure has been partly confirmed by Litovitz et al[62] and Ambrus[63] who

measured the velocity at lower frequencies just within the relaxation range, i.e, at temperatures where velocity dispersion was occuring at higher frequencies. The low frequency velocity was found to be linear with temperature, a finding confirmed by others[15,16,17,28], however K(0) has also been reported[62,63,64] to be linear with temperature. M(∞) is determined from the high frequency velocity obtained at low temperatures and/or high pressures. This was the most inaccurate measurement made and has always been open to doubt especially about its temperature relationship, Powell[28] found that it was linear with temperature. When measurements of V(∞) are unobtainable then it is assumed that $\left[K(\infty) - K(0) \right] = G(\infty)$ or some suitable multiple of G(∞) and this value is used to reduce the data.

The above assumption has been used to calculate M(∞) from equation (6.1),

$$M(\infty) = K(0) + xG(\infty) + \tfrac{4}{3} G(\infty) \qquad ..(6.1)$$

where x = 1 or some suitable value.

The velocity (V(∞)) can be obtained from M(∞) and the density; for Di-2-ethylhexyl phthalate[16], Bis(m-(m-phenoxy phenoxy)phenyl) ether[17] and Triorthotolyl phosphate[15] it was about 2300 m s^{-1}, the same value as obtained in the present work.

There are three quantities which must be extrapolated, namely V(0) (or K(0)), V(∞) (or M(∞)) and J(∞) (or G(∞)). V(0) and V(∞) have been taken to be linear and assumed to be linear into the relaxation range. J(∞) has been shown to be linear but only until Tg is reached, below this temperature J(∞) (or G(∞)) is constant. The range of temperature and/or pressure over which measurements are made is small and it is possible that other functions would fit these measurements within the experimental error. However, in the present circumstances and because of previous literature given above, it would not be justified to fit the experimental values to a more complicated expression.

Finally, when the reduced variables plots are obtained for shear and bulk moduli, the real parts and imaginary parts are compared. If the shapes of the curves for the real part of the reduced shear modulus and the real part of the reduced bulk modulus are identical and also the shapes of the curves for the imaginary part of the reduced shear and bulk moduli are the same then it can be assumed that the relaxation spectra for the shear and bulk (or compressional) processes are the same. Although the shapes may be the same the two plots may not superimpose, but since they are the same shape they could be superimposed by a shift of one relative to the other along the reduced frequency axis. Since, in both sets of reduced plots, the shear viscosity is used to calculate the reduced frequency, this shift is related to the moduli and viscosities by the following expression,

$$\text{Shift} = \frac{\eta_v}{\eta_s} \cdot \frac{G(\infty)}{(K(\infty) - K(0))} \qquad ..(6.2)$$

If the shapes of the reduced moduli curves are not the same then the two processes must be different. On the other hand, if the real parts are the same and the imaginary parts different or vice versa, then either the results are suspect or linear theory is inadequate.

6.2 4-phenyl dibenzofuran.

$G'(\omega)$ and $G''(\omega)$ were calculated from equation (2.42) (with $k = 0.9$) at the frequencies and temperatures at which the absorption coefficient and velocity were measured. $M'(\omega)$ and $M''(\omega)$ were calculated from equations (2.14) and (2.15) and $K(0)$ was obtained from the low frequency velocity and density. From the above values $K'(\omega)$ and $K''(\omega)$ were calculated from equations (2.50) and (2.51). The relaxational bulk modulus $\left[K(\infty) - K(0)\right]$ was calculated from the values of $K(0)$, $M(\infty)$ and $G(\infty)$ using equation (6.3),

$$K(\infty) - K(0) = M(\infty) - K(0) - \tfrac{4}{3} G(\infty) \qquad ..(6.3)$$

The values of $\left[K(\infty) - K(0) \right]$ as a function of temperature and the ratio to $G(\infty)$ are given in Table AVI.1. This ratio is not constant throughout the temperature range but within the relaxation range it has a value of 1.40 ± 0.05. The values of the normalised bulk moduli are given in Table AVI.2 as a function of reduced frequency and illustrated in Figure 6.1, curve II, $K''(\omega)/K(\infty) - K(0)$, is shifted by 1.0 on the logarithm scale. The curves have the same shape as the normalised shear moduli shown on Graph 2 (in the back cover) but to superimpose the two figures, Graph 2 must be shifted by 0.48 ± 0.04 on the logarithm scale. The value of η_v/η_s calculated from equation (6.2) is therefore 4.2 ± 0.6. This is higher than the values obtained by Powell[28] but lower than that obtained for Bis(m-(m phenoxy phenoxy) phenyl) ether[17]. The various moduli as a function of temperature are shown in Figure 6.2.

6.3 Epoxy Resin MY 750.

6.3.1 Atmospheric pressure.

Values of $G'(\omega)$, $G''(\omega)$, $M'(\omega)$ and $M''(\omega)$ were calculated as described in the previous section. $K(0)$ and $M(\infty)$ were calculated from $V(0)$ and $V(\infty)$ respectively and the density. $K'(\omega)$, $K''(\omega)$ and $\left[K(\infty) - K(0) \right]$ were calculated and the values of $K(\infty) - K(0)$ together with the ratio of $\left[K(\infty) - K(0) \right]$ to $G(\infty)$ are given in Table AVI.3 as a function of temperature. The ratio was not constant with temperature but within the relaxation range it was 1.20 ± 0.05. The values of the normalised bulk moduli are given in Table AVI.4 and shown in Figure 6.3. (Curve II is shifted along the logarithm of reduced frequency axis by 1.0). Comparison with Graph 2 shows that the shape of the curves are identical and the shift required to superimpose the two curves is 0.43 ± 0.03 on the logarithm scale. The value of η_v/η_s obtained is 3.2 ± 0.3. The moduli as a function of temperature are given in Figure 6.4.

6.3.2 Pressures above atmospheric.

There is no apparatus available to measure the imaginary part

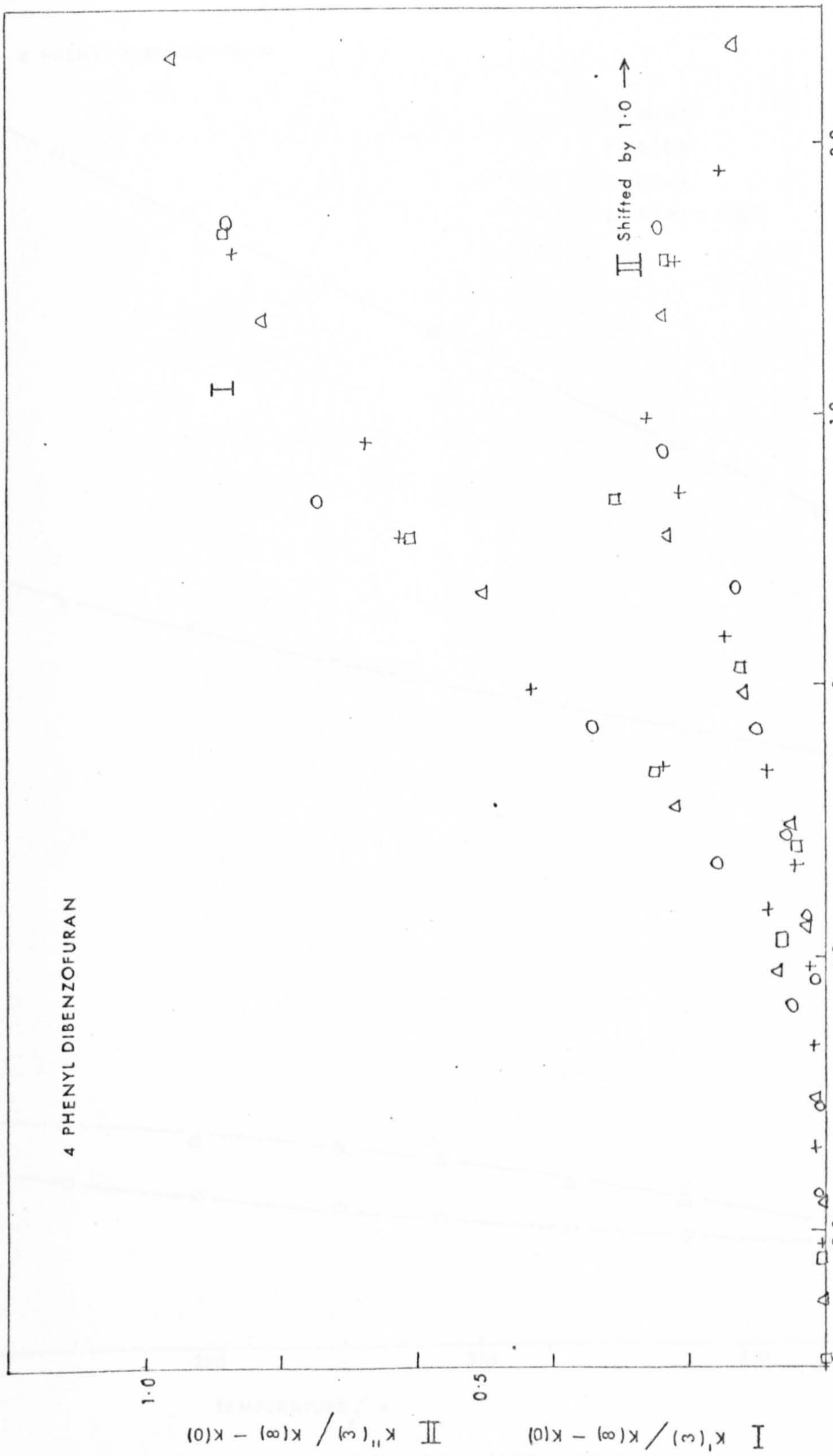

FIG. 6·1 THE VARIATION OF THE BULK STORAGE. I. AND LOSS. II. MODULI AS A FUNCTION OF REDUCED FREQUENCY

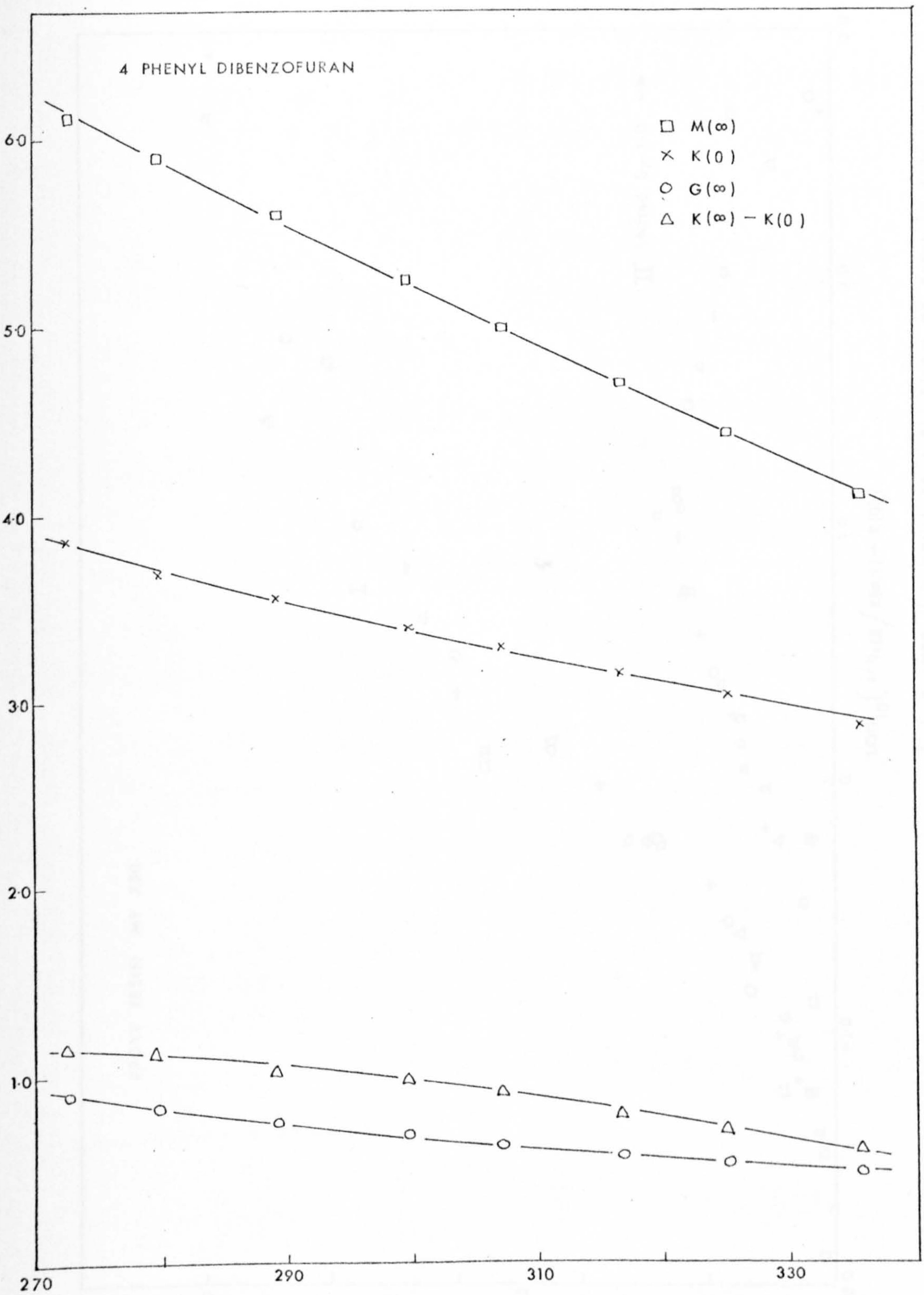

FIG. 6·2. THE VARIATION OF THE MODULI WITH TEMPERATURE

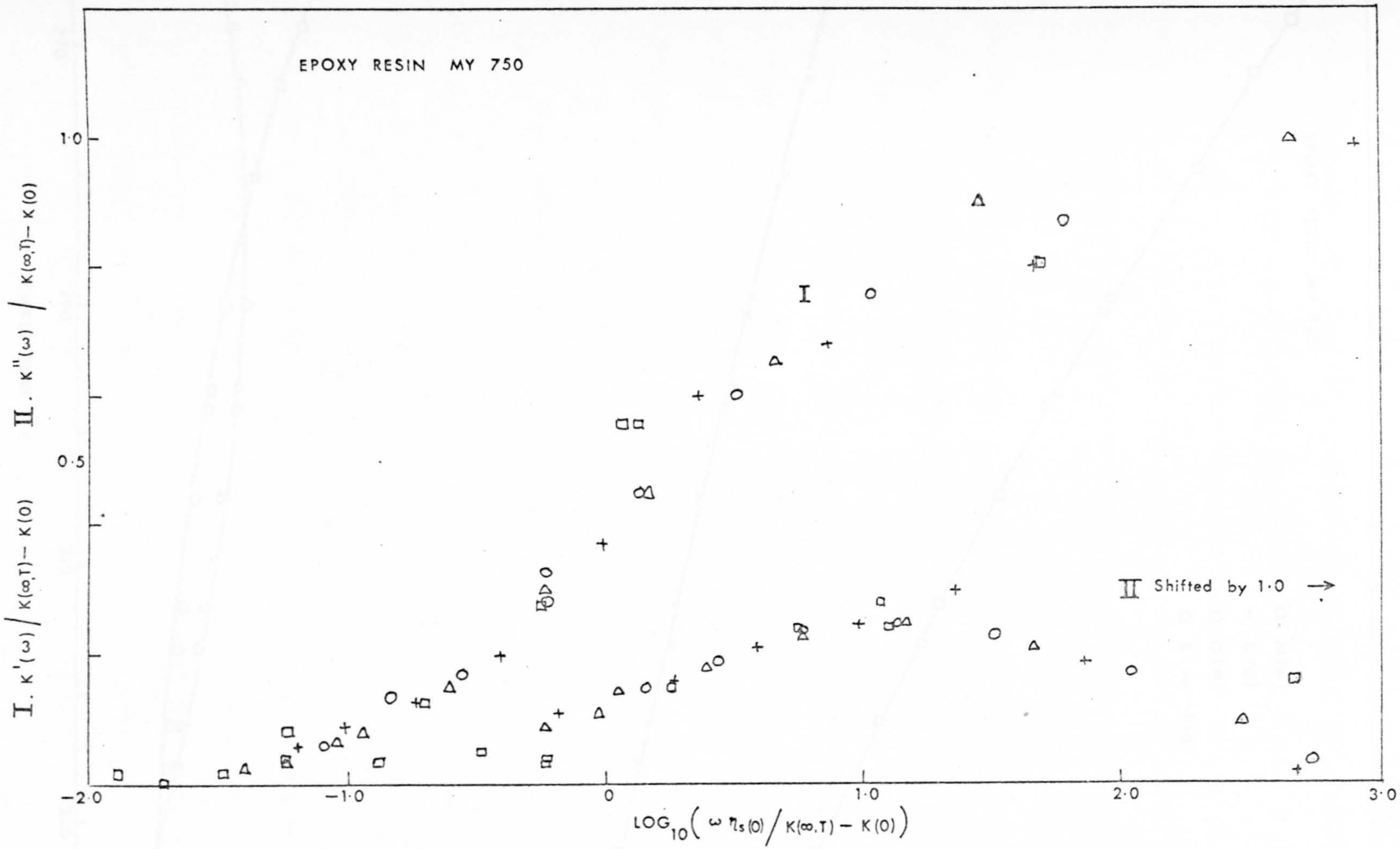

FIG. 6·3 THE VARIATION OF THE BULK STORAGE, I, AND LOSS, II, MODULI AS A FUNCTION OF REDUCED FREQUENCY

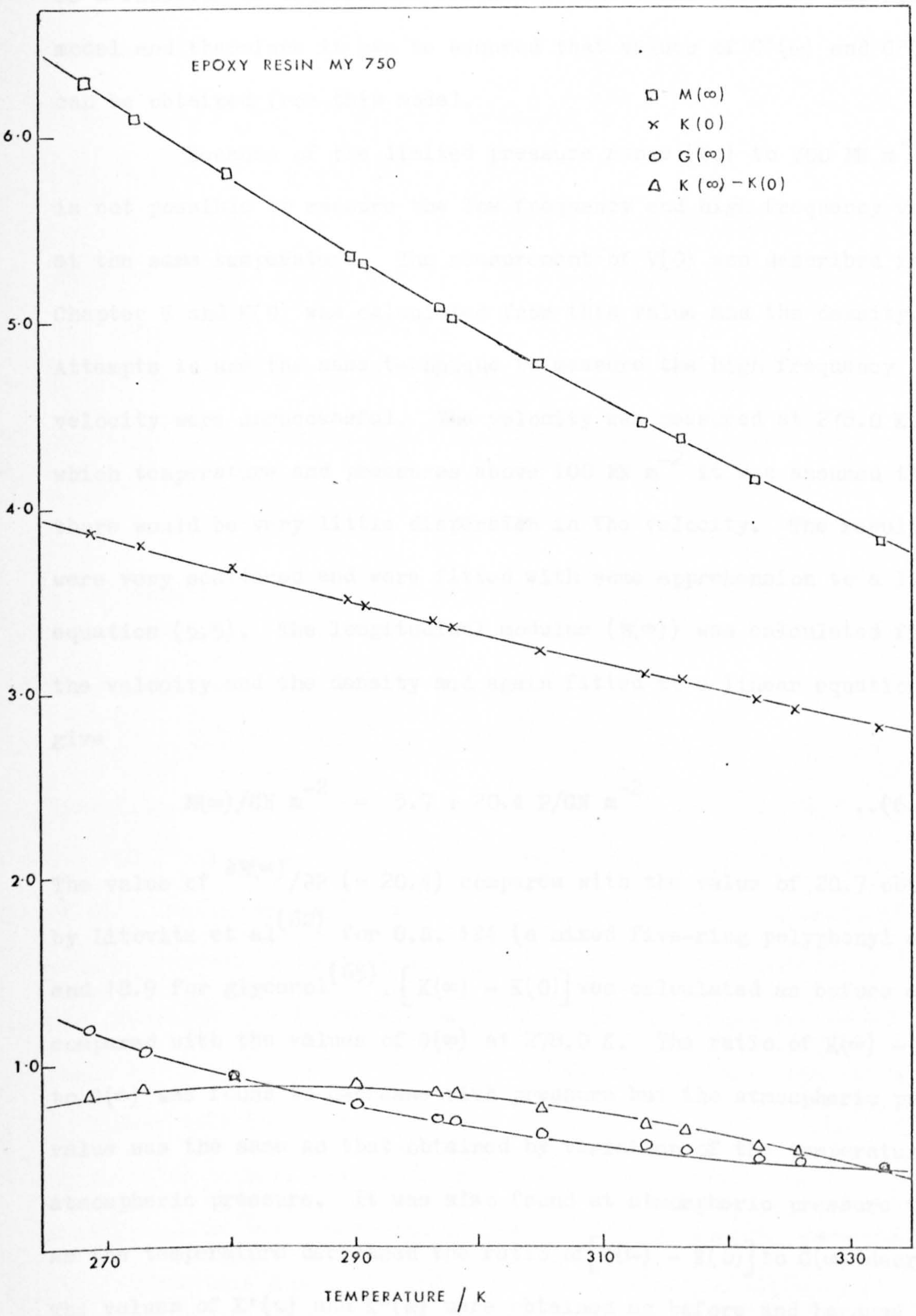

FIG. 6·4 THE VARIATION OF THE MODULI WITH. TEMPERATURE

of the shear impedance at pressures above atmospheric and therefore it is not possible to check experimentally the values of $G'(\omega)$ and $G''(\omega)$ obtained using the B.E.L. model. However, as seen in Figure 5.9b, the normalised values of the real part of the shear impedance as a function of the reduced frequency can be described by the B.E.L. model and therefore it can be assumed that values of $G'(\omega)$ and $G''(\omega)$ can be obtained from this model.

Because of the limited pressure range (0.1 to 700 MN m^{-2}) it is not possible to measure the low frequency and high frequency velocity at the same temperature. The measurement of V(0) was described in Chapter V and K(0) was calculated from this value and the density. Attempts to use the same technique to measure the high frequency velocity were unsuccessful. The velocity was measured at 278.0 K, at which temperature and pressures above 100 MN m^{-2} it was assumed that there would be very little dispersion in the velocity. The results were very scattered and were fitted with some apprehension to a linear equation (5.5). The longitudinal modulus ($M(\infty)$) was calculated from the velocity and the density and again fitted to a linear equation to give

$$M(\infty)/GN\ m^{-2} = 5.7 + 20.4\ P/GN\ m^{-2} \qquad ..(6.4)$$

The value of $\partial M(\infty)/\partial P$ (= 20.4) compares with the value of 20.7 obtained by Litovitz et al[62] for O.S. 124 (a mixed five-ring polyphenyl ether) and 18.9 for glycerol[65]. $[K(\infty) - K(0)]$ was calculated as before and compared with the values of $G(\infty)$ at 278.0 K. The ratio of $K(\infty) - K(0)$ to $G(\infty)$ was found to decrease with pressure but the atmospheric pressure value was the same as that obtained by variation of the temperature at atmospheric pressure. It was also found at atmospheric pressure that as the temperature decreased the ratio of $[K(\infty) - K(0)]$ to $G(\infty)$ decreased. The values of $K'(\omega)$ and $K''(\omega)$ were obtained as before and because of the difficulty in obtaining $V(\infty)$ and hence $M(\infty)$, $G(\infty)$ was used to reduce the

values of $K'(\omega)$ and $K''(\omega)$ and the frequency. The normalised values are given in Table AVI.5 as a function of pressure and shown in Figure 6.5. The curves are identical in shape to those of the reduced shear moduli but shifted by 0.45 on the logarithm scale, giving the ratio of η_v/η_s equal to 2.8 ± 0.04, this is of the same order as the value at atmospheric pressure.

6.4 S.E.P. in Di-2-ethylhexyl phthalate.

6.4.1 Atmospheric pressure.

$G'(\omega)$ and $G''(\omega)$ were calculated from the B.E.L. model at the same frequencies and temperatures at which the absorption coefficient and velocity had been measured, the latter quantities were used to obtain. $M'(\omega)$ and $M''(\omega)$. $K'(\omega)$ and $K''(\omega)$ were calculated as described previously. In Chapter V the high frequency velocity was taken to be linear with temperature, however, when the experimental values were used to calculate $M(\infty)$ and $^1/M(\infty)$ they were both found to be linear with temperature. The linear equations were as follows,

$$M(\infty)/GN\ m^{-2} = 16.89 - 0.055\ T/K \qquad ..(6.5)$$

$$^1/M(\infty)/(GN\ m^{-2})^{-1} = 0.179 + 0.00175\ T/K \qquad ..(6.6)$$

Therefore, depending on which equation is used, we have three values for $M(\infty)$, the highest values are given by equation (6.6). Three values of $K(\infty) - K(0)$ were obtained at each temperature and compared with the values of $G(\infty)$. When $V(\infty)$ was taken to be linear the ratio $K(\infty) - K(0)/G(\infty)$ decreased with increase in temperature but within the relaxation range it varied between 1.0 ± 0.2. Likewise, when $M(\infty)$ was taken to be linear with temperature the ratio $(K(\infty) - K(0)/G(\infty))$ decreased with increase in temperature and at high temperature $[K(\infty) - K(0)]$ was negative. The ratio was constant when $^1/M(\infty)$ was taken to be linear with temperature but was high, 2.0 ± 0.1. This is considerably higher than expected when compared with Di-2-ethylhexyl phthalate[16,28].

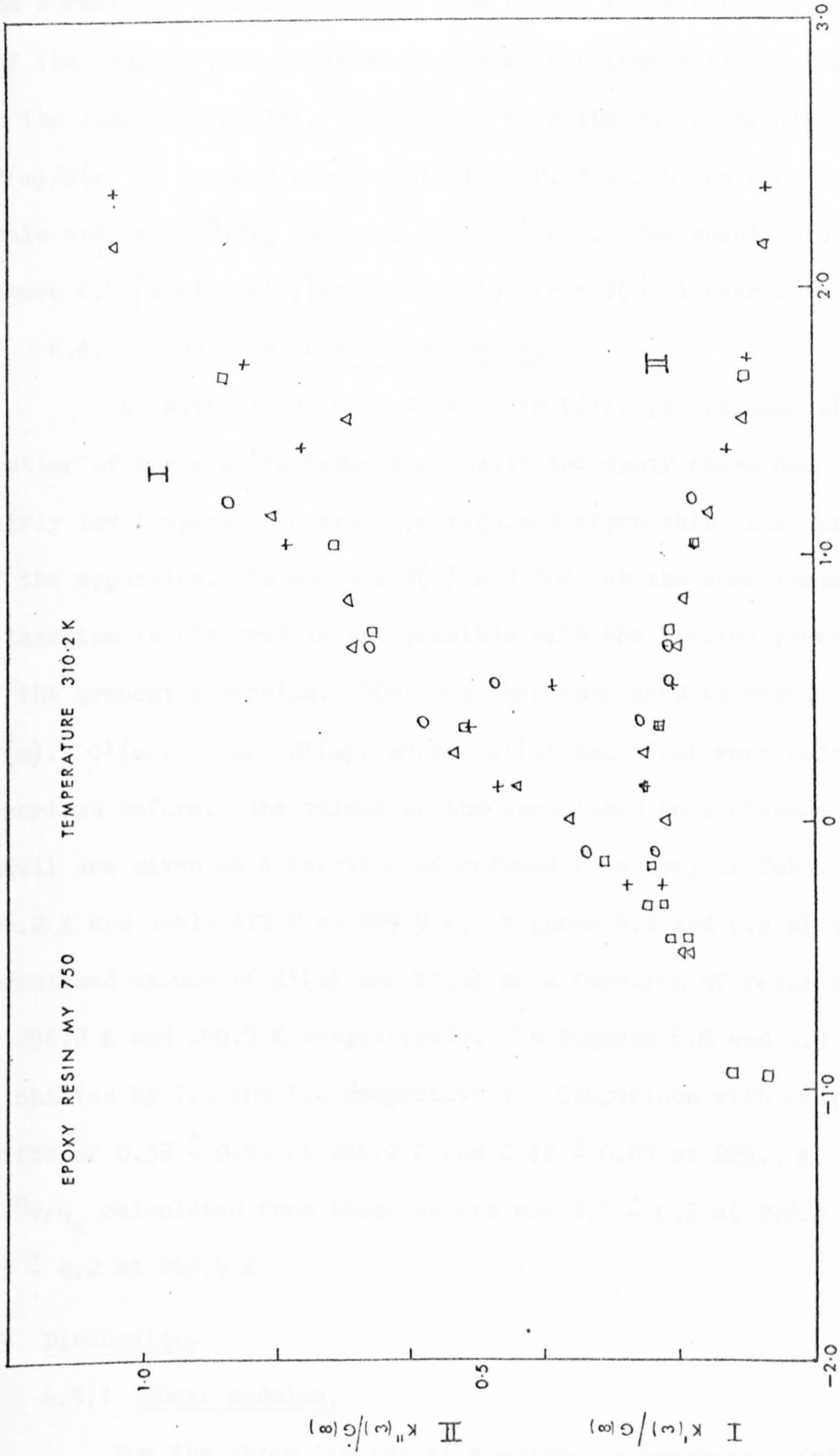

FIG. 6·5 THE VARIATION OF THE BULK STORAGE, I, AND LOSS, II, MODULI AS A FUNCTION OF REDUCED FREQUENCY

The normalised values calculated using $^1/M(\infty)$ linear with temperature were obviously too small and $K'(\omega)/(K(\infty) - K(0))$ was not approaching 1.0 even at fairly low temperatures (~ 210 K). It was decided to use $G(\infty)$ instead of $[K(\infty) - K(0)]$ to reduce $K'(\omega)$ and $K''(\omega)$. The values of the normalised bulk storage and loss moduli are given in Table AVI.6 and the reduced plot is shown in Figure 6.6 (Curve II is offset by 0.5 on the logarithm scale). Comparison with the curves of $G'(\omega)/G(\infty)$ and $G''(\omega)/G(\infty)$ in Graph 2 gives a shift of 0.43 ± 0.03 on the logarithm scale and hence η_v/η_s is equal to 2.7 ± 0.2. The moduli are shown in Figure 6.7, $[K(\infty) - K(0)]$ was calculated from $V(\infty)$ linear with temperature.

6.4.2 Pressures above atmospheric.

No attempt was made to measure $V(\infty)$, (a) because of the scatter of the results experienced with the epoxy resin and (b) because fairly low temperatures would be required approaching the safety limit of the apparatus. To measure $V(0)$ and $V(\infty)$ at the same temperature as relaxation is observed is not possible with the limited pressure range of the present apparatus. $G(\infty)$ was therefore used to reduce $K'(\omega)$ and $K''(\omega)$. $G'(\omega)$, $G''(\omega)$, $M'(\omega)$, $M''(\omega)$, $K'(\omega)$ and $K''(\omega)$ were calculated as described before. The values of the normalised bulk storage and loss moduli are given as a function of reduced frequency in Table AVI.7 at 296.2 K and Table AVI.8 at 269.9 K. Figures 6.8 and 6.9 show the normalised values of $K'(\omega)$ and $K''(\omega)$ as a function of reduced frequency at 296.2 K and 269.9 K respectively. In Figures 6.8 and 6.9 Curve II is shifted by 1.5 and 1.0 respectively. Comparison with Graph 2 gives shifts of 0.35 ± 0.03 at 296.2 K and 0.40 ± 0.03 at 269.9 K. The values of η_v/η_s calculated from these shifts are 2.2 ± 0.2 at 296.2 K and 2.5 ± 0.2 at 269.9 K.

6.5 Discussion.

6.5.1 Shear modulus.

For the three liquids at atmospheric pressure, $J(\infty)$ was found

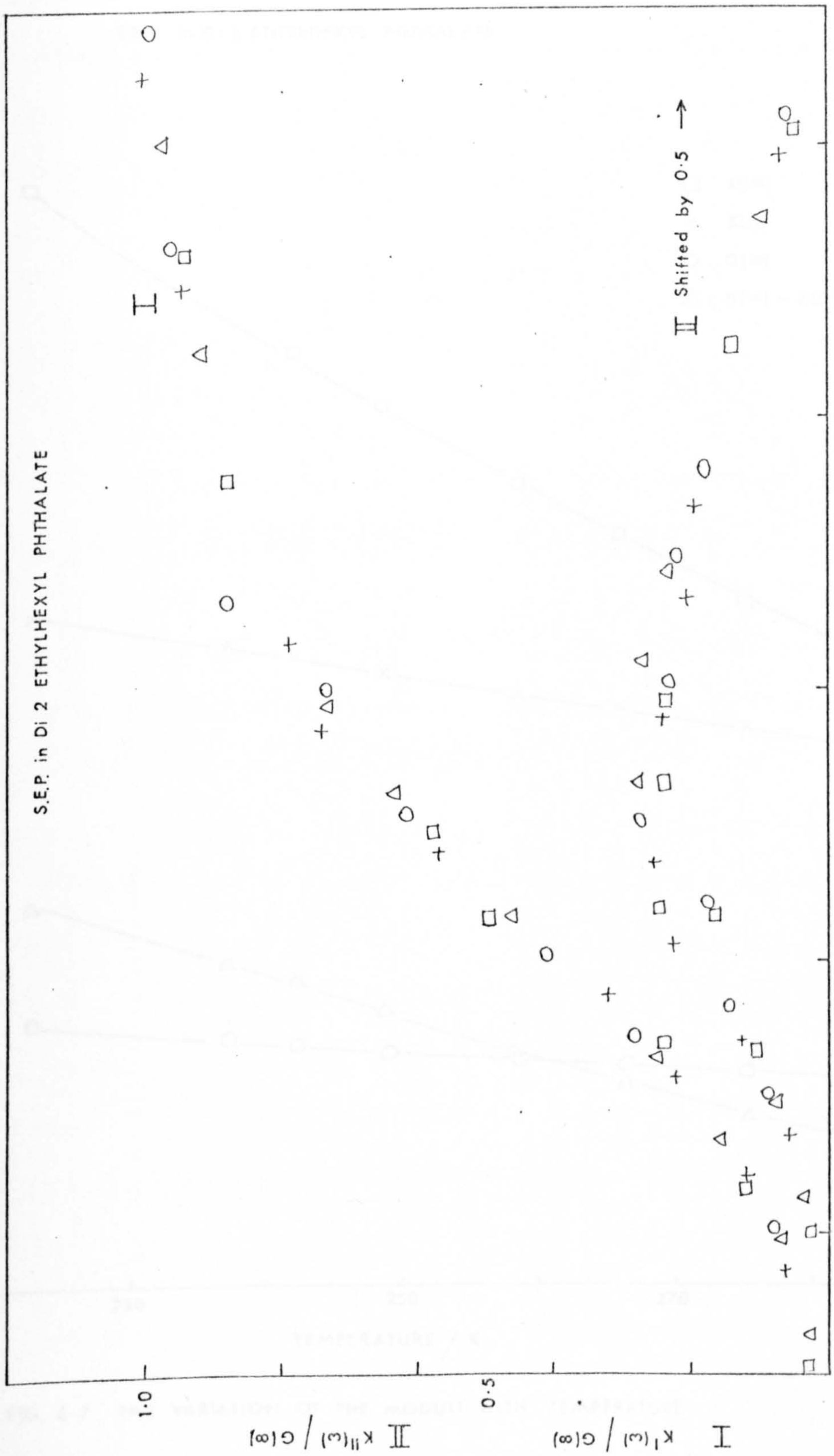

FIG. 6·6 THE VARIATION OF THE BULK STORAGE, I, AND LOSS, II, MODULI AS A FUNCTION OF REDUCED FREQUENCY

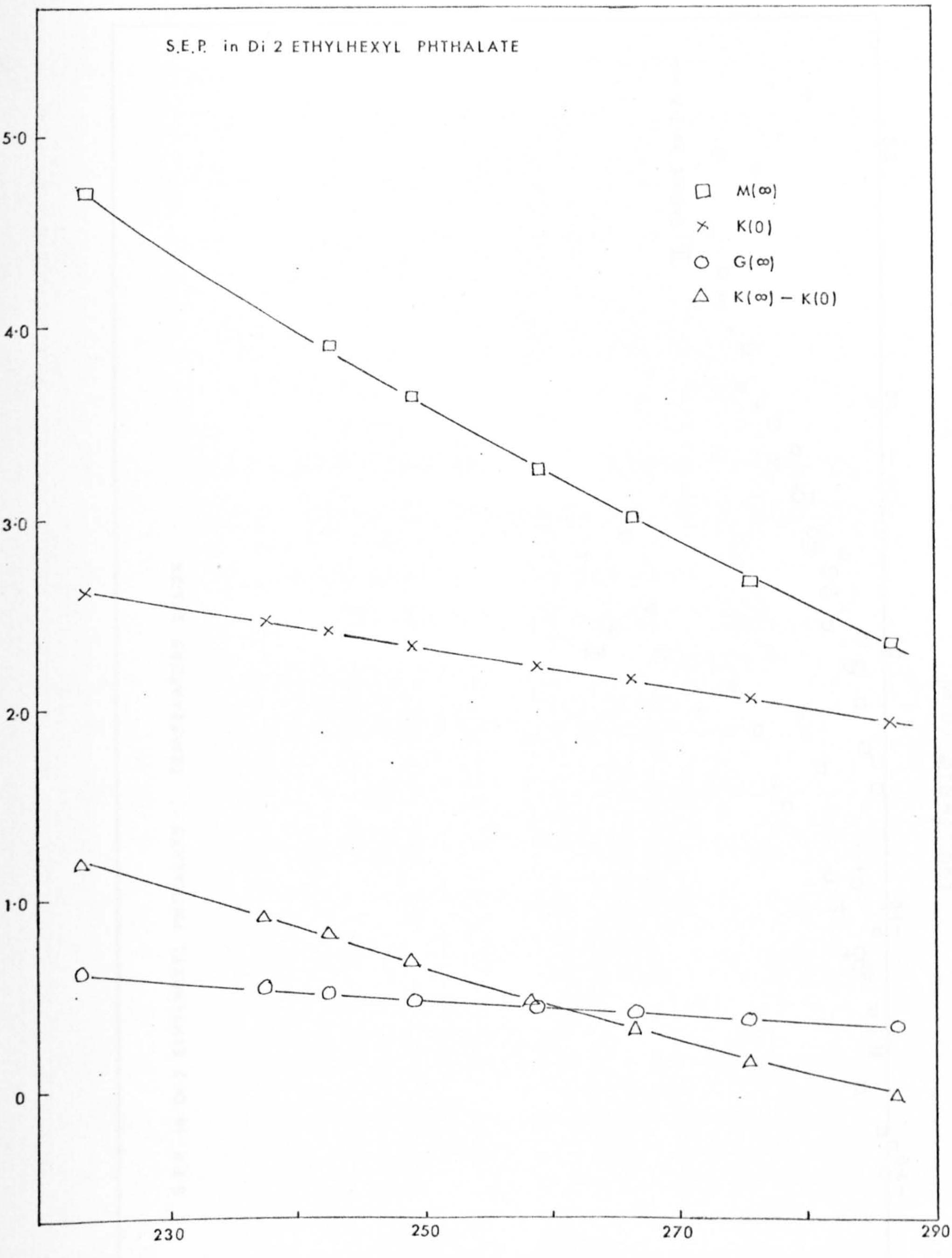

FIG. 6·7 THE VARIATION OF THE MODULI WITH TEMPERATURE

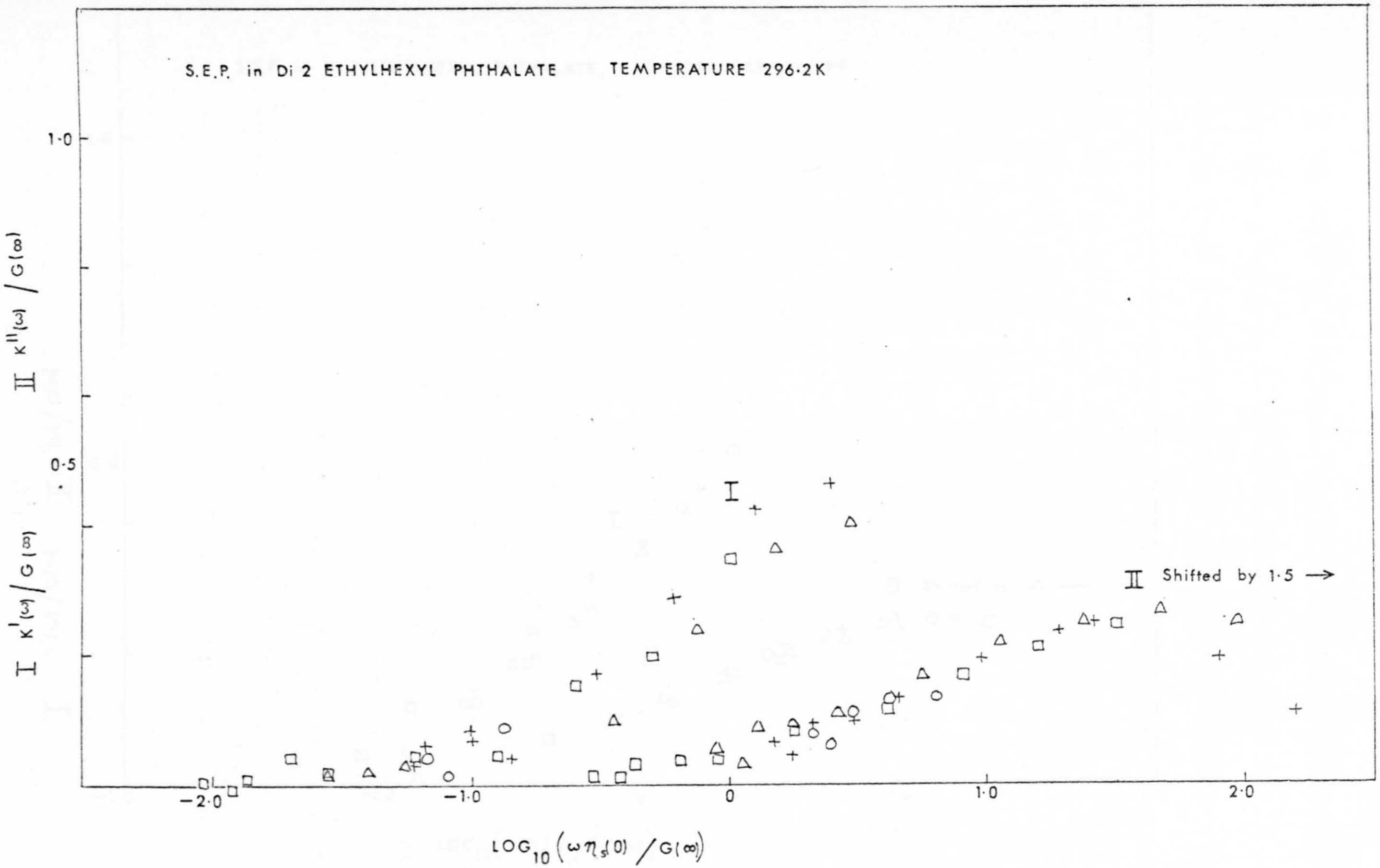

FIG. 6·8 THE VARIATION OF THE BULK STORAGE, I, AND LOSS, II, MODULI AS A FUNCTION OF REDUCED FREQUENCY

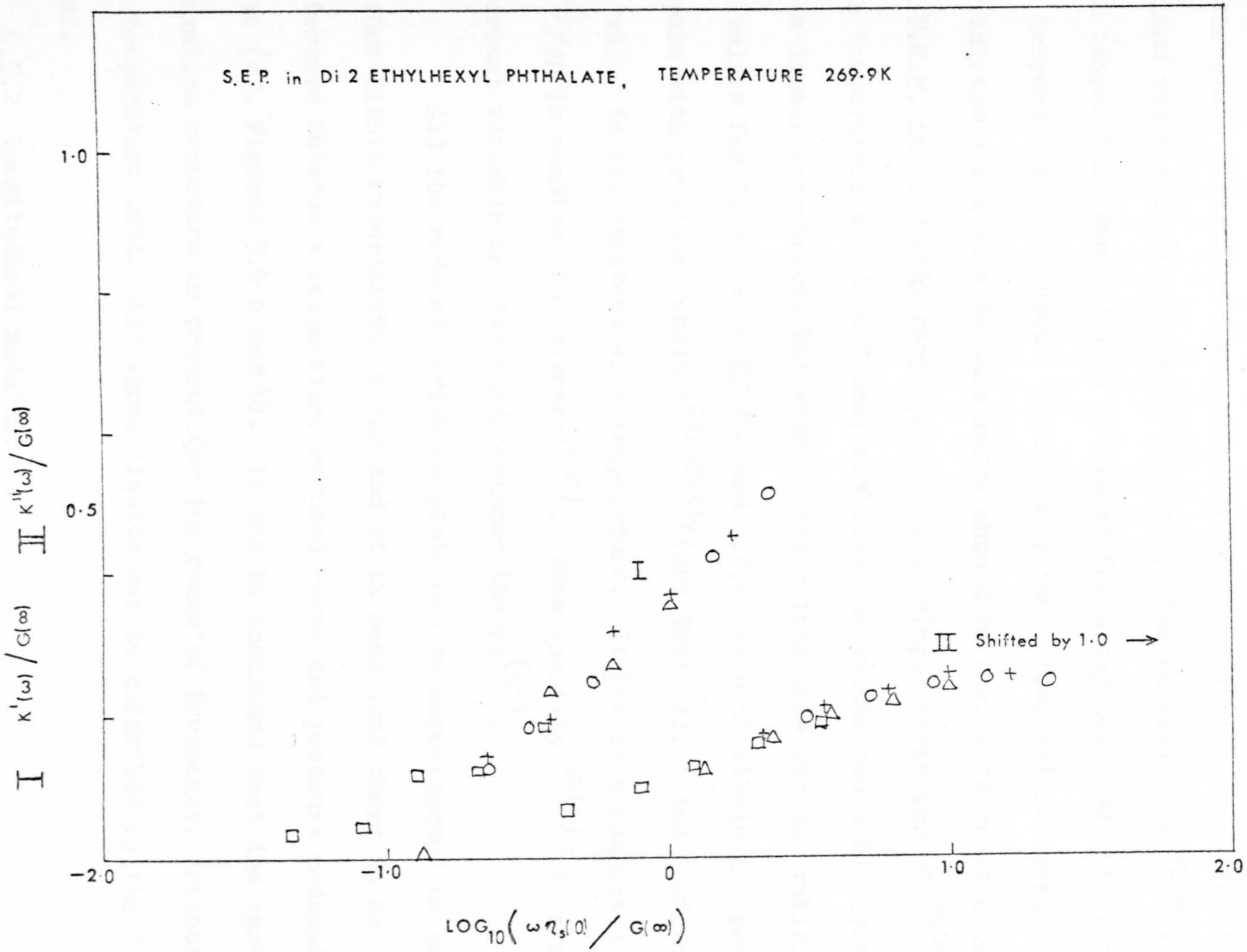

FIG. 6·9 THE VARIATION OF THE BULK STORAGE, I, AND LOSS, II, MODULI AS A FUNCTION OF REDUCED FREQUENCY

to vary linearly with temperature, the values of $G(\infty)$ were about the same order of magnitude for the three liquids and other liquids[11,21] with maximum values between 1.0 and 1.5 GN m^{-2}. Above atmospheric pressure $G(\infty)$ was found to vary linearly with pressure (although for Epoxy Resin MY 750 and S.E.P. in Di-2-ethylhexyl phthalate $R_s(\infty)$ was also found to vary linearly with pressure at each temperature), maximum values of $G(\infty)$ were greater than those obtained at atmospheric pressure (~ 2 GN m^{-2}). At the glass transition temperature or pressure $G(\infty)$ approaches its maximum value and thereafter is constant. The variation of $\partial G(\infty)/\partial P$ with temperature was found to be linear for Epoxy Resin MY 750, within the temperature range used. (Since only three temperatures were used any extrapolation outside this range should be used with great care). For S.E.P. in Di-2-ethylhexyl phthalate no simple variation of $\partial G(\infty)/\partial P$ with temperature could be found, although the values could be forced to fit a linear expression, but with so few points this was not valid. The values for Epoxy Resin MY 750 and S.E.P. in Di-2-ethylhexyl phthalate compare with previous results[28,58,66] (see Table AI.2) and confirm that the value is not constant with temperature. It has been suggested that $\partial G(\infty)/\partial P$ is constant for glycerol[65]. This quantity $\partial G(\infty)/\partial P$ is an important variable in elastohydrodynamic theory[67].

All the reduced variables plots can be superimposed on one-another within experimental error and it is seen that there is no difference between a temperature reduced curve and pressure reduced curve (cf. Figures 5.9 a and b). It can be concluded that the same relaxation mechanism is present for the range of frequency, pressure and temperature used. All three liquids can be described by the B.E.L. model.

6.5.2 Longitudinal modulus.

The data available on this quantity is sparse but recent work using light scattering techniques[62,63] has shown that $M(\infty)$ is linear with temperature and also pressure. As far as is known there is no work

to show what happens at low temperatures and/or high pressures when the glass transition is reached. The magnitude of $M(\infty)$ and to a certain extent $K(0)$ depends on the density. For liquids with densities of about 1000 Kg m^{-3} at ambient temperature, HVI 330 oil, MVI 170 oil, Di-2-ethylhexyl phthalate[28] and S.E.P. in Di-2-ethylhexyl phthalate $K(0)$ is about 3.0 GN m^{-2} and $M(\infty)$ less than 5.0 GN m^{-2} at the low temperature end of the relaxation region, whereas liquids with higher densities, Aroclor 1254[28], 4-phenyl dibenzofuran and Epoxy Resin MY 750 have values of $K(0)$ equal to about 4.0 GN m^{-2} and $M(\infty)$ about 6.0 GN m^{-2}. It appears that the density is a more important quantity than the velocity in determining the magnitude of $M(\infty)$. The above seems to be true for organic covalent compounds but ionic compounds have much higher values of $K(0)$ and $M(\infty)$, for aqueous calcium nitrate solution Ambrus et al[63] gives $K(0)$ about 5.5 GN m^{-2} and $M(\infty)$ about 18 GN m^{-2}, the density is also higher than organic covalent compounds. Attempts to put some quantitative measure on the value of $M(\infty)$ failed, calculation of $M(\infty)$ at a fixed density (i.e. 1000 Kg m^{-3}) gave similar values for oils but for Aroclor 1254 and Epoxy Resin MY 750 very low values were obtained. Zwanzig and Mountain[68] gave the following formula for $K(\infty)$

$$K(\infty) = {}^{5}/_{3}\, G(\infty) + 2(P - \rho k_B T) \qquad ..(6.7)$$

where ρ is the number density $^{N}/_{V}$ (where V is the total volume of N molecules),

k_B is Boltzmann's constant ($= {}^{R}/_{N} = 1.3805 \times 10^{-23}$ J K^{-1}),

P is the thermodynamic pressure of the fluid.

Substituting in (6.7) for $K(\infty)$ ($= M(\infty) - {}^{4}/_{3}\, G(\infty)$) we have

$$M(\infty) = 3G(\infty) + 2(P - \rho k_B T) \qquad ..(6.8)$$

$$\text{now} \quad \rho k_B T = \frac{N}{V} \cdot \frac{R}{N} T \qquad ..(6.9)$$

(for 4-phenyl dibenzofuran at 270 K, $\rho k_B T = 0.011$ GN m^{-2})

The quantity $\rho k_B T$ can be neglected in comparison with $M(\infty)$ and $G(\infty)$ and therefore

$$M(\infty) \simeq 3\,G(\infty) + 2P \qquad ..(6.10)$$

In the present work and that of Powell[28] it is found that $M(\infty)$ is equal to about 6 $G(\infty)$. Thus P has values between 1.0 and 2.0 GN m^{-2}. Gopala Rao and Nammalvar[69] using Henderson's equation of state for P, found good agreement between the observed and calculated value for $G(\infty)$. However, calculation of P from Henderson's equation for glycerol using the quantities given yields 0.24 GN m^{-2}, less than calculated in the present work.

The value of $\partial M(\infty)/\partial P$ obtained in this work is very similar to that obtained by others, but this may have been fortuitous. The value of $M(\infty)$ like that of $G(\infty)$ is higher at pressures above atmospheric by a factor of 1.5 to 2.0 that of the atmospheric value at the end of the relaxation region.

6.5.3 Bulk modulus.

The low frequency bulk modulus has been discussed earlier. The accuracy of the high frequency bulk modulus depends on the value of $M(\infty)$, since $G(\infty)$ has been well established. $K(\infty)$ is important in determining $[K(\infty) - K(0)]$ which has been found to be of the same order of magnitude as $G(\infty)$ and to have a similar temperature and pressure dependence. With all three liquids the reduced variables plots of the real and imaginary parts of the bulk modulus were found to have the same shape as the real and imaginary parts of the shear modulus but in all instances they were shifted to the left of the shear values. It can be assumed that the same mechanism is involved in both shear and bulk relaxations. All the data can be fitted by assuming a distribution of relaxation times. The majority of the literature on viscoelastic relaxation has shown that the results can only be accounted for by assuming a distribution of relaxation times. However, there have been

claims that a single relaxation time is obtained, for Soya bean and Cotton seed oils[24] for both bulk (volume) and shear viscosities. The shear relaxation is attributed to a reorientational mechanism and bulk relaxation to a molecular packing rearrangement. In two other liquids, Castor and Tung oils, both processes are thought to be strongly coupled and therefore lead to a wide spectrum of relaxation times for both bulk and shear viscosities. A dubious paper[70] also assumes a single relaxation time for bulk and shear relaxation of an ethyl alcohol-water mixture.

6.5.4 The ratio of volume to shear viscosity.

The value of this ratio was found to be about 3 for three liquids. These values compare with those previously obtained by the same method (cf. Table AI.1). For Di-2-ethylhexyl phthalate, S.E.P., in Di-2-ethylhexyl phthalate and Epoxy Resin MY 750 the value of η_v/η_s was smaller at pressures above atmospheric pressure, but the difference between the two values is hardly significant. Slie and Madigosky[65] found for glycerol at 299.2 K that the ratio was 0.80 ± 0.03 for pressures up to 200 MN m^{-2}. Their value was obtained from ultrasonic measurements from the formula given in (6.11).

$$\eta_v/\eta_s = 4/3 \quad \alpha_{obs}/\alpha_{cl} - 1 \qquad ..(6.11)$$

Another later investigation of glycerol[71] found by changing the pressure from 0.1 to 100 MN m^{-2} the ratio changed from 1.24 to 1.16 (i.e. 1.20 ± 0.04).

All the evidence to date suggests that for viscous liquids the ratio is constant at temperatures and pressures.

6.5.5 The magnitude of α.

In previous work[28] and this work, the value of logarithm of maximum α/f^2 against logarithm of f at atmospheric pressure was shown to fit the linear relationship of Singh and Mishra[23]. This relationship seems to be applicable to covalent organic compounds. The results

of Ambrus et al[63] for calcium nitrate and Bogdanov et al[72] for boric oxide gave much higher values of maximum α/f^2 at a fixed frequency than predicted by Singh and Mishra. Nevertheless, all the literature seen to date gives values of α for a structural relaxation process which are always higher than those obtained from rotational isomerisation, vibrational relaxation and chemical equilibria. The values differ by a factor of 2 upwards. Therefore the value of α will give some indication of whether a structural relaxation is present when shear measurements are not available. It is doubtful if any other process could be detected if it takes place on the same time scale as the viscoelastic relaxation, Matheson and Dexter[10] found two processes for sec-butyl benzene but they were separated in time, the high temperature mechanism was due to internal rotation of the sec-butyl group and the low temperature process due to viscoelastic relaxation. A recent Russian paper[73] suggests different mechanisms for the low and high frequency measurements on butyric esters.

6.5.6 Polymer solutions.

The values obtained in this work for S.E.P. in Di-2-ethylhexyl phthalate have been compared with those of Di-2-ethylhexyl phthalate obtained by Powell[28]. The various quantities are given in Table AVI.9. There is really no significant difference between the two sets of values, except perhaps in the value of η_v/η_s (Di-2-ethylhexyl phthalate = 1.9 $\pm$ 0.2, S.E.P. in Di-2-ethylhexyl phthalate = 2.7 $\pm$ 0.2), but differences of this magnitude have been quoted before[16].

Polymers have been studied by others, Barlow et al[74] investigated polydimethylsiloxane liquids of varying viscosity in the frequency ranges 10 kHz to 125 kHz and 6 to 78 MHz and temperatures from 223.2 to 323.2 K. The data for each liquid could be reduced onto a single curve, but at low frequency the combined data could not be reduced onto a single curve. The values of the real and imaginary parts of the shear modulus were found to increase with increase in viscosity

at the same reduced frequency. However, as the frequency was increased (6 to 78 MHz) the curves merged together. The results were in close agreement with the theory of Rouse[75]. This theory proposes that the molecule is composed of sub-units whose movement is damped by the solvent viscosity, but the velocity of the solvent is unaffected by the presence of the polymer. The relaxation time of the modes of motion depends on the molecular weight and the viscosity. Further work by Barlow et al[54] on Poly-1-butenes (later[76] described as isomeric butenes) of varying molecular weight, the lowest molecular weight equivalent to eight monomer units, at low (64 kHz) and high (6-30 MHz) frequencies showed that the polymer of lowest molecular weight was similar to that of pure liquids whereas the higher molecular weight samples were found to have a second relaxation process at the low frequency. Similar results were found for polyethylacrylates and poly-n-butylacrylates[76]. The relaxation process at high frequencies could be described by the B.E.L. model, whereas the relaxation process at lower frequencies arose from the modes of motion of the flexible polymer chain.

The above work was concerned with 'pure' polymers, nevertheless work on polymers in solution has shown similar effects. Dilute solutions of high molecular weight polystyrene in Aroclor and Di-2-ethylhexyl phthalate at low frequencies (0.016 to 400 Hz) have been investigated by Frederick et al[77], they found that the observed frequency dependence of the real and imaginary shear modulus ranged from the predictions of Rouse to that of Zimm[78]. The Zimm theory is similar to that of Rouse but assumes that the solvent is retarded at the centre of the coiled chain. The viscoelastic properties of high molecular weight polystyrene in a few solvents have been investigated by Lamb and Matheson[79] again at low frequency (40 - 73 kHz). In a good solvent, e.g. toluene and fairly dilute solutions 1 - 3% $^{w}/_{v}$ the results could be fitted to the Zimm theory with some deviations at lower frequencies,

but as the solvent power decreased greater deviations were obtained from both the Rouse and the Zimm theories. The values of G' and G"-$\omega\eta_s$ were not self-consistent and this was attributed to the viscosity term. The viscosity was adjusted to make the values self-consistent and the results were then found to fit the theory of Rouse. From this adjusted viscosity it was found that 25% of the polymer contribution to the viscosity does not take part in the viscoelastic relaxation. For the poor solvent, e.g. methyl ethyl ketone the behaviour could be described by the Rouse or Zimm theory depending on the polymer contribution to the viscosity.

There has been very little work on the ultrasonic absorption of dilute polymer solutions, Mikhailov and Polunin[80] found a slight increase in absorption for a 3% solution of polyisobutylene (molecular weight 118,000) in transformer oil compared to the pure oil at various pressures. They attributed the cause of the increase in absorption to be due to the friction between the polymer chains and the solvent.

It can be seen from the above brief survey of polymers and their solutions that the effects of polymers are only seen at low frequency where the molecular modes are active, at higher frequency the viscosity has relaxed and the solution behaves like a low molecular weight liquid. This has been confirmed in the present work. However, the effect on the absorption coefficient of the longitudinal waves was small and therefore suggests that in this solution (S.E.P. in Di-2-ethylhexyl phthalate) there is very little friction between the polymer chains and the solvent.

CHAPTER VII

MICELLE SYSTEMS

7.1 Introduction.

This chapter is devoted to a preliminary investigation of micelle solutions. It was intended to measure the absorption coefficient, velocity and density at pressures above atmospheric pressure. However, in the presence of these solutions the transducer was detached from the quartz rod and therefore only the velocity and density were measured. Section 7.2 deals with the effects of pressure on solutions of decyltrimethylammonium bromide, while in Section 7.3 the shear properties of a liquid crystal system are investigated.

7.2 Attempts to determine the critical micelle concentation at various pressures.

7.2.1 Introduction.

At the start of this work only a few studies had been made of the effect of pressure on the critical micelle concentration (c.m.c.) in aqueous solutions. Hamann[81] studied the effect of pressure (to 200 MN m^{-2}) on solutions of sodium dodecyl sulphate. He argued that an increase in pressure should raise the c.m.c. This was found to be true for sodium dodecylsulphate at pressures below 100 MN m^{-2}, however, above 100 MN m^{-2} the c.m.c. decreased with increase in pressure. Hamann suggested that the micelles were more dense than the free ions which may have been caused by either the partial freezing of the hydrocarbon chains within the micelle, or the hydrocarbon interior within the micelle was more compressible than the hydrocarbon chains of the free ions in water. Tuddenham and Alexander[82] investigated the effect of pressure (to 300 MN m^{-2}) on octyl, decyl and dodecyltrimethylammonium bromide. They found the same effect as Hamann, that is, the c.m.c. increased followed by a decrease with increase in pressure. The partial molar volume change ($\Delta\bar{V}$) was found to change sign with increasing pressure, at low pressures (up to 100 MN m^{-2}) it was positive whereas above this pressure it was negative. Several plausible explanations were put forward including the fact that the viscosity of water passes through

a minimum at about 100 MN m^{-2} and then rises rapidly with increase in pressure. Dodecyl ammonium chlorides were also found to show the same pattern of behaviour up to 500 MN m^{-2} (83,84). In all the above investigations the c.m.c. was determined from conductivity measurements, therefore it would be useful to compare with measurements obtained by another technique. A series of sodium alkylsulphates have been studied at atmospheric pressure and 303.2 K by Shigehara(85). The c.m.c. was determined from the compressibility which in turn was obtained from the measurements of velocity and density. The graph of velocity against density shows a break at the c.m.c. The compressibility is closely related to the hydration of the solute in solution. Shigehara showed that the compressibility of the micelle and the molar volume of the methylene group in the micellar state were constant and independent of the number of carbon atoms in the alkylsulphate molecule. The value was nearer to that of a liquid rather than solid hydrocarbon. It was concluded that the hydrocarbon interior was liquid in nature. Sound velocity measurements were also used by Rassing et al(86) to determine the c.m.c. of a larger series of alkylsulphates (C_5 to C_{11}). The values obtained compared with those from reaction rates (c.m.c. = k_a/k_d, where k_a and k_d are the association and dissociation rate constants respectively) and from other published c.m.c. data. The success of the velocity method prompted an investigation of decyltrimethylammonium bromide at pressures above atmospheric.

7.2.2 Theory.

The change of c.m.c. with pressure has been shown by Tuddenham and Alexander(82) to be related to the partial molar volume change by the following equation.

$$\Delta \bar{V} = RT \frac{\partial(\ln \text{ c.m.c.})}{\partial P} \qquad ..(7.1)$$

The formula was derived by two different methods each one making certain assumptions.

The compressibility is related to the velocity and density by the Laplace equation (7.2),

$$\beta = \frac{1}{V^2\rho} \qquad ..(7.2)$$

Therefore from the density and velocity all the above quantities can be calculated.

7.2.3 Experimental and results.

Decyltrimethylammonium bromide (ex. Pfaltz and Bauer) was used to prepare the following aqueous solutions 0.005, 0.01, 0.04, 0.05, 0.2, 0.1, 0.5 and 1.0 molar. The density was measured at a few temperatures at atmospheric pressure and at 298.2 K at pressures above atmospheric. The apparatus for both sets of measurement was described in Chapter III (3.5). At atmospheric pressure the density varied linearly with temperature, the parameters for the linear equation for the solutions are given in Table AVII.1. The high pressure measurements which are shown in Figure 7.1 were fitted to the linear secant modulus equation, the parameters of which are given in Table AVII.2.

The velocity was measured with the velocimeter described in Chapter III (3.4.2). The apparatus is capable of providing very accurate measurements of velocity which are required to detect the break in the curve of velocity against concentration to give the c.m.c. Difficulties were experienced with these measurements. At atmospheric pressure with the Townson and Mercer bath the measurements were reproducible to $\pm$ 0.01% with both cells. (Atmospheric pressure cell, spacer length 5.5 mm and high pressure cell, described by Powell[28]). Nevertheless, when the cell was used in the high pressure apparatus the results were only reproducible to $\pm$ 0.2%, which was unsatisfactory for the calculation of the c.m.c. The poor reproducibility was attributed to poor temperature stability and/or pressure stability. The temperature stability was not better than 0.1 of a degree, which was inadequate. The glass matting, surrounding the aluminium bath, had cracked through

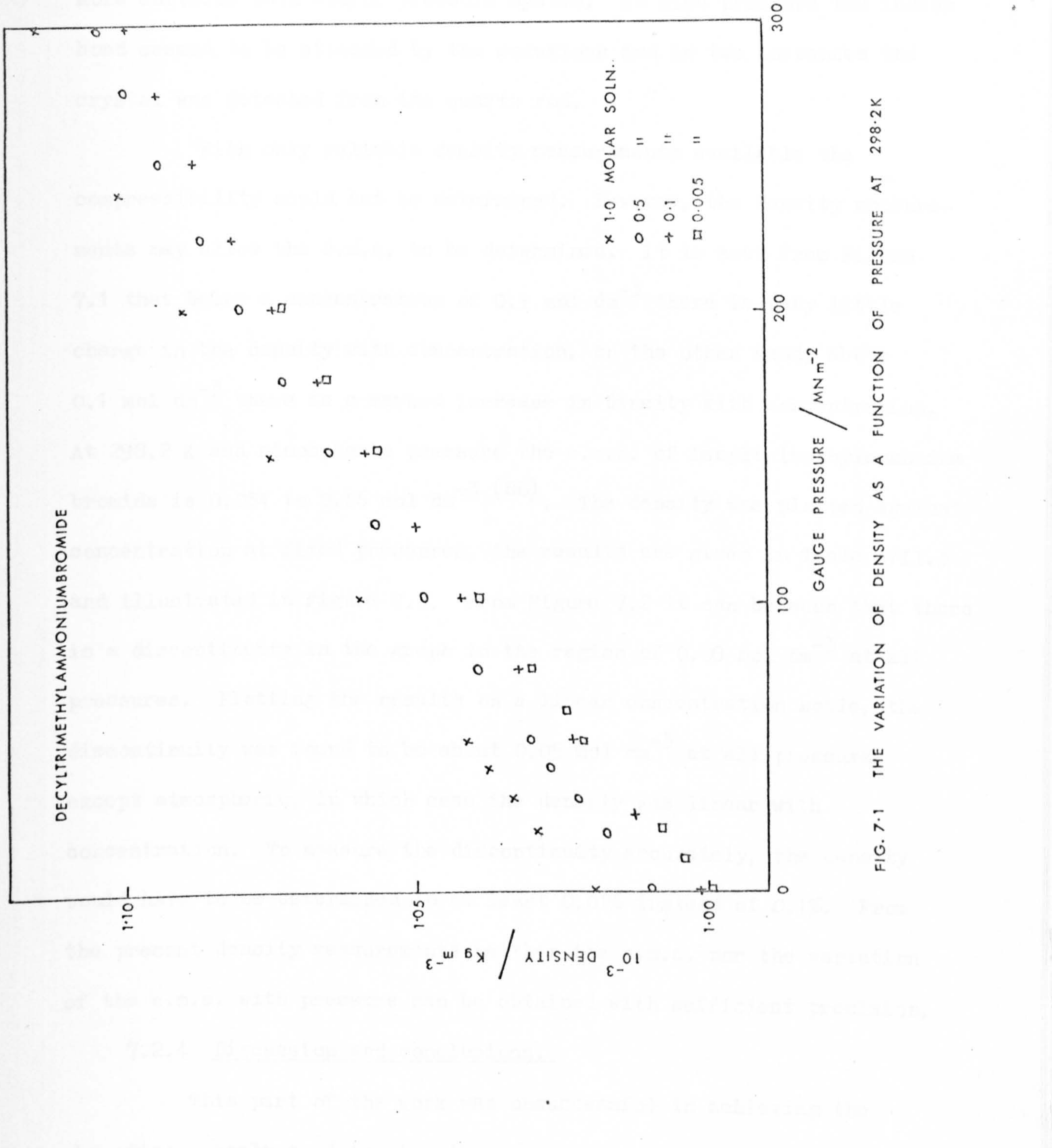

FIG. 7·1 THE VARIATION OF DENSITY AS A FUNCTION OF PRESSURE AT 298·2K

constant use at low temperature and was therefore renewed, but the slight improvement in temperature stability was still insufficient to achieve accurate measurements of velocity. After extensive measurements had been made it was decided not to pursue the velocity measurements, which would probably only be improved by the construction of a more suitable bath and/or pressure system. At high pressure the indium bond seemed to be attacked by the solutions and in two instances the crystal was detached from the quartz rod.

With only reliable density measurements available the compressibility could not be determined. However, the density measurements may allow the c.m.c. to be determined. It is seen from Figure 7.1 that below a concentration of 0.1 mol dm^{-3} there is very little change in the density with concentration, on the other hand, above 0.1 mol dm^{-3} there is a marked increase in density with concentration. At 298.2 K and atmospheric pressure the c.m.c. of Decyltrimethylammonium bromide is 0.054 to 0.06 mol dm^{-3} (86). The density was plotted against concentration at fixed pressures, the results are given in Table AVII.3 and illustrated in Figure 7.2. From Figure 7.2 it can be seen that there is a discontinuity in the graph in the region of 0.08 mol dm^{-3} at all pressures. Plotting the results on a linear concentration scale, the discontinuity was found to be about 0.05 mol dm^{-3} at all pressures except atmospheric, in which case the density was linear with concentration. To measure the discontinuity accurately, the density would have to be determined to at least 0.01% instead of 0.1%. From the present density measurements neither the c.m.c. nor the variation of the c.m.c. with pressure can be obtained with sufficient precision.

7.2.4 Discussion and conclusions.

This part of the work was unsuccessful in achieving the objective, namely to determine the c.m.c. at various pressures from the compressibility and hence to calculate the partial molar volume. After this work had progressed, i.e. all the density and some velocity

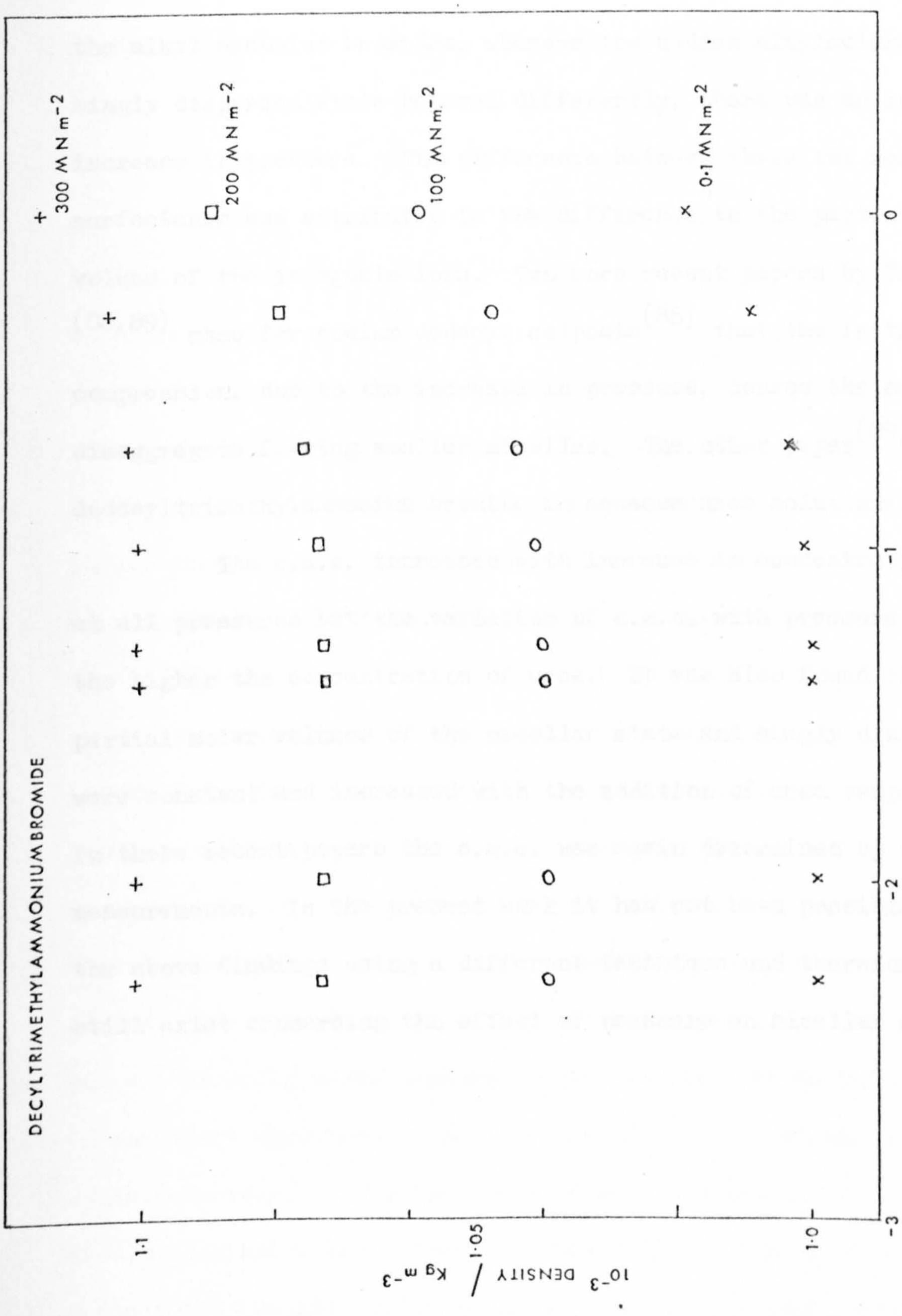

FIG. 7·2 THE VARIATION OF DENSITY WITH CONCENTRATION AND PRESSURE AT 298·2 K

measurements had been made, a paper by Tanaka et al[87] was published on the partial molar volumes of surfactants under high pressure. Among the compounds studied was decyltrimethylammonium bromide. They found the partial molar volume decreased with increase in pressure in the micelle state for all compounds and in the singly dispersed state for the alkyl ammonium bromides, whereas the sodium alkylsulphates in the singly dispersed state behaved differently, there was an increase with increase in pressure. The difference between these two series of surfactants was attributed to the difference in the partial molar volume of the inorganic ions. Two more recent papers by Tanaka et al [88,89] show for sodium dodecyl sulphate[88] that the initial compression, due to the increase in pressure, causes the micelle to disaggregate forming smaller micelles. The other paper[89] deals with dodecyltrimethylammonium bromide in aqueous urea solutions.

The c.m.c. increased with increase in concentration of urea at all pressures but the variation of c.m.c. with pressure was less the higher the concentration of urea. It was also found that the partial molar volumes of the micellar state and singly dispersed state were constant and increased with the addition of urea respectively. In these recent papers the c.m.c. was again determined by conductivity measurements. In the present work it has not been possible to confirm the above findings using a different technique and therefore doubts still exist concerning the effect of pressure on micellar systems.

7.3 Shear properties of a 'liquid crystal'.

7.3.1 Introduction.

The properties of 'liquid crystals' or crystalline phases are becoming increasingly important, especially in the field of medicine and detergents. Winsor[90] has reviewed the amphiphilic compounds of liquid crystalline solutions with regard to phase changes and other physical properties. However, to date only a few reports have appeared of the response to shear and ultrasonic waves. Lee et al[91] have shown that liquid crystals have different values of the shear impedance when orientated in different directions. The nematic and isotropic states of p-methoxybenzylidene-p-n-butylaniline gave values of the real (R_s) and imaginary (X_s) parts of the shear impedance which were equal for the three orientations in the isotropic state but varied according to the direction for the nematic state. The real part was larger than the imaginary part and both values were very close to that expected from a Newtonian liquid. Barlow and Letcher[92] found that in the nematic state of ethyl p(p-methoxybenzylidene amino) cinnamate R_s was equal to the Newtonian value within experimental error at 30 and 450 MHz. On the other hand, the smectic states of ethyl-p-azoxy-benzoate and heptyloxyazoxybenzene gave R_s values lower than those expected from Newtonian liquids. The latter was attributed to either the material being viscoelastic or the shear impedance was a measure of the low viscosity component. The only significant increase in R_s was obtained for ethyl-p-azoxybenzoate at its melting point, attributed to the shear wave transmission into the solid. Both shear and ultrasonic measurements have been made by Dyro and Edmonds[93,94] on C-18 unsaturated fatty acid esters of cholesteral. The shear wave measurements show a slight deviation from Newtonian behaviour as the cholesteric phase is reached and then a greater increase in deviation from the cholesteric to smectic phase. The values of R_s and X_s were not affected by the orientation. The highest values of $G'(\omega)$ were

mainly confined to the smectic phase and were three orders of magnitude less than G(∞) obtained for typical organic liquids. In the ultrasonic measurements (10 to 70 MHz) there was no anomalous behaviour of the absorption coefficient or velocity at either of the two phase transitions namely isotropic to cholesteric and cholesteric to smectic. From the temperature dependence of the ratio η_V/η_S, they suggested that both structural and thermal relaxations were taking place. This was in partial agreement with Zvereva and Kapustin[95] who thought that only a structural relaxation (a phase transition type) was taking place in cholesteryl caprate.

The system chosen for study in the present work was an aqueous solution of cetyltrimethylammonium bromide (cetrimide - antiseptic detergent). This system has been studied semi-quantitatively in the presence of naphthalene derivatives by Nash[96,97]. The solutions were found to have peculiar mechanical properties. Ekwall et al[98] have investigated the system cetrimide, hexanol and water and found different phases, depending on concentration. There was a phase change for the binary mixture cetrimide-water at 25 to 27% $^{w}/_{w}$ cetrimide, and several phase changes in the ternary mixtures. The homogeneous phases L_1, E and D were an isotropic aqueous solution, two dimensional hexagonal mesophase and lamellar mesophase respectively. The shear properties of these phases have now been studied.

7.3.2 Preparation of phases and shear measurements.

All measurements were made at 298.2 K using the shear spectrometer described in Chapter III (3.2). Cetrimide (ex. B.D.H., m.p. 503.2 - 513.2 K with decomposition) was used as received to prepare a 40% $^{w}/_{w}$ solution in water (Phase E). After measurements of R_s it was diluted slowly with water to give a 10% $^{w}/_{w}$ solution. There was no evidence of the rigid fairly clear gel at 40% $^{w}/_{w}$ described by Ekwall[98]. A further sample of cetrimide (ex. B.D.H.) was obtained and recrystallised from acetone and ethanol to give a white powder (m.p. 503.2 -

513.2 K with decomposition). Preparation of phase E gave, after removal of the foam by centrifugation, (2000 r.p.m., 300 s) a fairly clear rigid gel. The gel was diluted with water to give a 30% $^{w}/_{w}$ cetrimide in water and a gelatinous solution, and then 20% $^{w}/_{w}$, giving a solution. The ternary mixture cetrimide, water and hexanol (ex. B.D.H.) 40 : 40 : 20 (phase D) gave a mucoid cloudy mass. The viscosity of phase E was measured with a Ferranti-Shirley viscometer; other viscosities with suspended level viscometers.

7.3.3 Results and discussion.

The results are tabulated in Table AVII.4. With all the phases measured, R_s was found to be less than 0.02 MN s m^{-3}, i.e. within the experimental error of the apparatus. Values of R_s expected for a Newtonian liquid for the 10% $^{w}/_{w}$ and 40% $^{w}/_{w}$ solutions were of the same order of magnitude. However, the Newtonian value of R_s for the gel would be greater than 0.5 MN s m^{-3} and would be measureable with the present apparatus. The viscosity of the rigid gel (49.3% $^{w}/_{w}$ cetrimide) was shear rate dependent. It ranged from 2.85 N s m^{-2} at 86.5 s^{-1} to 0.002 N s m^{-2} at 3,460 s^{-1} and was independent of the previous history of the sample. The ternary mixture supported its own weight for about two months and thereafter began to flow, but the bulk of the material was still gel-like, it was only the surface which had lost its gelatinous nature.

7.3.4 Conclusions.

There was no change in the measured shear properties across any of the phases, L, E or D. The present spectrometer may not have been sufficiently sensitive to detect any small changes. Viscosity measurements on phase E showed it to be thixotropic.

CHAPTER VIII

CONFORMATIONAL ANALYSIS

8.1 Introduction.

The passage of an ultrasonic longitudinal wave in a liquid takes place adiabatically. Pressure variations of 0.03 atmospheres and temperature variations of 0.002 degrees[99] take place in the liquid due to the passage of the wave. The local temperature variations will affect the equilibrium constant. At sufficiently low frequencies the equilibrium constant will fluctuate with the temperature variations, but as the frequency is increased then the chemical equilibrium does not adjust so quickly and there is a phase lag which gives rise to excess sound absorption. The frequency range in which this occurs is related to the chemical reaction rates and the relaxation time. In principle the ultrasonic technique can be used to measure reaction rates and enthalpy changes. It is an accepted physical chemistry method for rates of conformational changes and has been used for many years by several workers in various countries[100-110]. The majority of the above papers are concerned with rotational isomerisation at atmospheric pressure. The isomerisation is readily perturbed by the small pressure and temperature changes within the sound wave, if the relaxation frequency is of the same order of magnitude as the experimental frequency range. However, to date there has been a paucity of works dealing with the effect of increased pressure on such systems. The relaxation frequency of Triethylamine was found to be independent of pressure up to 300 MN m^{-2} [111]. Slie and Litovitz[112] studied the rotational relaxation in ethylacetate at pressures up to 100 MN m^{-2}, but their work was in disagreement with the work of Kal'yanov and Nozdrev[113]. Slie and Litovitz found that the relaxation frequency was independent of pressure but was not constant at constant density, whereas Kal'yanov and Nozdrev found at constant density, f_c, was independent of density. Mamedov[114] has found similar behaviour for crotonaldehyde, namely the relaxation frequency was independent of density. A search of the chemical literature including the Science

Citation Index for reference 112 revealed very little on this topic. Therefore, with the exception of some Russian papers[115,116], it is concluded that there are no other references to ultrasonic work on the effect of pressure on rotational isomerisations.

In the application of the ultrasonic method to determine equilibrium parameters, two assumptions are made, first, that we are concerned with a first order reaction and secondly, that $^{\Delta V}/_{V} \cdot {}^{C_p}/_{\Delta H\theta}$ is small compared with 1.0 (see later). For ethylacetate this was shown to be a correct assumption, but Wyn-Jones et al[117,118] have shown that for certain compounds the second assumption is incorrect. Volume changes of the order of 2% were found and the sign of these volume changes appeared to depend on the dielectric constant of the medium. The effect of these volume changes will affect the equilibrium constant (K) and therefore should have some effect on the relaxation frequency. To test this hypothesis a compound was chosen which has been shown to have a volume change, when investigated in solution. 1,1,2 Trichloroethane, which has been studied by Padmanaban[105] in the pure state and by Wyn-Jones et al[117] in various solvents, was chosen. At atmospheric pressure 1,1,2 Trichloroethane has a relaxation frequency within the experimental frequency range at temperatures between 275 and 330 K.

8.2 Theory.

A two state process is assumed $I \rightleftharpoons II$ with I being the lower energy state. The process is characterised by a single relaxation time. The absorption coefficient (α) and frequency (f) are related to the relaxation frequency ($f_c = {}^1/2\pi\tau$) by the following equation:

$$\frac{\alpha}{f^2} = \frac{A}{1 + ({}^f/f_c)^2} + B \qquad ..(8.1)$$

where A is a relaxation parameter,

B represents the contribution to ${}^{\alpha}/f^2$ from shear viscosity and

any other relaxation processes having a relaxation much greater than f_c.

When a two state unimolecular equilibrium is perturbed by a sound wave, then the relationship between the relaxation parameters and the thermodynamic equilibrium parameters is given by Matheson[119] namely;

$$A\, V_L\, f_c\, C_p / (\gamma - 1)\, \pi = R\left[\frac{\Delta H}{RT}\right]^2 \left[1 - \frac{\Delta V\, C_p}{V \Delta H \theta}\right]^2 \frac{\exp(-\Delta G/RT)}{(1 + \exp(-\Delta G/RT))^2} \quad ..(8.2)$$

where C_p is the specific heat at constant pressure,

V_L is the velocity of sound in the liquid,

γ is the ratio of specific heats,

V is the molar volume,

ΔV is the volume change,

ΔG is the Gibbs free energy difference,

ΔH is the enthalpy of activation,

θ is the thermal expansion coefficient,

R is the gas constant.

ΔH obtained from ultrasonic measurements has not always agreed with ΔH obtained by other technqüies (infrared spectroscopy). The assumption $\left|\Delta V/V \;\; C_p/\theta\right| \ll \Delta H$, which simplifies equation (8.2), has been thought to be a possible reason for this discrepancy. Measurements at pressures greater than atmospheric should allow us to test this assumption.

8.3 1,1,2 Trichloroethane.

Trichloroethane exists in the following conformations,

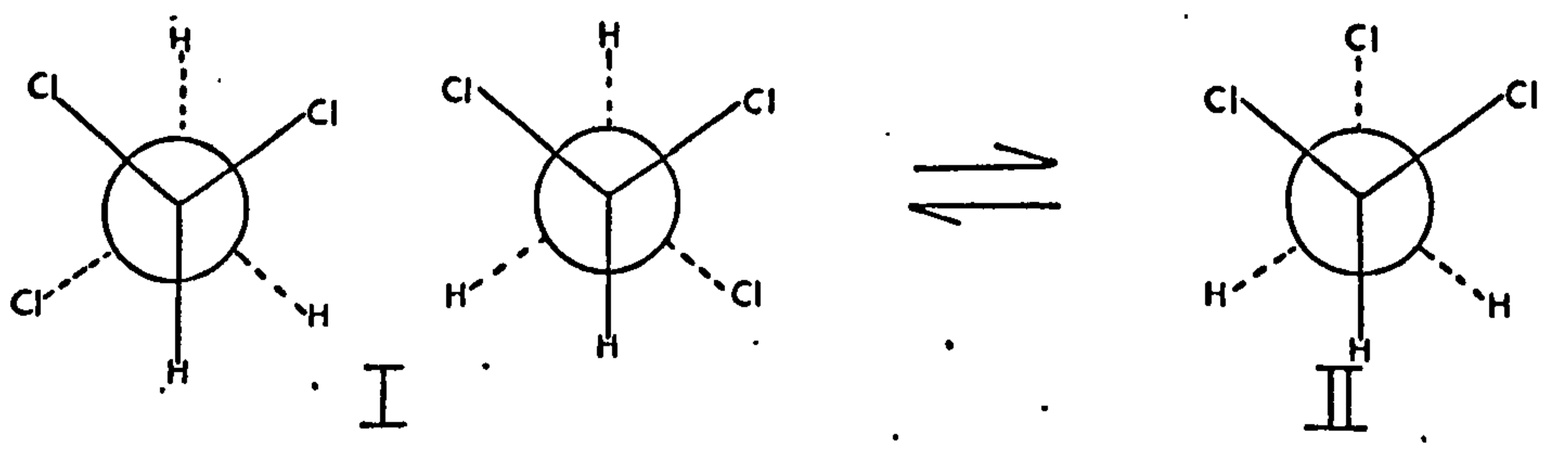

the more stable trans isomer I which has two optical isomers of equal energy and the gauche isomer II of higher energy. The infrared spectrum of the compound has been studied by Harrison and Kobe[120] and the fundamental bands assigned. Some of these bands were found to disappear on solidification[121] indicating that only one isomer is present in the solid state. The solid form was also produced by pressure at ambient temperatures (much higher pressures than used in the present work). The initial high pressure solid was primarily the more polar gauche isomer[122]. Relaxation times and free energy of activation in solution have been obtained from dielectric studies[123], N.M.R. spin relaxation times[124] and activation energy from N.M.R. studies[125] have been obtained in solution.

8.4 Experimental.

1,1,2 Trichloroethane (ex. R.N. Emanuel) has to be stabilised and therefore, was used as received. It was not expected that any small amounts of impurities would affect the results, this assumption has been supported by Padmanaban[105]. The absorption coefficient was measured at four frequencies (5, 15, 25, 35 MHz) in the pressure range 0.1 to 250 MN m^{-2} at three temperatures (283.4, 293.2 and 313.2 K) using the apparatus described in Chapter III (3.3.2). Under the same conditions of temperature and pressure the velocity was measured by the method described in Chapter III (3.4.1).

8.5 Analysis of results.

The velocity was found to be independent of frequency over the range of pressure and temperature used and to increase with increasing pressure. The absorption coefficient decreased with increasing pressure. The variation of absorption coefficient and velocity at 293.2 K are illustrated in Figure 8.1. The limited frequency range (5 to 35 MHz) made the analysis extremely difficult. However, a comprehensive survey of the experimental data showed it to be consistent with the following;

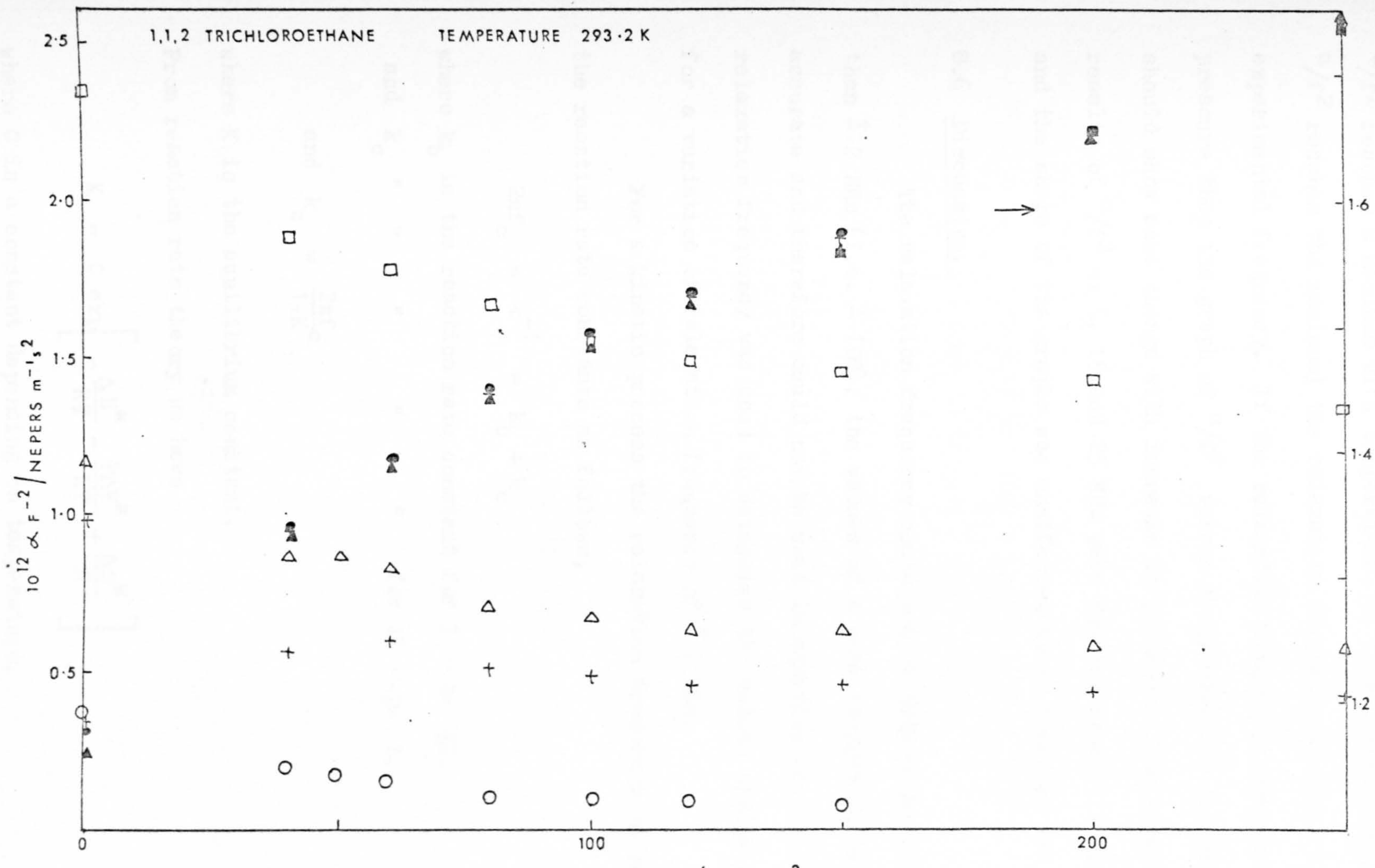

FIG. 8·1 THE VARIATION OF αF^{-2} (open symbols + ○ △ □) AND VELOCITY (closed symbols ● ▲) WITH PRESSURE

A and B decrease with increasing pressure and f_c remains fairly constant, to within $\pm$ 2 MHz. In conformational analysis, at a fixed frequency, α/f^2 reaches a maximum with temperature, at this temperature (at which α/f^2 reaches the maximum) the relaxation frequency is equal to the experimental frequency. If the relaxation frequency changes with pressure then the graph of α/f^2 versus temperature at a fixed frequency should show some change with increase in pressure. The experimental results of α/f^2 at 5, 15 and 25 MHz were plotted against temperature and the shape of the graphs was unaffected by an increase in pressure.

8.6 Discussion.

The relaxation frequency could not be determined to better than $\pm$ 2 MHz (i.e. $\pm$ 10%), the values of A were thought to be less accurate and therefore could not be used in equation (8.2). The relaxation frequency was used to determine the volume change expected for a variation of relaxation frequency of $\pm$ 2 MHz.

For a kinetic process the relaxation frequency is related to the reaction rate constants as follows;

$$2\pi f_c = \tau^{-1} = k_b + k_c \qquad ..(8.3)$$

where k_b is the reaction rate constant for I $\longrightarrow$ II,

and k_c " " " " " for II $\longrightarrow$ I,

$$\text{and } k_c = \frac{2\pi f_c}{1+K} \qquad ..(8.4)$$

where K is the equilibrium constant.

From reaction rate theory we have

$$K = C \exp\left[-\frac{\Delta E^{\ddagger}}{RT} - \frac{P\Delta V^{\ddagger}}{RT} + \frac{\Delta S^{\ddagger}}{R} \right] \qquad ..(8.5)$$

where C is a constant depending on temperature,

$\Delta E^{\ddagger}$ is the energy difference between the activated state and the less stable isomer,

$\Delta S^{\ddagger}$ is the entropy difference between the activated state and the

less stable isomer,

$\Delta V^{\ddagger}$ is the volume difference between the activated state and the less stable isomer.

Now from equations (8.4) and (8.5) we have

$$\log_{10}\left[\frac{f_{c_2}}{f_{c_1}}\right] = \frac{(P_1 - P_2)\,\Delta V^{\ddagger}}{2.303\ RT} \qquad ..(8.6)$$

and substituting the limits for f_c from section 8.5 into equation (8.6) for the pressure range 0.1 to 250 MN m^{-2} and temperature range 283.4 to 313.2 K gives values of $\frac{\Delta V^{\ddagger}}{V}$ equal to about $\pm$ 2%. Therefore, for any increase in pressure to have any effect on the relaxation frequency a volume change greater than $\pm$ 2% would be required. The above findings show that this work is not inconsistent with previous work, nevertheless it does not show conclusively that a volume change occurs in the transition from I to II for 1,1,2 Trichloroethane.

CHAPTER IX

ASSESSMENT AND CONCLUSIONS

This work has shown the versatility of the ultrasonic technique. The technique has been used to study intramolecular movement of atoms, i.e. rotation within a molecule, movement of molecules to and from a group of molecules (micelle state) and lastly structural movement.

Discussing the latter first, the ultrasonic and viscoelastic properties of the three liquids, 4-phenyl dibenzofuran, Epoxy Resin MY 750 and S.E.P. polymer in Di-2-ethylhexyl phthalate, agree with previous findings and show that the shear and bulk properties of these liquids have a common origin, described by the relaxation of defects within the liquid. The chemical nature seems to be of very little significance, although the chemical nature determines to some extent whether the liquid supercools and therefore, can be investigated by this method. A fair number of compounds have been investigated over the years but the number is small in comparison with the possible number of compounds available. Some theoretical treatments have also shown that the shear and bulk properties should have a common origin[126] and that the shear and bulk viscosities are approximately the same. The ratio of volume to shear viscosity in the three liquids was approximately the same and was constant with temperature and pressure. For rotational and thermal mechanisms this is not so; with increase in pressure the ratio of volume to shear viscosity decreases and increases with increase in temperature. The frequency region of excess ultrasonic absorption depends on the temperature in shear and rotational mechanisms but the vibrational frequency is unaffected by temperature. The magnitude of the absorption coefficient and velocity dispersion predict a structural relaxation which can be easily confirmed by shear measurements.

Once a structural relaxation has been confirmed then the reduced variables plot can be obtained. These plots are very similar for many liquids studied. Therefore, once the viscosity function is known, most other behaviour (shear and bulk) can be calculated, i.e. the effect at frequency, temperature and pressure. The shear modulus

does not vary much throughout the temperature range, and for most liquids studied $G(\infty)$ is of the same order of magnitude for each liquid.

Because the viscosity is such an important quantity, then it may be possible to design lubricants with specific properties[60]. The viscosity required could be achieved by introducing specific groups at strategic points in a molecule or the introduction of impurities. However, it is doubtful from previous evidence if compounds can be designed with rheologically different properties from those which exist at present.

Theoretical treatments of viscosity and shear and bulk moduli have been many and varied and often only applicable to a few closely related compounds and not universally applicable.

Although the work has shown common features for most liquids the work on bitumens shows that care must be taken before the method is applied universally. The time temperature superposition principle cannot be applied without some previous knowledge. Initially there was nothing to suggest that Kuwait bitumen would not obey this rule. A closely related material (although different from most bitumens) Miri 150/250 did obey the rule. Bitumens are complex materials whose chemical and structural properties are not fully known.

A disadvantage of the technique at present is that it can only be applied to fairly viscous liquids which are usually supercooled. A lot of information would be obtained if symmetrical molecules could be studied; we may find that these molecules have a single relaxation time or perhaps a much narrower distribution of relaxation times.

The other two parts of the work were hindered by the fact that the apparatus had been designed for the above work and different types of liquids, where extreme accuracy of temperature and pressure were not so important. In particular the rotational isomerisation work required a slightly different absorption cell. Nevertheless, some useful results were obtained which will help future work. To establish

the theory about volume changes and relaxation frequency much more work should be carried out, namely the dilution technique[118] should be applied to ethylacetate, where there was no change in the relaxation frequency with pressure. At present only 1,1,2 Trichloroethane has been studied by the dilution technique and pressure variation, which was inconclusive.

The technique has been used for a number of years but it is still in its infancy. If it is to gain wide support and use the apparatus would have to be automated. It can be compared with other spectroscopic techniques where it was not until they were widely used that the full potential was realised. It has an advantage over infra-red spectroscopy in that prominent relaxations can be observed when there is less than 1% of the molecules in the excited state. Any technique which is sensitive at this level must surely be significant.

APPENDICES.

APPENDIX I

Table AI.1. Literature values of the ratio of volume viscosity (η_v) to shear viscosity (η_s) as a function of pressure or temperature.

Compound	Temperature or Pressure	η_v/η_s	Reference
Glycerol	0.01 MN m^{-2}	0.78	65
(299.2 K)	4.73 "	0.77	
	10.14 "	0.79	
	19.43 "	0.83	
Carbon tetrachloride	253.2 K	2.5 ± 1.5	127
Toluene	193.2 K	1.7 ± 0.2	
Chlorobenzene	243.2 K	1.6 ± 0.2	
Cyclohexanone	253.2 K	0.4 ± 0.1	
Propane	153.2 K	1.1 ± 0.1	
Cyclopentane	183.2 K	< 0.7	
Acetone	193.2 K	< 2.0	
n-hexane	423.2 K	7.0 ± 1.0	
n-heptane	"	6.0 ± 1.0	
n-octane	"	6.0 ± 1.0	
Argon	123.2 K - 83.2 K	0.9 ± 0.5	128
Isobutyl bromide	273.2 K	0.44	129
Hydrocarbon oil (M.W. 300)	223.2 K - 323.2 K	1.33	130
Dichloromethane	293.2 K	1.4	131
Liquid metals		< 0.4 - 4.0	132
Fused salts		1 to 27	127
Calcium nitrate solution		8.3	63
Di-2-ethylhexyl phthalate	223.2 K - 273.2 K	3.0 ± 0.3	16
	243.2 K - 333.2 K	1.9 ± 0.2	28
	0 - 400 MN m^{-2}	1.2 ± 0.2	28

(cont..)

Table AI.1 cont..			
Tri-orthotolyl phosphate	230 K - 310 K	3.0 ± 0.3	15
3-phenyl propyl chloride		1.61	10
sec. butyl benzene		3.86	
Bis -[m(m-phenoxy phenoxy) phenyl] ether	267.2 K - 370.2 K	5.3	17
Hydrocarbon oil			
HVI 330	243 - 303 K	0.64 ± 0.2	28
" LVI 260	247 - 303 K	1.05 ± 0.2	
" MVI 170	249 - 300 K	0.93 ± 0.2	
Aroclor 1254	240 - 300 K	3.2 ± 0.2	

Table AI.2. Literature values of moduli.

$$X = A + BY$$

where $X = G,\ J,\ K,\ M(\omega, P, T)$ in GN m^{-2}.

$Y = T$ in K or P in GN m^{-2}.

Compound and Modulus	A	B	Reference
OS 124 (mixed isomeric 5 ring polyphenyl ether)			
M (∞, 0, T)	19.9	-0.051	62
K (0, 0, T)	6.64	-0.0122	
J (∞, 0, T)	-0.474	0.0051	12
Di-2-ethylhexyl phthalate			
J(∞, 0, T)	-1.664	0.0138	16
"	-2.31	0.017	21
Bis-[m-(m-phenoxy phenoxy) phenyl] ether			
K (0, 0, T)	7.193	-0.0135	16,12
J (∞, 0, T)	-1.011	0.0075	"
Tri-orthotolyl phosphate			
J (∞, 0, T)	-0.167	0.0041	15
Benzyl benzoate			
J(∞, 0, T)	-2.454	0.0168	133
3-Phenylpropyl chloride			
J(∞, 0, T)	-1.573	0.0144	10
Sec. butylbenzene			
J(∞, 0, T)	-1.186	0.0138	10,21
Isopropyl bromide			
J(∞, 0, T)	-1.826	0.020	21
n-Propylbromide			
J(∞, 0, T)	-1.839	0.0198	21
Di-isobutyl phthalate			
J(∞, 0, T)	-1.676	0.0126	21

(cont..)

Table AI.2 (cont..)

Di-n-butyl phthalate			
J(∞, 0, T)	-2.712	0.0193	21
Castor oil			
J(∞, 0, T)	0.054	0.005	12
Lubricating oil HVI 330			
M(∞, 0, T)	9.38	-0.0223	28
K(0, 0, T)	5.5	-0.012	"
J(∞, 0, T)	-4.734	0.0276	"
Lubricating oil MVI 170			
M(∞, 0, T)	9.55	-0.0232	28
K(0, 0, T)	4.6	-0.009	"
J(∞, 0, T)	-3.341	0.0202	"
Lubricating oil LVI 260			
J(∞, 0, T)	-2.660	0.0172	28
Aroclor 1254			
M(∞, 0, T)	14.17	-0.0301	28
K(0, 0, T)	6.85	-0.013	"
J(∞, 0, T)	-1.886	0.0103	"
Glycerol			
M(∞, 0, T)	11.59	-0.0815	65
K(0, 0, T)	4.91	0.0125	"
G(∞, 0, T)	2.65	0.0274	"
OS 124			
M(∞, P, 295)	4.83	20.7	62
K(0, P, 295)	3.01	3.2	"
K(∞, P, 295)	4.12	13.9	"
G(∞, P, 295)	0.53	5.1	"
Bis-[m-(m-phenoxy phenoxy) phenyl] ether			
G(∞, P, 303)	0.79	5.0	66

(cont..)

Table AI.2 (cont..)

Di-2-ethylhexyl phthalate			
G(∞, P, 303)	0.50	2.5	66
G(∞, P, 303)	0.28	1.6	57
G(∞, P, 243)	0.54	2.6	57
Lubricating Oil LVI 260			
G(∞, P, 288)	0.33	2.0	28
G(∞, P, 303)	0.31	1.6	"
Aroclor 1254			
G(∞, P, 303)	0.86	3.8	28
G(∞, P, 313)	0.64	3.7	"
Castor Oil			
G(∞, P, 303)	0.637	1.5	58
Glycerol			
K(0, P, T)	K(0, 0, T)	10.8	65
K(∞, P, T)	K(∞, 0, T)	14.6	"
M(∞, P, T)	M(∞, 0, T)	18.9	"
G(∞, P, T)	G(∞, 0, T)	3.2	"

APPENDIX III

Preparation of 4-phenyldibenzofuran.

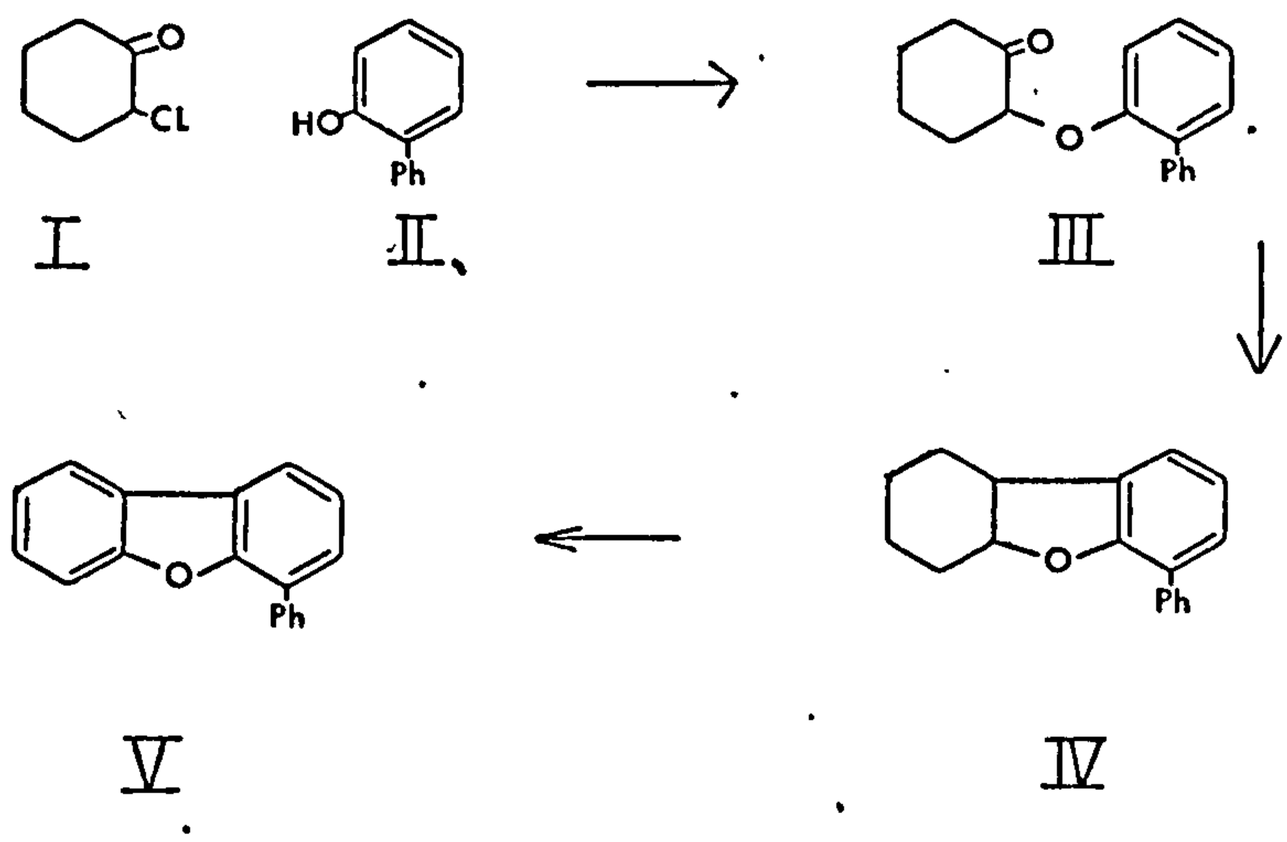

I II III IV V

(i) 2-(2'-phenylphenoxy) cyclohexanone, III.

2-chlorocyclohexanone, I (358 g), dry sodium ortho phenyl phenate (424 g) and ortho phenyl phenate, II (1600 g) were heated (410 - 420 K) for 12 hours. After cooling the mixture was poured into water and the resulting brown oil was ether extracted. The ether extract was washed well with dilute sodium hydroxide solution followed by water and then dried (Na_2SO_4). The ether was distilled off and the residue distilled in vacuo to give a pale yellow oil (b.p.. 435 - 440 K/0.6 mm).

(ii) Cyclodehydration of 2-(2'-phenylphenoxy) cyclohexanone.

2-(2'-phenylphenoxy) cyclohexanone, III (~ 200 g), phosphorus pentoxide (400 g) and phosphoric acid (0.2 L) were heated (373 K) for 3 hours. After cooling the reaction mixture was poured into water and ether extracted. The ether extract was washed twice with dilute sodium hydroxide solution followed by water and dried (Na_2SO_4). The solvent was distilled off leaving a solid material which was recrystallised from ethanol to give yellow crystals (m.p. 315.5 K).

(iii) Dehydrogenation of 4-phenyltetrahydrodibenzofuran IV.

4-phenyltetrahydrodibenzofuran (147.5 g) and 5% palladium on

charcoal (52.2 g) were heated (573 K) for 16 hours. The dehydrogenation product was dissolved in benzene and hot filtered to remove the catalyst. The concentrated solution was distilled to give 4-phenyl dibenzofuran, a pale yellow oil (b.p. 451 - 453 K/0.6 mm). The infra-red spectrum showed no OH or CH_2. Gas chromatographic analysis showed less than 1% impurity to be present.

Preparation of S.E.P. in Di-2-ethylhexyl phthalate solution.

Styrene-ethylene propylene (S.E.P.) (45.0 g, 0.56×10^{-3} g. mole.) was dissolved with stirring into warm (327.0 - 337.0 K) di-2-ethylhexyl phthalate (ex Lankro Chemicals Ltd.) (3.0 litres, 7.55 g. mole.). After standing at room temperature the solution was filtered through glass wool to remove some gelatinous particles. The residue was taken up into toluene and the polymer precipitated with methanol (0.833 g of polymer).

S.E.P. in Di-2-ethylhexyl phthalate sol. = 1.47% $^{w}/_{v}$

Molar ratio $\approx 1 : 7.4 \times 10^{-5}$

APPENDIX IV

Table AIV.1. Fit of density-temperature results to a linear equation.

$$\rho/\mathrm{Kg\ m^{-3}} = A + BT/K$$

Bitumen	A	B
Kuwait S.B. 80/100	1207.3	-0.623
Miri 150/250	1179.2	-0.523

Table AIV.2. Fit of viscosity-temperature results.

Kuwait S.B. 80/100

$$\log_{10}(\eta/\mathrm{N\ s\ m^{-2}}) = -0.54 + \frac{4.22}{(T/K - 101)^2}$$

Miri 150/250

$$\log_{10}(\eta/\mathrm{N\ s\ m^{-2}}) = 17.189 - \frac{17.970 \times 10^3}{T/K} + \frac{4.219 \times 10^6}{T^2/K^2}$$

Table AIV.3. Bitumen Kuwait S.B. 80/100.

Values of the normalised shear resistance as a function of the reduced frequency and temperature.

Temperature/K	$R_s(\omega,T)/R_s(\omega,T)$	$\log_{10}[\ \omega\ \eta_s(0)/G(\infty)\ ]$
389.7	0.164	-1.312
	0.259	-0.834
	0.319	-0.612
	0.406	-0.198
375.1	0.315	-0.311
	0.373	-0.090
358.1	0.395	0.417
	0.466	0.639
348.1	0.459	0.920
	0.536	1.142
342.2	0.496	1.248
	0.594	1.470
342.1	0.496	1.254
	0.594	1.452
332.9	0.554	1.818
	0.648	2.039
	0.765	2.454
327.7	0.587	2.167
	0.687	2.389
323.6	0.613	2.461
	0.705	2.683
	0.825	3.098
322.7	0.618	2.527
	0.717	2.749
	0.829	3.164
313.9	0.686	3.223
	0.775	3.445
	0.877	3.860

(cont..)

Table AIV.3 (cont..)

313.7	0.611	2.765
	0.686	3.242
313.3	0.790	3.498
	0.949	3.913
304.9	0.839	4.259
	0.912	4.674
299.7	0.776	4.080
	0.815	4.557
	0.892	4.780
292.7	0.884	5.326
	0.946	5.548
	0.946	5.963
291.1	0.902	5.516
	0.958	5.737
	0.945	6.152
283.7	0.949	5.976
	0.955	6.453
	1.002	6.675
	0.955	7.090
273.4	0.974	7.488
	0.974	7.966
	1.037	8.187
	0.974	8.602
273.0	0.978	8.030
	1.034	8.252
	0.978	8.667
266.2	1.000	8.719
	1.000	9.196
	1.000	9.418
	1.000	9.833
264.2	0.996	9.093
	1.050	9.792

(cont..)

Table AIV.3 (cont..)

263.8	1.000	9.645
	1.053	9.867
	1.000	10.282
259.2	1.003	10.086
	1.003	10.563

Table AIV.4. Bitumen Miri 150/250.
Values of $R_s(\infty, T)$ and calculated values of $G(\infty)$.

Temperature/K	$R_s(\infty, T)$/MN s m^{-3}	$G(\infty)$/GN m^{-2}
298.5	0.835	0.682
289.7	0.893	0.778
285.5	0.916	0.817
276.6	0.992	0.956
272.7	1.016	1.002
270.0	1.040	1.050
268.7	1.042	1.053
266.7	1.061	1.091
265.0	1.089	1.055
261.1	1.047	1.060
257.3	1.085	1.137
253.5	1.057	1.078

Table AIV.5. Bitumen Miri 150/250.

Values of the normalised shear resistance as a function of the reduced frequency and temperature.

Temperature/K	$R_s(\omega,T)/R_s(\omega,T)$	$\log_{10}\left[\omega\,\eta_s(0)/G(\infty)\right]$
373.2	0.107	-1.655
	0.227	-1.178
	0.253	-0.956
353.2	0.255	-0.914
	0.423	-0.437
	0.529	-0.215
343.1	0.337	-0.424
	0.537	0.054
	0.620	0.276
	0.637	0.690
334.9	0.483	0.042
	0.675	0.519
	0.733	0.741
333.4	0.596	0.612
	0.715	0.834
324.0	0.702	0.769
	0.805	1.247
	0.849	1.468
	0.908	1.883
314.6	0.820	1.511
	0.939	2.210
309.5	0.884	1.965
	0.995	2.442
	1.020	2.664
303.5	0.966	2.546
	1.000	3.023
	1.005	3.245

(cont..)

Table AIV.5 (cont..)

298.5	0.990	3.077
	0.990	3.554
	1.004	3.775
289.7	0.992	4.120
	1.024	4.597
	0.975	4.819
276.6	1.012	5.972
	1.004	6.449
	1.020	6.671
272.7	1.010	6.604
	0.995	7.081
	1.006	7.303

Table AIV.6. Experimental and calculated values for the steady flow viscosity.

Sample	Temperature /K	Frequency /MHz	Viscosity from experiment /N s m^{-2}	Viscosity from calculation* /N s m^{-2}
Kuwait Bitumen	303.2	6	8.16×10^{4}	9.19×10
		18	"	7.97×10
		30	"	5.55×10
	323.6	6	1.28×10^{3}	2.37×10
		18	"	2.64×10
		30	"	1.71×10
	348.1	18	3.17×10	5.07
		30	"	4.61
	358.1	18	9.42	2.21
		30	"	1.34
	389.7	18	0.45	0.51
		30	"	0.49
		78	"	0.89
Miri Bitumen	334.9	18	14.05	18.25
		30	"	13.61
	343.1	18	4.50	4.46
		30	"	5.18
Epoxy Resin MY 750	343.2	18	0.119	0.115
		30	"	0.136
4-phenyl dibenzo-furan	335.0	18	0.035	0.036
		30	"	0.039
S.E.P. in Di-2-ethylhexyl phthalate	292.6	18	0.093	0.113
		30	"	0.117
	298.2	18	0.068	0.063
		30	"	0.130

* $\eta/N\ s\ m^{-2} = \dfrac{(R_s^2 + X_s^2)^2}{2\,\rho\,\omega\,X_s^2}$

R_s, X_s in N s m^{-3}

ρ in Kg m^{-3}

ω in s^{-1}

APPENDIX V

Table AV.1. Fit of temperature-density results to a linear equation.

$$\rho/\mathrm{Kg\ m^{-3}} = A + BT/K$$

Liquid	A	B
4-phenyl dibenzofuran	1390	-0.712
Epoxy Resin MY 750	1381.3	-0.730
S.E.P. in Di-2 ethyl-hexyl phthalate	1203.0	-0.742

Table AV.2. Fit of temperature viscosity results to Roelands' equation.

$$\log_{10}\left[\log_{10}\eta_s(0)/\mathrm{N\ s\ m^{-2}} + 4.2\right] = A + B\log_{10}\left[\frac{T/K - 138}{135}\right]$$

Liquid	A	B
4-phenyl dibenzofuran	0.8754	-2.661
Epoxy Resin MY 750	0.8647	-1.942
S.E.P. in Di-2 ethyl-hexyl phthalate	0.5751	-1.258

Table AV.3. Fit of pressure-density results to the Linear Secant Modulus Equation.

$$\rho/\mathrm{Kg\ m^{-3}} = \frac{1 + AP/\mathrm{MN\ m^{-2}} + BT/K}{C + DP/\mathrm{MN\ m^{-2}}}$$

Liquid	10^3 A	10^3 B	10^3 C	10^6 D
Epoxy Resin MY 750	0.7418	-0.7843	0.6558	0.4553
S.E.P. in Di-2-ethyl-hexyl phthalate	1.721	-0.6195	0.8296	1.337
Di-2-ethylhexyl phthalate ⁂	1.462	-0.5716	0.8442	1.085
Isopentane⁂	3.428	-1.010	1.135	3.541

Table AV.4. Fit of pressure-viscosity results to Roelands' equation.

$$\log_{10}(\log_{10}\eta/\mathrm{N\ s\ m^{-2}} + 4.2) = A + BPr + CTr + DPrTr$$

$$\text{where } Pr = \log((200 + P/\mathrm{MN\ m^{-2}})/200)$$

$$Tr = \log((T/K - 138)/135)$$

Liquid	A	B	C	D
Epoxy Resin MY 750	0.8729	0.9239	-2.102	-1.768
S.E.P. in Di-2-ethyl-hexyl phthalate	0.5765	0.6096	-1.713	0.9212
Isopentane⁂	-0.185	0.784	-1.126	0.952
Di-2-ethylhexyl phthalate ⁂	0.5746	0.6065	-1.295	-0.0505

⁂ Ref. 35

Table AV.5a. Fit of temperature-velocity (V(0)) results to a linear equation.

$$V(0)/m\ s^{-1} = C + DT/K$$

Liquid	C	D
4-phenyl dibenzofuran	2666.5	-3.25
Epoxy Resin MY 750	2841	-3.85
S.E.P. in Di-2-ethyl-hexyl phthalate	2292.2	-3.12

Table AV.5b. Fit of pressure-velocity (V(0)) results to a linear equation.

$$V(0)/m\ s^{-1} = C + DP/MN\ m^{-2}$$

Liquid	Temperature K	C	D
Epoxy Resin MY 750	310.2	1647	2.95
S.E.P. in Di-2-ethyl-hexyl phthalate	296.2	1368	3.30
	269.9	1450	3.30

Table AV.6. 4-phenyl dibenzofuran.

The values of longitudinal velocity and absorption coefficient, α, as a function of frequency and temperature.

Temperature / K	Frequency/MHz	Velocity/m s^{-1}	10^{-3} α/Nepers m^{-1}
273.6	5.37	2200	0.367
272.2	15.01	2241	0.552
271.2	24.77	2249	0.676
272.3	34.78	2252	0.835
282.6	5.37	2021	0.896
279.5	14.92	2141	1.38
279.1	24.92	2165	1.68
279.7	34.78	2167	2.32
291.3	5.37	1826	1.16
288.8	14.92	1951	2.70
289.0	24.77	1986	3.86
289.2	34.78	2031	5.41
298.8	5.37	1721	0.548
298.2	15.01	1783	2.56
298.7	24.77	1796	4.24
298.9	34.78	1828	6.31
309.0	5.37	1657	0.196
307.0	15.38	1693	1.41
307.0	24.97	1701	2.94
306.8	35.09	1718	4.52
318.8	5.37	1631	0.070
316.3	15.38	1644	0.616
316.4	24.97	1645	1.49
316.3	35.13	1654	2.52
328.3	5.37	1600	0.029
325.1	15.35	1612	0.292
325.0	24.97	1614	0.705
325.5	35.05	1613	1.24
337.4	5.37	1570	0.014
335.5	15.35	1577	0.121
335.5	24.97	1577	0.308
335.4	35.09	1578	0.597

(cont..)

Table AV.6 (cont..)

347.2	5.37	1539	0.012
345.6	15.35	1543	0.073
345.6	24.97	1540	0.156
345.5	35.05	1546	0.317
357.3	15.43	1508.	0.057
358.1	25.26	1503	0.076
357.1	35.15	1506	0.174

Table AV.7. 4-phenyl dibenzofuran.

Values of the resistive part of the shear impedance as a function of frequency and temperature.

Temperature/K	Frequency/MHz	$R_s(\omega,T)$/MN s m^{-3}
258.2	18	1.184
	30	1.175
	78	1.096
265.1	18	1.112
	30	1.128
	78	1.120
274.2	18	1.011
	30	1.039
	78	1.035
283.4	18	0.873
	30	0.885
	78	0.933
298.6	18	0.400
	30	0.524
	78	0.641
314.4	6	0.088
	18	0.137
	30	0.180
	78	0.309
323.5	18	0.076
	30	0.105
	78	0.201
335.0	6	0.027
	18	0.048
	30	0.065
	78	0.108

Table AV.7. 4-phenyl dibenzofuran.

Values of the resistive part of the shear impedance as a function of frequency and temperature.

Temperature/K	Frequency/MHz	$R_s(\omega,T)$/MN s m^{-3}
258.2	18	1.184
	30	1.175
	78	1.096
265.1	18	1.112
	30	1.128
	78	1.120
274.2	18	1.011
	30	1.039
	78	1.035
283.4	18	0.873
	30	0.885
	78	0.933
298.6	18	0.400
	30	0.524
	78	0.641
314.4	6	0.088
	18	0.137
	30	0.180
	78	0.309
323.5	18	0.076
	30	0.105
	78	0.201
335.0	6	0.027
	18	0.048
	30	0.065
	78	0.108

Table AV.8. Comparison of experimental and calculated values of G' and η'.

Liquid	Temperature/K	Frequency/MHz	k	G'/MN m^{-2}		η'/N s m^{-2}	
				Experimental	Calculated	Experimental	Calculated
Bitumen	348.1	18	4.0	91	97	0.615	0.604
Kuwait SB 80/100	"	30	5.0	115	122	0.388	0.366
	358.1	18	4.0	53	52	0.487	0.395
	"	30	5.0	76	67	0.327	0.283
Bitumen	334.9	18	1.0	206	204	0.96	1.06
Miri 150/250	"	30	1.0	244	242	0.65	0.628
	343.1	18	1.0	107	102	0.970	0.853
		30	1.0	154	139	0.59	0.568
Epoxy Resin MY 750	343.2	18	1.0	1.5	2.2	0.100	0.087
		30	1.0	4.2	4.2	0.105	0.080
4-phenyl dibenzofuran	335.0	18	1.0		0.42	0.037	0.031
		30	1.0	0.78	0.85	0.035	0.029
S.E.P. in Di 2-ethylhexyl phthalate	292.6	18	1.0	2.01	1.83	0.091	0.071
		30	1.0	3.36	3.53	0.090	0.065
	298.2	18	1.0			0.06	0.054
		30	1.0	2.4	2.39	0.051	0.050

Table AV.9. Parameters in the linear equation for the shear compliance with temperature.

$$J(\infty)/(GN\ m^{-2})^{-1} = A + BT/K$$

Liquid	A	B
4-phenyl dibenzofuran	-3.023	0.0151
Epoxy Resin MY 750	-5.18	0.0224
S.E.P. in Di-2-ethyl-hexyl phthalate	-3.34	0.022

Table AV.10. Parameters in the linear equation for the shear modulus with pressure.

$$G(\infty)/GN\ m^{-2} = A + BP/GN\ m^{-2}$$

Liquid	Temperature K	A	B
Epoxy Resin MY 750	310.2	0.493	2.99
		0.675	2.65
	298.0	0.724	3.48
		0.742	3.44
	278.0	1.01	4.3
S.E.P. in Di-2-ethyl-hexyl phthalate	296.2	0.225	2.05
	269.9	0.375	2.26
	252.2	0.435	2.67

Table AV.11. 4-phenyl dibenzofuran.

Values of the normalised shear resistance as a function of the logarithm of reduced frequency.

Temperature/K	$R_s(\omega,T)/R_s(\infty,T)$	$\log_{10}[\omega\eta_s(0)/G(\infty,T)]$
258.2	1.009	5.019
	1.001	5.241
	0.934	5.656
265.1	1.004	3.657
	1.019	3.879
	1.011	4.294
274.2	0.978	2.233
	1.005	2.455
	1.000	2.870
283.4	0.897	1.113
	0.910	1.335
	0.959	1.750
298.6	0.449	-0.246
	0.588	-0.024
	0.720	0.383
314.4	0.107	-1.703
	0.167	-1.226
	0.219	-1.004
	0.376	-0.589
323.5	0.096	-1.655
	0.133	-1.433
	0.255	-1.019
335.0	0.036	-2.570
	0.064	-2.093
	0.086	-1.871
	0.144	-1.456

Table AV.12. Epoxy Resin MY 750.

Values of the longitudinal velocity and absorption coefficient, α, at atmospheric pressure as a function of frequency and temperature.

Temperature/K	Frequency/MHz	Velocity/m s^{-1}	10^{-3} α/Nepers $/m^{-1}$
268.6	15.00	2280	0.621
"	24.78	2284	0.743
"	34.85	2284	0.722
272.9	5.08	2182	0.476
279.8	15.02	2144	1.24
"	24.86	2136	1.33
280.3	34.70	2153	1.80
291.2	5.16	1903	0.885
289.8	15.02	1981	2.28
290.0	24.86	2001	3.34
289.7	34.70	2030	4.16
296.9	5.16	1832	0.849
298.0	15.40	1853	2.70
297.8	25.20	1902	4.66
297.9	35.25	1911	5.62
305.1	5.10	1705	0.58
"	15.40	1759	2.48
305.2	25.20	1787	4.27
304.7	35.25	1816	6.02
316.7	5.08	1632	0.272
313.6	15.40	1676	1.83
313.7	25.20	1691	3.53
313.8	35.25	1721	5.33
325.8	5.37	1591	0.161
322.7	15.40	1617	1.211
322.6	25.20	1628	2.44
322.2	35.25	1641	4.01

(cont..)

Table AV.12 (cont..)

333.9	5.31	1557	0.092
332.7	15.40	1567	0.653
332.6	25.20	1575	1.42
332.8	35.12	1582	2.56
344.9	5.16	1515	0.088
342.8	15.35	1524	0.371
343.0	25.15	1526	0.862
343.5	35.14	1526	1.49

Table AV.13. Epoxy Resin MY 750.

Values of the resistive part of the shear impedance as a function of frequency and temperature.

Temperature/K	Frequency/MHz	$R_s(\omega,T)$/MN s m^{-3}
248.4	18	1.102
	30	1.087
	78	1.102
259.6	30	1.300
	78	1.358
261.5	18	1.195
	30	1.208
	78	1.203
264.1	6	1.124
	18	1.198
	30	1.147
	78	1.147
273.7	18	1.019
	30	1.058
	78	1.085
282.7	18	0.901
	30	0.901
	78	0.991
297.2	6	0.437
	18	0.576
	30	0.672
	78	0.716
304.3	18	0.484
	30	0.572
	78	0.640
313.2	6	0.169
	18	0.307
	30	0.383
	78	0.529

(cont..)

Table AV.13 (cont..)

318.4	18	0.230
	30	0.305
	78	0.492
331.9	18	0.125
	30	0.150
	78	0.273
343.4	18	0.073
	30	0.124
	78	0.233

Table AV.14. Epoxy Resin MY 750.

Values of the normalised shear resistance as a function of $\log_{10}(\omega\,\eta_s(0)/G(\infty,T))$.

Temperature/K	$R_s(\omega,T)/R_s(\infty,T)$	$\log_{10}(\omega\,\eta_s/G(\infty,T))$
248.4	0.624	5.261
	0.615	5.483
	0.624	5.898
259.6	0.949	3.850
	0.991	4.265
261.5	0.901	3.390
	0.911	3.612
	0.907	4.027
264.1	0.885	2.605
	0.943	3.082
	0.903	3.304
	0.903	3.719
273.7	0.914	2.081
	0.949	2.303
	0.973	2.718
282.7	0.892	1.401
	0.892	1.623
	0.971	2.038
297.2	0.492	-0.143
	0.649	0.334
	0.757	0.562
	0.806	0.977
304.3	0.575	-0.069
	0.679	0.153
	0.760	0.568
313.2	0.213	-0.945
	0.387	-0.468
	0.483	-0.246
	0.668	0.169

(cont..)

Table AV.14 (cont..)

318.4	0.300	-0.685
	0.397	-0.461
	0.641	-0.048
331.9	0.176	-1.171
	0.211	-0.949
	0.384	-0.534
343.4	0.109	-1.505
	0.185	-1.283
	0.347	-0.868

Table AV.15. Epoxy Resin MY 750.

Values of the resistive part of the shear impedance as a function of temperature, pressure and frequency.

Temperature/K	Pressure/MN m^{-2}	Frequency/MHz	$R_s(\omega)$/MN s m^{-3}
278.0	0.1	6	0.94
		18	0.97
		30	1.03
"	50	6	1.11
		18	1.15
		30	1.18
"	100	6	1.29
		18	1.32
		30	1.34
"	150	6	1.41
		18	1.43
		30	1.43
"	200	6	1.49
		18	1.50
		30	1.50
"	225	6	1.57
		18	1.57
		30	1.57
"	250	6	1.62
		18	1.63
		30	1.625
278.0	275	6	1.64
		18	1.64
		30	1.65
"	310	6	1.62
		18	1.65
		30	1.65
"	350	6	1.61
		18	1.64
		30	1.63

(cont..)

Table AV.15 (cont..)

298.0	0	6	0.398
		18	0.543
		30	0.608
	50	6	0.677
		18	0.801
		30	0.857
	100	6	1.03
		18	1.09
		30	1.09
	150	6	1.18
		18	1.22
		30	1.23
	200	6	1.31
		18	1.31
		30	1.30
	250	6	1.41
		18	1.42
		30	1.42
	300	6	1.48
		18	1.48
		30	1.49
	350	6	1.56
		18	1.57
		30	1.55
	400	6	1.64
		18	1.63
		30	1.64
	450	6	1.72
		18	1.71
		30	1.73
310.2	100	6	0.648
		18	0.773
		30	0.853

(cont..)

Table AV.15 (cont..)

310.2	200	6	1.02
		18	1.11
		30	1.13
	300	6	1.30
		18	1.27
		30	1.28
	400	6	1.47
		18	1.44
		30	1.45
	450	6	1.57
		18	1.52
		30	1.53
	500	6	1.61
		18	1.60
		30	1.59
	550	6	1.67
		18	1.65
	600	6	1.70
		18	1.72

Table AV.16. Epoxy Resin MY 750.

Values of the normalised resistive part of the shear impedance as a function of reduced frequency at various pressures and temperatures.

Temperature/K	Pressure/MN m^{-2}	$R_s(\omega)/R_s(\infty)$	$\log(\omega\,\eta_s(0)/G(\infty))$
278.0	0.1	0.857	1.286
		0.884	1.763
		0.939	1.984
	50	0.918	2.729
		0.951	3.207
		0.976	3.428
	100	0.949	4.160
		0.970	4.637
		0.985	4.859
	150	0.99	5.571
		1.00	6.048
		1.00	6.270
	200	0.976	6.970
		0.983	7.447
		0.983	7.669
298.0	0	0.427	-0.273
		0.583	0.204
		0.653	0.426
	50	0.651	0.648
		0.770	1.125
		0.824	1.347
298.0	100	0.903	1.543
		0.955	2.021
		0.955	2.243
	150	0.956	2.417
		0.988	2.894
		0.996	3.116
	200	0.990	3.271
		0.990	3.748
		0.982	3.970

(cont..)

Table AV.16 (cont..)

	250	1.002	4.108
		1.01	4.585
		1.01	4.807
	300	0.995	4.930
		0.995	5.408
		1.00	5.630
	350	0.997	5.739
		1.003	6.216
		0.990	6.438
	400	1.00	6.536
		0.99	7.013
		1.00	7.235
310.2	100	0.614	0.436
		0.733	0.913
		0.809	1.135
	200	0.844	1.753
		0.918	2.230
		0.935	2.452
	300	0.965	2.999
		0.943	3.476
		0.950	3.698
	400	0.995	4.192
		0.975	4.669
		0.982	4.891
	450	1.021	4.770
		0.988	5.248
		0.998	5.470

Table AV.17. Epoxy Resin MY 750.

Values of the longitudinal velocity and absorption coefficient, α, at 310.2 K as a function of frequency and pressure.

Pressure/MN m^{-2}	Frequency/MHz	Velocity/m s^{-1}	10^{-3} α/Nepers m^{-1}
0.1	5.13	1666	0.432
40	"	1826	0.691
50	"	1875	0.729
60	"	1927	0.768
100	"	2140	0.726
125	"	2280	0.627
150	"	2400	0.499
200	"	2637	0.262
0.1	15.94	1702	2.04
40	"	1888	2.39
50	"	1947	2.42
60	"	2008	2.37
100	"	2217	1.78
125	"	2347	1.36
150	"	2429	0.959
200	"	2685	0.489
0.1	24.98	1729	3.98
40	"	1927	4.14
50	"	1980	3.88
60	"	2002	3.73
100	"	2252	2.57
125	"	2354	1.89
150	"	2649	1.34
200	"	2691	0.671
0.1	35.08	1749	5.94
40	"	1960	5.71
50	"	1987	5.29
60	"	2065	4.89
100	"	2280	3.36

Table AV.18. S.E.P. in Di-2-ethylhexyl phthalate.

Values of the longitudinal velocity and absorption coefficient, α, as a function of frequency and temperature.

Temperature/K	Frequency/MHz	Velocity/m s^{-1}	10^{-3} α/Nepers m^{-1}
286.4	5.05	1404	0.087
	14.98	1404	0.460
	25.04	1409	1.10
	34.85	1413	2.24
275.7	5.05	1437	0.120
	14.98	1446	0.860
	25.04	1455	2.13
	34.85	1463	3.68
266.5	5.05	1472	0.240
	14.98	1493	1.55
	25.04	1509	3.69
	34.85	1523	4.69
259.2	5.05	1508	0.410
	14.98	1542	2.48
	25.04	1563	4.35
	34.85	1583	6.37
249.2	5.10	1577	0.692
	14.94	1641	2.85
	25.16	1672	4.42
	34.86	1689	5.88
242.2	5.10	1672	0.899
	14.94	1731	2.70
	25.16	1761	3.71
	34.86	1772	5.05
237.7	5.12	1731	0.903
	15.12	1791	2.32
	24.98	1812	3.14
	34.74	1834	3.97

(cont..)

Table AV.18 (cont..)

223.7	5.12	1938	0.424
	15.12	1958	0.835
	24.98	1966	1.04
	34.74	1971	1.21
217.2	5.12	2017	0.165
	15.12	2030	0.403
	24.98	2034	0.524
	34.74	2034	0.564

Table AV.19. S.E.P. in Di-2-ethylhexyl phthalate.

Values of the resistive part of the shear impedance as a function of frequency and temperature.

Temperature/K	Frequency/MHz	$R_s(\omega, T)$/MN s m^{-3}
194.7	6	1.060
	18	1.042
	30	1.089
	78	1.065
201.2	6	1.005
	18	1.008
	30	1.012
	78	0.996
202.5	6	0.982
	18	0.990
	30	0.991
	78	0.984
209.7	6	0.916
	18	0.902
	30	0.910
	78	0.914
217.6	6	0.810
	18	0.848
	30	0.824
	78	0.917
225.6	6	0.679
	18	0.754
	30	0.781
	78	0.815
234.4	6	0.561
	30	0.667
	78	0.691
239.5	6	0.481
	30	0.605
	78	0.613

(cont..)

Table AV.19 (cont..)

254.3	6	0.271
	18	0.379
	30	0.413
	78	0.455
263.2	18	0.247
	30	0.303
	78	0.371
274.4	30	0.152
	78	0.232
292.6	6	0.043
	18	0.065
	30	0.102
	78	0.151
298.2	6	0.032
	18	0.059
	30	0.093

Table AV.20. S.E.P. in Di-2-ethylhexyl phthalate.

Values of the normalised shear resistance as a function of the logarithm of reduced frequency.

Temperature/K	$R_s(\omega,T)/R_s(\infty,T)$	$\log[\omega\,\eta_s(0)/G(\infty,T)]$
194.7	1.001	5.547
	0.984	6.024
	1.028	6.246
	1.005	6.661
201.2	1.020	4.179
	1.023	4.656
	1.027	4.878
	1.011	5.293
202.5	1.010	3.944
	1.019	4.421
	1.020	4.643
	1.013	5.058
209.7	1.010	2.815
	0.995	3.292
	1.004	3.514
	1.008	3.929
217.6	0.955	1.844
	1.000	2.321
	0.971	2.543
	1.081	2.958
225.6	0.850	1.063
	0.944	1.540
	0.978	1.762
	1.020	2.177
234.4	0.746	0.378
	0.886	1.075
	0.918	1.492
239.5	0.660	0.043
	0.830	0.742
	0.841	1.157

(cont..)

Table AV.20 (cont..)

254.3	0.404	-0.736
	0.565	-0.259
	0.616	-0.037
	0.678	0.378
263.2	0.385	-0.624
	0.472	-0.402
	0.578	0.012
274.4	0.250	-0.783
	0.381	-0.368
292.6	0.076	-1.963
	0.115	-1.486
	0.181	-1.264
	0.268	-0.849
298.2	0.058	-2.083
	0.107	-1.606
	0.168	-1.384
		-0.969

Table AV.21. S.E.P. in Di-2-ethylhexyl phthalate.

Values of the resistive part of the shear impedance as a function of temperature, pressure and frequency.

Temperature/K	Pressure/MN m^{-2}	Frequency/MHz	$R_s(\omega, P)$/MN s m^{-3}
252.2	0.1	6	0.286
		18	0.315
		30	0.416
	75	18	0.561
		30	0.646
	102	6	0.626
		18	0.656
		30	0.674
	151	6	0.747
		18	0.793
		30	0.830
	203	6	0.84
		18	0.91
		30	0.91
	300	6	1.11
		18	1.11
		30	1.12
	350	6	1.21
		18	1.22
		30	1.23
	400	6	1.26
		18	1.25
		30	1.26
	450	6	1.37
		18	1.35
		30	1.37
	500	6	1.47
		18	1.46
		30	1.47

(cont..)

Table AV.21 (cont..)

269.9	0	6	0.12
		18	0.16
		30	0.215
		78	0.43
	66	6	0.29
		18	0.38
		30	0.46
		78	0.53
	100	30	0.515
	300	6	0.85
		18	0.94
		30	0.97
	448	6	1.11
		18	1.17
		30	1.20
	500	6	1.35
		18	1.37
		30	1.36
296.2	0	6	0.046
		18	0.087
		30	0.128
		78	0.190
	50	6	0.082
		18	0.147
		30	0.212
		78	0.303
	106	6	0.094
		18	0.203
		30	0.252
		78	0.335
	156	6	0.178
		18	0.319
		30	0.380
		78	0.447

(cont..)

Table AV.21 (cont..)

		204	6	0.233
			18	0.442
			30	0.483
			78	0.554
		257	6	0.368
			18	0.560
			30	0.656
		352	6	0.630
			18	0.767
			30	0.835
			78	0.911
		398	6	0.735
			18	0.840
			30	0.913
			78	0.826
		449	6	0.86
			18	0.96
			30	1.00
		500	6	0.98
			18	1.03
			30	1.10
		501	6	0.98
			18	1.06
			30	1.10

Table AV.22. S.E.P. in Di-2-ethylhexyl phthalate.

Values of the normalised shear resistance as a function of the logarithm of reduced frequency at various pressures and temperatures.

Temperature/K	Pressure/MN m^{-2}	$R_s(\omega,P)/R_s(\infty,P)$	$\log_{10}(\omega\eta_s(0)/G(\infty))$
252.2	0.1	0.45	-0.240
		0.49	0.237
		0.65	0.459
	75	0.736	1.020
		0.847	1.242
	102	0.806	0.808
		0.814	1.285
		0.836	1.507
	151	0.843	1.268
		0.895	1.745
		0.937	1.967
	203	0.865	1.732
		0.937	2.209
		0.937	2.431
	300	0.983	2.542
		0.983	3.019
		0.992	3.241
	350	1.00	2.936
		1.01	3.413
		1.02	3.635
	400	0.975	3.316
		0.967	3.793
		0.975	4.015
	450	0.997	3.683
		0.983	4.160
		0.997	4.382
	500	1.01	4.040
		1.00	4.517
		1.01	4.739

(cont..)

Table AV.22 (cont..)

269.9	0	0.20	-1.273
		0.26	-0.796
		0.35	-0.574
		0.70	-0.159
	66	0.40	-0.686
		0.52	-0.209
		0.63	0.013
		0.73	0.428
	100	0.65	0.302
	300	0.79	1.156
		0.87	1.633
		0.90	1.855
	448	0.89	2.182
		0.94	2.659
		0.96	2.881
	500	0.99	2.845
		1.01	3.322
		1.00	3.543
296.2	0	0.098	-2.102
		0.185	-1.624
		0.272	-1.403
		0.404	-0.988
	50	0.144	-1.798
		0.258	-1.321
		0.372	-1.099
		0.532	-0.684
	106	0.140	-1.442
		0.303	-0.965
		0.376	-0.743
		0.500	-0.328
	156	0.237	-1.123
		0.425	-0.646
		0.507	-0.424
		0.596	-0.009

(cont..)

Table AV.22 (cont..)

296.2	204	0.282	-0.818
		0.536	-0.341
		0.585	-0.119
		0.672	0.296
	257	0.410	-0.487
		0.624	-0.010
		0.731	0.212
	352	0.618	0.092
		0.752	0.569
		0.819	0.791
		0.893	1.206
	398	0.687	0.366
		0.785	0.843
		0.853	1.065
		0.772	1.480
	449	0.762	0.665
		0.851	1.142
		0.887	1.364
	500	0.831	0.958
		0.873	1.435
		0.932	1.657
	501	0.831	0.965
		0.898	1.442
		0.932	1.664

Table AV.23. S.E.P. in Di-2-ethylhexyl phthalate.

Values of the longitudinal velocity and absorption coefficient, α, as a function of frequency and pressure at 296.2 K.

Pressure/MN m^{-2}	Frequency/MHz	Velocity/m s^{-1}	10^{-3} α/Nepers m^{-1}
0.1	5.06	1368	0.035
	14.93	1364	0.288
	25.12	1372	0.675
	34.98	1371	1.31
25	5.06	1451	0.042
	14.93	1453	0.345
	25.12	1444	0.796
	34.98	1457	1.38
50	5.06	1534	0.058
	14.93	1536	0.425
	25.12	1541	1.01
	34.98	1529	1.78
75	5.06	1620	0.080
	14.93	1621	0.590
	25.12	1628	1.20
	34.98	1631	2.22
100	5.06	1700	0.101
	14.93	1698	0.722
	25.12	1708	1.55
	34.98	1699	2.47
150	5.06	1870	0.169
	14.93	1920	1.00
	25.12	1900	2.11
200	5.06	2040	0.241
	14.93	2060	1.30
	25.12	2100	2.39
250	5.06	2230	0.322
	14.93	2267	1.41
	25.12	2311	2.41

(cont..)

Table AV.23 (cont..)

300	5.06	2418	0.372
	14.93	2478	1.38
	25.12	2512	2.03
350	5.06	2631	0.396
	14.93	2680	1.23
	25.12	2600	1.71
400	5.06	2798	0.359
	14.93	-	1.01
	25.12	-	1.36

Table AV.24. S.E.P. in Di-2-ethylhexyl phthalate.

Values of the longitudinal velocity and absorption coefficient, α, as a function of frequency and pressure at 269.9 K.

Pressure/MN m^{-2}	Frequency/MHz	Velocity/m s^{-1}	10^{-3} α/Nepers m^{-1}
0.1	5.11	1509	0.192
	14.96	1510	1.16
	25.07	1531	2.52
	34.95	1540	4.05
25	5.11	1596	0.269
	14.96	1615	1.46
	25.07	1631	3.01
	34.95	1644	4.63
50	5.11	1687	0.357
	14.96	1716	1.72
	25.07	1738	3.33
	34.95	1754	4.93
75	5.11	1782	0.444
	14.96	1823	1.89
	25.07	1850	3.45
	34.95	1869	4.90
100	5.11	1883	0.520
	14.96	1936	1.95
	25.07	1966	3.36
	34.95	1987	4.62

Table AV.23 (cont..)

300	5.06	2418	0.372
	14.93	2478	1.38
	25.12	2512	2.03
350	5.06	2631	0.396
	14.93	2680	1.23
	25.12	2600	1.71
400	5.06	2798	0.359
	14.93	-	1.01
	25.12	-	1.36

Table AV.24. S.E.P. in Di-2-ethylhexyl phthalate.

Values of the longitudinal velocity and absorption coefficient, α, as a function of frequency and pressure at 269.9 K.

Pressure/MN m^{-2}	Frequency/MHz	Velocity/m s^{-1}	10^{-3} α/Nepers m^{-1}
0.1	5.11	1509	0.192
	14.96	1510	1.16
	25.07	1531	2.52
	34.95	1540	4.05
25	5.11	1596	0.269
	14.96	1615	1.46
	25.07	1631	3.01
	34.95	1644	4.63
50	5.11	1687	0.357
	14.96	1716	1.72
	25.07	1738	3.33
	34.95	1754	4.93
75	5.11	1782	0.444
	14.96	1823	1.89
	25.07	1850	3.45
	34.95	1869	4.90
100	5.11	1883	0.520
	14.96	1936	1.95
	25.07	1966	3.36
	34.95	1987	4.62

Table AV.25. The values of the limiting high frequency longitudinal velocity obtained with the normal reflection technique.

Liquid	Temperature/K	V/m s^{-1}		
		18 MHz	30 MHz	78 MHz
4-phenyl dibenzofuran	275.9	2252	2283	
	270.7	2304	2297	
	265.8	2309	2314	
	261.2	2324	2339	
Epoxy Resin MY 750	280.2	2222	2243	2201
	274.1	2222	2227	2232
	271.5	2275	2313	2261
	265.2	2331	2345	
	261.0	2377	2425	2388
S.E.P. in Di-2-ethylhexyl phthalate	211.7	2222	2246	
	206.2	2294	2282	
	203.2	2310	2317	
	199.2	2361	2384	
	195.7	2400	2396	

APPENDIX VI

Table AVI.1. 4-phenyl dibenzofuran.

Values of the relaxing part, $K(\infty) - K(0)$, of the bulk modulus and ratio to the shear modulus as a function of temperature.

Temperature/K	$K(\infty)-K(0)$ /GN m^{-2}	$K(\infty)-K(0)/G(\infty)$
273.6	1.145	1.27
272.2	1.150	1.25
272.1	1.152	1.26
272.3	1.150	1.26
282.6	1.098	1.38
279.5	1.117	1.35
279.1	1.120	1.34
279.7	1.116	1.35
291.3	1.034	1.44
288.8	1.054	1.42
289.0	1.008	1.36
289.2	1.051	1.42
298.8	0.968	1.46
298.2	0.974	1.46
298.7	0.969	1.46
298.9	0.967	1.46
309.0	0.869	1.45
307.0	0.889	1.45
307.0	0.889	1.45
306.8	0.891	1.45
318.8	0.768	1.40
316.3	0.794	1.41
316.4	0.793	1.41
316.3	0.794	1.41
328.3	0.668	1.31
325.1	0.702	1.35
325.0	0.703	1.35
325.0	0.698	1.34

(cont..)

Table AVI.1 (cont..)

337.4	0.571	1.21
335.5	0.591	1.23
335.5	0.591	1.23
335.4	0.593	1.23
347.2	0.468	1.06
345.6	0.485	1.09
345.6	0.485	1.09
345.5	0.486	1.09
357.3	0.364	0.88
358.1	0.356	0.87
357.1	0.366	0.88

Table AVI.2. 4-phenyl dibenzofuran.

Values of the normalised bulk storage, $K'(\omega)/K(\infty) - K(0)$, and loss, $K''(\omega)/K(\infty) - K(0)$, moduli as a function of $\log_{10}(\omega\,\eta_s(0)/K(\infty) - K(0))$.

Temperature/K	$\log_{10}\left[\frac{\omega\,\eta_s(0)}{K(\infty)-K(0)}\right]$	$K'(\omega)/(K(\infty)-K(0))$	$K''(\omega)/(K(\infty)-K(0))$
273.6	1.687	0.882	0.098
272.2	2.339	0.965	0.057
272.1	2.571	0.960	0.040
272.3	2.689	0.971	0.035
282.6	0.540	0.610	0.231
279.5	1.349	0.829	0.133
279.1	1.618	0.874	0.090
279.7	1.690	0.885	0.098
291.3	-0.334	0.245	0.307
288.8	0.342	0.507	0.242
289.0	0.560	0.622	0.212
289.2	0.670	0.752	0.238
298.8	-0.945	0.061	0.123
298.2	-0.454	0.221	0.223
298.7	-0.300	0.240	0.210
298.9	-0.141	0.340	0.235
309.0	-1.610	-0.030	0.047
307.0	-1.035	0.071	0.118
307.0	-0.825	0.082	0.148
306.8	-0.665	0.116	0.139
318.8	-2.107	0.002	0.018
316.3	-1.535	0.018	0.055
316.4	-1.329	0.017	0.082
316.3	-1.176	0.050	0.097
328.3	-2.486	0.002	0.008
325.1	-1.913	0.008	0.028
325.0	-1.700	0.015	0.042
325.5	-1.569	0.016	0.052
337.4	-2.771	0.000	0.004
335.5	-2.260	0.005	0.013
335.5	-2.049	0.004	0.020
335.4	-1.898	0.007	0.027

(cont..)

Table AVI.2 (cont..)

347.2	-3.002	0.007	0.005
345.6	-2.514	-0.002	0.009
345.6	-2.302	-0.020	0.011
345.5	-2.153	0.016	0.017
357.3	-2.711	0.025	0.010
358.1	-2.507	0.003	0.006
357.1	-2.350	0.000	0.011

Table AVI.3. Epoxy Resin MY 750.

Values of the relaxing part ($K(\infty) - K(0)$) of the bulk modulus and ratio to the shear modulus $G(\infty)$ as a function of temperature.

Temperature/K	$K(\infty) - K(0)/GN \cdot m^{-2}$	$K(\infty) - K(0)/G(\infty)$
268.6	0.8212	0.69
"	"	"
"	"	"
272.9	0.8750	0.82
279.8	0.9052	0.98
"	"	"
280.3	0.9059	1.00
291.2	0.8645	1.16
289.8	0.8733	1.15
290.0	0.8721	1.15
289.7	0.8739	1.14
296.9	0.8222	1.21
298.0	0.8125	1.21
297.8	0.8144	1.21
297.9	0.8135	1.21
305.1	0.7414	1.22
305.1	0.7429	1.23
305.2	0.7418	1.23
304.7	0.7471	1.23
316.7	0.6115	1.17
313.6	0.6481	1.20
313.7	0.6469	1.19
313.8	0.6495	1.20
325.8	0.5012	1.06
322.7	0.5393	1.10
322.6	0.5404	1.11
322.2	0.5453	1.11
333.9	0.4011	0.92
332.7	0.4159	0.95
332.6	0.4180	0.95
332.8	0.4143	0.94

(cont..)

Table AVI.3 (cont..)

344.9	0.2662	0.68
342.8	0.2917	0.73
343.0	0.2893	0.72
343.5	0.2992	0.75

Table AVI.4. Epoxy Resin MY 750.

Values of the normalised bulk storage and loss moduli as a function of $\log_{10}(\omega\,\eta_s(0)/K(\infty) - K(0))$.

Temperature/K	$\log_{10}[\omega\,\eta_s(0)/K(\infty) - K(0)]$	$K'(\omega)/K(\infty) - K(0)$	$K''(\omega)/K(\infty) - K(0)$
268.6	2.670	1.000	0.090
"	2.880	0.995	0.056
"	3.036	0.978	0.021
272.9	1.696	0.799	0.159
279.8	1.474	0.901	0.098
279.8	1.693	0.794	0.014
280.3	1.793	0.866	0.030
291.2	0.103	0.550	0.244
289.8	0.665	0.656	0.214
290.0	0.870	0.680	0.185
289.7	1.036	0.761	0.170
296.9	-0.268	0.280	0.027
298.0	0.140	0.453	0.250
297.8	0.368	0.599	0.304
297.9	0.507	0.599	0.230
305.1	-0.725	0.129	0.166
305.1	-0.246	0.294	0.235
305.2	-0.037	0.375	0.247
304.7	0.134	0.450	0.250
316.7	-1.233	0.044	0.088
313.6	-0.630	0.157	0.185
313.7	-0.421	0.198	0.213
313.8	-0.277	0.336	0.239
325.8	-1.515	0.023	0.057
322.7	-0.962	0.085	0.141
322.6	-0.745	0.129	0.165
322.2	-0.586	0.175	0.191
333.9	-1.726	0.009	0.039
332.7	-1.237	0.041	0.089
332.6	-1.026	0.092	0.113
332.8	-0.877	0.144	0.152

(cont..)

Table AVI.4 (cont..)

344.9	-1.919	0.022	0.039
342.8	-1.420	0.024	0.067
343.0	-1.210	0.049	0.093
343.5	-1.095	0.061	0.109

Table AVI.5. Epoxy Resin MY 750.

Values of the normalised bulk storage and loss moduli at 310.2 K.

Pressure/MN m^{-2}	$\log_{10}[\omega\eta_s(0)/G(\infty)]$	$K'/G(\infty)$	$K''/G(\infty)$
0.1	-0.956	0.068	0.125
40	-0.467	0.191	0.212
50	-0.325	0.245	0.222
60	-0.184	0.310	0.239
100	0.368	0.516	0.228
125	0.705	0.656	0.214
150	1.024	0.715	0.175
200	1.685	0.880	0.100
0.1	-0.491	0.189	0.194
40	-0.003	0.360	0.234
50	0.139	0.440	0.249
60	0.280	0.533	0.254
100	0.832	0.689	0.197
125	1.169	0.804	0.161
150	1.502	0.690	0.098
200	2.149	1.04	0.070
0.1	-0.268	0.275	0.226
40	0.221	0.467	0.250
50	0.362	0.510	0.228
60	0.503	0.381	0.201
100	1.055	0.780	0.172
125	1.392	0.759	0.125
150	1.724	0.844	0.094
200	2.372	1.04	0.061
0.1	-0.121	0.335	0.239
40	0.368	0.578	0.254
50	0.510	0.470	0.210
60	0.651	0.659	0.215
100	1.203	0.876	0.177

Table AVI.6. S.E.P. in Di-2-ethylhexyl phthalate.

Values of the normalised bulk storage and loss moduli as a function of the logarithm of reduced frequency.

$\log[\omega\eta_s(0)/G(\infty)]$	$K'(\omega)/G(\infty)$	$K''(\omega)/G(\infty)$
-1.824	0.041	0.028
-1.348	0.032	0.036
-1.126	0.062	0.050
-0.980	0.083	0.086
-1.488	0.031	0.028
-1.011	0.077	0.071
-0.789	0.121	0.114
-0.642	0.158	0.146
-1.128	0.060	0.058
-0.651	0.157	0.138
-0.429	0.219	0.223
-0.283	0.287	0.165
-0.820	0.120	0.103
-0.343	0.248	0.255
-0.121	0.321	0.250
0.025	0.403	0.268
-0.291	0.238	0.153
0.187	0.460	0.275
0.408	0.568	0.239
0.554	0.612	0.228
0.156	0.497	0.229
0.633	0.637	0.269
0.854	0.742	0.200
1.000	0.747	0.215
0.484	0.580	0.230
0.961	0.736	0.232
1.183	0.789	0.181
1.329	0.887	0.177

(cont..)

Table AVI.6 (cont..)

1.783	0.882	0.130
2.260	0.919	0.097
2.482	0.942	0.069
2.628	0.959	0.057
2.582	0.951	0.040
3.059	0.978	0.054
3.281	1.000	0.043
3.427	0.996	0.030

Table AVI.7. S.E.P. in Di-2-ethylhexyl phthalate.

Values of the normalised bulk storage and loss moduli as a function of reduced frequency at 296.2 K.

$\log_{10}(\omega\ \eta_s(0)/G(\infty))$	$K'(\omega)/G(\infty)$	$K''(\omega)/G(\infty)$
-1.932	-0.002	0.011
-1.461	-0.056	0.033
-1.235	0.031	0.043
-1.091	0.011	0.065
-2.027	0.005	0.018
-1.557	0.020	0.053
-1.332	-0.080	0.065
-1.188	0.049	0.082
-1.873	0.008	0.025
-1.402	0.019	0.062
-1.177	0.056	0.085
-1.033	-0.067	0.102
-1.714	0.037	0.037
-1.245	0.032	0.091
-1.019	0.078	0.098
-0.875	0.089	0.136
-1.554	0.012	0.046
-1.085	-0.025	0.110
-0.859	0.034	0.132
-0.715	0.061	0.137
-1.235	0.037	0.083
-0.765	0.360	0.179
-0.539	0.166	0.197
-0.918	0.042	0.122
-0.448	0.087	0.222
-0.222	0.290	0.235
-0.604	0.149	0.178
-0.134	0.239	0.258
0.092	0.429	0.254

(cont..)

Table AVI.7 (cont..)

-0.297	0.195	0.211
0.173	0.362	0.270
0.399	0.466	0.196
0.006	0.346	0.247
0.476	0.398	0.252
0.702		0.110
0.304	0.618	0.521

Table AVI.8. S.E.P. in Di-2-ethylhexyl phthalate.

Values of the normalised bulk storage and loss moduli as a function of reduced frequency at 269.9 K.

$\log (\omega \eta_s(0)/G(\infty))$	$K'(\omega)/G(\infty)$	$K''(\omega)/G(\infty)$
-1.343	0.035	0.067
-0.877	0.007	0.128
-0.653	0.141	0.168
-0.508	0.182	0.192
-1.116	0.046	0.094
-0.650	0.129	0.168
-0.426	0.195	0.203
-0.281	0.248	0.222
-0.895	0.122	0.128
-0.428	0.235	0.203
-0.204	0.317	0.231
-0.060	0.373	0.242
-0.678	0.126	0.163
-0.212	0.271	0.229
0.012	0.362	0.246
0.157	0.424	0.250
-0.466	0.188	0.198
0.000	0.362	0.246
0.224	0.451	0.249
0.369	0.517	0.246

Table AVI.8. S.E.P. in Di-2-ethylhexyl phthalate.

Values of the normalised bulk storage and loss moduli as a function of reduced frequency at 269.9 K.

$\log (\omega \eta_s(0)/G(\infty))$	$K'(\omega)/G(\infty)$	$K''(\omega)/G(\infty)$
-1.343	0.035	0.067
-0.877	0.007	0.128
-0.653	0.141	0.168
-0.508	0.182	0.192
-1.116	0.046	0.094
-0.650	0.129	0.168
-0.426	0.195	0.203
-0.281	0.248	0.222
-0.895	0.122	0!128
-0.428	0.235	0.203
-0.204	0.317	0.231
-0.060	0.373	0.242
-0.678	0.126	0.163
-0.212	0.271	0.229
0.012	0.362	0.246
0.157	0.424	0.250
-0.466	0.188	0.198
0.000	0.362	0.246
0.224	0.451	0.249
0.369	0.517	0.246

Table AVI.9. Comparison of Di-2-ethylhexyl phthalate and S.E.P. in Di-2-ethylhexyl phthalate.

Property	Di-2-ethylhexyl phthalate	S.E.P. in Di-2-ethylhexyl phthalate
T_g (experiment)	184 K	190 ± 3 K
T_g (calculated at $\eta_s(0) = 10^{12}$ N s m^{-2})	183.8 K	186 ± 1 K
Density/Kg m^{-3}	1202.0 - 0.689 T/K	1203.0 - 0.742 T/K
Velocity V(0)/m s^{-1}	2140.6 - 2.525 T/K	2292.2 - 3.12 T/K
Viscosity		
$\log_e \eta_s(0)$	-11.724 + 1305/(T/K-150.6)	
$\log_{10}(\log_{10} \eta+4.2)$		$0.5751 - 1.258 \log_{10} \frac{(T/K - 138)}{135}$
$J(\infty)/GN\ m^{-2}$	-2.16 + 0.0152 T/K	-3.34 + 0.022 T/K
max. α/f^2 at 15 MHz	$1.43 \cdot 10^{-11}$	$1.40 \cdot 10^{-11}$
max. α/f^2 at 25 MHz	$0.84 \cdot 10^{-11}$	$0.86 \cdot 10^{-11}$
max. α/f^2 at 35 MHz	$0.61 \cdot 10^{-11}$	$0.60 \cdot 10^{-11}$

* Ref. 28

Table AVI.9. Comparison of Di-2-ethylhexyl phthalate and S.E.P. in Di-2-ethylhexyl phthalate.

Property	Di-2-ethylhexyl phthalate	S.E.P. in Di-2-ethylhexyl phthalate
T_g (experiment)	184 K	190 ± 3 K
T_g (calculated at $\eta_s(0) = 10^{12}$ N s m^{-2})	183.8 K	186 ± 1 K
Density/Kg m^{-3}	1202.0 - 0.689 T/K	1203.0 - 0.742 T/K
Velocity V(0)/m s^{-1}	2140.6 - 2.525 T/K	2292.2 - 3.12 T/K
Viscosity		
$\log_e \eta_s(0)$	-11.724 + 1305/(T/K-150.6)	
$\log_{10}(\log_{10} \eta+4.2)$		0.5751 - 1.258 $\log_{10} \frac{(T/K - 138)}{135}$
$J(\infty)/GN\ m^{-2}$	-2.16 + 0.0152 T/K	-3.34 + 0.022 T/K
max. α/f^2 at 15 MHz	$1.43 \cdot 10^{-11}$	$1.40 \cdot 10^{-11}$
max. α/f^2 at 25 MHz	$0.84 \cdot 10^{-11}$	$0.86 \cdot 10^{-11}$
max. α/f^2 at 35 MHz	$0.61 \cdot 10^{-11}$	$0.60 \cdot 10^{-11}$

* Ref. 28

APPENDIX VII

Table AVII.1. Decyltrimethylammoniumbromide aqueous solutions.

Fit of atmospheric pressure density results to a linear equation.

$$\rho/\mathrm{Kg\ m^{-3}} = A + BT/K$$

Solution Concentration /mol dm^{-3}	A	B
0.005	1085.8	-0.2892
0.01	1102.5	-0.3467
0.05	1127.0	-0.4267
0.10	1125.9	-0.4175
0.50	1149.1	-0.4700
1.00	1194.1	-0.5882

Table AVII.2. Decyltrimethylammonium bromide.

Fit of pressure-density results to the linear secant modulus equation.

$$\rho/\mathrm{Kg\ m^{-3}} = \frac{1 + AP/\mathrm{MN\ m^{-2}} + BT/K}{C + DP/\mathrm{MN\ m^{-2}}}$$

Solution Concentration /mol dm^{-3}	10^3 A	10^4 B	10^4 C	10^6 D
0.005	1.314	-2.664	9.211	0.9102
0.01	1.295	-3.021	9.105	0.9008
0.05	1.495	-3.738	8.873	1.097
0.10	1.400	-3.901	8.825	1.007
0.50	1.332	-4.167	8.675	0.9522
1.00	1.469	-5.626	8.159	1.086

Table AVII.3. Decyltrimethylammonium bromide aqueous solutions.

Values of the density as a function of concentration and pressure at 298.2 K.

Pressure /MN m^{-2}	Concentration /mol. dm^{-3}	Density /Kg m^{-3}
0.1	0.005	998.9
"	0.01	999.1
"	0.04	999.4
"	0.05	999.8
"	0.10	1001
"	0.20	1003
"	0.50	1009
"	1.00	1019
100	0.005	1039
"	0.01	1039
"	0.04	1040
"	0.05	1041
"	0.10	1042
"	0.20	1044
"	0.50	1048
"	1.00	1059
200	0.005	1073
"	0.01	1072
"	0.04	1072
"	0.05	1073
"	0.10	1074
"	0.20	1076
"	0.50	1080
"	1.00	1090
300	0.005	1101
"	0.01	1100
"	0.04	1100
"	0.05	1099
"	0.10	1100
"	0.20	1102
"	0.50	1105
"	1.00	1115

Table AVII.4. Cetrimide - Hexanol - Water.

A. Values of R_s at 298.2 K

Composition, w/w %			R_s/MN s m^{-3}	$R_{s_{Newt}}$/MN s m^{-3}	Phase (a)
Cetrimide	Water	Hexanol			
40	60	0	<0.02	0.0406	E
10	90	0	<0.02	0.0123	L
49.3*	50.7	0	<0.02	>0.5	E
30*	70	0	<0.02		E
20*	80	0	<0.02		L
39.8*	40.3	19.9	<0.02		D

* Recrystallised cetrimide.

(a) Ref. 98.

B. Values of viscosity and density at 298.2 K

Composition, w/w %		Viscosity/N s m^{-2}	Density/Kg m^{-3}
Cetrimide	Water		
40	60	0.0174	1005.4
10	90	0.0016	998.8

APPENDIX VIII

Table AVIII.1. 1,1,2 Trichloroethane.

Values of α/f^2 and $V_L(\omega)$ as a function of frequency and pressure at 283.4 K.

Pressure/MN m^{-2}	Frequency/MHz	$10^{13}\ \alpha/f^2$ / Nepers $m^{-1} s^2$	$V_L(\omega)$/m s^{-1}
0.1	5.07	35.0	1210
	14.96	11.3	1212
	25.12	5.08	1214
	34.93	3.45	
40	5.07	28.6	1385
	14.96	8.11	1386
	25.12	3.03	
	34.93	1.60	1386
50	5.07	27.5	1415
	14.96	7.75	1415
	25.12	3.18	
	34.93	1.54	
60	5.07	24.3	1450
	14.96	7.78	1451
	25.12	2.60	
	34.93	1.49	
80	5.07	24.0	1490
	14.96	7.10	1492
	25.12	2.60	
	34.93	1.22	
100	5.07	22.6	1530
	14.96	6.22	1531
	25.12	2.29	1529
	34.93	1.00	
120	5.07	21.5	1570
	14.96	5.62	1569
150	5.07	18.3	1605
	14.96	5.01	1609
	25.12	2.01	
	34.93	0.80	

(cont..)

Table AVIII.1 (cont..)

200	5.07	16.6	
	14.96	4.83	1662
	25.12	1.79	1675
	34.93	0.70	
250	5.12	15.0	
	14.96	3.83	1723
	25.12	1.49	
	34.93	0.51	

Table AVIII.2. 1,1,2 Trichloroethane.

Values of α/f^2 and $V_L(\omega)$ as a function of frequency and pressure at 298.2 K.

Pressure/MN m^{-2}	Frequency/MHz	$10^{13}\ \alpha/f^2$ / Nepers $m^{-1}s^2$	$V_L(\omega)$/m s^{-1}
0.1	5.14	23.5	1165
	15.62	11.7	1161
	24.96	9.91	1160
	34.71	3.87	1180
40	5.14	18.9	1336
	15.62	8.76	1334
	24.96	5.62	1336
	34.71	2:01	1342
50	15.62	8.70	
	34.71	1.71	
60	5.14	17.8	1394
	15.62	8.26	1386
	24.96	6.01	1394
	34.71	1.61	1396
80	5.14	16.7	1446
	15.62	7.00	1441
	24.96	5.04	1446
	34.71	1.09	1450
100	5.14	15.5	1489
	15.62	6.72	1482
	24.96	4.82	1488
	34.71	1.00	1493
120	5.14	14.8	1526
	15.62	6.34	1516
	24.96	4.59	1526
	34.71	0.89	1530
150	5.21	14.5	1562
	15.60	6.19	1561
	24.97	4.57	1573
	34.86	0.80	1578

(cont..)

Table AVIII.2 (cont..)

200	5.21	14.3	1657
	15.60	5.71	1650
	24.97	4.32	1652
	34.86	0.61	1655
250	5.21	13.4	1737
	15.60	5.78	1746
	24.97	4.23	1737
	34.86	0.50	1738

Table AVIII.3. 1,1,2 Trichloroethane.

Values of α/f^2 and $V_L(\omega)$ as a function of frequency and pressure at 313.2 K.

Pressure/MN m^{-2}	Frequency/MHz	$10^{13}\ \alpha/f^2$ / Nepers $m^{-1}s^2$	$V_L(\omega)$/m s^{-1}
0.1	5.31	15.8	1103
	15.16	11.3	
	25.19	7.87	1105
	34.96	6.12	
40	5.31	12.6	1274
	15.16	8.57	
	25.19	7.57	1281
	34.96	3.87	
50	5.31	11.3	
60	5.31	11.1	1326
	15.16	7.31	1323
	25.19	6.80	1328
	34.96	2.97	
80	5.31	9.86	1382
	15.16	6.51	
	25.19	6.16	1384
	34.96	2.22	
100	5.31	8.85	1418
	15.16	4.26	1420
	25.19	3.92	1422
	34.96	2.19	
120	5.31	9.01	1452
	15.16	4.17	1457
	25.19	3.60	
	34.96	1.60	
150	15.16	4.08	1493
	34.96	1.50	

REFERENCES.

REFERENCES

1. Pinkerton, J.M.M., Proc. Phys. Soc. Lond., 1949, B62, 286.

2. Johnson, K.L., Cameron, R., Proc. Inst. Mech. Engrs., 1967-8, 182(1), 307.

3. Fein, R.S., J. of Lubr. Tech., 1967, 89, 127.

4. Paul, G.R., Cameron, A., Nature, 1974, 248(5445), 219.

5. Stokes, G.S., Trans. Camb. Phil. Soc., 1845, 8, 287.

6. Biquard, P., Comp. Rend., 1931, 193, 226.

7. Pellam, J.R., Galt, J.K., J. Chem. Phys., 1946, 14, 608.

8. Mason, W.P., McSkimin, H.T., J. Acoust. Soc. Amer., 1947, 19, 464.

9. Barlow, A.J., Lamb, J., Proc. Roy. Soc. Lond., Ser.A, 1959, 253, 52.

10. Dexter, A.R., Matheson, A.J., J. Chem. Phys., 1971, 54(8), 3463.

11. Barlow, A.J., Erginsav, A., Lamb, J., Proc. Roy. Soc. Lond., Ser.A, 1967, 298(1455), 481.

12. Barlow, A.J., Erginsav, A., Lamb, J., Proc. Roy. Soc. Lond., Ser.A, 1969, 309(1499), 473.

13. Phillips, M.C., Barlow, A.J., Lamb, J., Proc. Roy. Soc. Lond., Ser.A, 1972, 329(1577), 193.

14. Glarum, S.H., J. Chem. Phys., 1960, 33(3), 639.

15. Barlow, A.J., Singh, R.P., J.C.S. Faraday II, 1972, 68(8), 1404.

16. Barlow, A.J., Erginsav, A., Mclachlan, R.J., Singh, R.P., J.C.S. Faraday II, 1974, 70(7), 1288.

17. Barlow, A.J., Lamb, J., Taskĕprülü, N.S., J. Acoust. Soc. Amer., 1969, 46, 569.

18. D'Arrigo, G., J. Chem. Phys., 1975, 63(1), 61.

19. Hunter, A.N., Proc. Phys. Soc., 1951, 64B, 1086.

20. Hutton, J.F., Proc. Roy. Soc., Ser.A, 1968, 304(1476), 65.

21. Barlow, A.J., Lamb, J., Matheson, A.J., Padmini, P.R.K.L., Richter, J., Proc. Roy. Soc., Ser.A, 1967, 298(1455), 467.

22. Rassing, J., 'Chemical and Biological Applications of Relaxation Spectrometry', edited by E. Wyn-Jones, pub. D. Reidel Pub. Co., p.1.

23. Mishra, P.K., Singh, R.P., J. Appl. Phys., 1974, 45(12), 5478.

24. Mikhailov, I.G., Manuchorov, Yu.S., Khakimov, O., Ultrasonics, 1975, 13(2), 66.

25. Barlow, A.J., Erginsav, A., Proc. Roy. Soc., Ser.A, 1972, 327(1569), 175.

26. Barlow, A.J., Erginsav, A., J.C.S. Faraday II, 1973, 69, 1200.

27. Davidson, D.W., Cole, R.H., J. Chem. Phys., 1951, 19, 1484.

28. Powell, G., Ph.D. Thesis, University of Salford, 1973.

29. Lamb, J., Rheol. Acta., 1973, 12, 438.

30. Mason, W.P., "Piezoelectric crystals and their application to ultrasonics", Pub. D. van Nostrand and Co., Chapter 6.

31. O'Neil, H.T., Phys. Rev., 1949, 75(6), 928.

32. Hutton, J.F., Shell Research internal report.

33. Barlow, A.J., Subramanian, S., Brit. J. Appl. Phys., 1966, 17, 1201.

34. Bridgeman, P.W., "Physics of High Pressure", Pub. G. Bell and Son Ltd., London.

35. Phillips, M.C., Shell Research internal report.

36. Houck, J.C., J. Res. Natl. Bur. Stds., 1974, 78A(5), 617.

37. Andreae, J.H., Bass, R., Heasell, E.J., Lamb, J., Acustica, 1958, 8, 131.

38. Barlow, A.J., Yazgan, E., Brit. J. Appl. Phys., 1967, 18, 645.

39. Barlow, A.J., Yazgan, E., Brit. J. Appl. Phys., 1966, 17, 807.

40. McSkimin, H.J., J. Acoust. Soc. Amer., 1957, 29(11), 1185.

41. Angel. W.T., Bean, V.E., Rev. Sci. Inst., 1975, 46(5), 533.

42. Bundell, H.E., Wyn-Jones, E., Private communication.

43. Heyward, A.T.J., N.E.L. Report No. 486, 1971.

44. Roelands, C.J.A., Dissertation, T.H. Delft, 1966.

45. Hutton, J.F., Phillips, M.C., Shell Research internal report.

46. Newman, F.H., Searle, V.H.L., "General Properties of Matter", Pub. E. Benn Ltd., 1933, p.204.

47. Hutton, J.F., Phillips, M.C., Shell Research internal report.

48. Isayev, A.I., Zolotarev, V.A., Vinogradov, G.V., Rheol. Acta., 1975, 14(2), 135.

49. Jongepier, R., Kuilman, B., Rheol. Acta., 1970, 9(1), 102.

50. Hutton, J.F., Phillips, M.C., J. Chem. Phys., 1969, 51(3), 1065.

51. Jongepier, R., Kuilman, B., Rheol. Acta., 1970, 9(3), 460.

52. Schwarzl, F., Staverman, A.J., J. Appl. Phys., 1952, 23(8), 838.

53. Hraiki, S., Rheol. Acta., 1974, 13(3), 567.

54. Barlow, A.J., Dickie, R.A., Lamb, J., Proc. Roy. Soc. A., 1967, 300, 356.

55. Herzfeld, K.F., Litovitz, T.A., Absorption and Dispersion of Ultrasonic Waves, Academic Press, 1959, p.467.

56. Hayton, B., Lucas, A.G., Private communication.

57. Hutton, J.F., Phillips, M.C., Nature Physical Science, 1972, 238 (87), 141.

58. Barlow, A.J., Harrison, G., Kim, M.G., Lamb, J., J.C.S. Faraday II, 1973, 69, 1446.

59. Boelhouwer, J.W.M., Physica, 1967, 34, 484.

60. Jakobsen, J., Sanborn, D.M., Winer, W.O., Trans. ASME, J. Lub. Tech., 1974, 96, 410.

61. Miles, D.O., Hamamoto, A.S., Nature, 1962, 193, 644.

62. Dill, J.F., Drake, P.W., Litovitz, T.A., ASLE Trans., 1975, 18(3), 202.

63. Ambrus, J.H., Dardy, H., Moynihan, C.T., J. Phys. Chem., 1972, 76, 3495.

64. Slie, W.M., Donfor, A.R., Litovitz, T.A., J. Chem. Phys., 1966, 44, 3712.

65. Slie, W.M., Madigosky, W.M., J. Chem. Phys., 1968, 48, 2810.

66. Barlow, A.J., Harrison, G., Irving, J.B., Kim, M.G., Lamb, J., Pursley, W.C., Proc. Roy. Soc. Lond., Ser.A, 1972, 327, 403.

67. Dyson, A., Phil. Trans. Roy. Soc. Lond., 1970, A266, 1.

68. Zwanzig, R., Mountain, R.D., J. Chem. Phys., 1965, 43, 4464.

69. Gopala Rao, R.V., Nammalvar, T., Acustica, 1975, 34, 51.

70. Kono, R., Yamaoka, T., Nomoto, O., Acustica, 1975, 32, 286.

71. Mikhailov, I.G., Polunin, V.M., Akust. Zh., 1972, 18, 286.

72. Bogdanov, V.N., Mikhailov, I.G., Nemilov, S.V., Sov. Phys. Acoust., 1975, 20, 310.

73. Pulatova, D., Khabibullaev, P.K., Khaliulin, M.G., Sharipov, Sh., Akust. Zh., 1975, 21, 308. (Sov. Phys. Acoust., 1975, 21, 194).

74. Barlow, A.J., Harrison, G., Lamb, J., Proc. Roy. Soc. Lond., Ser.A, 1964, 282, 228.

75. Rouse, P.E., J. Chem. Phys., 1953, 21, 1272.

76. Barlow, A.J., Day, M., Harrison, G., Lamb, J., Subramanian, S., Proc. Roy. Soc. Lond., Ser.A, 1969, 309, 497.

77. Frederick, J.E., Tschoegl, N.W., Ferry, J.D., J. Phys. Chem., 1964, 68, 1974.

78. Zimm, B.H., J. Chem. Phys., 1956, 24, 269.

79. Lamb, J., Matheson, A.J., Proc. Roy. Soc. Lond., Ser.A, 1964, 281, 207.

80. Mikhailov, I.G., Polunin, V.M., Sov. Phys. Acoust., 1973, 19, 142.

81. Hamann, S.D., J. Phys. Chem., 1962, 66, 1359.

82. Tuddenham, R.F., Alexander, A.E., J. Phys. Chem., 1962, 66, 1839.

83. Osugi, J., Sato, M., Ifuku, N., Rev. Phys. Chem. Jap., 1965, 35, 32.

84. Osugi, J., Sato, M., Ifuku, N., Rev. Phys. Chem. Jap., 1968, 38, 58.

85. Shigehara, K., Bull. Chem. Soc. Jap., 1965, 38, 1700.

86. Rassing, J., Sams, P.J., Wyn-Jones, E., J.C.S. Faraday II, 1974, 70, 1247.

87. Tanaka, M., Kaneshina, S., Shinno, K., Okajima, T., Tomida, T., J. Colloid Interface Sci., 1974, 46, 132.

88. Kaneshina, S., Tanaka, M., Tomida, T., J. Colloid Interface Sci., 1974, 48, 450.

89. Tanaka, M., Kaneshina, S., Kuramdo, S., Matuura, R., Bull. Chem. Soc. Jap., 1975, 48, 432.

90. Winsor, P.A., Chem. Revs., 1968, 68, 1.

91. Lee. Y.S., Golub, S.L., Brown, G.H., J. Phys. Chem., 1972, 76, 2409.

92. Letcher, S.V., Barlow, A.J., Phys. Rev. Lett., 1971, 26, 172.

93. Dyro, J.F., Edmonds, P.D., Mol. Cryst. Liquid Cryst., 1975, 29, 263.

94. Dyro, J.F., Edmonds, P.D., Mol. Cryst. Liquid Cryst., 1974, 25, 175.

95. Zvereva, G.E., Kapustin, A.P., Soviet Phys. (Acoust.), 1964, 10, 97.

96. Nash, T., J. Appl. Chem., 1956, 6, 539.

97. Nash, T., J. Colloid Sci., 1958, 13, 134.

98. Ekwall, P., Mandell, L., Fontell, K., J. Colloid Interface Sci., 1969, 29, 639.

99. Rassing, J., Chemical and Biological Applications of Relaxation Spectrometry, Ed. E. Wyn-Jones, Pub. D. Reidel Pub. Co., 1975, p.2.

100. Eccleston, G., Pethrick, R.A., Wyn-Jones, E., Hamblin, P.C., White, R.F.M., Trans. Faraday Soc., 1970, 66, 310.

101. Pethrick, R.A., Wyn-Jones, E., Trans. Faraday Soc., 1970, 66, 2483.

102. Crook, K.R., Wyn-Jones, E., Trans. Faraday Soc., 1971, 67, 660.

103. Eccleston, G., Walsh, B., Wyn-Jones, E., Morris, H., Trans. Faraday Soc., 1971, 67, 3223.

104. Lamb, J., Z. Electrochem., 1960, 64, 135.

105. Padmanaban, R.A., J. Sci. Ind. Res. (India), 1960, 19B, 336.

106. Padmanaban, R.A., J. Sci. Ind. Res. (India), 1960, 19B, 457.

107. Lamb, J., Andreae, J.H., Bird, R., Nature, 1948, 162, 993.

108. De Groot, M.S., Lamb, J., Nature, 1956, 177, 1231.

109. Lamb, J., Sherwood, J., Trans. Faraday Soc., 1955, 51, 1674.

110. Lamb, J., De Groot, M.S., Trans. Faraday Soc., 1955, 51, 1676.

111. Litovitz, T.A., Carnevale, E.H., J. Acoust. Soc. Amer., 1958, 30, 134.

112. Slie, W.M., Litovitz, T.A., J. Chem. Phys., 1963, 39, 1538.

113. Kal'yanov, B.I., Nozdrev, N.F., Soviet Phys. Acoust., 1959, 5, 377.

114. Mamedov, I.A., Akust. Zh., 1975, 21(2), 241.

115. Nozdrev, V.F., Mamedov, I.A., Pulatov, D.K., Zh. Fiz. Khim., 1972, 46, 746.

116. Nozdrev, V.F., Mamedov, I.A., Pulatov, D.K., Zh. Fiz. Khim., 1972, 46, 1705.

117. Crook, K.R., Wyn-Jones, E., J. Chem. Phys., 1969, 50, 3445.

118. Crook, K.R., Wyn-Jones, E., Orville-Thomas, W.J., Trans. Faraday Soc., 1970, 66, 1597.

119. Matheson, A.J., Molecular Acoustics, Pub. Wiley Intersciences, 1971, Chapter 12.

120. Harrison, R.H., Kobe, K.A., J. Chem. Phys., 1957, 26, 1411.

121. Kuratani, K., Mizushima, S., J. Chem. Phys., 1954, 22, 1403.

122. Brasch, J.W., J. Chem. Phys., 1965, 43, 3473.

123. Crossley, J., Smyth, C.P., J. Amer. Chem. Soc., 1969, 91, 2482.

124. Miller, C.R., Gordon, S.L., J. Chem. Phys., 1970, 53, 3531.

125. Heatley, F., Allen, G., Molecular Phys., 1969, 16, 77.

126. Mikhailov, I.G., Polunin, V.M., Sov. Phys. Acoust., 1972, 18, 236.

127. Piercy, J.E., Seshagiri Rao, M.G., J. Acoust. Soc. Amer., 1967, 41, 1063.

128. Naugle, D.G., J. Chem. Phys., 1966, 44, 741.

129. Clark, A.E., Litovitz, T.A., J. Acoust. Soc. Amer., 1960, 32, 1221.

130. Tasköprülü, N.S., Barlow, A.J., Lamb, J., J. Acoust. Soc. Amer., 1961, 33, 278.

131. Hanes, G.R., Turner, R., Piercy, J.E., J. Acoust. Soc. Amer., 1965, 38, 1057.

132. Jarzynski, J., Proc. Phys. Soc., 1963, 81, 745.

133. Barlow, A.J., Erginsav, A., J.C.S. Faraday II, 1974, 70, 885.